2016

Interplay Effects in Highly Modulated Stereotactic Body Radiation Therapy Lung Cases Treated with Volumetric Modulated Arc Therapy

Desmond Joseph Fernandez
Louisiana State University and Agricultural and Mechanical College, desmondfernandez38@yahoo.com

INTERPLAY EFFECTS IN HIGHLY MODULATED STEREOTACTIC BODY RADIATON THERAPY LUNG CASES TREATED WITH VOLUMETRIC MODULATED ARC THERAPY

A Thesis

Submitted to Graduate Faculty of the
Louisiana State University and
Agricultural and Mechanical College
in partial fulfillment of the
requirements for the degree of
Master of Science

in

The Department of Physics and Astronomy

by
Desmond Joseph Fernandez
B.S., Southern University, 2013
August 2016

Acknowledgments

I take this opportunity to thank Dr. Kenneth L. Matthews, Dr. James Matthews, and Dr. Joseph P. Dugas for their service on my committee. Their advice and guidance were essential in the development and completion of this project. I express a special thanks to my major thesis advisor, Dr. Jonas D. Fontenot, for his patience, time and counseling throughout the entire process.

Special thanks go to Mr. Connel Chu for taking immense interest in my project and providing immeasurable insight. Additional thanks goes to my classmates, David Heins, Erin Chambers and Joe Steiner, for aiding in my academic success and the completion of this project.

I recognize the staff at Mary Bird Perkins Cancer Center for their interest in me and my project. Their help, support, and encouragement will always be remembered. Furthermore, sincerest gratitude goes to Mrs. Yolanda Augustus and Mrs. Susan Hammond for being true friends and showing care and compassion during my time at Mary Bird Perkins Cancer Center.

Lastly, I thank my family for being a great source of love, support and encouragement throughout my life; especially my parents, Donald and Patricia Fernandez, who are the driving force behind my success.

Table of Contents

List of Tables

List of Figures

Abstract

Purpose: To evaluate the influence of tumor motion on dose delivery in highly modulated stereotactic body radiotherapy (SBRT) of lung cancer using volumetric modulated arc therapy (VMAT).

Methods: 4D-CT imaging data of the quasar respiratory phantom were acquired, using a GE Lightspeed 16-slice CT scanner, while the phantom reproduced patient specific respiratory traces. Flattening filter-free (FFF) dual-arc VMAT treatment plans were created on the acquired images in Pinnacle^3 treatment planning system. Each plan was generated with varying levels of complexity characterized by the modulation complexity score. Static and dynamic measurements were delivered to GafChromic EBT^3 film inside the respiratory phantom using an Elekta Versa HD linear accelerator. The treatment prescription was 10 Gy per fraction for 5 fractions. Comparisons of the planned and delivered dose distribution were performed using Radiological Imaging Technology (RIT) software.

Results: For the motion amplitudes and periods studied, the interplay effect is insignificant to the GTV coverage. The mean dose deviations between the planned and delivered dose distribution never went below -2.00% and a minimum dose difference of -5.05% was observed for a single fraction. However for amplitude of 2 cm, the dose error could be as large as 20.00% near the edges of the PTV at increased levels of complexity. Additionally, the modulation complexity score showed an ability to provide information related to dose delivery. A correlation value (R) of 0.65 was observed between the complexity score and the gamma passing rate for GTV coverage.

Conclusions: As expected, respiratory motion effects are most evident for large amplitude respirations, complex fields, and small field margins. However, under all tested conditions target coverage was maintained.

Chapter 1
Introduction

1.1 Background and Significance

1.1.1 Lung Cancer

Lung cancer is the second most diagnosed cancer in men and women, but the leading cause of cancer death in both (American Lung Association, 2015). Lung cancer accounts for approximately 37% of all cancer mortality and the stage of the disease at diagnosis is heavily related to outcome, as shown in Figure 1. When an individual is diagnosed after the cancer has metastasized, the expected 5-year survival is approximately 4%. In contrast, when an individual is diagnosed in the localized stage of the disease the expected 5-year survival is approximately 54%. Figure 1 likewise displays the relative number of individuals diagnosed at the corresponding stages. Although the number of individuals with a localized diagnosis represents a small percentage of the total number of diagnosed lung cancers, this number is expected to increase with the use of computed tomography (CT) scans as a lung cancer screening tool for high-risk individuals.

For localized lung cancers, surgical resection is currently considered the standard of care. However, many patients diagnosed with lung cancer are elderly or have health deficits that make them unsuitable candidates for surgery. Radiation therapy is the preferred treatment option for patients unwilling or unsuitable for surgery (National Comprehensive Cancer Network, 2015).

Radiation therapy is the use of ionizing radiation to destroy cancerous cells. Radiation therapy can be administered internally or externally. Internal radiation therapy, or brachytherapy, involves the administration of radiation from within the patient's body. In contrast, external radiation therapy, most commonly delivered with a medical electron accelerator, involves the

administration of radiation beams to the patient and is the primary method of lung cancer treatment.

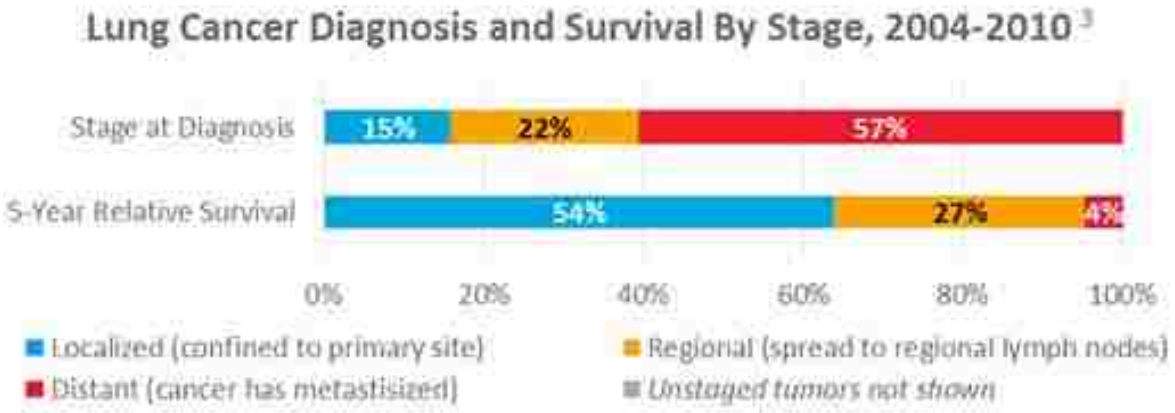

Figure 1: Percentage of lung cancer patients diagnosed at the localized, regional and distant stage of the disease with corresponding 5-year survival. (American Lung Association, 2015)

1.1.2 Stereotactic Body Radiation Therapy

Stereotactic body radiation therapy (SBRT) is one specialized form of external beam radiation therapy treatment that utilizes hypofractionated radiation doses delivered in a limited number of fractions. The hypofractionated doses in SBRT are believed to not only result in clonogenic cell death but also in vascular damage, stromal damage and immune system activation, all of which help improve local control. Stereotactic treatments are also characterized by small treatment volumes and sharp dose fall off into the surrounding healthy tissue.

SBRT's hypofractionated doses have shown to be very effective at treating localized lung cancer (Bezjak et al., 2014). The small treatment volumes and sharp dose fall-off limit the amount of healthy lung tissue treated; which is desirable considering that mean lung dose correlates with lung complications (Yorke *et al.*, 1996). Though effective, SBRT necessitates careful targeting of the tumor volume. Therefore, the use of image guidance, immobilization and motion management is required.

Image guidance is the use of imaging before, during, or after a radiotherapy course for the purpose of improving the precision and accuracy of each treatment delivery (RadiologyInfo, 2014). Most modern linear accelerators utilize onboard kilo-voltage cone beam computed tomography (kV-CBCT) imaging systems to acquire volumetric images before each treatment (Figure 2).

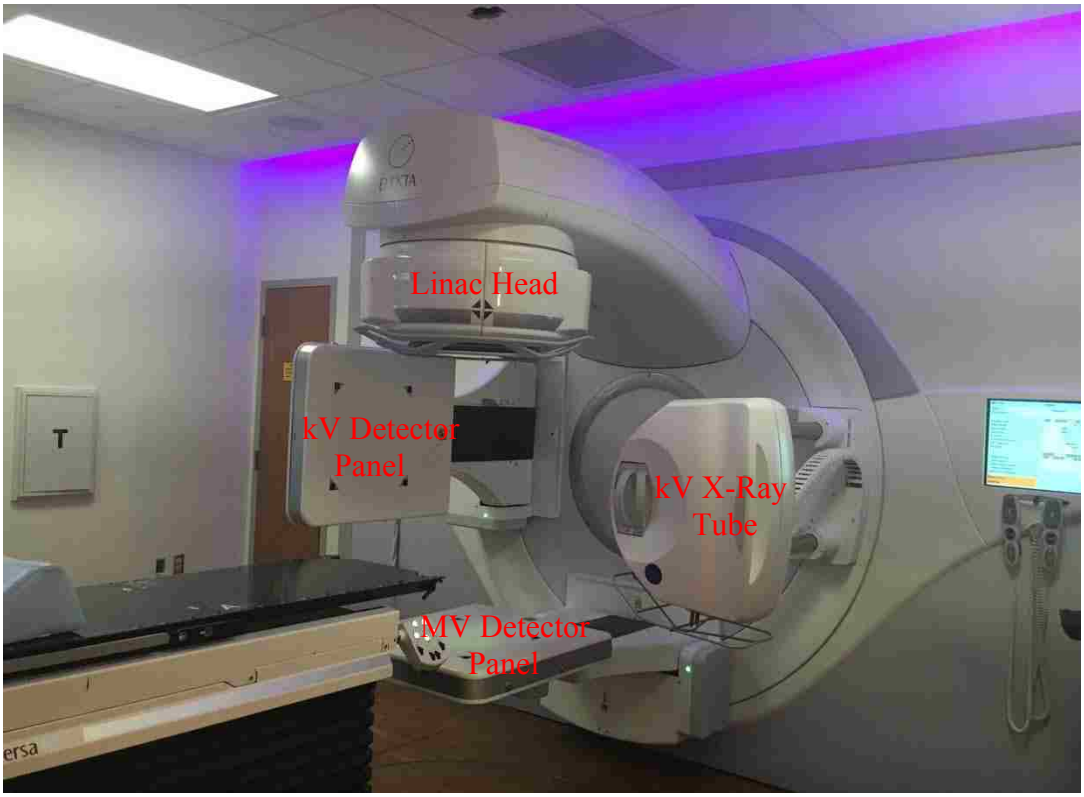

Figure 2: Mary Bird Perkins Cancer Center Elekta Versa HD linear accelerator with onboard MV-CBCT and orthogonal kV-CBCT imaging.

These systems allow for verification of location, shapes, and volumes of treatment targets, organs at risk, and surrounding normal tissues, leading to a reduction in daily setup errors. Image guidance is crucial for treating tumors in areas of the body that are prone to movement or located near critical organs and tissues. When considering SBRT treatments, image guidance is particularly important in that it provides quality setup prior to each treatment.

Immobilization helps establish and maintain the patient in a fixed, well-defined position to minimize daily setup differences (inter-fraction motion) and patient motion during treatment (intra-fraction motion) over a radiotherapy course (RadiologyInfo, 2014). Immobilization must be considered in SBRT since large fractional doses considerably increase treatment time, which increase the likelihood of patient motion. Common immobilization devices to reduce voluntary patient motion for stereotactic procedures include stereotactic body frames, stereotactic head frames, thermoplastic shells, and bite blocks, among others. Unfortunately, respiratory motion is a major component of patient intra-fraction motion and is particularly difficult to manage. As a result, additional motion management techniques are needed to limit or account for patient respiratory motion.

Respiratory motion can complicate the radiation therapy imaging, treatment planning and delivery processes by introducing a temporal component which is not customarily accounted for in radiotherapy. For example, respiratory motion can affect the location of the tumor, make it difficult to detect microscopic disease, and distort the target volume causing incorrect positional and volumetric information during the CT image acquisition process, as seen in Figure 3. Distorted and incorrect imaging data becomes problematic when trying to determine and delineate treatment planning margins during the planning process, typically resulting in the use of larger margins around the tumor, which consequently results in more normal tissue being treated. Respiratory motions can also cause averaging or blurring of the dose distribution over the path of the motion during radiation delivery; thus giving unintended deviations between the planned and delivered dose distribution. Hence, respiratory motion is very important and requires careful assessment.

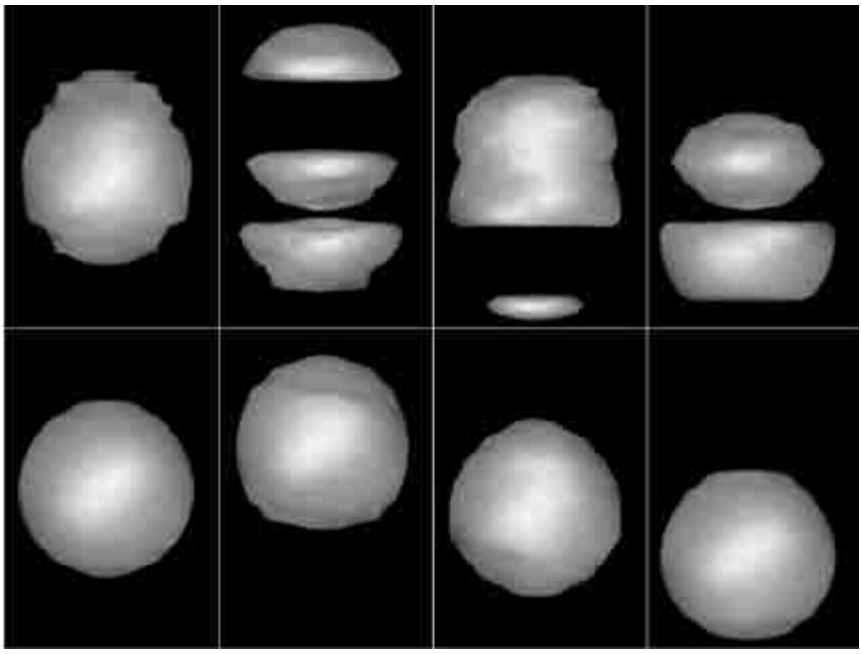

Figure 3: Example of motion artifacts from scanning a moving sphere. Top row: Artifacts of the moving sphere when scanned with a helical free breathing-CT. Bottom row: true geometry of the sphere. (Rietzel *et al.*, 2005)

1.1.3 Four-Dimensional Computed Tomography

Four-dimensional computed tomography (4D-CT) scan involves the acquisition of standard CT data sets at various phases throughout the breathing cycle. This method has been used to address the issues presented by respiratory motion in the imaging acquisition process. In 4D-CT acquisition, a cine CT is acquired by obtaining a continuous series of timed images over an entire breathing cycle at each fixed couched position, as the couch is indexed throughout the entire field of view (FOV).

During cine image-acquisition, respiratory surrogates are used to generate a respiratory trace. The respiratory trace is used to tag each acquired cine image with a respiratory phase value. Both, the cine data and respiratory trace are sent to binning software where the images are sorted into bins based on phase value. Each bin, representing a 3D-CT data set, is part of the 4D-CT data set that together represents the entire breathing cycle.

The 4D-CT binning software also has the ability to create unique intensity projection data sets. The maximum intensity projection (MIP) data set is particularly important in that it shows all possible positions of the tumor throughout the respiratory cycle. This data set is generated by displaying the greatest pixel value (highest attenuation) across all phases, Figure 4. Currently, the MIP data set is used in treatment planning to delineate a motion encompassing region of interest (ROI) that fully encompasses the extent of the tumor's motion.

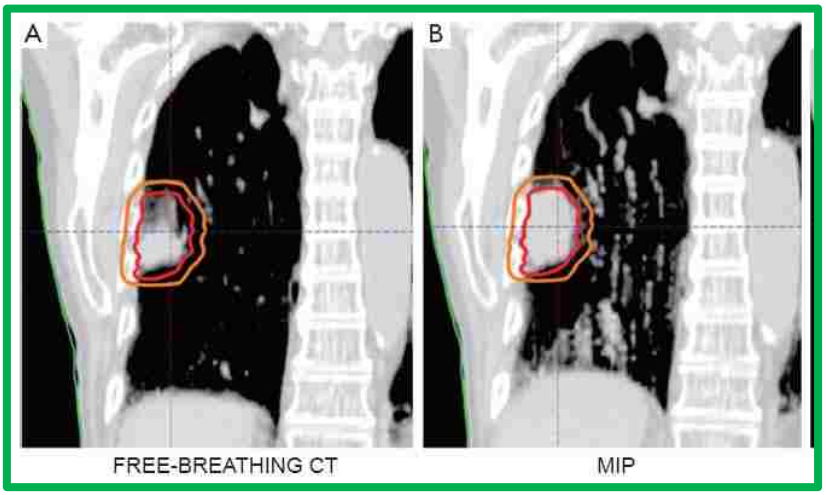

Figure 4: Positional differences between the tumor positions on the free-breathing (A) and the MIP (B) data sets. Contours represent the ITV (red) and PTV (orange). (Glide-Hurst *et al*., 2014)

1.1.4 Volumetric Modulated Arc Therapy (VMAT)

Volumetric Modulated Arc Therapy (VMAT) is an advanced radiation delivery technique that delivers fluence modulated radiation fields while the gantry of a linear accelerator is rotating through one or more arcs. During arc delivery, near continuous variations of gantry rotation speed, dose rate and multi leaf collimator (MLC) position modulate the beam's fluence in an effort to deliver a conformal dose distribution. The MLCs are leaves made of tungsten material located in the head of a linear accelerator and are the driving force behind conformal dose distributions and fluence modulated fields in VMAT (see Figure 5).

VMAT has several advantages over other fluence modulated techniques. VMAT has the ability to deliver radiation therapy treatments in shorter periods of time and with increased monitor unit efficiency, while maintaining comparable or more conformal target coverage and critical structure sparing than Intensity Modulated Radiation Therapy (IMRT) (Li *et al*., 2013; Ong *et al*., 2011; Ramsey *et al*., 2001; Rao *et al.*, 2012). As a result, VMAT treatments are more tolerable for the patient and provide additional time for image guidance, which are important considerations when treating with SBRT.

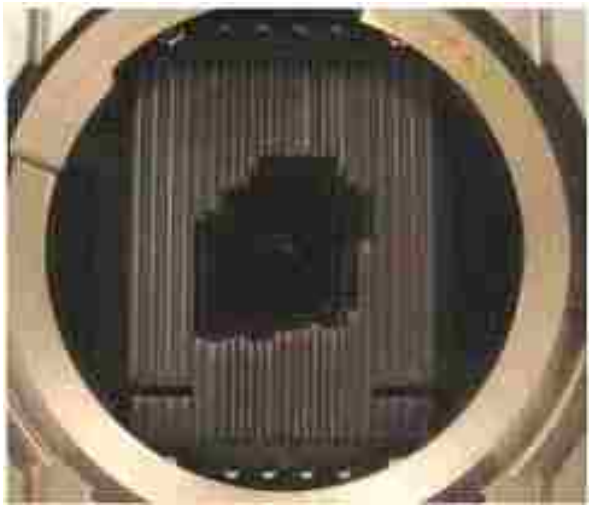

Figure 5: MLC leaves from both leaf banks forming desired shape (looking into gantry head). (Garcia-Garduno *et al*. 2008)

1.2 Research Motivation

When using fluence modulated techniques there are concerns of interplay between moving tumors and dynamically changing parameters, most notably MLC motion. Interplay is the result of treatment planning dose calculations on stationary CT data sets. A treatment volume, assumed to be stationary in treatment planning, is modulated by segments of time-dependent changes in MLC and gantry positions. During delivery, the displacement of this

volume, relative to the moving MLC leaves, results in deviations between the planned and delivered dose distributions.

Previous investigations of interplay have been reported for lung cases using conventional fractionation schemes (e.g. 30 fractions at 2 Gy per fraction). For sliding widow and step-and-shoot IMRT, Jiang et al., (2003) used a motor driven platform to simulate one-dimensional sinusoidal movements. Solid water was placed on top this platform with a Farmer chamber inside and clinical lung cancer treatment plans were delivered. This study observed that interplay effects could result in an 18% dose variation for a single fraction.

Seco et al., (2007) used an in-house made motor driven platform to simulate one-dimensional sinusoidal breathing motion. An ionization chamber and Kodak X-Omat films were used to measure the dose in the moving phantom. Interplay's dose variations were observed to be greatest for IMRT beam segments with low monitor units (MU).

Chui et al., (2003) developed a computational algorithm that calculates the effects of respiration-induced organ motion on delivered dose for sliding widow and step-and-shoot IMRT. This study reported that the effects of organ motion broadened the penumbra and degraded the coverage of the planning target volume for lung treatments.

For conventionally fractionated VMAT, Court et al., (2008) exported static dose distributions were to written software, which recalculated the dose distribution being delivered to a moving target. Moreover, an experimental dynamic phantom, on which an ion chamber array was mounted, was programmed to simulate various motions as treatments plans delivered. The results indicated that dose variations were largest for small MLC separation and fast moving MLCs. Also, it was observed that dose variations are largest for complicated MLC sequences, large amplitudes and single arcs.

However, under clinical conditions, all studies above concluded that the use of multiple beams per fraction and several fractions per treatment course causes the interplay effect to be averaged out and dosimetrically insignificant for conventional fractionation schemes (Chui *et al*., 2003; Court *et al*., 2010.; Jiang *et al*., 2003; Seco *et al*., 2007).

The use of fewer treatment fractions and increased dose per fraction could result in very different statistics of interplay. Kang *et al*., (2010) recalculated the dose distributions of nine clinical hypofractionated IMRT lung cancer treatments plans, simulating one-dimensional tumor motion, to assess perturbations in delivered doses from respiratory motion. This study indicated that variations in target coverage had minimal dependence on respiratory period or initial phase. Dose variations were more dependent on amplitude, degree of modulation and field margin; all of which led to significant changes in target coverage for highly modulated fields.

Stambaugh *et al*., (2013) used a 4D dose reconstruction method on SBRT VMAT plans by applying perturbations to the treatment planning system calculated static 3D dose. Their results showed that intra-fraction interplay is minimal for clinical conditions (<0.2%). It is also small (0.9% average, 2.2% maximum) when the target excursion is increased to 2–3 cm. Additionally, when comparing single and multiple fractionations, interplay effects are reduced as you increase the number of fractions.

Li *et al*., (2013) considered interplay effect in flattening filter-free dual-arc VMAT SBRT plans. Their process entailed a 3D dose calculation from the Eclipse treatment planning system being processed by in-house software to generate a 4D VMAT plan. The 4D VMAT plan is the original static 3D dose distribution where radiation is delivered only during the respiratory phase or phases that receives dose from a corresponding control point. Their results showed that the coverage difference between the 3D and 4D dose calculations were either unchanged or slightly

increased up to 1.2%, and the variations of their minimum doses were less than 3.2% for the 6 patients studied. However, there were significant changes in the PTV coverage and, therefore, it was concluded that with significant margin the interplay effect would be insignificant.

Rao *et al*., (2011) studied the interplay effect in VMAT SBRT lung treatments. This simulation study conducted a planning based investigation on 4D-CT phase sets. 3D dose calculations were performed on the end-of-exhale phase set and compared to its recalculated dose distribution distributed on all phase sets (i.e. 4D dose calculation) by copying the 3D phase set planning parameters. This study observed negligible interplay effects for all plans studied. However, one stated weakness of their study was the minimal use of modulation in their treatment plans. This was indicated by majority of their aperture shapes conforming to the PTV and few aperture shapes containing MLC leaves that block part of the target.

SBRT treatments have been implemented at Mary Bird Perkins Cancer Center (MBPCC) with VMAT since 2009. Over the course of the program, the treatment team has observed some circumstances of high plan modulation; such as lung tumors that are in close proximity to critical structures where significant dose sparing is required. Therefore, the goal of this study is to assess VMAT SBRT dose delivery under increased levels of modulation. Evaluation of target coverage was used to gage interplay effects on the delivered dose distributions in effort to evaluate its clinical importance. Additionally, correlation of target coverage to a plan-based modulation metric was used to provide an indication of potentially risky plans.

1.3 Hypothesis and Specific Aims

The hypothesis of this work is that treatment plan modulation will correlate ($R > 0.60$) with changes in target coverage between planned and delivered dose distributions. The three specific aims that have been formulated to address the hypothesis of this work are:

Aim 1: Generate Flattening Filter Free (FFF) -VMAT treatment plans with a range of Modulation Complexity Scores (MCS).

Aim 2: Measure dose distributions for VMAT treatment plans and evaluate interplay's impact on the target's delivered dose distribution.

Aim 3: Evaluate MCS for correlation with target coverage for respective VMAT plans.

Chapter 2
Methods and Materials

2.1 Aim 1

In this aim, a respiratory motion phantom was imaged while simulating patient specific respiratory traces. Subsequently, treatment plans were generated using the acquired images with varying degrees of complexity characterized by a treatment plan complexity metric.

2.1.1 Respiratory Phantom

In this study, a dynamic phantom (Quasar Respiratory Phantom, Modus Medical Devices, Ontario, Canada) was used as a surrogate for patient geometry. The phantom is composed of an acrylic body and an electric drive unit designed to simulate one-dimensional internal lung motion with various cylindrical "lung" inserts that move in the longitudinal direction while simultaneously simulating one-dimensional external chest motion with a platform that moves in the anterior-posterior direction. The phantom's acrylic body, internal and external motion features, and array of cylindrical inserts makes the device suitable for mimicking a breathing patient. This device, shown in Figure 6, was used throughout the imaging, planning and treatment process.

In this study, the cedar lung tumor insert was used. The insert is composed of cedar wood and contains an offset, 3 cm diameter, plastic sphere to be used as lung and tumor surrogates, respectively. Cedar and plastic are typically used as surrogates for lung and tumor, respectively, due to their similar properties. The cedar CT numbers and densities range from 290-400 and 0.25-0.32 g/cm^3 as compared to 140-300 and 0.15-0.33 g/cm^3 for lung. The CT number and density of the plastic sphere are 950 and 0.98 g/cm^3 compared to 1000 and 1.02 g/cm^3 for patient tumors (Yorke *et al.*, 1996). This insert, inside the phantom's acrylic body,

provides the desired imaging conditions of an actual lung tumor patient. Figure 7 shows the cylindrical insert which splits in half for film dosimetry.

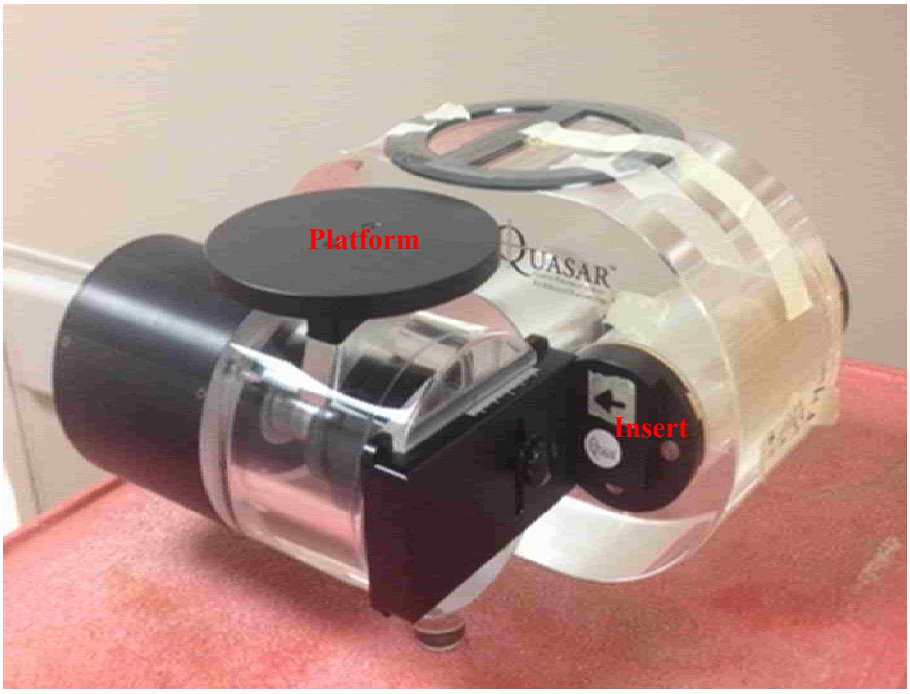

Figure 6: Quasar respiratory motion phantom

Figure 7: Cedar lung tumor insert (left) and CT scan of cedar lung tumor insert (right).

2.1.2 Respiratory Motion Models

The control software for the phantom supports import of 1D respiratory traces that can be reproduced by the phantom. Using this feature, three anonymized patient-specific breathing traces acquired with the external tracking system (Varian Real-Time Positioning (RPM), Varian Medical Systems, Palo Alto, CA) used at MBPCC were attained. Two traces were selected where the amplitude and period of the respiratory cycles where consistent, see Figure 8-9. Additionally, one irregular trace was selected where the amplitude and period of the respiratory cycles varied, see Figure 10. The provided software utilizes a waveform editor that allows the user to filter, compress, stretch, and scale the amplitude of a given waveform. The software's wave editor was used to set each waveform at fixed amplitudes of 1 and 2 cm, for a total of 6 traces. Amplitudes of 1 and 2 cm were chosen, because respiratory amplitudes over 2 cm are relatively uncommon. This software and phantom have demonstrated the ability to reproduce traces to sub-millimeter accuracy (Modus QA, 2016).

Figure 8: Patient specific breathing trace one (PS1) at 2 cm amplitude.

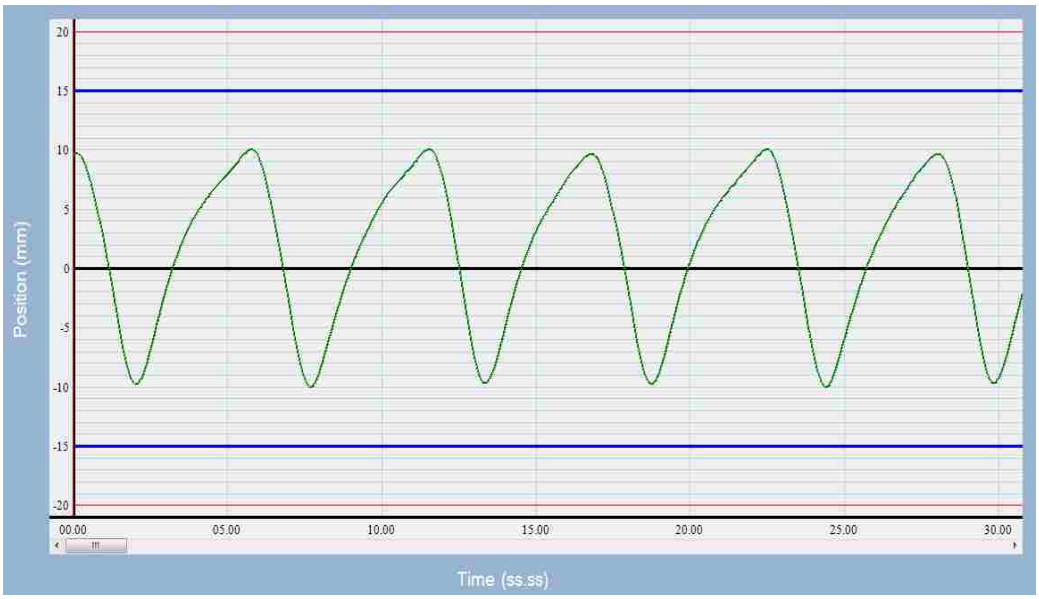

Figure 9: Patient specific breathing trace two (PS2) at 2 cm amplitude.

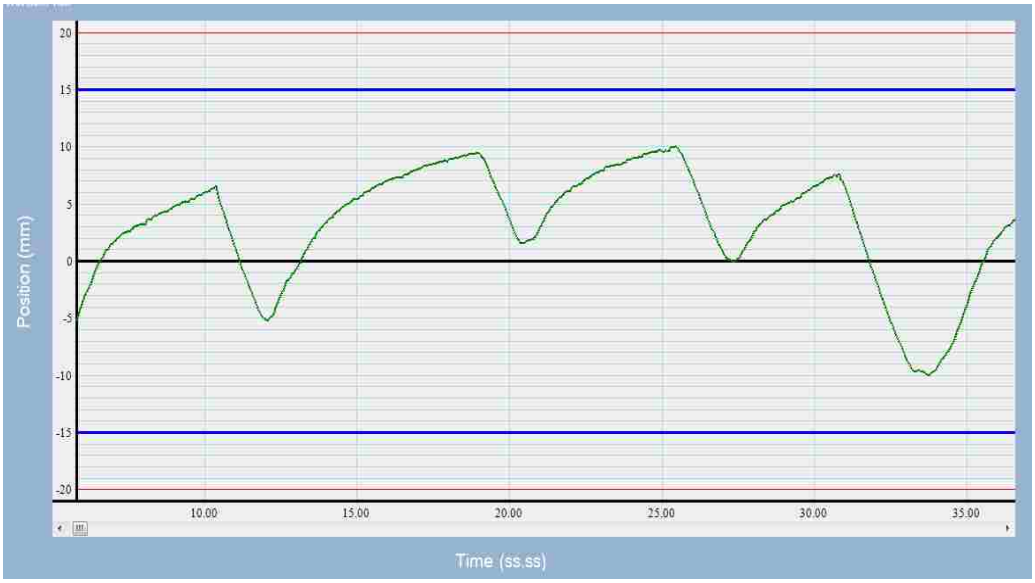

Figure 10: Irregular patient specific breathing trace at 2 cm amplitude.

2.1.3 Treatment Planning Image Acquisition

Currently, MBPCC employs a motion encompassing imaging technique for managing intra-fraction respiratory motion during treatment planning and delivery of lung SBRT. Again, this technique involves creating a region of interest (ROI) that encompasses the target and its envelope of motion. To reproduce this, images of the phantom were acquired with a General

Electric Lightspeed multi-slice CT scanner (General Electric Company, Waukesha, WI) using MBPCC's standard clinical 4-Dimensional Computed Tomography (4D-CT) gating protocol. The parameters and values for the 4D-CT gating protocol are shown in Table 1.

Table 1: MBPCC 4D-CT Gating Protocol

Parameter	**Value**
Slice Thickness	2.5 mm
Matrix Size	512 x 512
mAs	400
Field of View	30 cm
kVp	120
Cine Duration	(variable)

The MBPCC 4D-CT protocol consists of taking an initial scout scan, a free-breathing (FB) CT scan and then a cine scan. During cine image-acquisition, Varian's Real-time Position Management (RPM) system, which consists of an infrared (IR) tracking camera and a reflective marker box (Figure 11), monitors the external chest motion of the phantom and generates a breathing trace.

Figure 11: The Varian RPM system 4D-CT infrared camera (left) and the Varian RPM system reflective marker box (right).

Once acquired, the cine volumetric data and the RPM breathing trace were sent to the Advantage 4D-CT v1.6 binning software (GE Healthcare, Buckinghamshire, England) and a 4D-CT data set generated. Additionally, the Advantage software was used to create a MIP data set.

2.1.4 Pinnacle^3 Treatment Planning

After imaging the FB and MIP CT data sets, Figure 12, were exported to a treatment planning system (TPS) (Pinnacle^3, Fitchburg, Wisconsin, U.S.). The data sets were fused and the MIP data set was used to contour the ITV on the FB-CT data set. A uniform margin of 0.5 mm was added to the ITV to form the PTV.

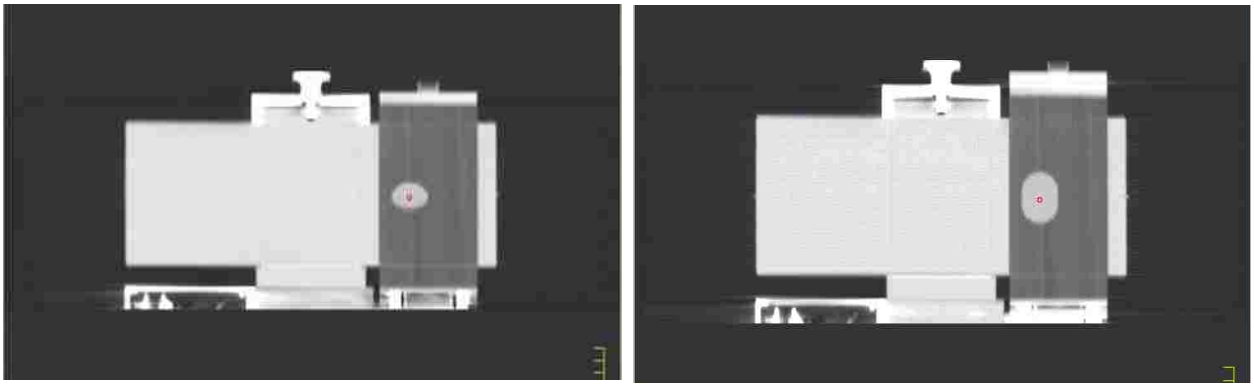

Figure 12: Coronal slice of free breathing-CT data set and MIP CT data set in Pinnacle^3 treatment planning system.

Flattening filter free (FFF) VMAT plans were created according to the Radiation Therapy Oncology Group (RTOG) 0813 and MBPCC clinical protocols on the FB-CT data sets. Several protocol requirements are shown in Table 2. Each FFF-VMAT plan consisted of two full 360° treatment arcs at 6 megavoltage (MV) photon beam energy. The collimator angle was set to 45° and the coach angle was 0°. VMAT plans were generated using Pinnacle^3 SmartArc inverse planning module (Bzdusek *et al.*, 2009). Inverse planning allows the optimization algorithm to determine the best method of accurately irradiating the target volume while minimizing dose to surrounding critical structures. All plans were optimized using a 4° control points spacing and a 0.46 cm/degree leaf motion constraint.

The PTV prescription was set to 1000 cGy per fraction for 5 fractions and the dose was calculated on a dose grid of 3x3x3 mm^3. This dose fractionation scheme was selected as it is

allowed by the RTOG 0813 protocol, the current standard at MBPCC for most cases, and common in the literature (Li *et al.*, 2013; Ong *et al.*, 2011; Ramsey *et al.*, 2001; Rao *et al.*, 2012).

Table 2: RTOG 0813 Protocol Requirements

Normalization	≥60% and ≤90%
PTV Coverage	Prescription isodose should cover 95% of PTV
High Dose Spillage	Any dose >105% should occur in PTV
Low Dose Spillage	Dose falloff must be rapid

Plans were created at varying degrees of complexity characterized by the modulation complexity score (see Section 2.1.5). This was achieved by contouring approximating regions of interest to represent normal anatomy. The insert inside the phantom represents a left lung tumor. Therefore, contours representing right lung, spinal cord, left ribs, and esophagus were delineated. Additionally, a region of interest (ROI) was contoured inside the ITV and PTV volume adjacent to the GTV, per RTOG protocol, to generate modulation in the more complex cases see, Figure 13. The right lung, spinal cord, left ribs, and esophagus were sequentially added to increase plan modulation. A contour was added and then the initial dose objective value was set according to the RTOG critical organ dose-volume limit with an objective weight of one. The contour's dose objective value was progressively reduced until an objective value of 0.01 was reached. Then, the next contour would be delineated until the final desired modulation complexity score was reached. Once the desired modulation complexity score was achieved, analysis of dose-volume metrics, for agreement within protocol requirements, was performed. The plans and images were then exported from Pinnacle[3] and imported into MOSAIQ Record and Verify System (Elekta AB, Mountainview, CA) information system for treatment delivery.

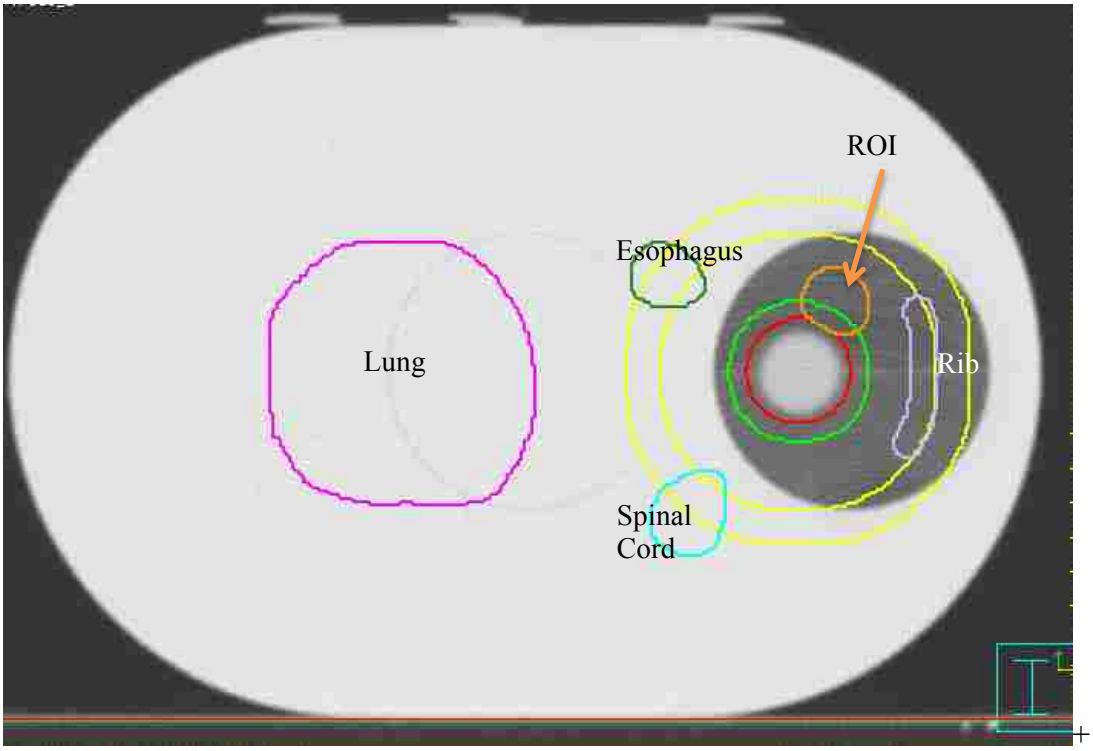

Figure 13: Axial CT-slice of respiratory motion phantom with all contours delineated.

2.1.5 Modulation Complexity Score

The modulation complexity score (MCS) was utilized to quantify the MLC modulation of each plan. MCS was proposed by McNiven et al., (2012) for step-and-shoot IMRT and then adopted for VMAT as reported by Masi *et al.,* (2013). The MCS has a fixed range from 0-1, with lower scores indicating increased modulation. MCS is calculated based on three characteristics of each segment: area, weight and number of monitor units.

Segment shape is quantified using the leaf sequence variability (LSV) parameter. LSV is defined as the variability in segment shapes of each field. The segment shape is based on the difference in leaf position between adjacent MLC leaves for each leaf bank excluding those positioned under the jaws. The maximum distance between positions for a leaf bank is defined as

$$pos_{max}(CP) = \max(pos_{n\in N}) - \min(pos_{n\in N})_{leafbank}$$

The LSV is then calculated as follows:

$$LSV_{cp} = \left(\frac{\sum_{n=1}^{N-1}(pos_{max} - |(pos_n - pos_{n+1})|)}{(N-1)\ x\ pos_{max}}\right) x \left(\frac{\sum_{n=1}^{N-1}(pos_{max} - |(pos_n - pos_{n+1})|)}{(N-1)\ x\ pos_{max}}\right)$$

Segment area is quantified using aperture area variability (AAV). AAV is defined as the variation in segment area relative to the maximum aperture area. Segments that similar in area to the maximum aperture area contribute to a larger complexity score, i.e. less modulation. The AAV is calculated using the leaf position information as follows:

$$AAV_{cp} = \left(\frac{\sum_{a=1}^{A}\left(\langle pos_a\rangle_{leftbank} - \langle pos_a\rangle_{rightbank}\right)}{\sum_{a-1}^{A}\left(\langle \max(pos_a)\rangle_{leftbank\epsilon arc} - \langle \max(pos_a)\rangle_{rightbank\epsilon arc}\right)}\right)$$

where A is the number of leaves in the leaf bank.

Finally, the segment weight is incorporated into the complexity score. Control points with a larger number of MUs have a larger weighting and contribute more to the complexity score. The weighting is incorporated along with AAV and LSV into the final MCS calculation. The MCS for an entire arc, MCS_{arc}, is the product of the LSV_{cp} and AAV_{cp} weighted by the relative MU of each control point in the beam.

MCS_{arc} is defined as follows:

$$MCS_{arc} = \sum_{i=1}^{I-1}\left[\frac{\left(AAV_{cpi} + AAV_{cpi+1}\right)}{2}\ x \frac{\left(LSV_{cpi} + LSV_{cpi+1}\right)}{2}\ x\ \frac{MU_{cpi,i+1}}{MU_{arc}}\right]$$

2.2 Aim 2

In Aim 2, each treatment plan created in Aim 1 was delivered to the respiratory motion phantom. Static and dynamic dose were measured using radiochromic film inside the phantom.

2.2.1 Ion Chamber Measurements

Treatment plans were delivered to the respiratory phantom using an Elekta Versa HD linear accelerator (Elekta Oncology Systems, Crawley, UK). This accelerator has a 160-leaf

MLC supporting up to a 40 x 40 cm^2 field size, resulting in a leaf width of 0.5 cm at isocenter. This accelerator is used clinically for SBRT procedures at MBPCC.

Linear accelerator output was measured before each film measurement session using the protocol recommended by Task Group 51 of the American Association of Physicists in Medicine (Almond *et al*., 1999). A Physikalisch-Technische Werkstätten (PTW) GmbH farmer ionization chamber, SN: N30006-0074, (PTW, Freiburg, Germany) was placed in a solid water phantom (CIRS, Norfolk, VA) and irradiated with 100 MU. The farmer chamber was coupled with a CNMC Model 206 dosimetry electrometer, SN: 11207335, (CNMC Company, Nashville, TN) in order to measure the charge collected per MU. The output measurements were converted to dose and film dose calibration curves (Section 2.2.4) were adjusted accordingly to account for changes in daily output.

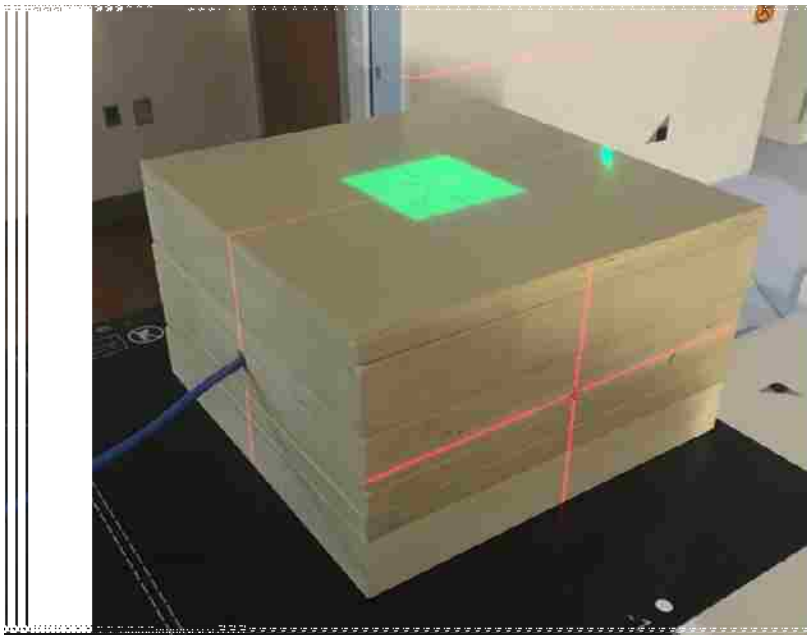

Figure 14: Linear accelerator output setup for a 6 MV beam at reference conditions of 100 SAD at 10 cm depth and 10 cm backscatter of solid water using a 10x10 cm^2 field size.

Per MBPCC clinical policies, the output was calibrated to a dose of 0.8 cGy/MU for a 6 MV beam at reference conditions. Reference conditions are at 100 SAD with 10 cm water for a

10x10 cm^2 field size, Figure 14. Three readings were taken and the corresponding output was calculated using Task Group 51 protocol facilitated by the use of an excel worksheet template in use at MBPCC for monthly output calibrators.

2.2.2 Radiochromic Film Measurements

Two-dimensional (2D) dose distributions of each treatment were measured using radiochromic film placed inside the cedar insert of the respiratory phantom. Radiochromic film was chosen because it is insensitive to ambient light, does not require wet chemical processing (i.e. self-developing), and has high spatial accuracy. Insensitivity to ambient lighting greatly simplifies the processes of handling, cutting, and loading film. Self-processing film eliminates any variations that may arise from wet chemical processing to be eliminated and high spatial accuracy is important when measuring dose distributions with steep dose gradients, such as those common in SBRT treatment.

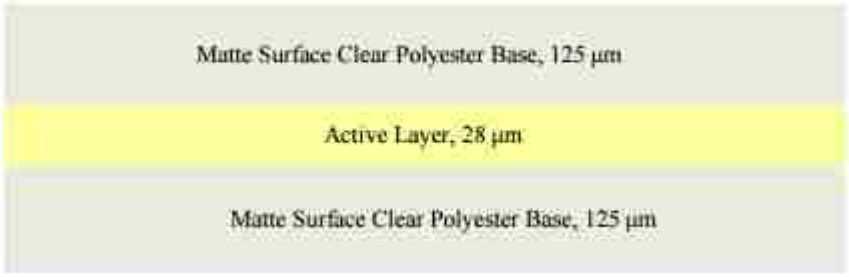

Figure 15: Structure of GafChromic EBT^3 Dosimetry Film (Ashland, 2016)

GafChromic EBT^3 (International Specialty Products, Wayne, NJ), was the type of radiochromic film used to measure the dose distributions. The structure of GafChromic EBT^3 film is shown in Figure 15. This film has been designed with a dynamic dose range of 10-2000 cGy and has been reported to have minimal photon energy dependence and is nearly tissue equivalent (Ashland, 2016).

A calibration curve was prepared for each batch of film. In this process, two sheets of 8x10 in^2 films were cut into twelve 3x3 in^2 pieces and marked for orientation purposes. With one film piece unirradiated representing background, eleven pieces of film were exposed to a range of doses from 250 to 1425 cGy. Figure 16 shows the cut film pieces for a batch of film and the planning doses received.

Each calibration film was set perpendicular to the radiation delivery in solid water at a 100 cm SSD and 1.5 cm depth, d_{max} for 6 MV radiations, with 10 cm of backscatter. Radiation was delivered with a 6 MV photon beam using an open 10x10 cm^2 field. Per manufacturer recommendations, each film was stored for a period greater than 24 hours before scanning to ensure that all polymer changes (self-development) had completed. Films were scanned in using an Epson Expression 10000XL flatbed scanner (Section 2.3.2**)** and a calibration curve was developed in Radiological Imaging Technology analysis software (Section 2.3.3) using a built in calibration procedure.

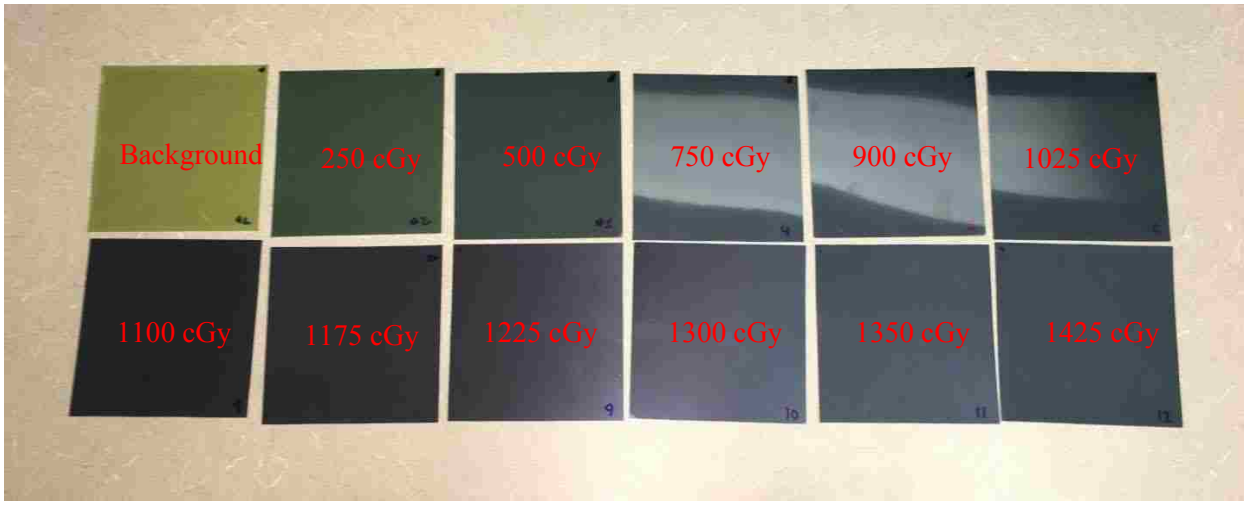

Figure 16: 3x3 in^2 pieces of GafChromic EBT^3 film with corresponding delivered dose for film's calibration curve.

Before treatment delivery on the linear accelerator, a piece of radiochromic film was prepared by cutting the film flush with the cedar film and tumor insert and punching registration

holes in each corner, Figure 17. The registration holes were punched using a hole puncher with consistent setting to punch a hole 7/16 and 1/2 inch from longitudinal and lateral edge of the film corner, respectively.

Figure 17: Radiochromic film piece cut flush with cedar film and tumor insert with punched registration holes before delivery (left) and after delivery (right).

The insert (now containing the film) was placed inside the phantom, which was aligned to the room lasers by radiopaque markers placed on the phantom during simulation. A kilovoltage cone beam computed tomography (kV-CBCT) scan was taken using the x-ray volume imaging (Elekta Versa HD, Elekta Ltd. Crawley, West Sussex, United Kingdom) system to align the phantom position with that in the planning CT data set exported from the TPS, Figure 18. Each kV-CBCT was acquired with a bow-tie filter (F1) and a small collimator field of view with an axial length of 26 cm (S20). Once the kV-CBCT was acquired, it was aligned to the reference CT using automatic grey-scale matching. The designated volume for registration (clipbox) was defined to encompass the stationary parts of the phantom. Treatment plans were then delivered to the phantom, and the resulting dose measured, with and without respiratory motion, for a total of 90 deliveries.

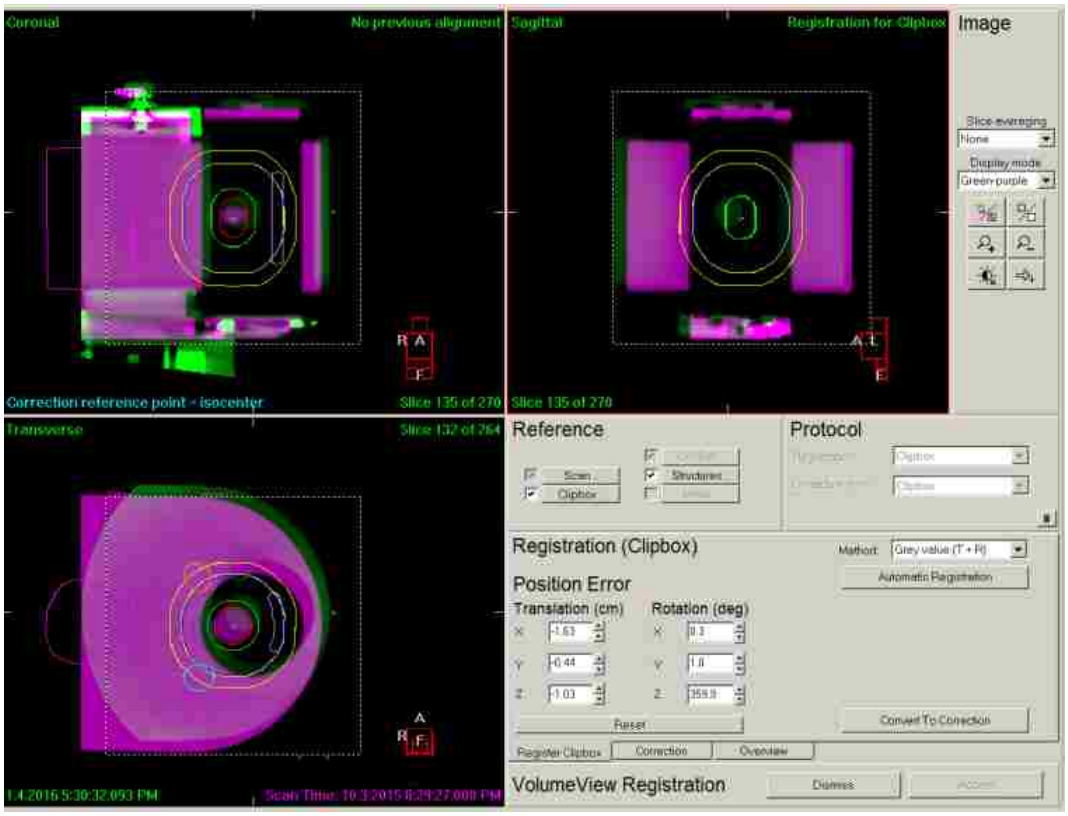

Figure 18: Screenshot of XVI 3D-kVCBCT registration window. (Green: Acquired CBCT; Purple: Pinnacle Export)

2.3 Aim 3

The film from the static and dynamic deliveries in Aim 2 will be compared to the Pinnacle[3] planar dose distributions in this aim.

2.3.1 Planar Dose Export

The coronal dose plane corresponding to the dose distribution measured by the film inside the phantom was exported from the TPS for each treatment plan. Planar doses were calculated for a 20x20 cm^2 square field. The planar dose tool, Figure 19**,** was used to create ASCII planar dose files at a resolution of 1 mm. The ASCII files were exported, and retrieved via file transfer protocol (FTP).

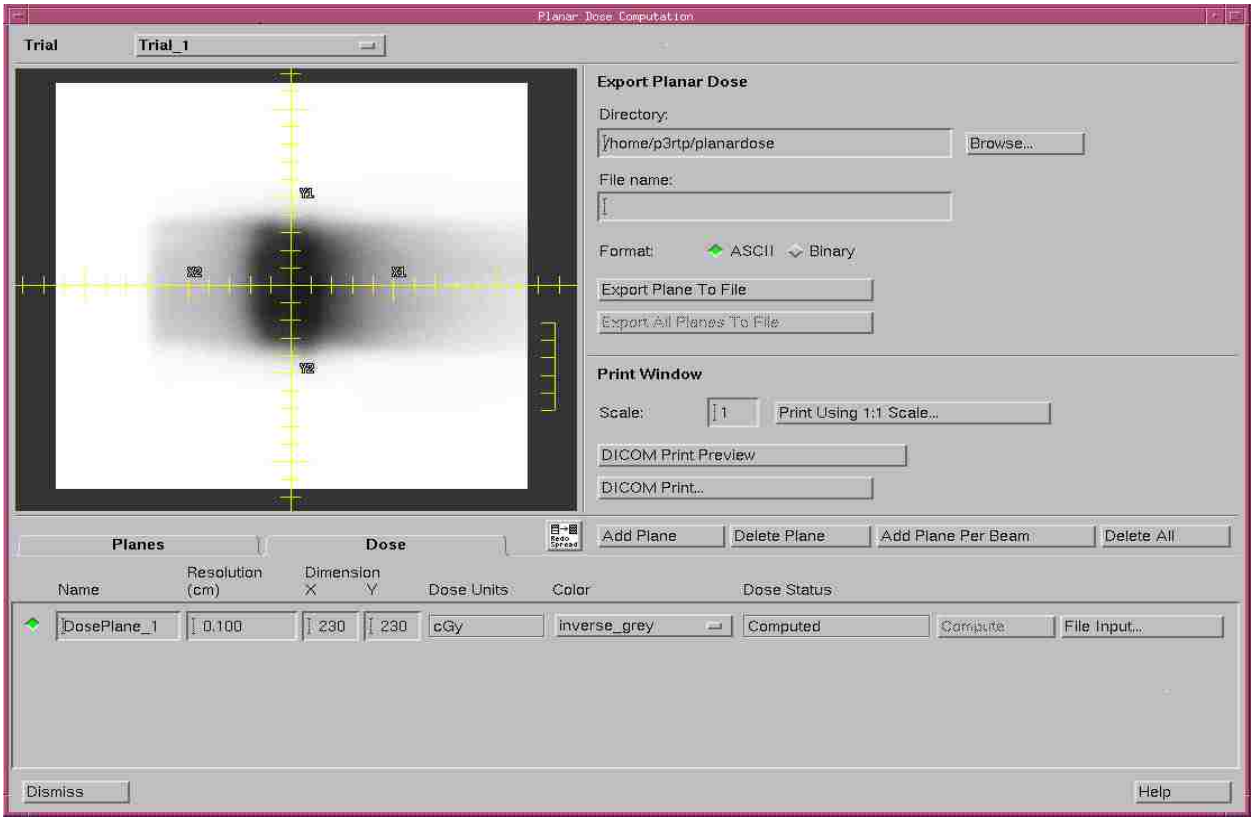

Figure 19: Screenshot of Pinnacle[3] Planar Dose Computation window.

2.3.2 Digitization of Exposed Films

Radiochromic film measurements were digitized using an Epson Expression 10000XL flatbed photo scanner (Seiko Epson Corporation, Nagano, Japan). This scanner was used to save 48-bit red-green-blue (RGB) images in tagged image file format (TIFF). Scanner settings are shown in Table 3.

Table 3: Film Scanner Settings

Parameter	Setting
Mode	Professional
Document Type	Film
Image Type	48-Bit Color
Resolution	150 dpi
Target Size	Variable
Image Adjustments	Off

As recommended by the manufacturer, the films were scanned in landscape orientation to reduce lateral response artifacts (Ashland, 2015). Care was taken to preserve film orientation and time between exposure and processing since both have shown to affect film response (Matney, 2008). Additionally, a cutout was designed to make sure that each film was placed in relatively the same position on the scanner during readout, as seen in Figure 20. Since the Epson scanner has no warm-up process, 10 repeated warm-up scans were performed on the scanner before actual image digitization. Each film was digitized at 0.178 mm per pixel in order to balance resolution and document size.

2.3.3 Film Registration

Delivered and planned dose distributions were registered and analyzed in Radiological Imaging Technology (RIT) v6.3 analysis software (Radiological Imaging Technologies, Inc., CO). The Epson scanned 48-bit RGB radiochromic film image was imported as a 16-bit

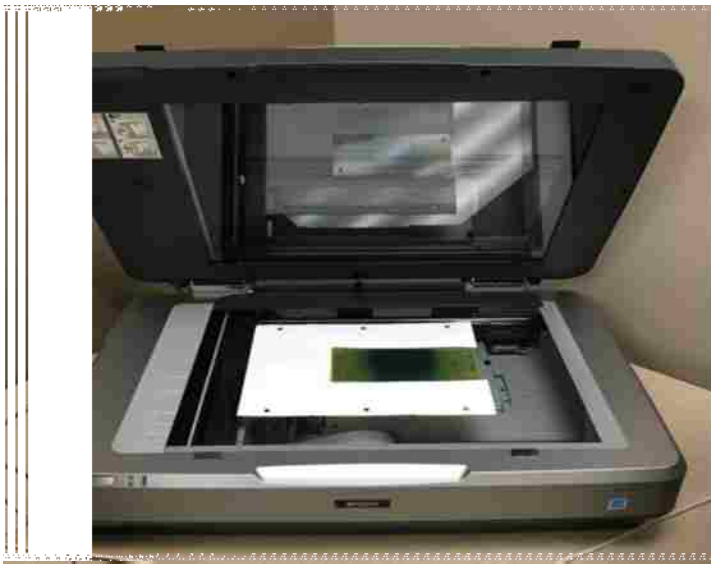

Figure 20: Epson Expression 10000XL Scanner with radiochromic film inside the cutout to ensure all film was scanned in the same relative position.

green channel image since fractionated doses were over 10 Gy (Ashland, 2015). A 2D median filter of 5x5 pixels was applied to all imported film to reduce inherent image noise. The

calibration curve, corresponding with the appropriate film batch, was applied to convert each film pixel value to dose. The planned planar dose ASCII file was also imported into RIT for image registration and analysis.

The planar dose image was registered to the film's measured dose distribution using a registration template created within the RIT software. The template was created by acquiring a CT scan of the phantom (stationary) with film inside and using the measurement tools in the TPS to determine the distances of the film registration holes from isocenter, Figure 21(a). Once the registration template was created and applied to the planar dose image, Figure 21(b), the film image and planar dose image were registered using a point-based rigid body registration tool. The registered images were than normalized and analyzed.

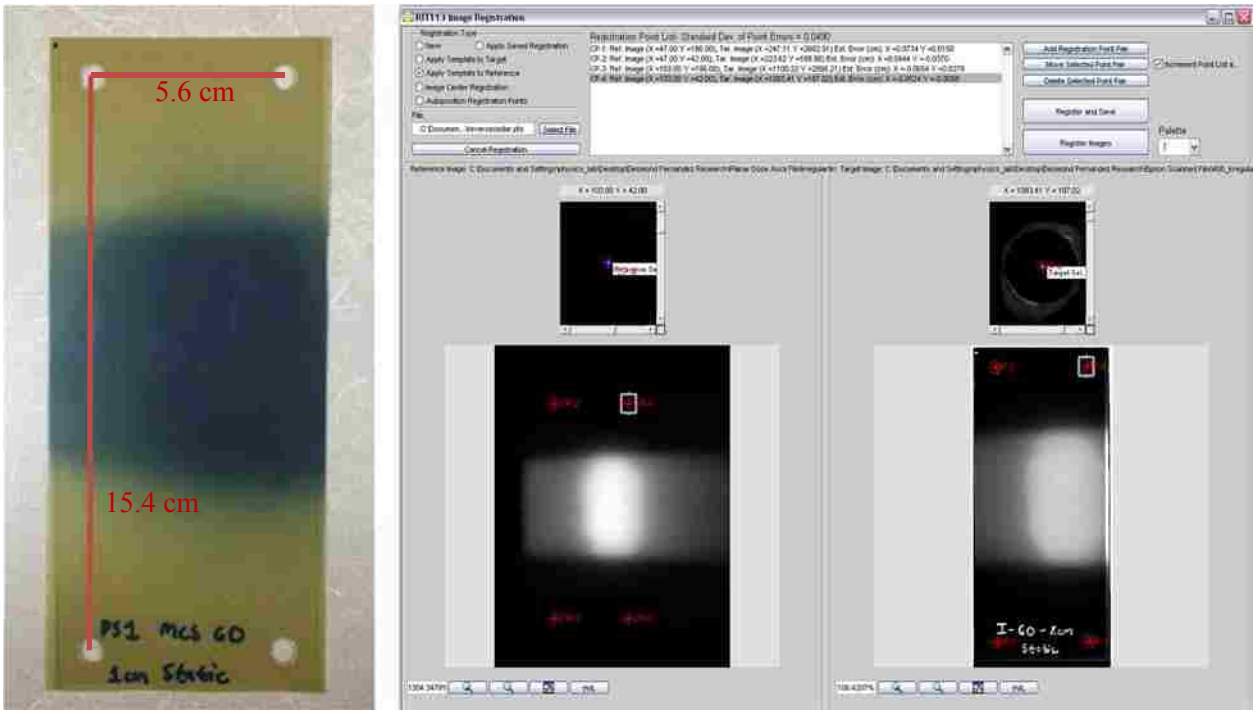

Figure 21: GafChromic film with punched holes for film registration (left) and RIT's image registration window (right).

2.3.4 Analysis

Uncertainty Measurements

The treatment delivery and film analysis processes are subject to error. The quality of the results presented herein is directly related to this error. Measurements were performed to quantify the uncertainty in these steps.

The uncertainty in the CBCT software registration algorithm was determined by a process similar to that described in Sutton et al., 2014. The phantom was initially aligned to isocenter by a kV-CBCT using grey-value registration with only translation shifts. This gave the best alignment possible without considering rotations that the couch is unable to account for. After the phantom was aligned, 6 repeated measurements were acquired without moving the phantom by re-calculating the registration. Ideally, these repeated measurements would have a mean and standard deviation of zero, with any deviations from that value indicating the inherent noise in the image guidance process.

The results from the kV-CBCT image guidance measurements are displayed in Table 4. The expected mean value is 0.00 mm in all directions, since the phantom was initially aligned using a kV-CBCT and the process was repeated without moving the phantom. However, the measurements indicate that the kV-CBCT has sub-millimeter accuracy.

Table 4: Registration results for repeated kVCBCT

	Mean & Standard Error (mm) (N=6)	**Standard Deviation (mm) (N=6)**
X-Lateral	0.17 ± 0.24	0.59
Y-Longitudinal	-0.50 ± 0.10	0.24
Z-Longitudinal	0.48 ± 0.21	0.51

The quality of the film and planar dose registration process was adopted from Vinci, 2007. The film registration software displays an estimated error value for each film registration

point (Δx_i, Δy_i) by evaluating the geometric relationship between registration points in the planar dose and film dose images. These values were taken to directly quantify the quality of the registration process, Q, as calculated by:

$$Q = \sigma_{RIT} = \left(\frac{1}{2N-1}\right)\sum_{j=1}^{N}\left[\left(\frac{\sum_{i=1}^{N}(\Delta x + \Delta y)}{2N} - \Delta x_j\right)^2 + \left(\frac{\sum_{i=1}^{N}(\Delta x + \Delta y)}{2N} - \Delta y_j\right)^2\right]$$

where N= the number of registration points.

The average Q values and spread of Q values from RIT's film registration are reported in Table 5. As a rule of thumb, the standard deviation (σ_{RIT}) should be less than or equal to 1/Pmm, where Pmm is the pixel size of the reference image in mm. For the 1 mm pixel size of our reference images, the Q value from each registration should be less than 1 mm to be considered appropriate. This served as a quality check for all films.

Table 5: Film Registration Quality (≤1mm)

Trace	Average (mm) (N=30)	Range (mm) (N=30)	σ (mm) (N=30)
PS1	0.67	0.35 - 0.96	0.18
PS2	0.55	0.33 - 0.95	0.16
Irregular	0.54	0.37 - 0.92	0.17
ALL	**0.60**	**0.33 - 0.96**	**0.18**

Additionally, one film was registered 10 times to it corresponding planar dose distribution and evaluated. The deviation in quality (Q) from this process (σ_Q = 0.03 mm) was far less than the deviations observed from registering different films. This indicated the error is in large part due to film preparation (*i.e.* the manual cutting of film to fit inside the insert and punching of film registration holes).

Lastly, one A/P plan was generated and delivered to the phantom three times in one session to measure the end-to-end variation in the phantom setup, treatment delivery and film analysis. Each film delivery was registered to the corresponding planar dose file in RIT.

Longitudinal and lateral profiles were acquired and the displacements between midpoints were determined using the 50% isodose line positions. This procedure includes all errors from kV-CBCT alignment, from treatment delivery, and from film registration and scanning.

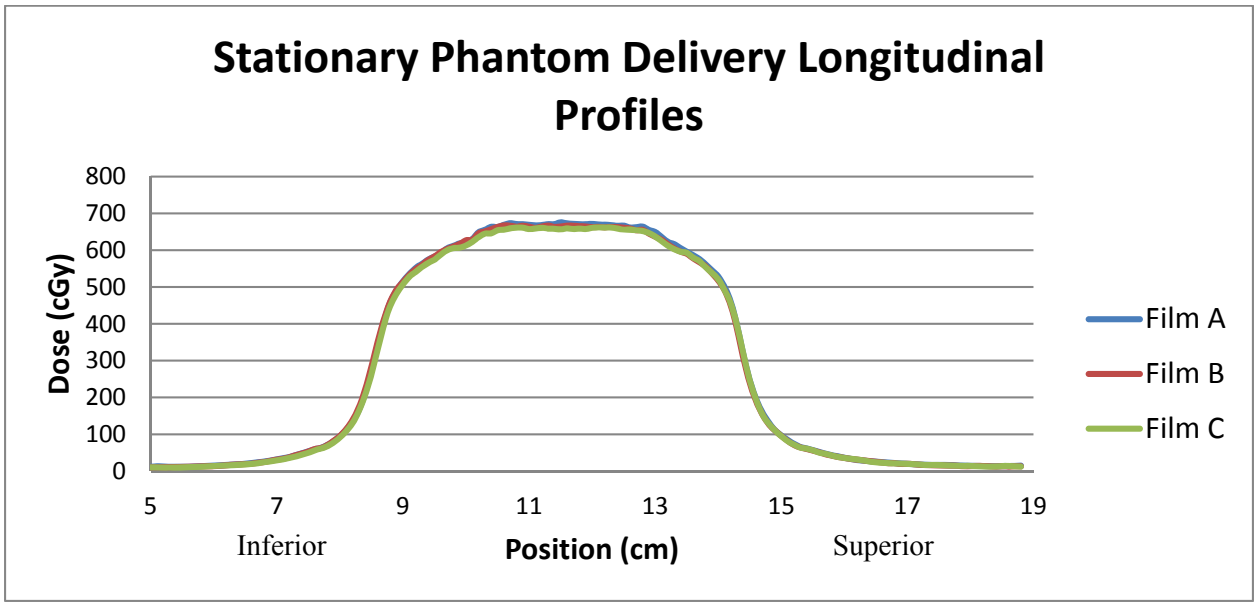

Figure 22: Longitudinal profiles of three repeated stationary film measurements inside the phantom.

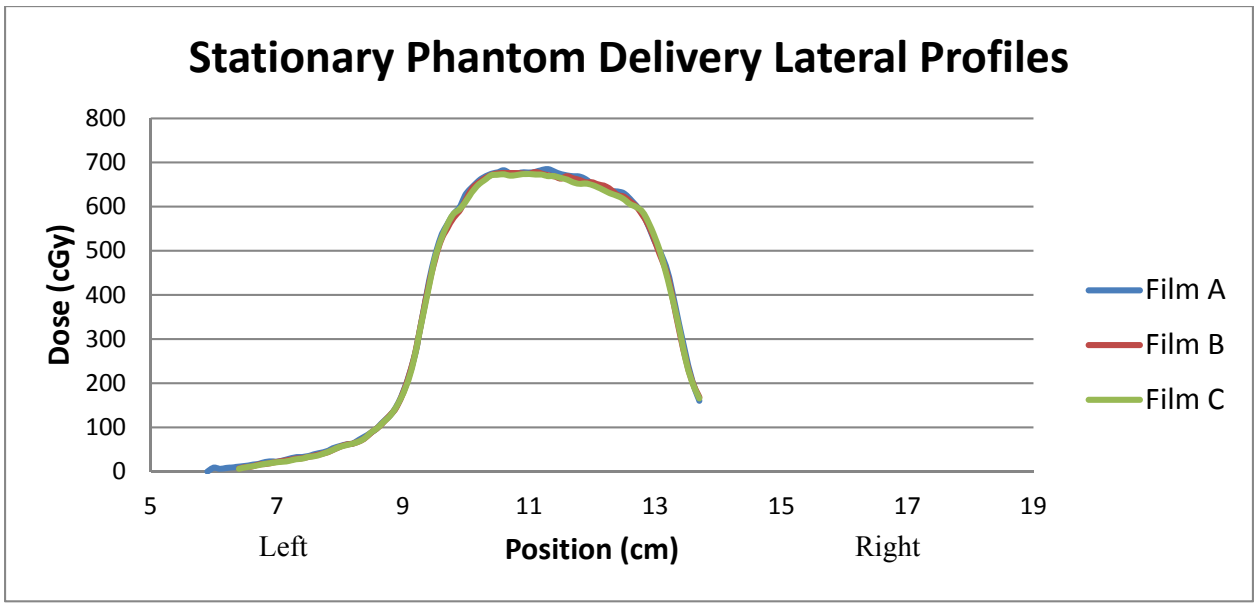

Figure 23: Lateral profiles of three repeated stationary film measurements inside the phantom.

The longitudinal and lateral profiles from the three repeated stationary phantom delivery are displayed in Figure 22-23. As measured from the data, the displacements of the midpoint at the 50% dose level between films are 1.21 mm in the longitudinal direction and 0.17 mm in the lateral direction for the film deliveries.

Analysis Metrics

Analysis was performed on all static and dynamic film deliveries using the RIT V6.3 software package. Once the film and planned dose distributions were registered, five 1-D profile measurements along the longitudinal (superior-inferior) and lateral (right-left) axis were acquired for each film. One profile through isocenter and four profiles adjacent to isocenter were acquired summed and averaged.

Target coverage was evaluated using the profile measurements. The analysis metrics evaluated the position of the measured dose distributions compared to the calculated distributions. The width of the 100% prescription dose, the width of the 95% prescription dose, and relative dose and percent dose error at the edges of the GTV, ITV and PTV between planned and delivered dose were evaluated. Insufficient target coverage will be considered a relative dose below 95% of the prescription in the GTV and a relative dose below 90% of the prescription in the PTV. Additionally, the mean, minimum and maximum dose difference for all points inside the GTV, ITV, and PTV were calculated between the planned and delivered distributions. Figure 24 shows longitudinal profiles through both the calculated and measured dose distribution. The red line is the measured film profile, compared to the blue line which is the calculated TPS profile.

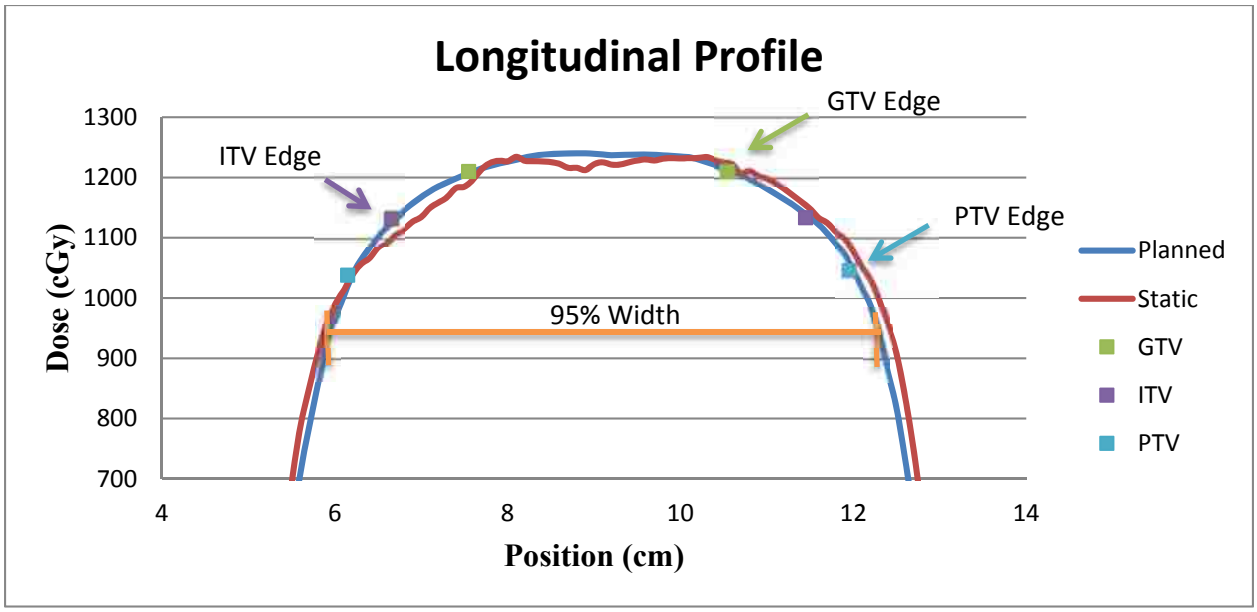

Figure 24: Profile plots illustrating the edges and width of the dose distributions at the 95% (950 cGy) prescription dose level.

Additionally, the RIT software has the ability to perform gamma analysis. Gamma analysis (Low *et al*., 1998) was used to compare the agreement between planned and delivered distributions with the TPS calculation. Gamma analysis considers the dose difference and spatial displacement between each point. RIT's gamma analysis method (Ju *et al*., 2008) was performed at gamma criteria of 3% dose difference and 3 mm distance to agreement and 5%/3 mm. Gamma analysis was performed on the area representing the GTV (sphere), the ITV (MIP) and the PTV in the dose distribution. Since the exact positon of isocenter is known on the pinnacle planar dose export, it was used to crop a region of interest that fully encompasses these areas. Additionally, the gamma analysis results were compared with the corresponding MCS values.

Chapter 3
Results and Discussion

3.1 Plan Complexity

In Aim 1, VMAT SBRT treatment plans of varying modulation complexity score values were generated. The planning process began by producing very simple treatment plans with only planning volumes and dose fall-off objectives. The calculated complexity score for these plans resulted in a complexity score of 0.70 and 0.75 for the 1 cm and 2 cm target amplitude, respectively. Critical structures were subsequently contoured in the phantom geometry to increase complexity and decrease the MCS in increments of 0.05. Successive treatment plans were created and the complexity score was steadily decreased until a complexity score of 0.40 was reached, for a total of 45 treatment plans. The complexity score value of 0.40 was chosen as an end point since such values are comparable to those observed in head and neck IMRT treatment plans (McNiven *et al.*, 2010).

3.2 Plan Monitor Units

The total number of monitor units was recorded on the basis that the number of monitor units has generally been associated with the degree of complexity in a treatment plan (Masi *et al.*, 2013; McNiven *et al.*, 2010). Table 6 shows the number of MU in each plan generally increases with increasing plan modulation (i.e., decreasing MCS) for all three patients. Figure 25 depicts the relationship between the number of MU and the MCS for each plan evaluated. The graph shows that there is a strong linear correlation (R=0.92) between MCS and number of MU in this study.

Table 6: Total Number of monitor units (MU)

	Patient Trace 1		Patient Trace 2		Patient Trace 3	
MCS	**1 cm**	**2 cm**	**1cm**	**2 cm**	**1 cm**	**2 cm**
.75	--	1715 MU	--	1719 MU	--	1716 MU
.70	1765 MU	1792 MU	1705 MU	1803 MU	1775 MU	1776 MU
.65	1799 MU	1960 MU	1945 MU	1901 MU	1903 MU	1856 MU
.60	2046 MU	2149 MU	2050 MU	2107 MU	2074 MU	2047 MU
.55	2538 MU	2352 MU	2285 MU	2320 MU	2287 MU	2384 MU
.50	2770 MU	2785 MU	2492 MU	2805 MU	2749 MU	2597 MU
.45	3073 MU	3286 MU	2701 MU	2937 MU	2866 MU	2986 MU
.40	3129 MU	3711 MU	3149 MU	3057 MU	3154 MU	3092 MU

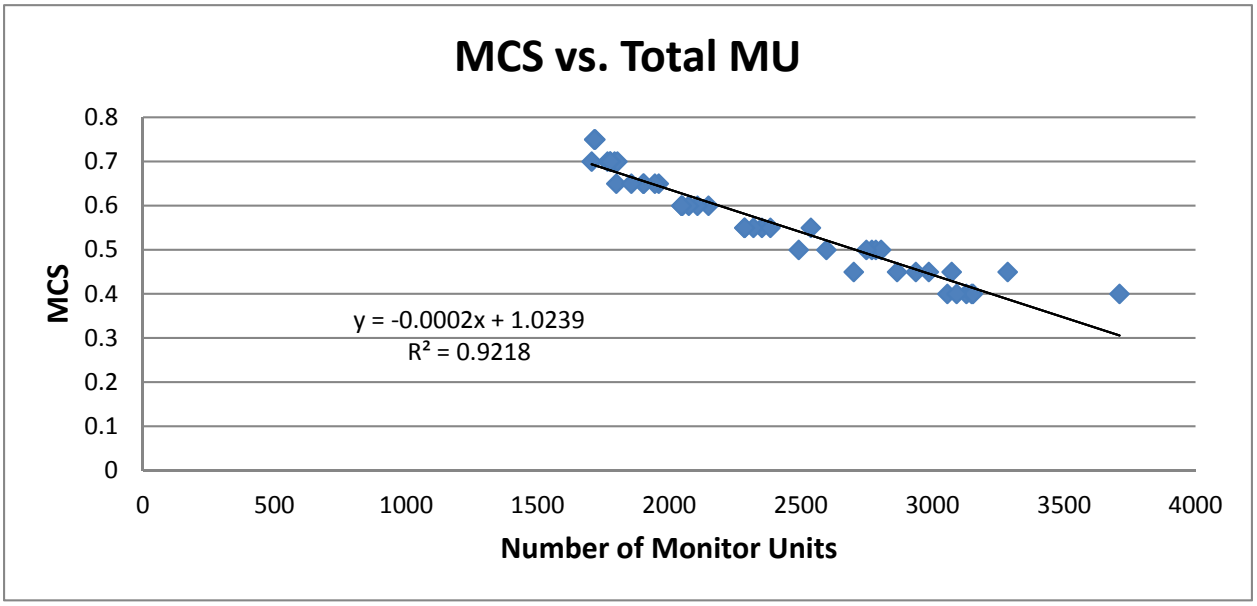

Figure 25: Plot of MCS and the total number of monitor units for each plan in this study.

3.3 Film Analysis

Calculated dose distributions from the TPS were compared with measured static and dynamic film dose distributions via profile assessment and gamma analysis.

3.3.1 Profile Assessment

Longitudinal and lateral profiles of each film measurement were taken. Figures 26-29 display profile measurements between static, dynamic and calculated dose distributions for several cases. The plots also display the isocenter and the extent of the GTV, ITV and PTV at the 95% prescription level (950 cGy).

Figure 26 shows longitudinal profile measurements for a simplified case (MCS=0.70) at an amplitude of 2 cm. The static delivery agrees with the planned dose distribution. The effects of respiratory motion on the dynamic dose distribution are visble in the edges of the profile. In the dynamic profile there is penumbra broadening and loss of coverage in the shoulder regions near the PTV. Due to the nature of the respiratory traces, as most patient spend more time in the exhale phase, the coverage in the inferior shoulder is less influenced by the respiratory motion and has more penumbra broadening.

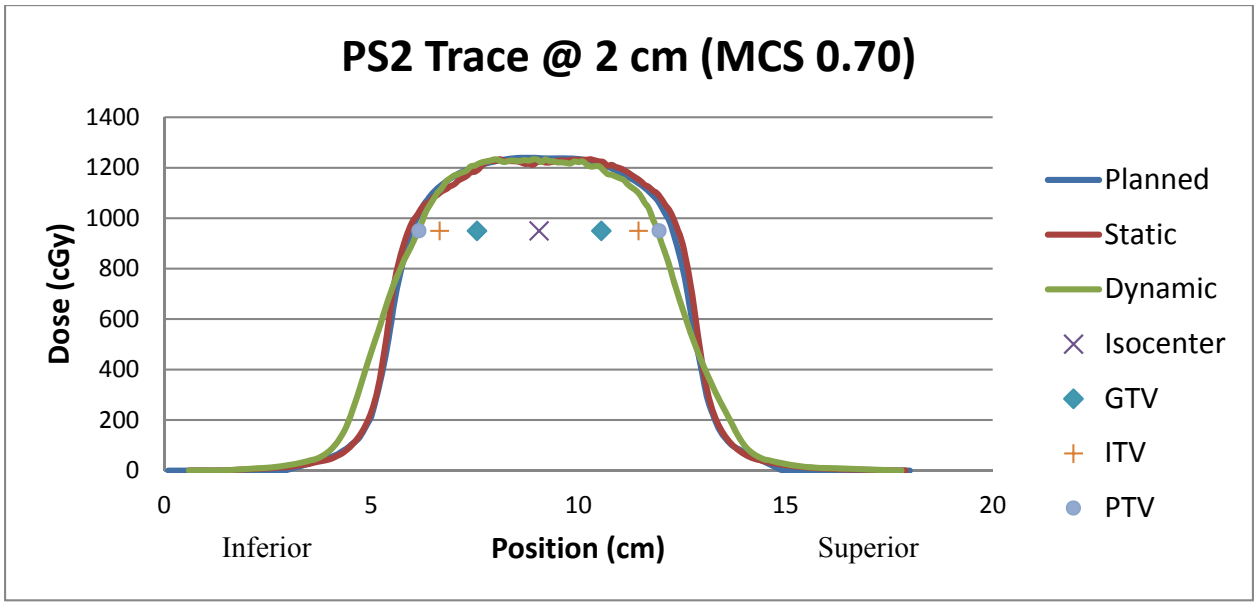

Figure 26: Longitudinal profiles for patient trace #2 at 2 cm amplitude with a plan MCS of 0.70.

Figure 27 shows longitudinal profile measurements for a simplified case (MCS = 0.70) at an amplitude of 1 cm. In this plot the static and dynamic profiles agree with the planned dose distribution. The dynamic profile at 1 cm shows less penumbra broadening and less coverage loss in the shoulder of the PTV compared to the dynamic case at an amplitude of 2 cm.

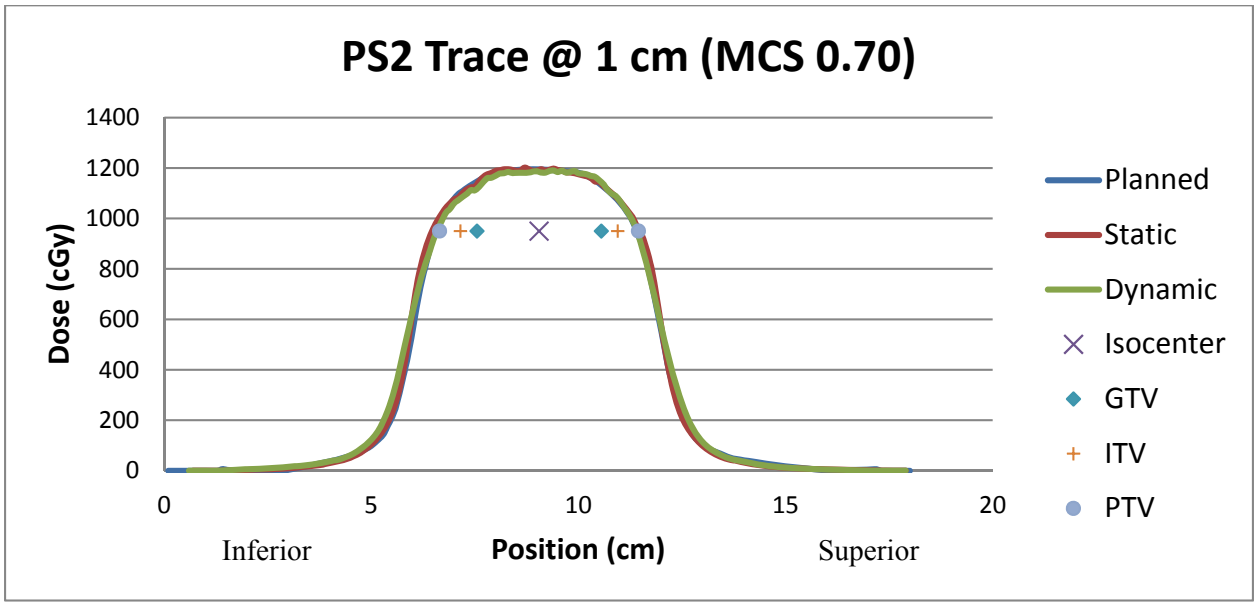

Figure 27: Longitudinal profiles for patient trace #2 at 1 cm amplitude with a plan MCS of 0.70.

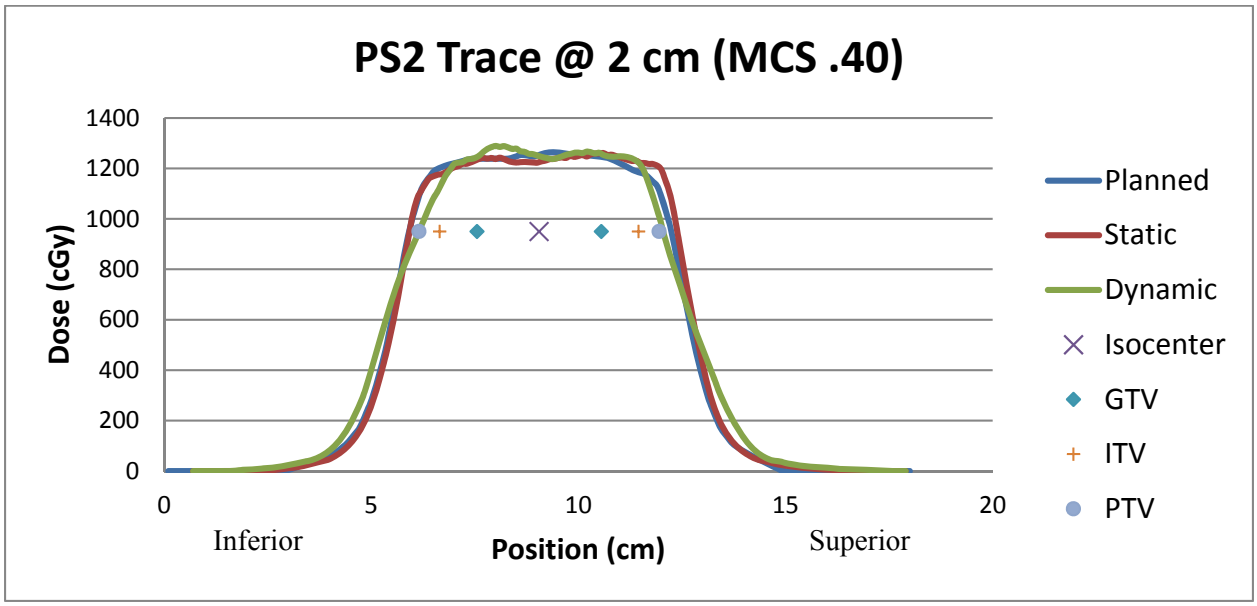

Figure 28: Longitudinal profiles for patient trace #2 at 2 cm amplitude with a plan MCS of 0.40.

Longitudinal profile measurements for a complex case (MCS=0.40) at an amplitude of 2 cm are shown in Figure 28. Again, there is penumbra broadening and loss of coverage in the shoulder region. Additionally, the profiles show greater dose fluctuations in the target region for the more complex case compared to the simplified (MCS=0.70) case.

Figure 29 shows profile measurements for a complex case (MCS=.40) at an amplitude of 1 cm. Again, there are dose fluctuations in the target region compared to the simplified case (MCS=0.70) and there is a less penumbra broadening compared to the 2 cm amplitude case.

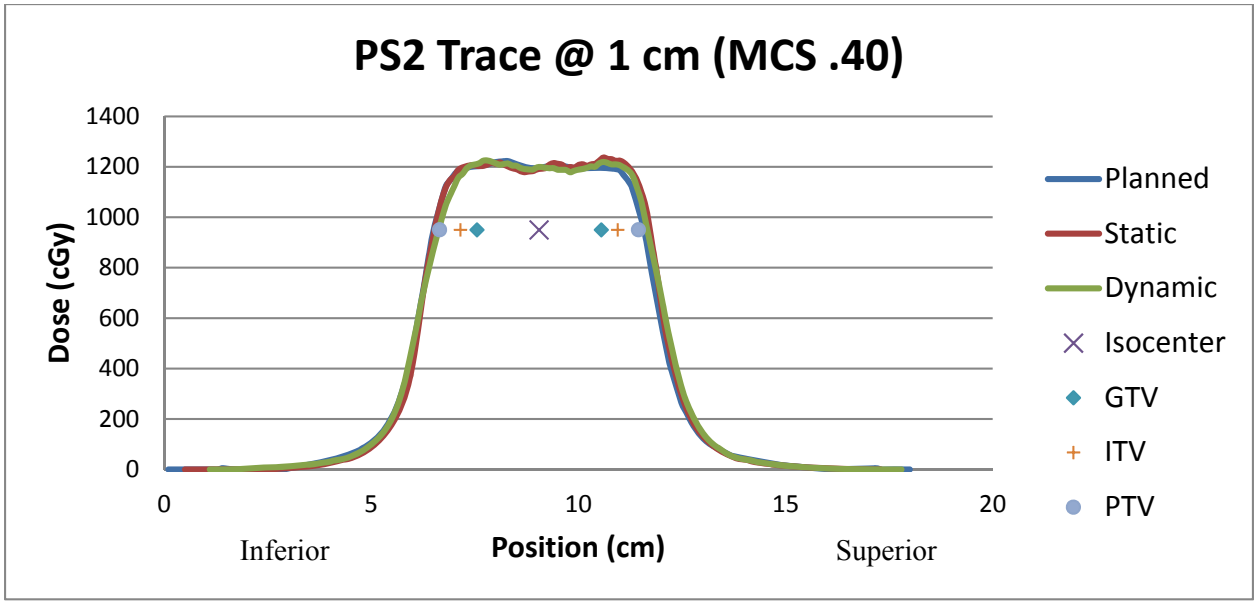

Figure 29: Longitudinal profiles for patient trace #2 at 1 cm amplitude with a plan MCS of 0.40.

Lateral profiles were also taken for each film delivery. Due to the design of the insert and the dose distribution in the phantom's geometry only partial lateral profiles could be obtained. Figures 30-33 display lateral profiles for simple and complex cases at amplitudes of 1 and 2 cm. Note a lateral profile is the perpendicular to the direction of phantom motion and it is seen from each measurement that there is relatively no change due to respiratory motion between profiles for any given amplitude and complexity. Any error is likely due to the treatment delivery, film response, film registration, or TPS model quality.

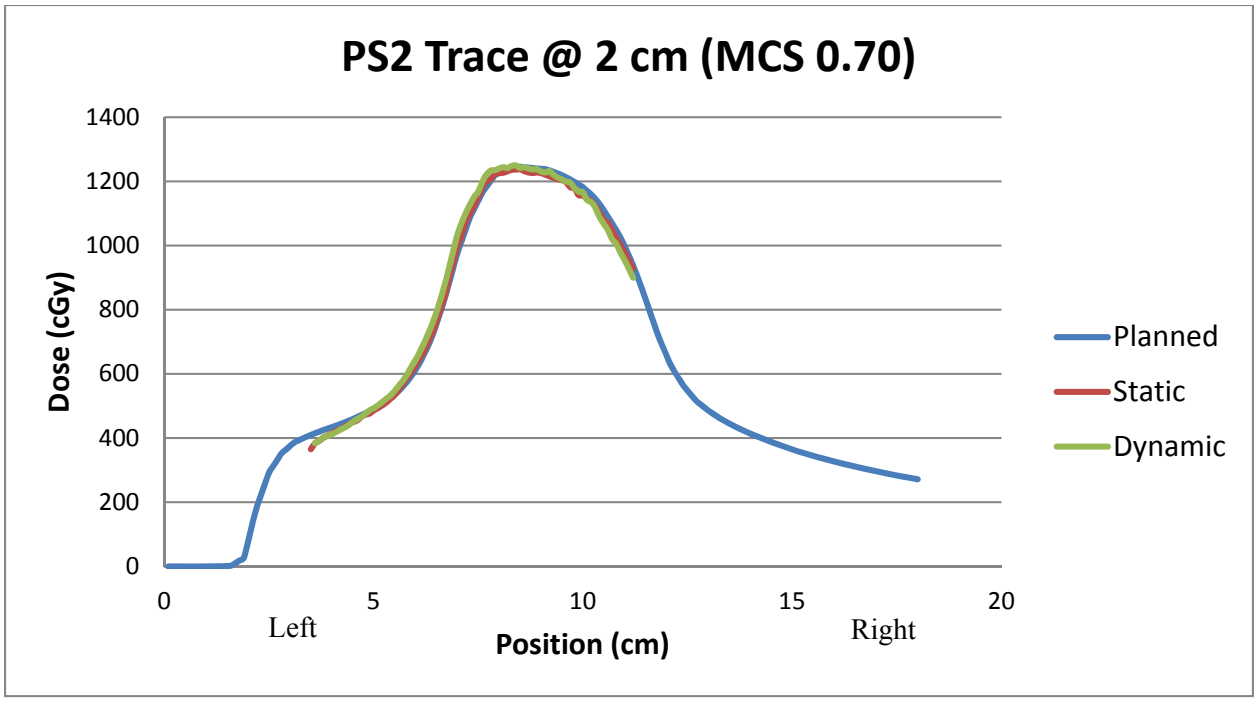

Figure 30: Lateral profiles for patient trace #2 at 2 cm amplitude with a plan MCS of 0.70.

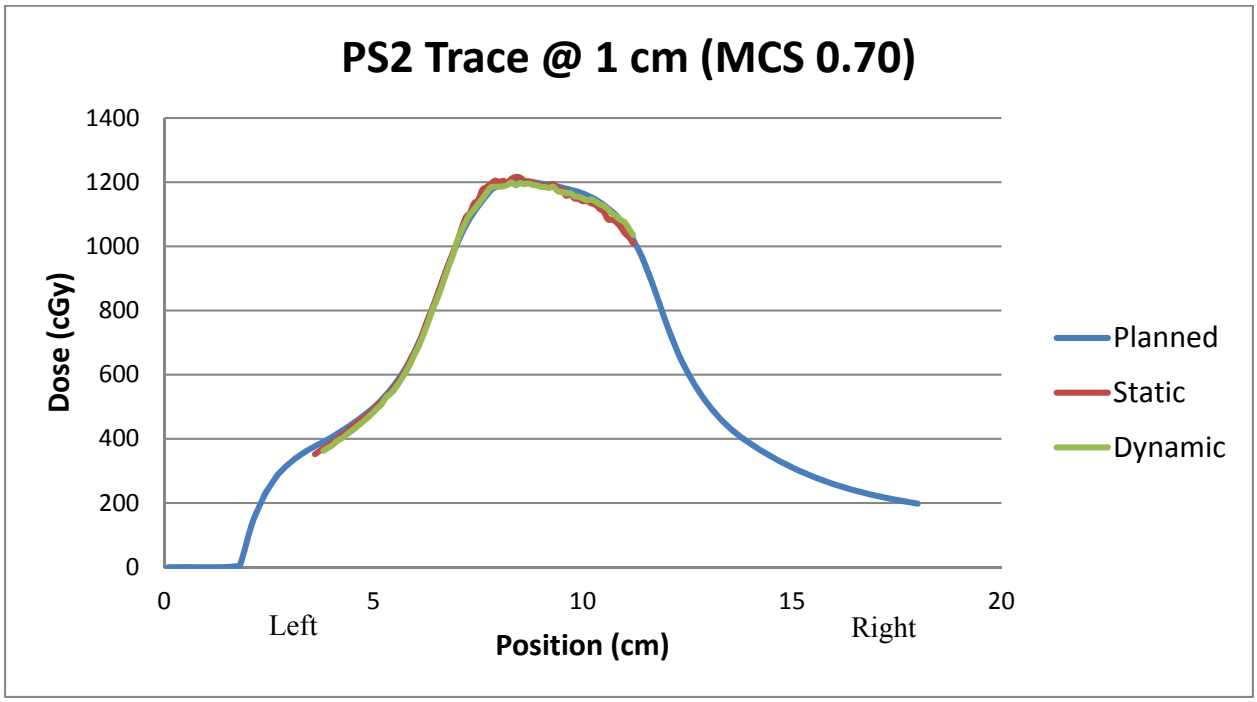

Figure 31: Lateral profiles for patient trace #2 at 1 cm amplitude with a plan MCS of 0.70.

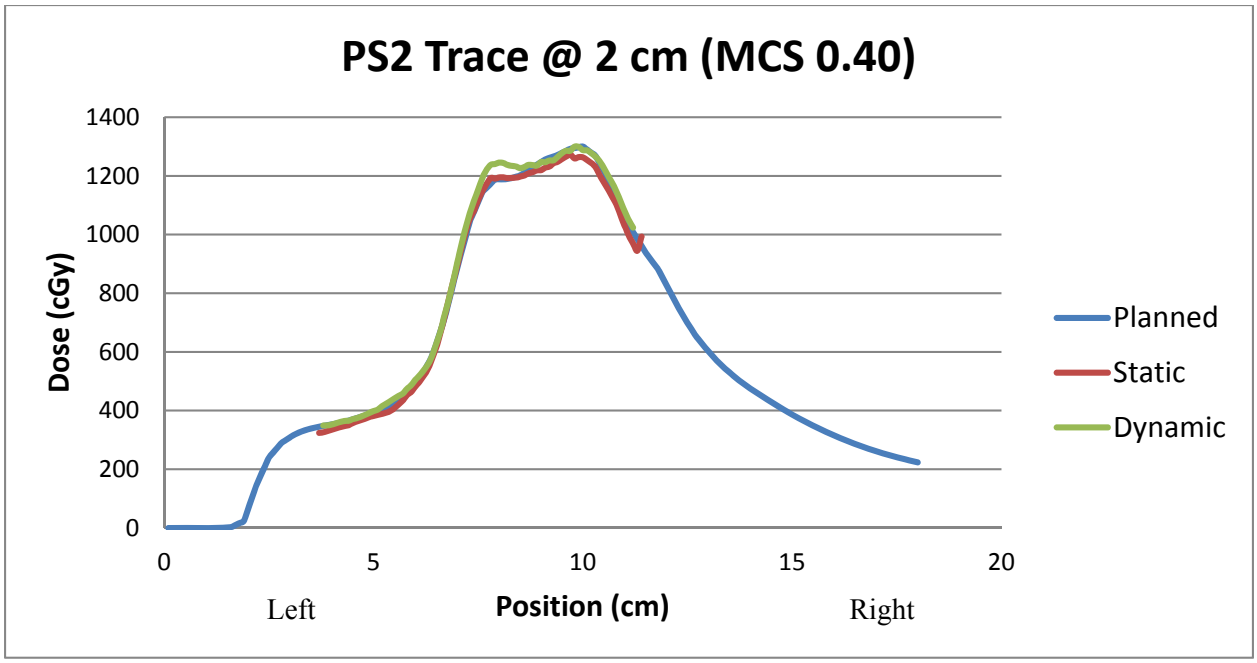

Figure 32: Lateral profiles for patient trace #2 at 2 cm amplitude with a plan MCS of 0.40.

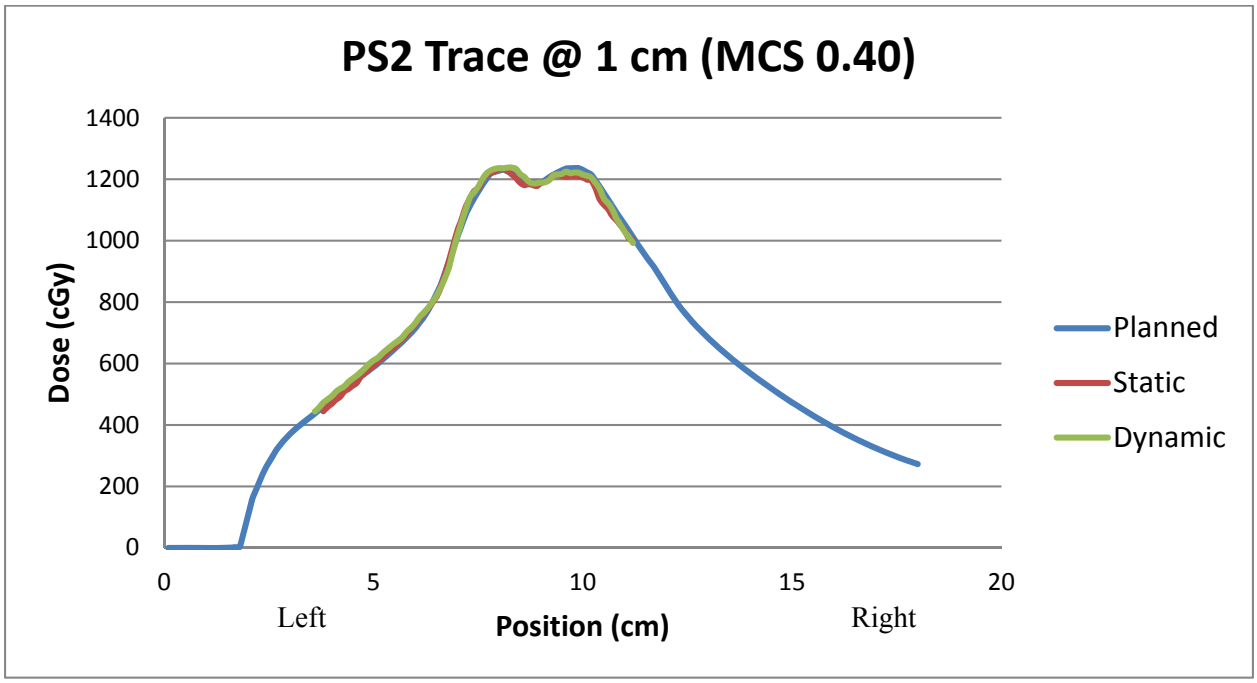

Figure 33: Lateral profiles for patient trace #2 at 1 cm amplitude with a plan MCS of 0.40.

Profile Width

Since the longitudinal profile corresponds to the direction of phantom motion and experiences changes in the dose distribution due to phantom motion, only the longitudinal profiles will be evaluated.

The width of the 100% (1000 cGy) and 95% (950 cGy) prescription dose along the longitudinal axis for patient trace 1 are shown in Figures 34-37. In each measurement it can be seen that the width of static dose distribution is wider the planned dose distribution. For the 2 cm deliveries, Figures 34 and 35, it can be seen that the dynamic dose distributions have the shortest width and that the 95% width fails to meet the required 6 cm to cover the entire PTV as prescribed. However, all the 1 cm dynamic deliveries, Figures 36 and 37, meet the required 5 cm width to cover the entire PTV. A correlation coefficient of -0.31, 0.03, and -0.06 was calculated between the MCS and the dynamic deliveries at 2 cm, 1 cm and all deliveries combined, respectively. This indicates that there is no correlation between the MCS and the width of the distribution.

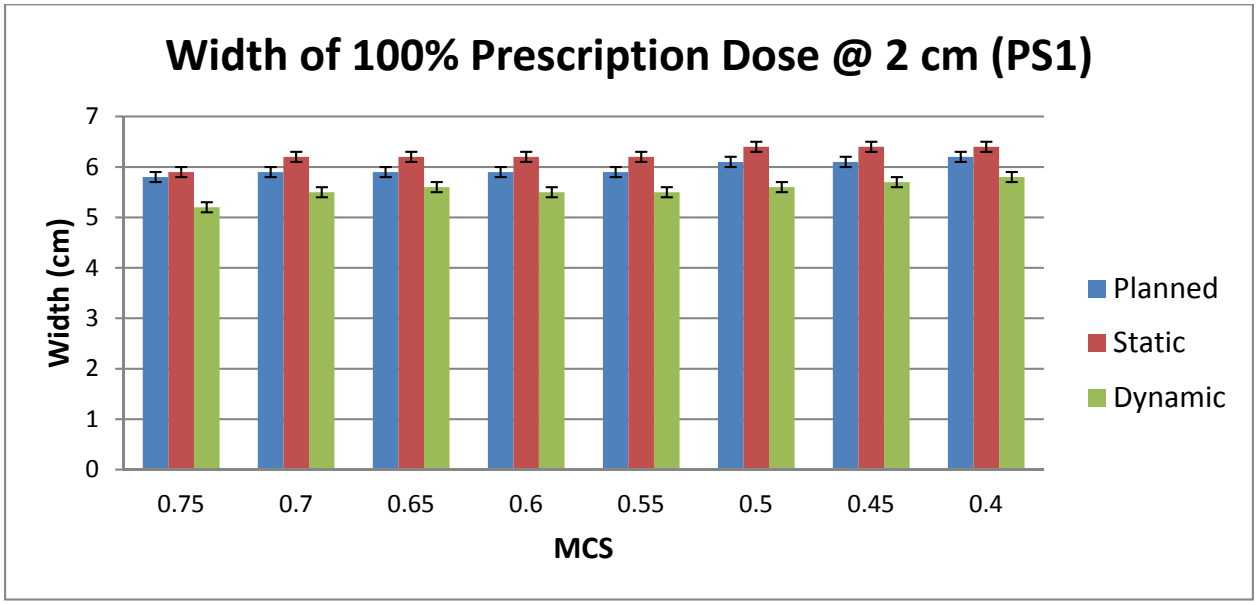

Figure 34: Width of the 100% prescription dose (1000 cGy) of planned, static and dynamic dose distribution for patient trace 1 at an amplitude of 2 cm.

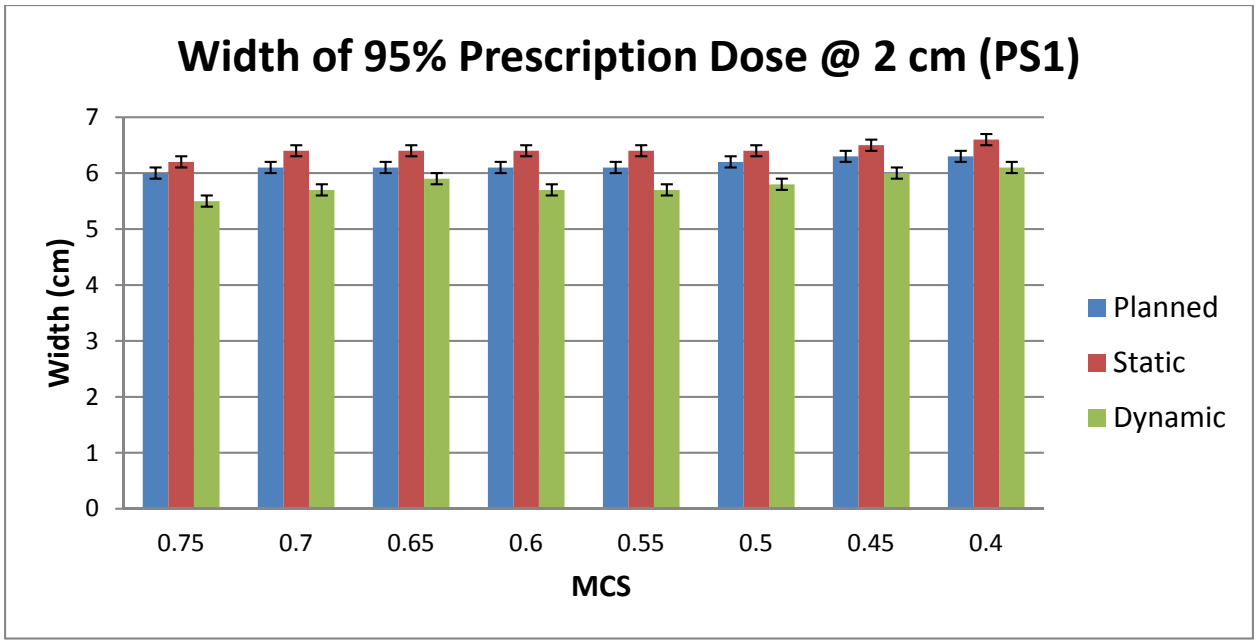

Figure 35: Width of the 95% prescription dose (950 cGy) of planned, static and dynamic dose distribution for patient trace 1 at an amplitude of 2 cm.

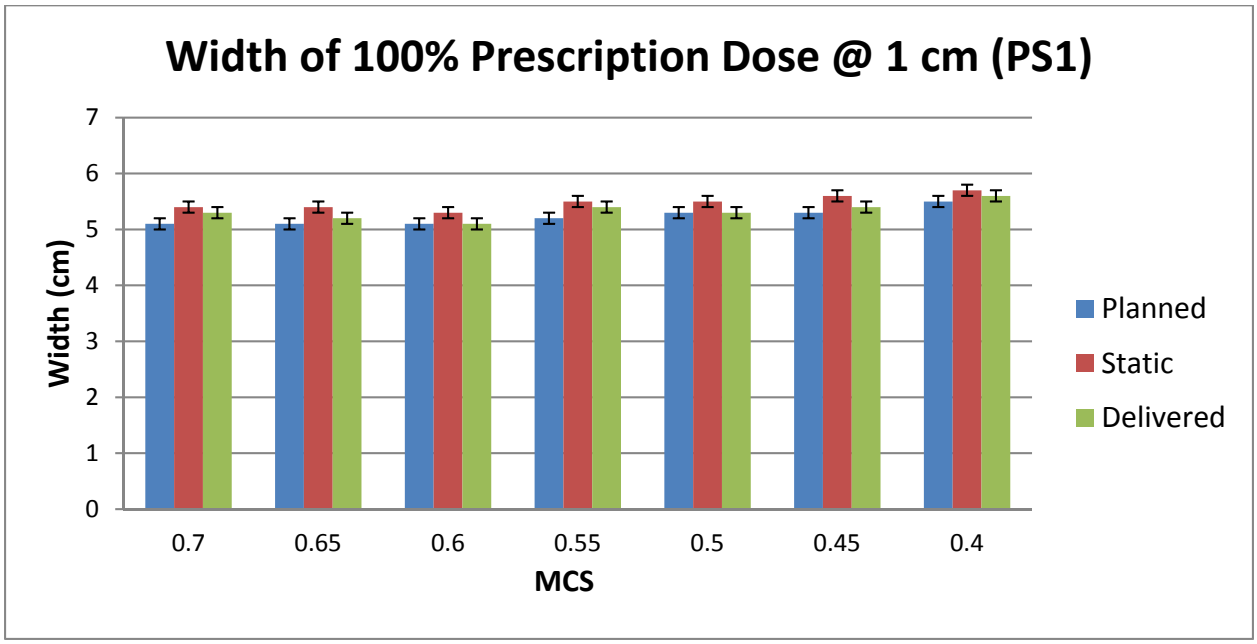

Figure 36: Width of the 100% prescription dose (1000 cGy) of planned, static and dynamic dose distribution for patient trace 1 at an amplitude of 1 cm.

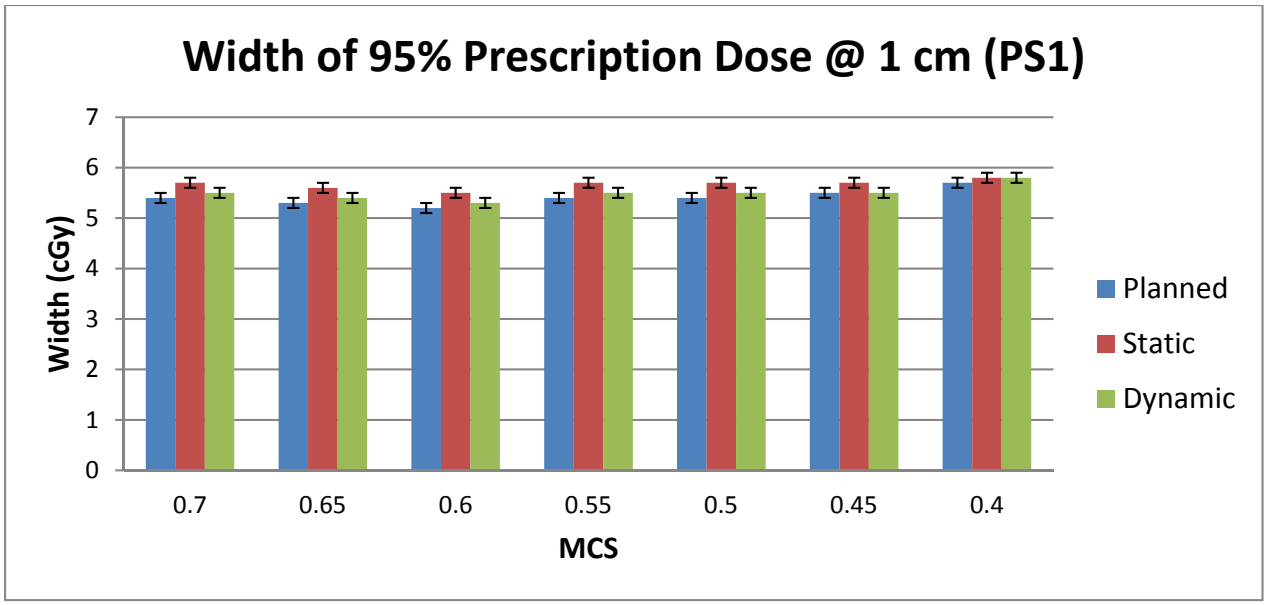

Figure 37: Width of the 95% prescription dose (950 cGy) of planned, static and dynamic dose distribution for patient trace 1 at an amplitude of 1 cm.

Percent Error

The percent dose error between the planned and delivered dose distributions at the longitudinal edges of each delivery can be seen in Tables 7-12. For the dynamic deliveries at 2 cm, Tables 7, 9 and 11, it can be seen that the percent error at the superior edge (range: -4.06 thru -22.43) is generally lower than that for the inferior edge (range: +6.96 thru -14.02). Again, this is influenced by the breathing trace as a patient spends more time in the end-of-exhale phase corresponding to the inferior edge. This trend is not evident in the dynamic deliveries at 1 cm, Tables 8, 10 and 12. The percent dose error at the GTV edge was never less than 2.58% for all static and dynamic cases. As you extend out to the ITV and PTV edges the percent dose error decreases. This indicates that with sufficient margin the target coverage can be maintained. Additionally, the dynamic 2 cm irregular trace, Table 11, has positive values in the inferior direction of motion for all cases, whereas the dynamic 2 cm regular traces, Table 7 and 9, has negative values in the inferior direction. This is due to the nature of the irregular respiratory trace; as the irregular trace spends an abnormally large amount of time in the inferior direction.

Table 7: Percent dose error at GTV, ITV, and PTV edges for patient trace 1 @ 2 cm

	GTV				ITV				PTV			
	Static		Dynamic		Static		Dynamic		Static		Dynamic	
MCS	**S**	**I**	**S**	**I**	**S**	**I**	**S**	**I**	**S**	**I**	**S**	**I**
0.75	-0.09	-2.21	-2.22	-1.64	0.61	1.07	-2.27	-1.65	2.60	9.81	-10.96	1.26
0.70	0.20	-2.14	-1.05	0.72	1.13	-0.94	-2.23	-1.34	2.71	4.52	-12.63	-2.98
0.65	0.13	-0.75	1.64	-0.55	1.11	-0.44	-1.73	-1.02	4.47	5.74	-16.62	0.88
0.60	0.61	-2.03	1.50	-0.84	2.63	-0.50	-3.99	-3.94	5.29	5.17	-18.02	-0.77
0.55	1.37	-1.13	-2.29	-2.39	3.54	-0.68	-2.52	-5.94	6.22	6.15	-14.44	-4.21
0.50	0.52	-2.63	2.25	-2.58	1.66	-0.88	-7.18	-7.55	6.04	4.52	-22.43	-5.53
0.45	2.36	-2.51	4.54	-0.04	4.75	-1.67	-2.25	-6.04	7.17	4.18	-16.31	-4.76
0.40	2.40	0.36	2.25	-0.64	1.76	-0.31	-10.00	-5.89	4.76	1.52	-21.77	-5.83

Table 8: Percent dose error at GTV, ITV, and PTV edges for patient trace 1 @ 1 cm

	GTV				ITV				PTV			
	Static		Dynamic		Static		Dynamic		Static		Dynamic	
MCS	**S**	**I**	**S**	**I**	**S**	**I**	**S**	**I**	**S**	**I**	**S**	**I**
0.70	0.35	4.22	0.71	3.72	0.62	0.02	0.52	0.37	3.59	-0.10	1.59	0.15
0.65	0.53	1.06	-0.60	1.08	0.68	1.08	0.50	1.91	2.73	6.82	1.30	4.17
0.60	0.90	-0.69	2.15	1.83	2.23	-0.36	1.74	2.07	5.31	4.23	0.36	5.16
0.55	3.24	-0.13	0.02	0.68	4.40	-0.94	0.02	-0.47	7.97	0.23	-0.59	2.03
0.50	3.88	0.79	2.93	-0.33	3.41	1.39	2.85	-0.37	6.50	2.53	0.87	-0.40
0.45	3.23	-1.21	2.04	-2.58	4.46	-1.63	4.21	-2.99	6.76	1.73	0.74	-2.58
0.40	4.04	1.53	2.57	1.75	4.06	0.91	2.24	2.98	7.57	1.62	-1.20	0.20

Table 9: Percent dose error at GTV, ITV, and PTV edges for patient trace 2 @ 2 cm

	GTV				ITV				PTV			
	Static		Dynamic		Static		Dynamic		Static		Dynamic	
MCS	**S**	**I**	**S**	**I**	**S**	**I**	**S**	**I**	**S**	**I**	**S**	**I**
0.75	2.87	1.54	-0.69	-0.34	2.81	1.06	-2.12	-1.81	3.11	1.15	-10.61	-5.97
0.70	1.05	-1.07	-1.58	0.66	1.33	-2.27	-3.83	-1.20	2.93	0.03	-13.64	-5.75
0.65	1.74	1.22	-1.48	-0.83	2.12	1.67	-2.44	-5.05	3.58	2.29	-8.65	-10.09
0.60	1.84	1.01	0.19	-1.09	1.20	1.32	-2.46	-1.93	3.11	1.85	-13.97	-5.75
0.55	0.04	-1.09	0.56	-0.31	2.51	-0.52	-1.28	-3.58	4.83	3.10	-12.81	-8.59
0.50	1.00	1.47	0.76	-0.26	3.12	2.75	-5.30	-4.13	7.61	2.98	-19.36	-8.88
0.45	0.79	-0.21	1.15	-0.33	1.26	-0.76	-0.01	-7.92	7.41	1.27	-19.56	-14.02
0.40	1.34	-0.04	0.72	0.93	3.34	-2.32	2.61	-5.28	9.98	-0.37	-9.87	-12.78

Table 10: Percent dose error at GTV, ITV, and PTV edges for patient trace 2 @ 1 cm

	GTV				ITV				PTV			
	Static		Dynamic		Static		Dynamic		Static		Dynamic	
MCS	**S**	**I**	**S**	**I**	**S**	**I**	**S**	**I**	**S**	**I**	**S**	**I**
0.70	0.34	-0.37	1.01	-2.24	0.48	-0.68	0.61	-2.05	3.80	1.39	-0.61	-1.42
0.65	2.58	-0.24	0.57	-1.44	5.31	0.54	0.96	-1.52	10.21	0.94	1.69	-2.35
0.60	3.15	0.98	2.07	-0.31	4.36	0.24	2.99	-1.44	13.29	-1.84	4.28	-3.10
0.55	3.41	0.36	1.92	-0.37	6.94	0.09	-0.82	1.01	14.59	5.00	-1.80	6.04
0.50	2.32	0.54	1.16	-0.39	5.67	0.53	2.09	-1.83	12.42	2.22	4.68	-5.78
0.45	4.07	1.31	2.82	-0.96	6.40	1.85	4.10	-2.03	14.01	1.31	6.63	-0.96
0.40	3.47	-0.02	2.02	0.91	3.29	0.54	1.73	-1.62	10.48	-0.01	7.10	-7.14

Table 11: Percent dose error at GTV, ITV, and PTV edges for irregular trace @ 2 cm

	GTV				ITV				PTV			
	Static		Dynamic		Static		Dynamic		Static		Dynamic	
MCS	**S**	**I**	**S**	**I**	**S**	**I**	**S**	**I**	**S**	**I**	**S**	**I**
0.75	0.02	1.94	1.07	3.39	2.00	2.41	-0.43	3.15	4.02	3.19	-6.36	5.61
0.70	0.62	2.41	-1.04	2.11	3.78	3.58	-3.13	3.23	7.15	5.40	-15.58	4.93
0.65	-0.34	2.94	-0.05	2.87	3.90	4.30	-0.03	2.52	6.42	6.76	-4.06	3.37
0.60	-0.17	0.86	-0.16	1.80	4.83	1.42	0.51	1.65	8.31	3.79	-6.48	3.27
0.55	-0.83	1.31	0.28	-0.69	3.72	2.53	-3.70	-1.21	1.12	7.28	-16.96	0.05
0.50	-2.56	0.81	-1.23	-0.08	4.32	0.73	-1.62	1.19	8.46	3.41	-12.98	6.96
0.45	-1.88	1.16	4.44	1.19	4.09	1.76	1.55	3.09	6.39	7.33	-6.79	5.06
0.40	-1.54	-1.04	-0.03	1.01	3.84	-0.37	-4.65	-0.28	9.87	5.29	-13.88	4.37

Table 12: Percent dose error at GTV, ITV, and PTV edges for irregular trace @ 1 cm

	GTV				ITV				PTV			
	Static		Dynamic		Static		Dynamic		Static		Dynamic	
MCS	**S**	**I**	**S**	**I**	**S**	**I**	**S**	**I**	**S**	**I**	**S**	**I**
0.70	-1.04	-0.42	-2.51	1.14	0.52	1.79	-1.24	4.11	1.46	5.40	-0.68	5.47
0.65	0.39	-0.85	-0.54	1.40	3.31	1.91	-0.73	3.71	3.85	4.64	-0.48	6.84
0.60	0.63	0.40	1.01	-0.23	2.12	3.38	1.35	1.90	2.29	6.28	1.07	4.61
0.55	-1.15	-0.84	1.15	-0.49	0.63	1.92	1.33	1.43	1.12	4.86	3.14	4.87
0.50	0.32	-0.48	2.32	-1.01	1.75	0.97	3.71	0.67	2.13	4.35	0.63	4.98
0.45	5.04	0.06	4.35	2.43	8.32	-1.32	4.91	2.78	16.81	4.28	4.90	8.23
0.40	1.85	-2.54	1.39	0.05	3.06	-0.98	1.79	0.57	9.65	2.37	-3.41	2.89

Relative Dose

The relative dose at the longitudinal edge of each dose distribution can be seen in Tables 13-18. Although the dose variations between planned and delivered dose distribution may seem substantial, the relative dose at the GTV edges (range: 1137-1366 cGy) and ITV edges (range: 1054-1263cGy) for the dynamic deliveries were above the prescription at all amplitudes and complexity level studied. This means that the GTV and ITV coverage was satisfactorily maintained. The relative dose at the PTV edge (range: 934-1131 cGy) for the dynamic deliveries at 1 cm, were above 90% of the prescription dose for all plans; where planning constraints suggest the PTV should not receive doses below 90%. However, the relative dose at the PTV edge (range: 826-1163 cGy) for the dynamic 2 cm deliveries were below 90% of prescription dose for several cases.

The 2 cm dynamic deliveries show that the relative dose at the superior edge is generally lower than the inferior edge. Again, this is influenced by the breathing trace as a patient spends more time in the end-of-exhale phase corresponding to the inferior edge. For the 1 cm dynamic deliveries, the superior edge of the PTV for the irregular trace of the two most complex plans (MCS = 0.45 and 0.40) drop below 95% of the prescription dose, Table 18. This is likely as the planned width of the 95% dose distribution for these profiles are exactly the required 5 cm to cover the PTV (Appendix D, Figure 148). The 2 cm amplitude dynamic irregular trace, Table 17, has the largest relative dose values in the inferior direction and the lowest relative dose values in the superior direction compared to all the dynamic traces at an amplitude of 2 cm, Table 13, 15 and 17. Again, this is due to the nature of the irregular respiratory trace; as the irregular trace spends an abnormally large amount of time in the inferior direction and consequently a small amount of time in the superior direction.

Table 13: Relative dose at GTV, ITV, and PTV edges for patient trace 1 @ 2 cm (cGy)

	GTV				ITV				PTV			
	Static		Dynamic		Static		Dynamic		Static		Dynamic	
MCS	**S**	**I**	**S**	**I**	**S**	**I**	**S**	**I**	**S**	**I**	**S**	**I**
0.75	1183	1160	1157	1160	1113	1087	1082	1057	1055	969	916	894
0.70	1207	1176	1192	1210	1148	1121	1110	1116	1078	1046	917	971
0.65	1200	1195	1218	1198	1159	1147	1126	1141	1101	1066	878	1017
0.60	1222	1202	1233	1217	1191	1171	1114	1131	1116	1074	869	1013
0.55	1229	1222	1185	1207	1208	1172	1137	1110	1146	1088	923	982
0.50	1249	1241	1270	1242	1273	1229	1162	1146	1225	1127	896	1019
0.45	1235	1184	1285	1214	1296	1188	1209	1135	1247	1112	974	1017
0.40	1247	1225	1245	1213	1279	1225	1131	1156	1219	1144	910	1061

Table 14: Relative dose at GTV, ITV, and PTV edges for patient trace 1 @ 1 cm (cGy)

	GTV				ITV				PTV			
	Static		Dynamic		Static		Dynamic		Static		Dynamic	
MCS	**S**	**I**	**S**	**I**	**S**	**I**	**S**	**I**	**S**	**I**	**S**	**I**
0.70	1173	1174	1177	1177	1126	1111	1125	1114	1066	1038	1045	1033
0.65	1213	1225	1200	1225	1154	1138	1152	1147	1074	1052	1059	1026
0.60	1199	1216	1214	1247	1165	1135	1159	1163	1095	1029	1044	1038
0.55	1297	1252	1257	1262	1254	1178	1201	1184	1174	1040	1081	1059
0.50	1275	1242	1263	1229	1228	1211	1222	1190	1160	1090	1099	1059
0.45	1269	1204	1255	1188	1266	1190	1263	1174	1198	1114	1130	1067
0.40	1338	1321	1319	1325	1294	1256	1271	1282	1232	1152	1131	1136

Table 15: Relative dose at GTV, ITV, and PTV edges for patient trace 2 @ 2 cm (cGy)

	GTV				ITV				PTV			
	Static		Dynamic		Static		Dynamic		Static		Dynamic	
MCS	**S**	**I**	**S**	**I**	**S**	**I**	**S**	**I**	**S**	**I**	**S**	**I**
0.75	1204	1185	1162	1163	1130	1098	1076	1067	1052	993	912	923
0.70	1223	1197	1192	1218	1148	1107	1090	1119	1078	1038	904	978
0.65	1234	1229	1195	1204	1163	1171	1111	1094	1082	1067	954	938
0.60	1237	1238	1217	1213	1176	1184	1133	1146	1091	1083	910	1002
0.55	1213	1214	1219	1223	1208	1180	1163	1144	1138	1117	947	991
0.50	1223	1211	1220	1190	1210	1207	1111	1127	1146	1097	859	971
0.45	1219	1187	1223	1186	1164	1163	1150	1079	1160	1105	869	938
0.40	1261	1238	1254	1250	1222	1178	1214	1142	1196	1111	980	972

Table 16: Relative dose at GTV, ITV, and PTV edges for patient trace 2 @ 1 cm (cGy)

	GTV				ITV				PTV			
	Static		Dynamic		Static		Dynamic		Static		Dynamic	
MCS	**S**	**I**	**S**	**I**	**S**	**I**	**S**	**I**	**S**	**I**	**S**	**I**
0.70	1130	1147	1137	1126	1069	1101	1071	1086	955	1019	1006	991
0.65	1236	1234	1212	1219	1185	1181	1136	1156	1008	1019	1030	985
0.60	1244	1238	1231	1222	1187	1175	1171	1156	1006	977	1026	964
0.55	1253	1237	1235	1228	1172	1152	1087	1163	993	975	951	985
0.50	1247	1227	1233	1216	1227	1181	1186	1154	1078	1048	1004	966
0.45	1264	1249	1249	1221	1249	1212	1222	1166	1104	1149	1032	1121
0.40	1237	1203	1220	1214	1225	1198	1206	1172	1108	1072	1074	995

Table 17: Relative dose at GTV, ITV, and PTV edges for irregular trace @ 2 cm (cGy)

	GTV				ITV				PTV			
	Static		Dynamic		Static		Dynamic		Static		Dynamic	
MCS	**S**	**I**	**S**	**I**	**S**	**I**	**S**	**I**	**S**	**I**	**S**	**I**
0.75	1173	1177	1186	1194	1084	1098	1058	1105	998	1009	899	1033
0.70	1206	1209	1187	1205	1129	1146	1054	1142	1048	1070	826	1065
0.65	1209	1226	1212	1225	1139	1176	1096	1156	1032	1106	931	1071
0.60	1218	1210	1218	1222	1165	1168	1117	1171	1060	1098	915	1092
0.55	1222	1223	1236	1199	1164	1198	1081	1154	1062	1151	1083	1072
0.50	1240	1250	1257	1239	1204	1196	1136	1202	1098	1111	881	1149
0.45	1235	1283	1340	1283	1202	1243	1173	1259	1061	1175	930	1150
0.40	1346	1297	1366	1324	1253	1259	1151	1260	1134	1174	889	1163

Table 18: Relative dose at GTV, ITV, and PTV edges for irregular trace @ 1 cm (cGy)

	GTV				ITV				PTV			
	Static		Dynamic		Static		Dynamic		Static		Dynamic	
MCS	**S**	**I**	**S**	**I**	**S**	**I**	**S**	**I**	**S**	**I**	**S**	**I**
0.70	1159	1170	1142	1189	1116	1129	1096	1155	1049	1075	1027	1076
0.65	1183	1187	1172	1214	1154	1150	1109	1171	1076	1080	1031	1103
0.60	1187	1198	1191	1191	1144	1171	1136	1154	1051	1101	1039	1084
0.55	1178	1193	1205	1197	1146	1168	1154	1162	1036	1108	1083	1108
0.50	1224	1161	1248	1155	1200	1147	1223	1144	1102	1109	1086	1116
0.45	1275	1234	1267	1263	1242	1163	1203	1211	1055	995	947	1033
0.40	1228	1183	1223	1214	1200	1187	1185	1205	1024	1056	934	1062

Mean, Minimum and Maximum

The mean, minimum and maximum dose errors between the dynamic and planned distributions were recorded for the GTV, ITV, and PTV regions for all longitudinal profiles measurements. The results for each patient trace at specified amplitude of this analysis can be seen in Tables 19-24.

The results show that the mean dose difference for the GTV never dropped below 2% at any amplitude or complexity level. Also, the minimum dose in the GTV only fell below 5% for one case under irregular respirations, Table 23. The minimum dose in the PTV decreases considerably for the dynamic deliveries at 2 cm, Table 20, 22, and 24. This is influenced by the loss of coverage in the shoulder of the profiles. This was concluded as the magnitude of the minimum doses in the PTV does not appear in the GTV or ITV which are subsets of the PTV. Additionally, the loss of coverage in PTV shoulder appears to influence the PTV mean dose. Table 20 and 22 shows the mean dose is negative for all 2 cm dynamic deliveries for patient traces 1 and 2.

Table 19: Percent dose error in dynamic delivery of patient trace 1 @ 1 cm

	GTV			**ITV**			**PTV**		
MCS	**Mean**	**Min**	**Max**	**Mean**	**Min**	**Max**	**Mean**	**Min**	**Max**
0.70	-0.33	-2.24	1.22	-0.44	-2.59	1.22	-0.51	-2.59	1.22
0.65	-0.81	-1.90	0.77	-0.70	-1.90	1.51	-0.57	-2.35	2.48
0.60	-0.27	-1.15	2.07	-0.09	-1.44	2.99	0.04	-3.51	4.72
0.55	-0.10	-1.18	2.50	0.03	-1.18	2.50	0.26	-1.80	6.04
0.50	-1.13	-3.37	1.16	-0.87	-3.37	2.09	-0.81	-6.15	4.68
0.45	-0.28	-1.99	2.82	0.00	-2.03	4.01	0.26	-4.99	7.25
0.40	-0.24	-1.79	2.02	-0.04	-1.79	2.02	-0.05	-7.14	7.10

Table 20: Percent dose error in dynamic delivery of patient trace 1 @ 2 cm

	GTV			ITV			PTV		
MCS	**Mean**	**Min**	**Max**	**Mean**	**Min**	**Max**	**Mean**	**Min**	**Max**
0.75	-1.09	-2.22	0.13	-1.59	-3.08	0.13	-1.57	-10.96	1.26
0.70	-0.23	-1.60	1.94	-0.69	-2.29	1.94	-0.85	-12.63	1.94
0.65	-0.84	-2.10	1.83	-0.79	-2.10	1.83	-0.80	-16.62	1.83
0.60	0.17	-1.40	2.46	-0.70	-3.99	2.46	-0.94	-18.02	2.46
0.55	-0.62	-2.39	1.09	-1.73	-6.17	1.09	-2.11	-14.44	1.09
0.50	0.49	-2.58	3.89	-0.91	-7.55	3.89	-1.57	-22.43	3.89
0.45	0.97	-2.17	6.54	0.69	-6.04	6.59	-0.02	-16.31	6.59
0.40	0.37	-2.52	2.97	-1.05	-10.00	2.97	-1.61	-21.77	2.97

Table 21: Percent dose error in dynamic delivery of patient trace 2 @ 1 cm

	GTV			ITV			PTV		
MCS	**Mean**	**Min**	**Max**	**Mean**	**Min**	**Max**	**Mean**	**Min**	**Max**
0.70	0.05	-1.22	1.12	0.05	-1.22	1.12	0.36	-1.22	3.72
0.65	-0.31	-0.93	1.39	-0.10	-0.93	1.91	0.21	-0.93	4.17
0.60	0.57	-1.18	2.87	0.77	-1.18	2.87	1.17	-1.18	5.16
0.55	-0.43	-1.68	0.68	-0.37	-1.68	0.68	-0.32	-1.68	2.03
0.50	0.27	-0.89	2.93	0.18	-0.89	3.49	0.55	-1.48	3.49
0.45	1.15	-2.79	5.87	0.48	-3.30	5.87	0.61	-4.02	5.87
0.40	0.97	-1.45	4.59	1.15	-1.45	4.59	1.28	-1.45	4.59

Table 22: Percent dose error in dynamic delivery of patient trace 2 @ 2 cm

	GTV			ITV			PTV		
MCS	**Mean**	**Min**	**Max**	**Mean**	**Min**	**Max**	**Mean**	**Min**	**Max**
0.75	-0.56	-1.49	0.51	-0.82	-2.12	0.51	-1.61	-10.61	0.51
0.70	-0.70	-1.65	0.67	-0.92	-3.83	0.67	-1.81	-13.64	0.67
0.65	-0.78	-1.48	0.03	-1.37	-5.05	0.03	-2.26	-10.09	0.03
0.60	-0.63	-1.70	1.04	-0.89	-2.46	1.04	-1.84	-13.97	1.04
0.55	-0.10	-1.40	1.28	-0.52	-3.58	1.28	-1.61	-12.81	1.28
0.50	-0.21	-2.85	1.47	-0.77	-5.30	1.47	-2.48	-19.36	1.47
0.45	-0.87	-2.61	1.15	-0.75	-7.92	3.35	-2.65	-19.56	3.35
0.40	1.00	-2.09	4.08	0.84	-5.28	4.08	-0.60	-12.78	4.08

Table 23: Percent dose error in dynamic delivery of irregular trace @ 1 cm

	GTV			ITV			PTV		
MCS	**Mean**	**Min**	**Max**	**Mean**	**Min**	**Max**	**Mean**	**Min**	**Max**
0.70	-0.12	-2.51	1.62	-0.04	-3.27	4.11	0.35	-3.27	5.52
0.65	-0.04	-1.61	1.75	0.07	-1.92	3.71	0.55	-1.92	6.83
0.60	0.04	-1.38	1.52	0.19	-1.38	1.90	0.58	-1.38	4.61
0.55	-0.10	-0.93	1.51	0.06	-0.93	1.51	0.67	-0.93	4.87
0.50	0.44	-1.00	2.32	0.59	-1.40	3.77	0.96	-1.40	4.98
0.45	1.51	-1.28	4.35	2.03	-1.28	4.91	2.54	-1.28	8.23
0.40	-1.82	-5.05	1.39	-1.10	-5.05	1.78	-0.78	-5.05	2.88

Table 24: Percent dose error in dynamic delivery of irregular trace @ 2 cm

	GTV			ITV			PTV		
MCS	**Mean**	**Min**	**Max**	**Mean**	**Min**	**Max**	**Mean**	**Min**	**Max**
0.75	1.48	-0.04	3.99	1.52	-0.43	3.99	1.37	-6.36	5.61
0.70	0.10	-1.36	2.78	0.15	-3.13	3.23	-0.29	-15.58	4.93
0.65	0.44	-0.67	3.19	0.77	-0.84	3.19	0.71	-4.06	3.37
0.60	-0.47	-2.21	2.96	0.05	-2.21	2.95	-0.01	-6.48	3.27
0.55	-0.27	-1.39	0.83	-0.48	-3.69	0.83	-1.30	-16.95	0.83
0.50	-1.60	-4.80	1.52	-1.08	-4.80	1.52	-1.26	-12.98	6.95
0.45	1.66	-2.95	6.44	1.92	-2.96	6.44	1.71	-6.79	6.44
0.40	0.29	-1.91	2.64	-0.21	-4.65	2.64	-0.88	-13.87	4.37

Systematic Shift

The width of the 100% and 95% prescription dose and the percent dose error and relative dose seen at the edges of the static dose distributions are influenced by a systematic shift seen in the film data. Looking at the dose profiles for these film measurements, a 1–2 mm shift in the longitudinal direction was observed in almost every film analyzed, Figure 38. A similar shift was also observed in Mancuso's, (2011) study. The systematic shift was attributed to uncertainties in precisely identifying the isocenter within a 2.5 mm CT slice width. This uncertainty means that

there is no guarantee that the isocenter defined in the TPS is at the exact same location as the actual isocenter of the phantom.

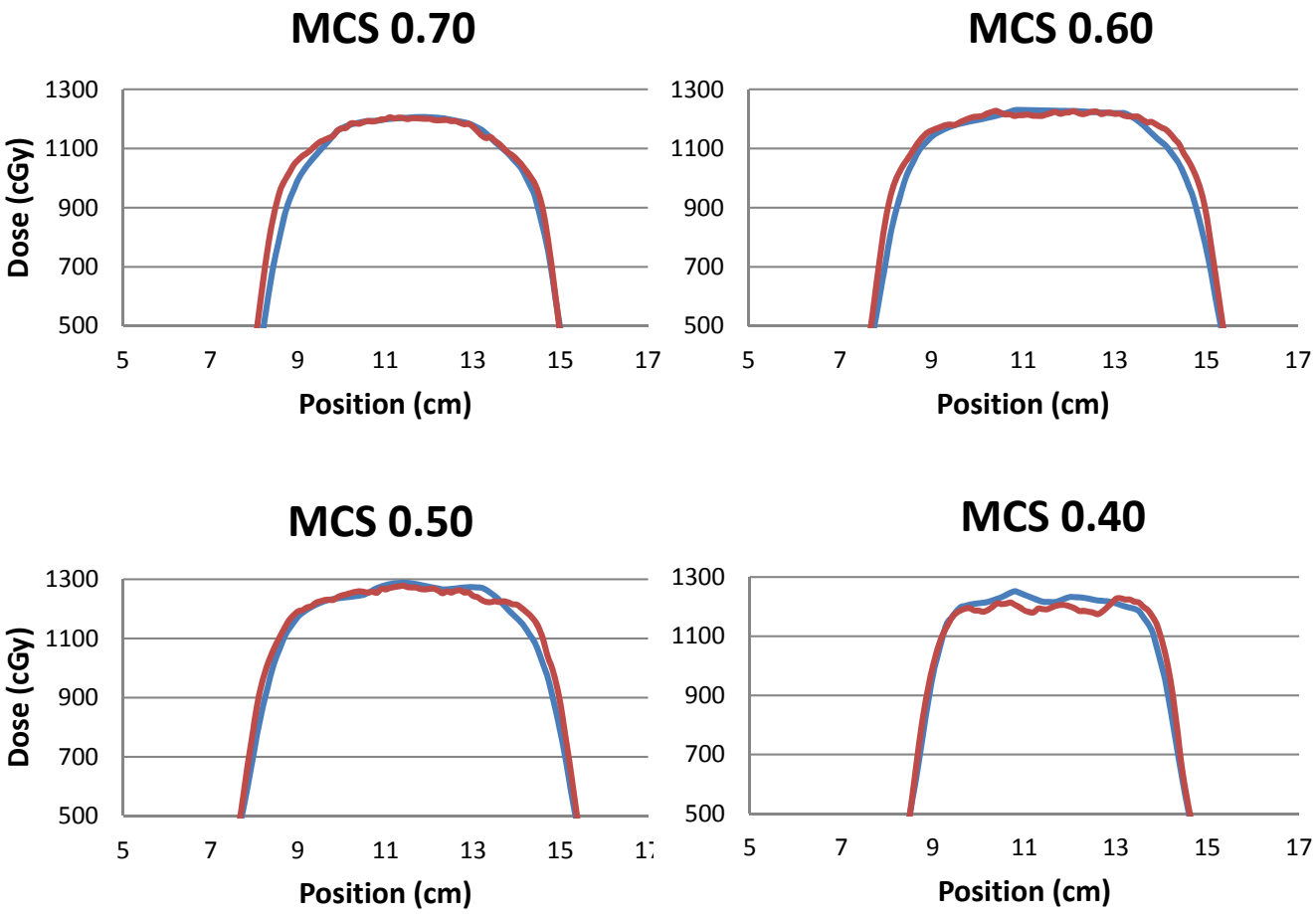

Figure 38: Longitudinal film profiles displaying a systematic shift between the film (red line) and the planed dose data (blue line).

3.3.2 Gamma Analysis

Gamma analysis was also used to assess the agreement between planned and delivered dose. Figure 39 shows RIT's gamma analysis results for select cases at 5%/5 mm gamma criteria. The software reports the percent of pixels passing the gamma test for the registered dose distributions. The red pixels in the images indicate pixels that failed to meet the gamma criteria for each comparison.

Tables 25-30 show gamma analysis passing rates for a region of interest encompassing the GTV for static and dynamic deliveries. The results show that as plan complexity increases (i.e. decreasing modulation complexity score) the gamma analysis passing rate decreases. Additionally, the results show that the dynamic deliveries generally have lower gamma passing rates compared to its corresponding static delivery and commonly the 2 cm dynamic deliveries have the lowest gamma passing rate.

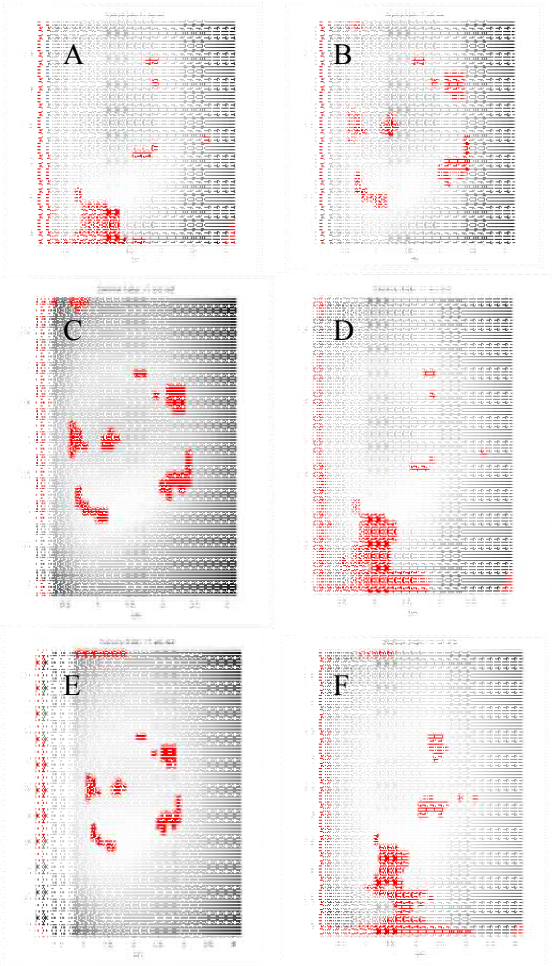

Figure 39: RIT gamma analysis results for patient trace 1 at 1 cm amplitude and MCS of 0.60. (A) Static GTV: 92.51% (B) Dynamic GTV: 96.25% (C) Static ITV: 92.53% (D) Dynamic ITV: 84.82% (E) Static PTV: 91.58% and (F) Dynamic PTV: 86.56%. Gamma criteria of 5%/3mm.

Table 25: Patient trace 1 GTV gamma analysis results (1 cm)

MCS	Static Gamma (3%/3mm)	Dynamic Gamma (3%/3mm)	Static Gamma (5%/3mm)	Dynamic Gamma (5%/3mm)
0.70	96.57 %	95.42 %	96.98 %	96.05 %
0.65	99.27 %	98.75 %	99.38 %	98.96 %
0.60	92.09 %	95.53 %	92.51 %	96.25 %
0.55	92.47 %	90.55 %	92.72 %	90.95 %
0.50	90.53 %	83.77 %	91.78 %	84.70 %
0.45	89.07 %	80.54 %	91.99 %	81.69 %
0.40	85.54 %	80.12 %	86.37 %	81.17 %

Table 26: Patient trace 1 GTV gamma analysis results (2 cm)

MCS	Static Gamma (3%/3mm)	Dynamic Gamma (3%/3mm)	Static Gamma (5%/3mm)	Dynamic Gamma (5%/3mm)
0.75	96.05 %	93.13 %	96.46 %	94.80 %
0.70	98.23 %	90.11 %	98.75 %	91.05 %
0.65	95.11 %	91.47 %	95.53 %	92.51 %
0.60	93.03 %	89.18 %	93.55 %	90.32 %
0.55	95.53 %	88.76 %	96.36 %	89.49 %
0.50	93.55 %	84.18 %	93.66 %	85.43 %
0.45	89.28 %	81.79 %	89.70 %	83.36 %
0.40	87.51 %	85.64 %	88.35 %	86.26 %

Table 27: Patient trace 2 GTV gamma analysis results (1 cm)

MCS	Static Gamma (3%/3mm)	Dynamic Gamma (3%/3mm)	Static Gamma (5%/3mm)	Dynamic Gamma (5%/3mm)
0.70	94.90 %	96.88 %	96.15 %	98.75 %
0.65	90.32 %	93.34 %	91.26 %	95.01 %
0.60	93.86 %	88.97 %	94.17 %	90.74 %
0.55	89.91 %	90.01 %	91.05 %	91.57 %
0.50	87.41 %	83.87 %	88.03 %	85.02 %
0.45	84.29 %	80.85 %	85.33 %	82.10 %
0.40	83.87 %	81.17 %	84.50 %	82.10 %

Table 28: Patient trace 2 GTV gamma analysis results (2 cm)

MCS	Static Gamma (3%/3mm)	Dynamic Gamma (3%/3mm)	Static Gamma (5%/3mm)	Dynamic Gamma (5%/3mm)
0.75	98.54 %	98.34 %	99.27 %	98.44 %
0.70	94.17 %	91.26 %	95.73 %	93.65 %
0.65	95.21 %	92.09 %	96.15 %	93.76 %
0.60	95.84 %	90.22 %	96.25 %	92.82 %
0.55	95.11 %	90.22 %	95.94 %	91.68 %
0.50	91.47 %	90.53 %	93.03 %	91.57 %
0.45	89.29 %	81.17 %	90.74 %	83.66 %
0.40	89.49 %	78.36 %	90.74 %	79.08 %

Table 29: Irregular trace GTV gamma analysis results (1 cm)

MCS	Static Gamma (3%/3mm)	Dynamic Gamma (3%/3mm)	Static Gamma (5%/3mm)	Dynamic Gamma (5%/3mm)
0.70	97.81 %	90.53 %	98.02 %	90.84 %
0.65	93.44 %	87.41 %	93.55 %	88.03 %
0.60	90.84 %	91.16 %	91.36 %	91.88 %
0.55	95.42 %	92.20 %	95.94 %	92.51 %
0.50	83.56 %	80.96 %	84.50 %	82.02 %
0.45	85.95 %	81.06 %	86.78 %	82.01 %
0.40	82.83 %	73.26 %	83.45 %	74.26 %

Table 30: Irregular trace GTV gamma analysis results (2 cm)

MCS	Static Gamma (3%/3mm)	Dynamic Gamma (3%/3mm)	Static Gamma (5%/3mm)	Dynamic Gamma (5%/3mm)
0.75	94.69 %	80.44 %	95.53 %	81.69 %
0.70	93.86 %	82.78 %	94.69 %	83.25 %
0.65	91.57 %	88.14 %	93.34 %	89.59 %
0.60	92.40 %	83.45 %	92.72 %	85.74 %
0.55	92.09 %	80.65 %	94.07 %	80.96 %
0.50	89.59 %	82.52 %	91.36 %	83.25 %
0.45	91.36 %	85.12 %	92.72 %	87.10 %
0.40	90.43 %	73.26 %	91.68 %	82.00 %

Chapter 4
Discussion and Conclusion

4.1 Summary of Findings

In this study, we performed a comprehensive investigation of VMAT SBRT delivery for lung treatment. To achieve this, a respiratory motion phantom was taken through the radiotherapy imaging, planning and delivery stages. Interplay effects on dose delivery were studied under varying degrees of plan modulation. Comparisons of planned and delivered distributions were used to gauge interplay effects on the delivered dose. Additionally, correlation between target coverage and the MCS was used to gauge its ability to indicate potentially unsafe plans. I hypothesized that the amount of plan modulation will correlate ($R > 0.60$) with changes in target coverage between planned and delivered dose distributions.

The results indicated that as plan complexity increases so does the number of MUs seen in the treatment plan (R=0.92). This finding is inconsistent with previous work from McNiven *et al.*, 2010. In their study the MCS and number of MU was investigated for correlation between different treatment sites; in which no correlation was found. Also, their study found limited linear correlation (R=0.41) between the number of MU's and MCS for a variety of lungs plans. However, this study is less generalized as each plan was based on the exact same phantom geometry.

The profile assessment results show that the effects of respiratory motion are most evident for larger amplitude deliveries and at the edges of the dose distribution (*i.e.* the shoulder and penumbra). This was anticipated since previous studies have noted that the larger the amplitude the more dosimetric deviations from the planned distribution (Court et al., 2010; Kang et al., 2010). The dose variation between planned and delivered distribution at the edges were the largest for the most complex plans at the larger amplitudes (2 cm); where this variation reached

up to 22%. However, the relative dose values indicated that the GTV, ITV and PTV at amplitude of 1 cm maintained satisfactory coverage for the dynamic deliveries at all complexity level studied. Furthermore, the results showed that the relative dose at the PTV edge for the dynamic 2 cm deliveries were below 90% of prescription dose for several cases; where planning constraints suggest the PTV should not receive doses below 90%.

This data was further supported by the mean, minimum and maximum dose deviations between planned and delivered profile points. Again, the smallest deviations were seen in the GTV. Where the mean dose never dropped below 2% and the minimum dose seen was 5.05% for the irregular patient trace at the highest degree of complexity. Again, as you extend out to the ITV and PTV the magnitude of the dose variations increase. However the mean, minimum and maximum data are influenced by treatment planning system modeling quality. As MLC modulation increases, the quality of the TPS model becomes important to get an accurate plan. The fluctuations seen are due to limitations in the TPS to model plans with increased modulation. This is evident as the dose fluctuations appear in the static and dynamic deliveries. Therefore, the minimum and maximum dose may be influenced by the dose fluctuations from TPS modeling quality.

The hypothesis of this work was not supported, as indicated by the correlation values. The MCS did not correlate with the width, relative dose at GTV, PTV and ITV edges, mean dose deviation, or max dose deviation for all plans. No correlation was considered a correlation coefficient of less than 0.3. However, a limited correlation of 0.54 and 0.50 was observed for the minimum dose deviations in the ITV and PTV regions, respectively, between plan and delivered dose distributions.

As expected, the MCS values correlated with the gamma analysis results for static and dynamic deliveries. The results show that as the MCS decreases, the gamma analysis results generally decreases. The correlation values were 0.85, 0.87, 0.81, and 0.57 for the mean passing rates at 5%/5mm for the static 1 cm, dynamic 1 cm, static 2 cm and dynamic 2 cm cases of the GTV, respectively. Additionally, a correlation value of 0.65 was obtained for the mean passing rate with all GTV cases considered. This find is consistent with previous work from Masi et al., 2013. In their study the MCS displayed a positive correlation ($R > 0.6$) with gamma analysis results (2%/2mm) for static VMAT deliveries at 2 Gy. Also, their study showed that as the MCS values decreased (more modulation) the gamma analysis results dropped below 90% for EBT^2 film measurements. Again, these results are influenced by MLC positioning error and the limited accuracy of MLC modeling in the TPS.

In conclusion, due to the nature SBRT, where the maximum dose is recommended to be between 110% -140% of the prescription dose, dose in the target region and at the edges of the target region never dropped below the prescription dose. Additionally, the larger the respiratory amplitude the more dosimetric deviations between planned and delivered distributions are expected. Lastly, the MCS correlated well with the GTV gamma passing rates for the separate cases and similar correlation, between previous works, was noticed when all target cases were considered.

4.2 Limitations

One limitation to this work was the Quasar respiratory motion phantom simulates 1D motion in the longitudinal direction. Although respiratory motion is usually larger in the longitudinal direction, studies have shown that lung tumors move in all three directions (Zhang

et al., 2013). Thus, it would be interesting and useful to see the effect of 3D tumor motion on the dose delivery.

As the film dosimetry process is complex, the accuracy and reproducibility of the measurement procedure could be improved. The quality of the results is directly related to this process. This includes cutting of the film pieces to fit the insert, positioning of the film in the insert, the phantom ability to accurately reproduce the respiratory traces, etc. Additionally, another type of detector besides EBT^3 film can potentially be beneficial. The study by Masi *et al.*, (2011) showed that EBT film gave the worst gamma analysis results compared to other dosimetric systems, see Figure 40.

	ERGO++				Oncentra Vmat			
	Average (%)		Max (%)	Min (%)	Average (%)		Max (%)	Min (%)
	All plans	Comparative study			All plans	Comparative study		
EDR2	95.1	96.1	100.0	83.0				
EBT2	91.1	92.9	98.5	80.0	91.7	92.1	98.9	85.2
MAPCHECK	97.4	98.0	100.0	92.0	96.3	97.8	99.7	86.2
DELTA4	99.3	99.4	100.0	93.0	95.4	96.2	100.0	89.3
SEVEN29	99.6	99.8	100.0	99.1	98.0	97.5	100.0	88.0

Figure 40: Comparison of calculated and measured dose distributions for different dosimetric systems. Percentage of points passing gamma criteria of 3%/3mm. (Masi *et al*., 2011)

RIT image registration procedure estimates the error in the registration process. This error can result from the inaccuracy in cutting of film's registration holes, the determination of hole centers and the subpixel registration. Furthermore, it has been noted that an increase in the resolution of the planar dose file increases the accuracy of RIT's gamma analysis results (Mancuso, 2011).

Another limitation is that no statistical tests were performed on the film data because the given sample size lacked sufficient statistical power. Also, this project did not account for

deformation of the tumor. Previous studies have shown that in structures such as lungs, tumor and organ deformation can occur (Rosu *et al*., 2005).

4.3 Future Work

In the future one could expand the number of patient specific respiratory traces to be planned, delivered and analyzed, in order to provide a larger sample size for statistical analysis of the data.

The clinical practice of SBRT is expected to increase in use for other cancers; therefore one could also expand the range of treatment sites studied. The results can be very different due to the different planning constraints, levels of modulation, target sizes, and motion characteristics. For example, the liver is another site that has been widely treated with SBRT and has considerable amount of changes in inter-fraction position due to respiratory motion (Fontenot *et al.*, 2013).

References

Almond, P, P Biggs, B Coursey, W F Hanson, M Huq, R Nath, D W O Rogers, 'AAPM's TG-51 protocol for clinical reference dosimetry of high-energy photon and electron beams', Med Phys 26 (1999), 1847-1870.

American Lung Association. 'Breathe Easy', Retrieved Febrauary 23, 2015, from http://www.lung.org/lung-disease/lung-cancer/resources/facts-figures/lung-cancer-fact-sheet.html.

Ashland. 'Gafchromic Dosimetry Media, Type EBT-3', Retrieved April 26, 2016, from Ashland:http://www.ashland.com/Ashland/Content/Documents/ASI/OtherMedical/EBT3_Specifications.pdf.

Bezjak, A, L Papiez, J Bradley, et al. 'Seamless Phase I/II Study of Stereotactic Lung Radiotherapy (SBRT) for Early Stage, Centrally Located NSCLC', *NRG Oncology* (2014).

Bzdusek, K, H Friberger, B Hardemark, D Robinson, & M Kaus, 'Development and evaluation of an efficient approach to volumetric arc therapy planning', *Med Phys* **36** (2009), 2328-2339.

Centers for Diease Control and Prevention. Retrieved February 23, 2015, from http://www.cdc.gov/cancer/lung/basic_info/symptoms.htm (2013, November 20).

Chui, C, E Yorke, L Hong, 'The effects of intra-fraction organ motion on the delivery of intensity-modulated field with a multileaf collimator', *Med Phys* **30** (2003), 1736-1746.

Court, L, M Wagar, D Ionascu, R Berbeco, L Chin, 'Management of the interplay effect using dynamic MLC sequences to treat moving targets', *Med Phys* **35** (2008), 1926-1931.

Court, L, M Wager, R Berbeco, A Reisner, et al. 'Evaluation of the interplay effect when using RapidArc to treat targets moving in the craniocaudal or right-left direction', *Med Phys* **37** (2010), 4-11.

Fontenot, J, E Klein, 'Technical Challenges in Liver Stereotactic Body Radiation Therapy: Reflecting on the Progress', *Int J Radiat Oncol Biol Phys.* **87** (2013), No.5, 869-870.

Garcia-Garduno, O, et al. 'Radiation Transmission, Leakage and Beam Prenumbra Measurements of a Micro-Culitleaf Collimator using GafChromic EBT Film', *J Appl Clin Med Phys.* **9** (2008).

Radiololgy Info. 'Image-guided Radiation Therapy (IGRT)', Retrieved March 15, 2015, from http://www.radiologyinfo.org/en/info.cfm?pg=igrt (2014, July 2).

Jiang, S B, C Pope, K M A Jarrah, J H Kong, T Bortfeld, and G T Y Chen ’An experimental investigation on intra-fractional organ motion effects in lung IMRT treatments’, *Phys Med Biol.* **48** (2003), 1773–1784.

Kang, H, E Yorke, J Yang, CS Chui, K Rosenzweig, H Amols, ‘Evaluation of tumor motion effects on dose distribution for hypofractionated intensity-modulated radiotherapy of non-small-cell lung cancer’, *J Appl Clin Med Phys.* **11** (2010), 78-89.

Li, X, Y Yang, T Li, K Fallon, D Heron, M Huq, ‘Dosimetric effect of respiratory motion on volumetric-modulated arc therapy-based lung SBRT treatment delivered by TrueBeam machine with flattening filter-free beam’, *J Appl Clin Med Phys.* **14** (2013), 195-204.

Low, D, W Harms, S Mutic, and J Purdy, ‘A technique for the quantitative evalution of dose distributions’, *Med Phys* **25** (1998), No. 5, 656-661.

National Comprehensive Cancer Network,’ NCCN Quick Guide Non-Small Cell Lung Cancer Treatment Options’, Retrieved May 30, 2016, from https://www.nccn.org/patients/guidelines/quick_guides/nscl/treatment_options/index.html#2.

Mancuso, G M, 'Evaluation of Volumetric Modulated Arc Therapy (VMAT) Patient Specific Quality Assurance', *LSU Electronic Thesis & Dissertation Collection* (2011).

Masi, L, R Doro, V Favuzza, S Cipressi, L Livi, ‘Impact of plan parameters on the dosimetric accuracy of volumetric modulated arc’, *Med Phys* **40** (2013).

Matney, J, 'Determination of CTV-To-ITV Margin for Free-Breathing Respiratory-Gated Treatments Usind 4DCT and Novalis EXACTRAC Gating System with Implanted Fiducials', *LSU Electronic Thesis & Disseration Collection* (2008).

McNiven, A, M Sharpe, T Purdie, ‘A new metric for assessing IMRT modulation complexity and plan deliverability’, *Med Phys* **37** (2010), 505-515.

Ong, C, M Dahele, B Slotman, W Verbakel, ‘Dosimetric Impact of the Interplay Effect During Stereotactic Lung Radiation Therapy Delivery Using Flattening Filter-Free Beams and Volumetirc Modulated Arc Therapy’, *Int J Radiat Oncol Biol Phys.* **86** (2013), 744-748.

Ong, C, W Verbakel, J Cuijpers, B Slotman, S Senan, ‘Dosimetric Impact of Interplay Effect on RapidArc Lung Stereotactic Treatment Delivery’, *Int. J Radiat Oncol Biol Phys.* **79** (2011), 305-311.

Ramsey, C, et al. ‘Leaf position error during conformal dynamic arc and intensity modulated arc treatments’, *Med Phys* **28** (2001), 67-72.

Rao, M, J Wu, D Cao, T Wong, V Mehta, D Shepard, J Ye, ‘Dosimetric Impact of Breathing Motin in Lung Stereotactic Body Radiotherapy Treatment Using Image-Modulated

Radiotherapy and Volumetris Modulated Arc Therapy', *Int J Radiat Oncol Biol Phys.* **83** (2012), 251-256.

Rietzel, E, T Pan, G T Y Chen, 'Four-dimensional computed tomography: Image formation and clinical protocol', *Med Phys* **32** (2005), 874.

Rosu, M, I Chetty, J Balter, M Kessler, D McShan, R Haken, 'Dose reconstruction in deforming lung anatomy: Dose grid size effects and clinical implications', *Med Phys*. **32** (2005).

Seco, J, G C Sharpe, J Turcotte, D Gierga, T Bortfield, H Paganetti, 'Effects of Organ Motion in IMRT treatments with segments of few monitor units', *Med Phys* **34** (2007), 923-934.

Stambaugh, C, B Nelms, T Dilling, C Stevens, K Latifi, G Zhang, et al. 'Experimentally studied dynamic dose interplay does not meaningfully affect target dose in VMAT SBRT lung treatments', *Med Phys* **40** (2013).

Appendix A. Longitudinal Profiles

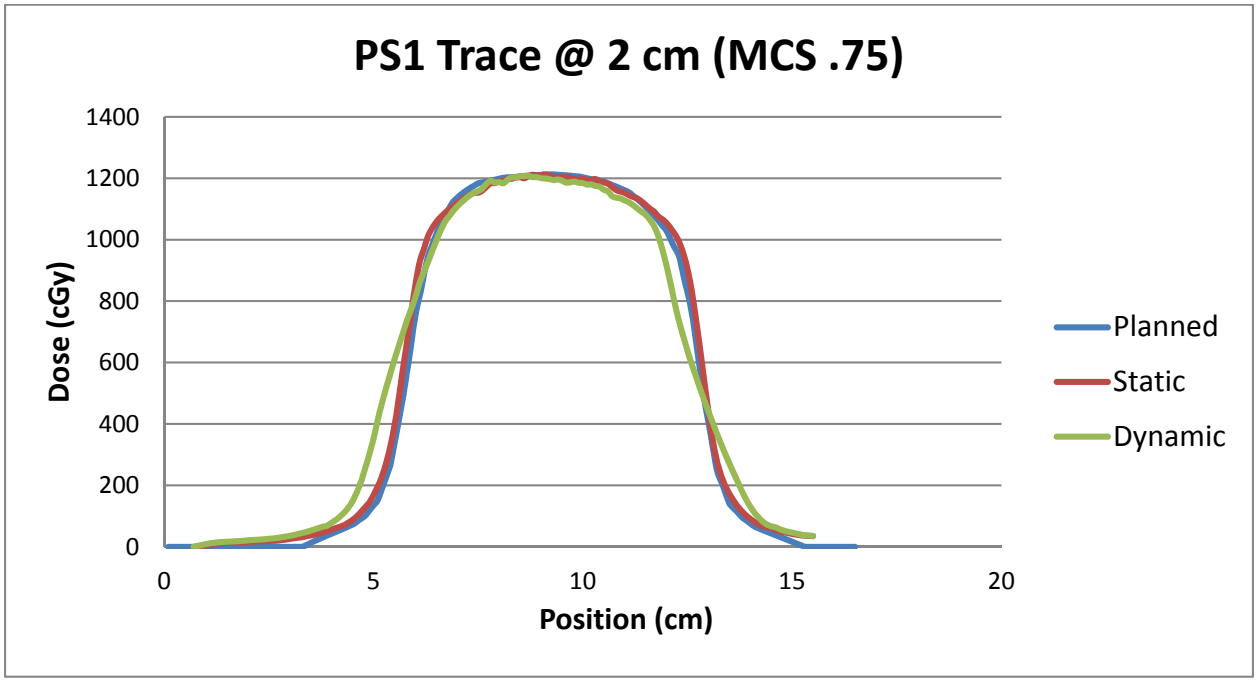

Figure 41: Longitudinal profiles for patient trace #1 at 2 cm amplitude with a plan MCS of 0.75.

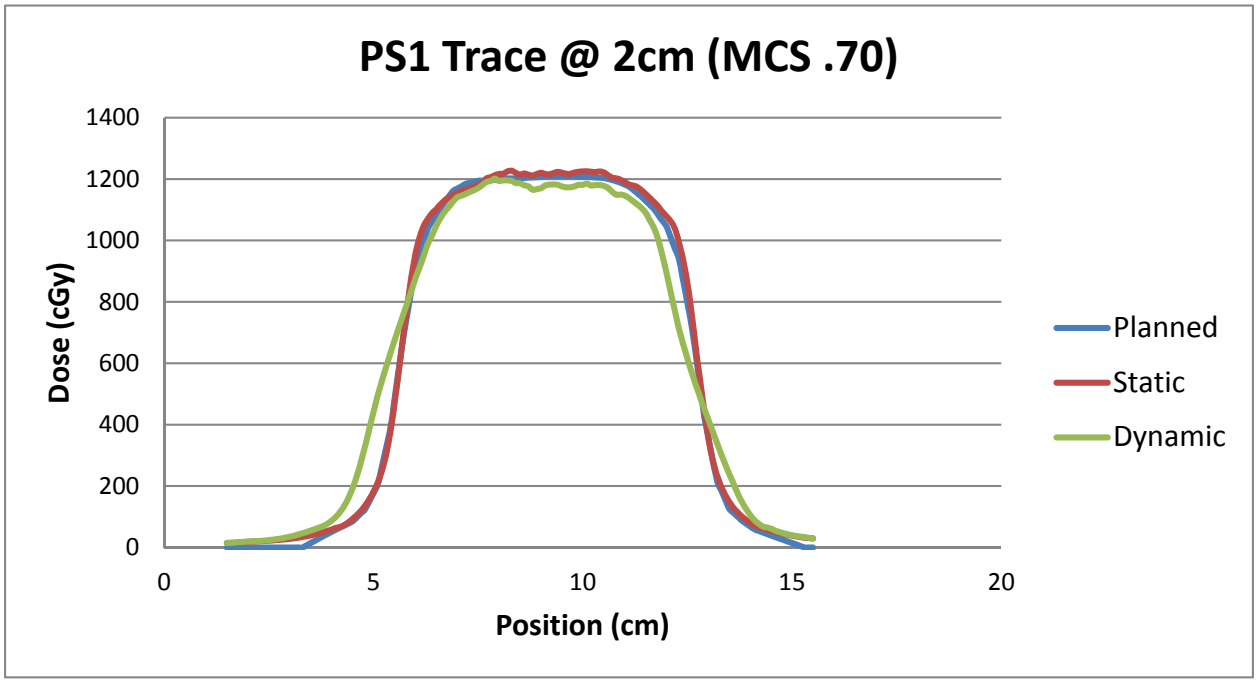

Figure 42: Longitudinal profiles for patient trace #1 at 2 cm amplitude with a plan MCS of 0.70.

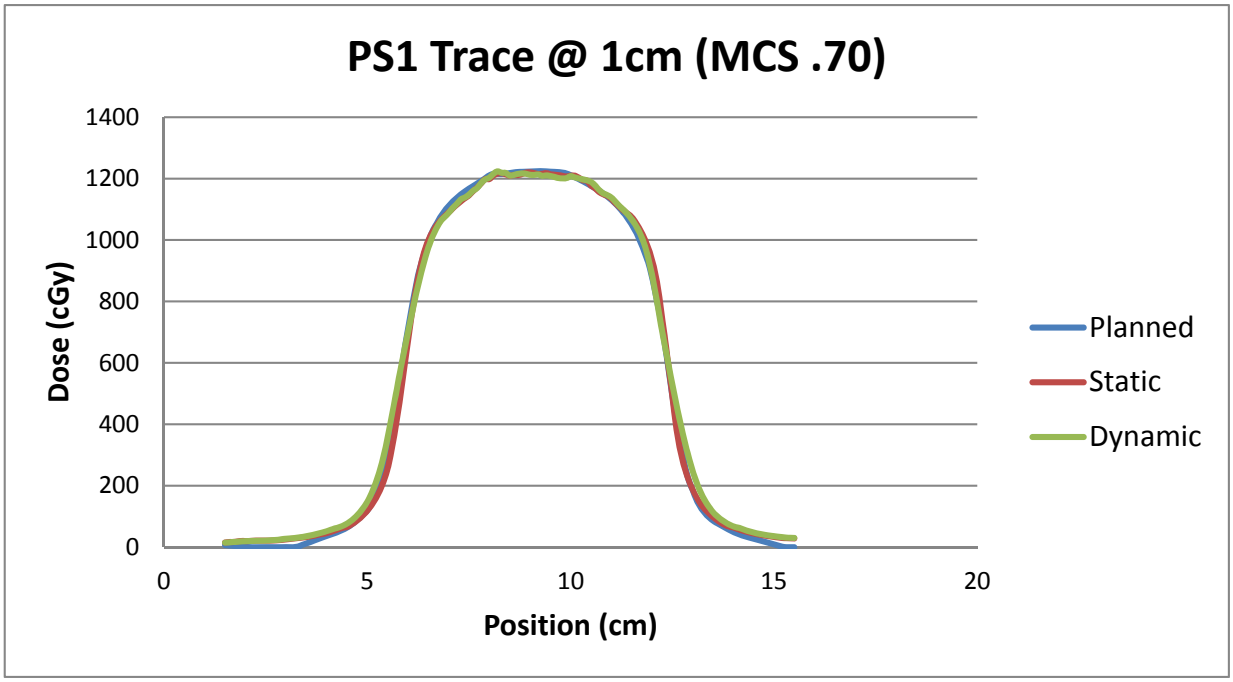

Figure 43: Longitudinal profiles for patient trace #1 at 1 cm amplitude with a plan MCS of 0.70.

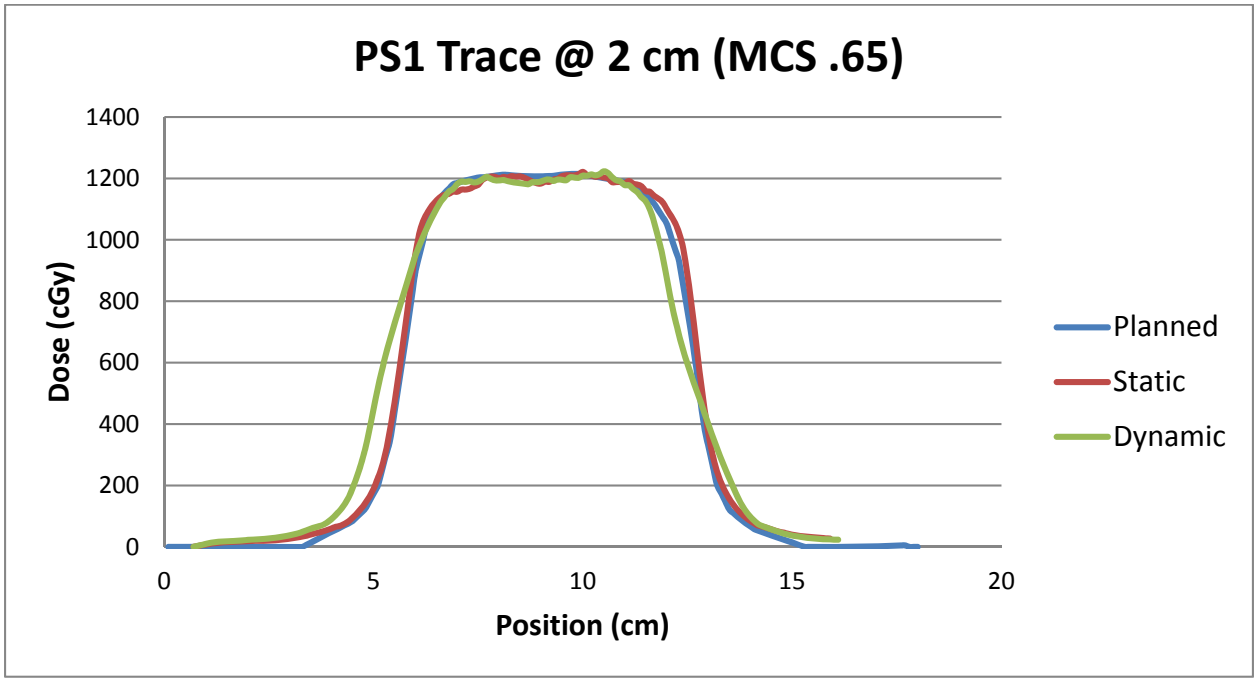

Figure 44: Longitudinal profiles for patient trace #1 at 2 cm amplitude with a plan MCS of 0.65.

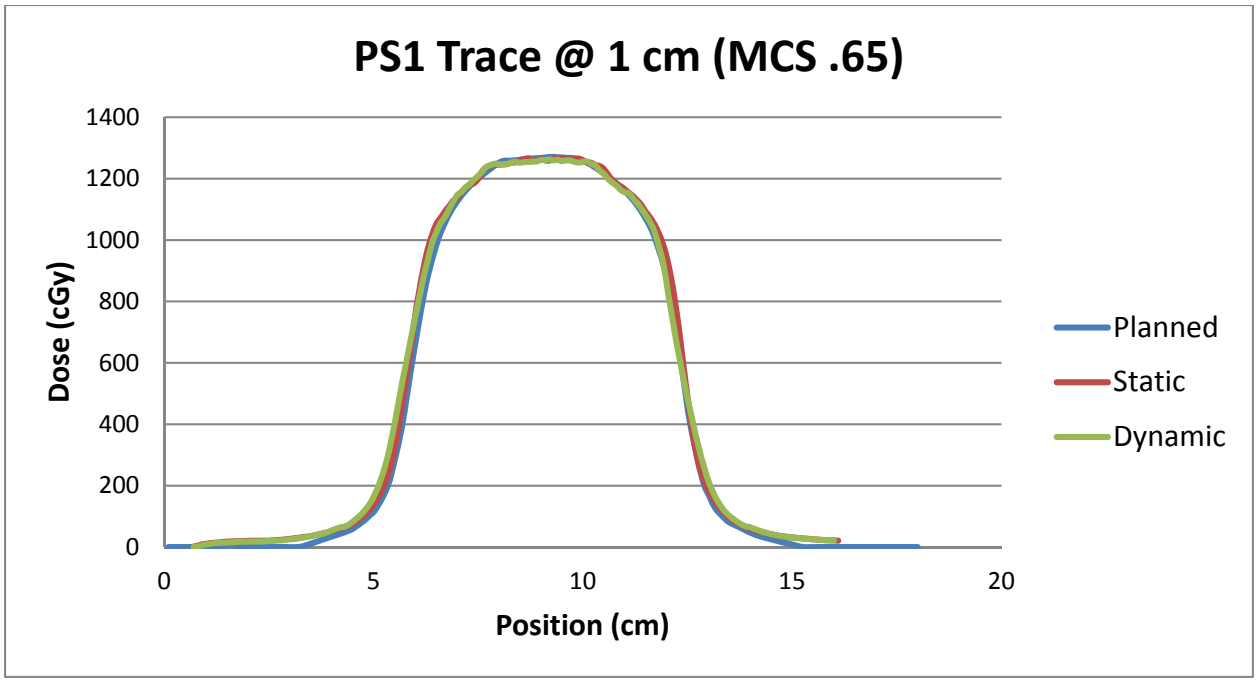

Figure 45: Longitudinal profiles for patient trace #1 at 1 cm amplitude with a plan MCS of 0.65.

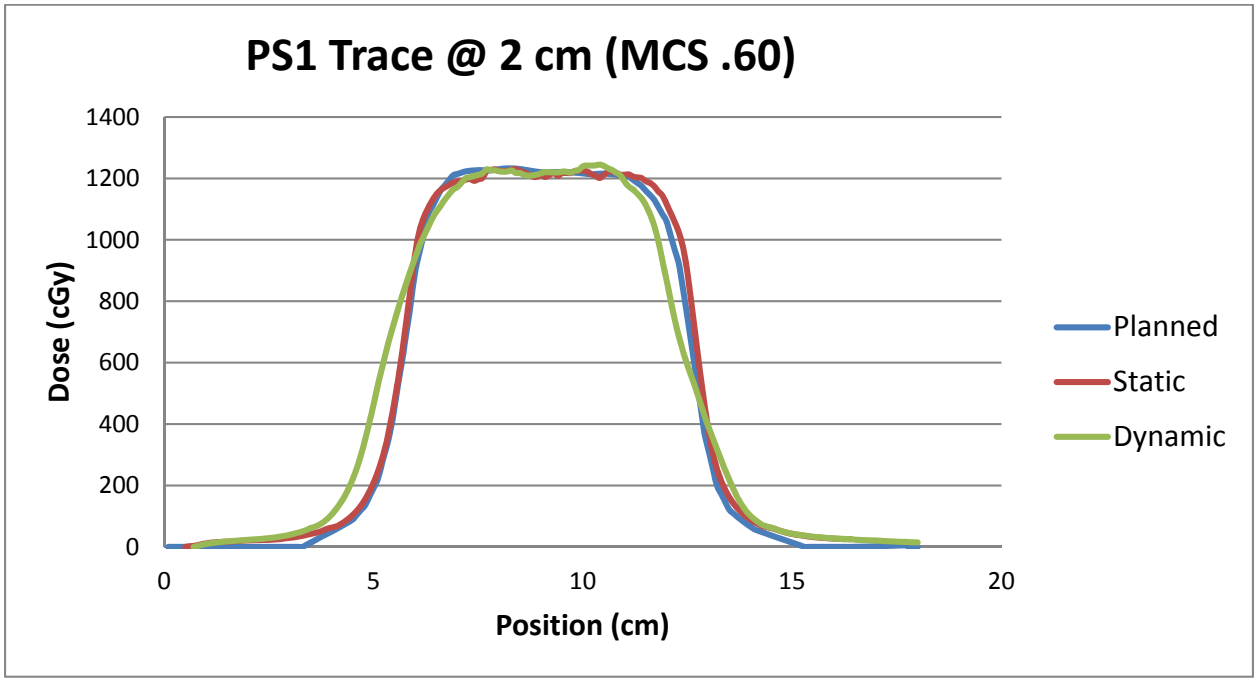

Figure 46: Longitudinal profiles for patient trace #1 at 2 cm amplitude with a plan MCS of 0.60.

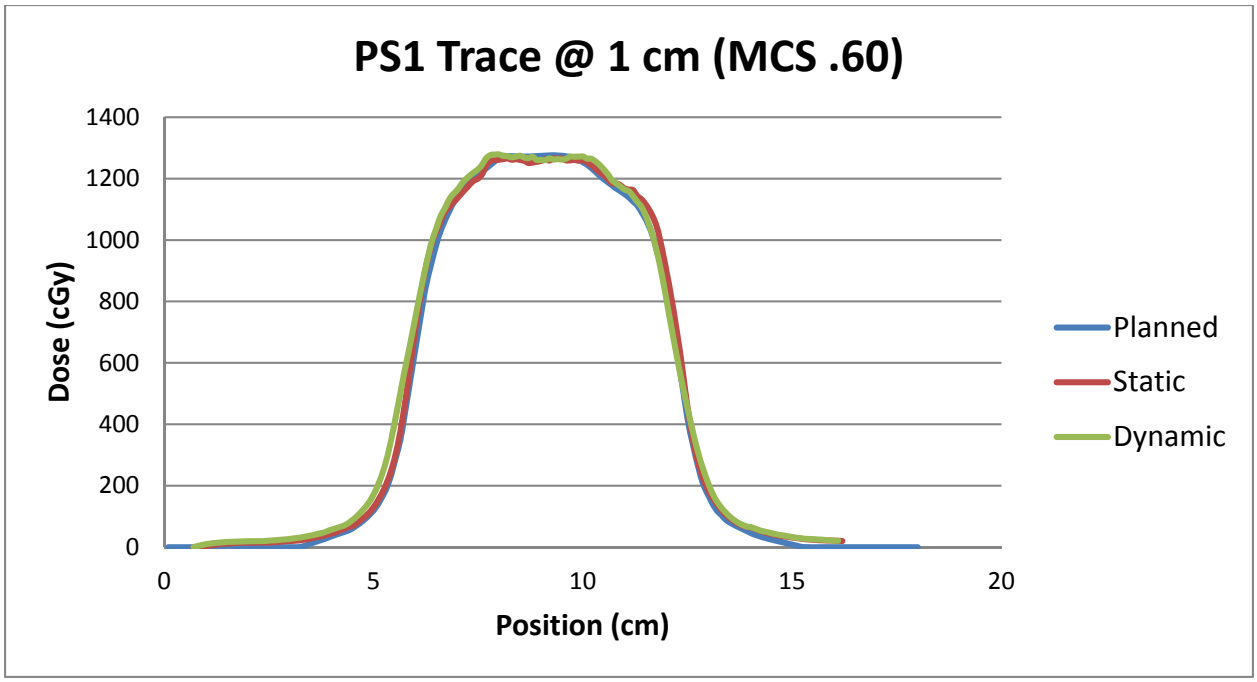

Figure 47: Longitudinal profiles for patient trace #1 at 1 cm amplitude with a plan MCS of 0.60.

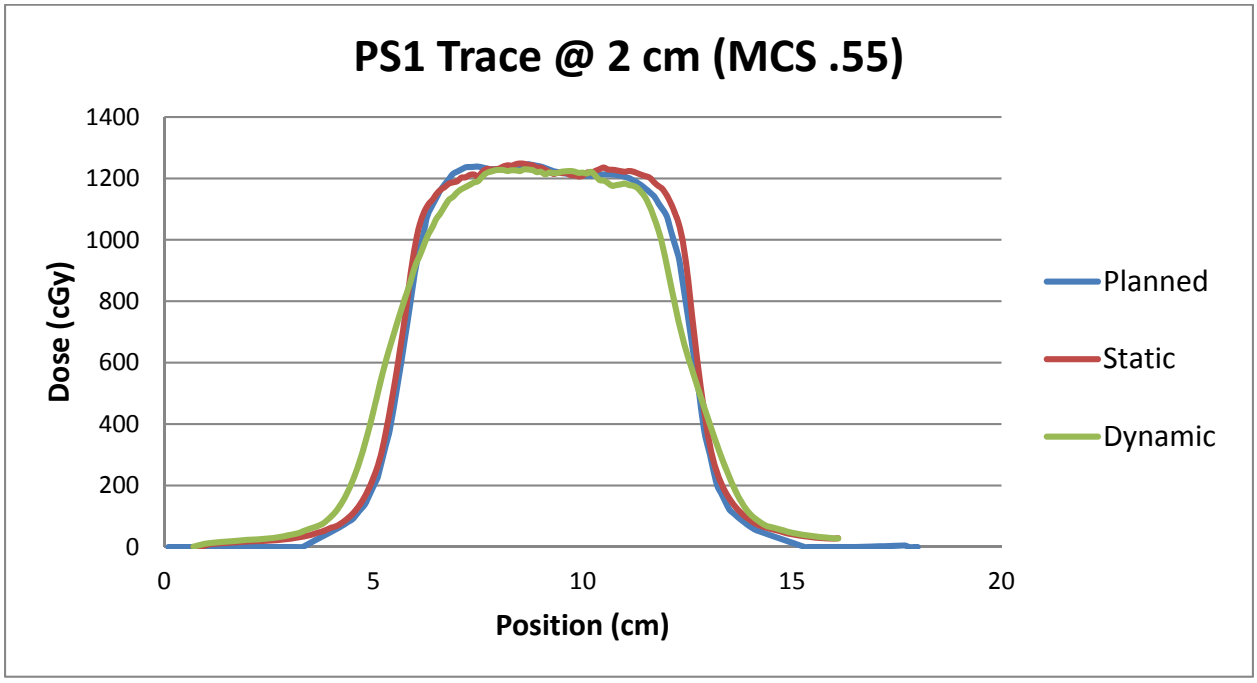

Figure 48: Longitudinal profiles for patient trace #1 at 2 cm amplitude with a plan MCS of 0.55.

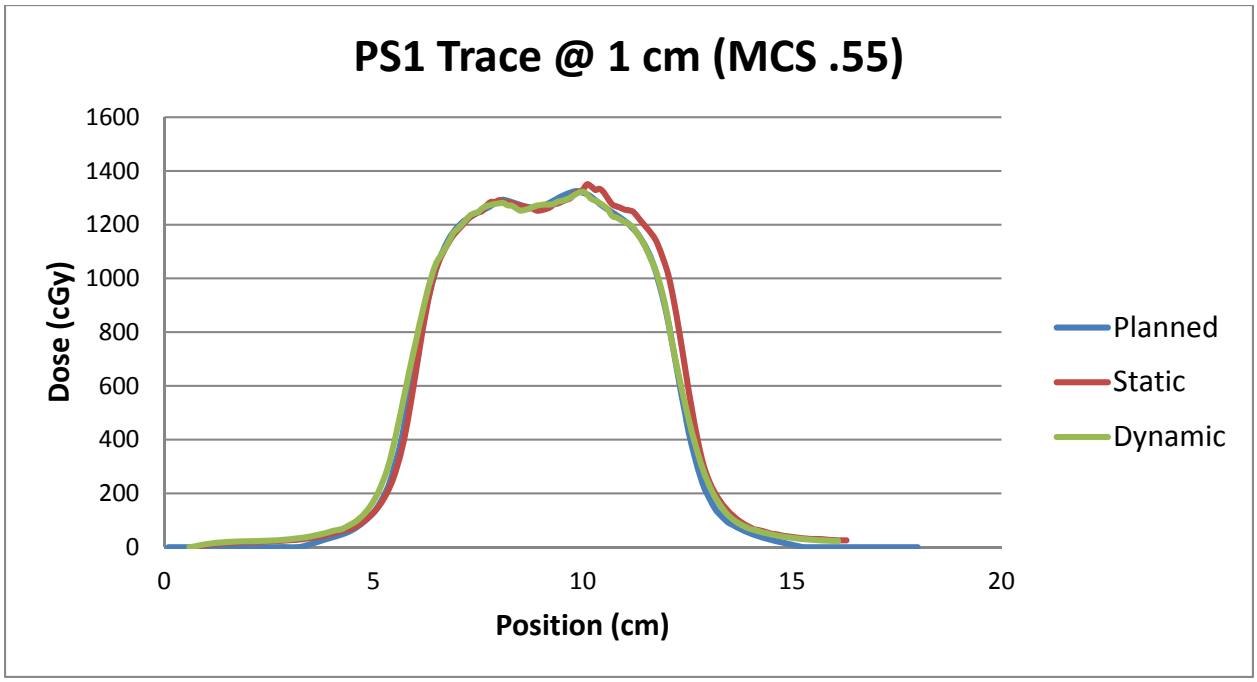

Figure 49: Longitudinal profiles for patient trace #1 at 1 cm amplitude with a plan MCS of 0.55.

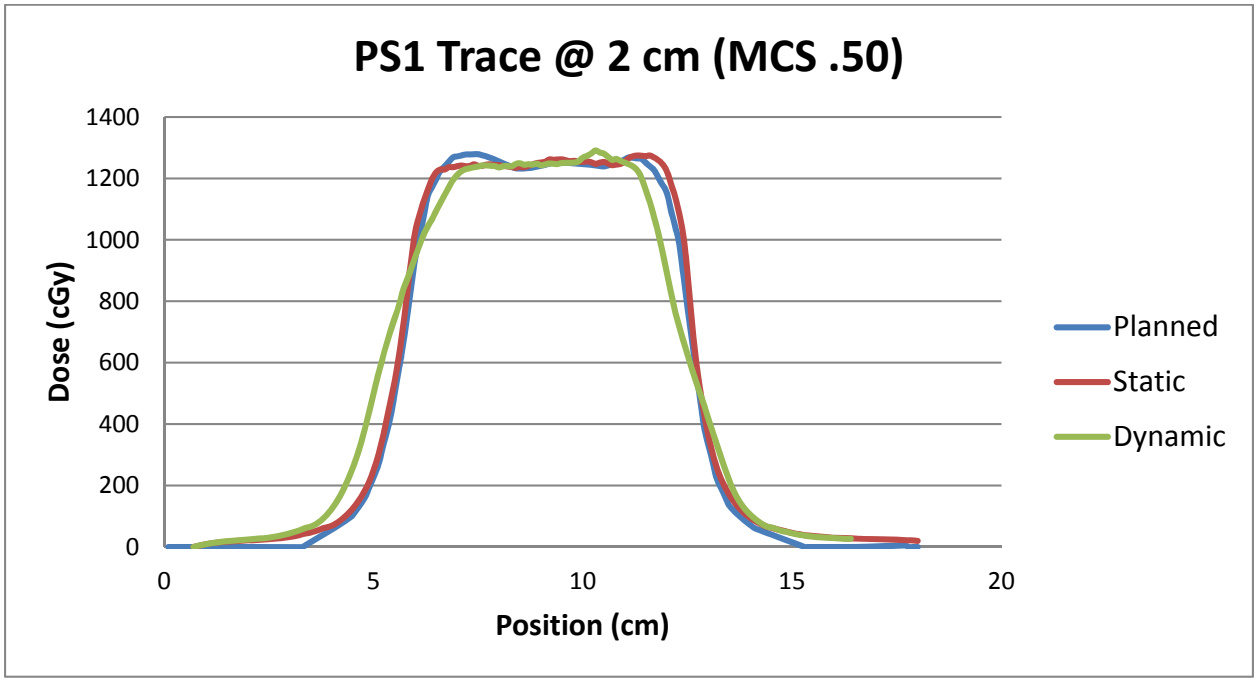

Figure 50: Longitudinal profiles for patient trace #1 at 2 cm amplitude with a plan MCS of 0.50.

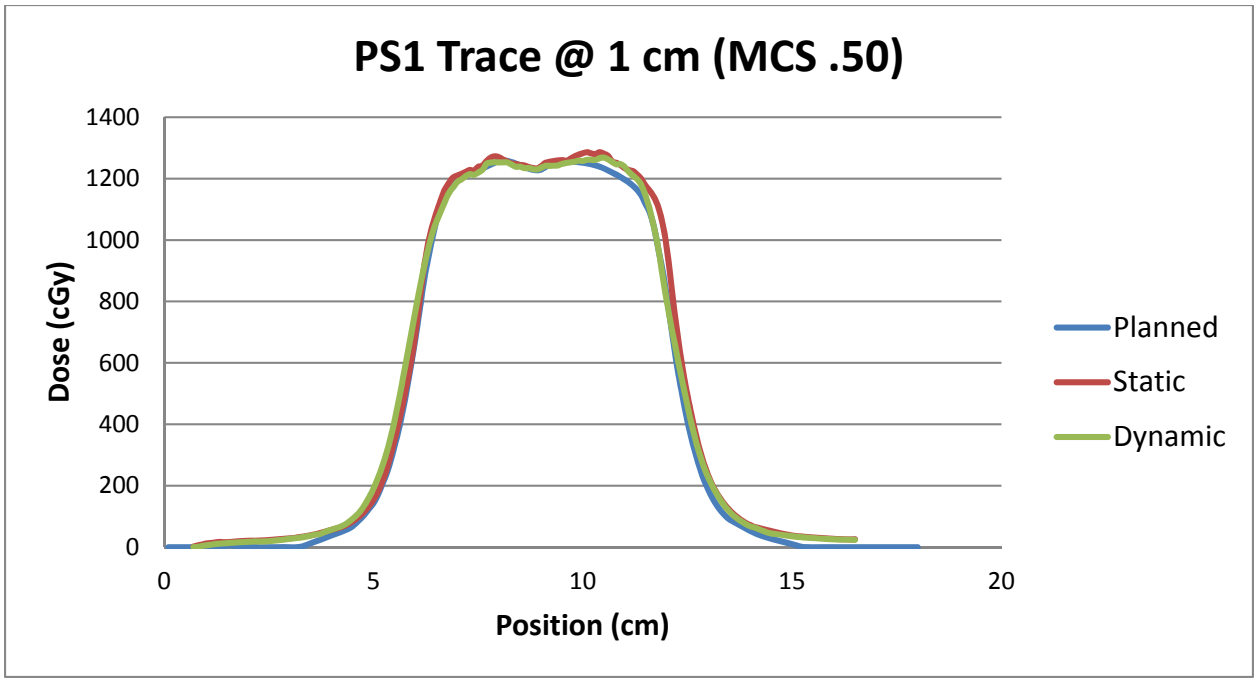

Figure 51: Longitudinal profiles for patient trace #1 at 1 cm amplitude with a plan MCS of 0.50.

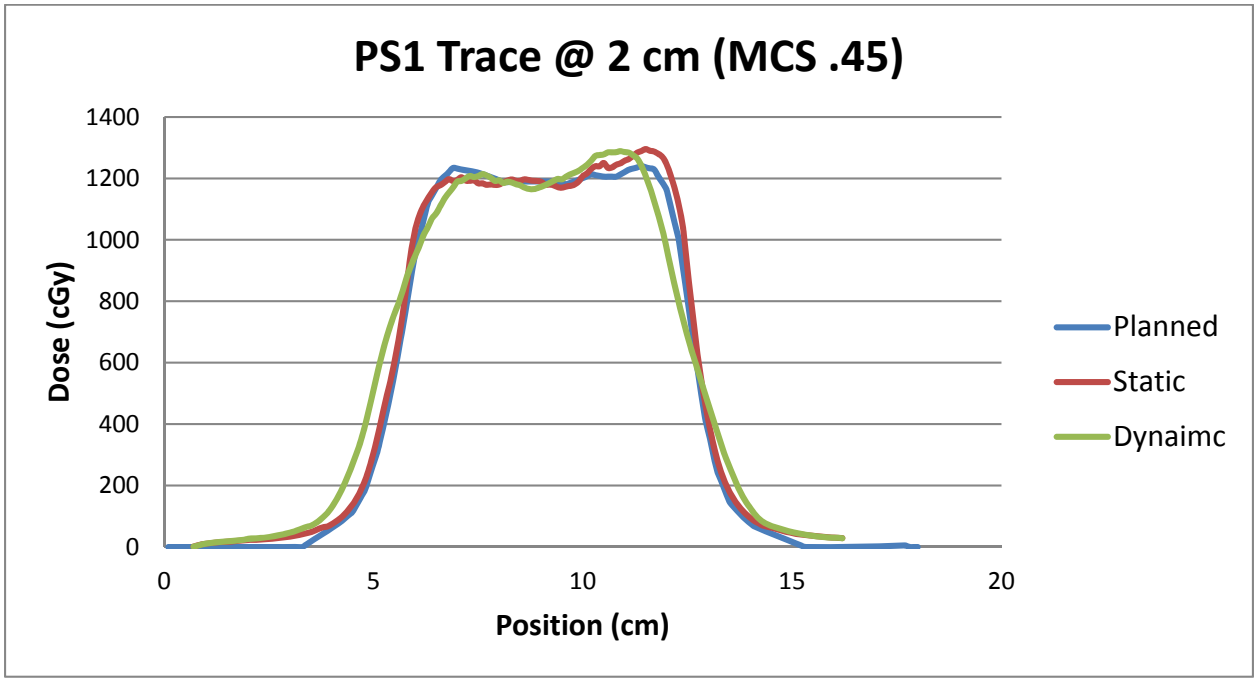

Figure 52: Longitudinal profiles for patient trace #1 at 2 cm amplitude with a plan MCS of 0.45.

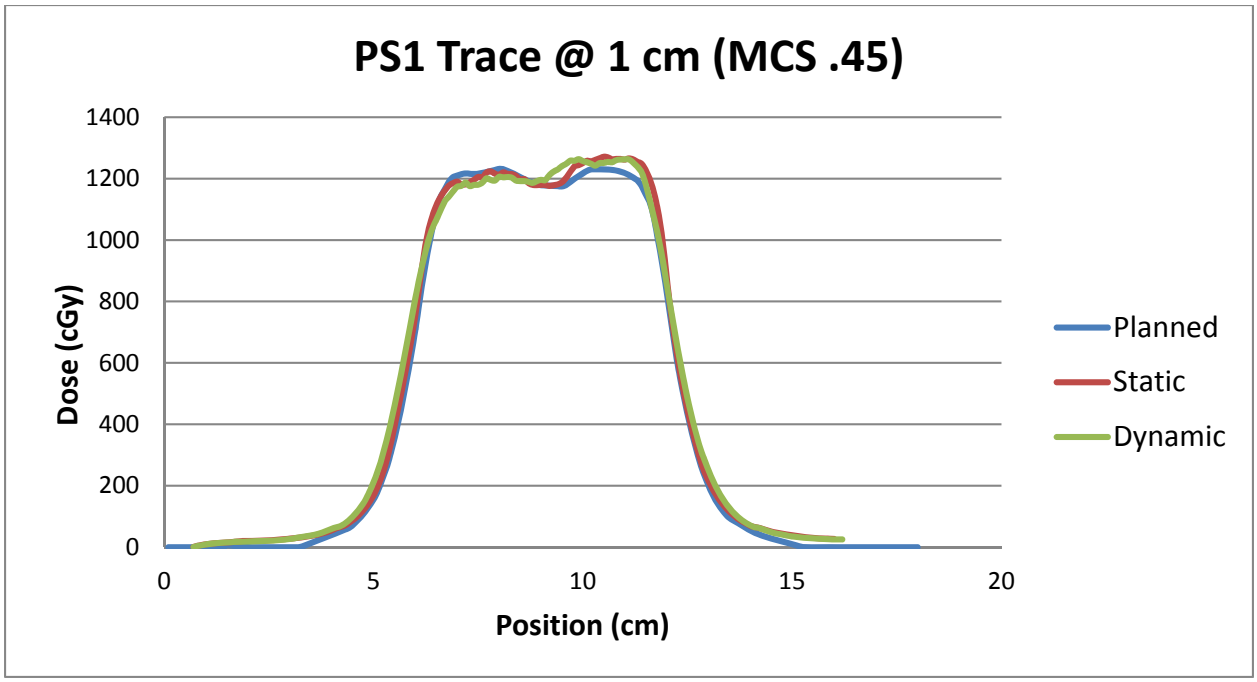

Figure 53: Longitudinal profiles for patient trace #1 at 1 cm amplitude with a plan MCS of 0.45.

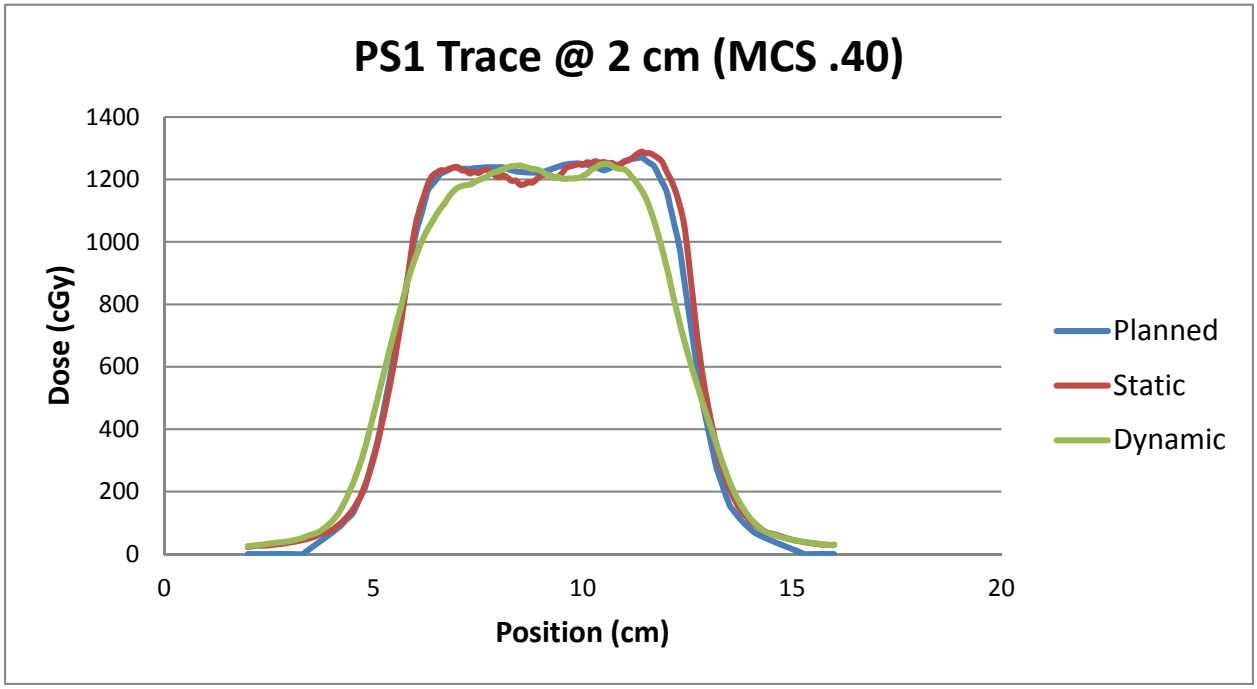

Figure 54: Longitudinal profiles for patient trace #1 at 2 cm amplitude with a plan MCS of 0.40.

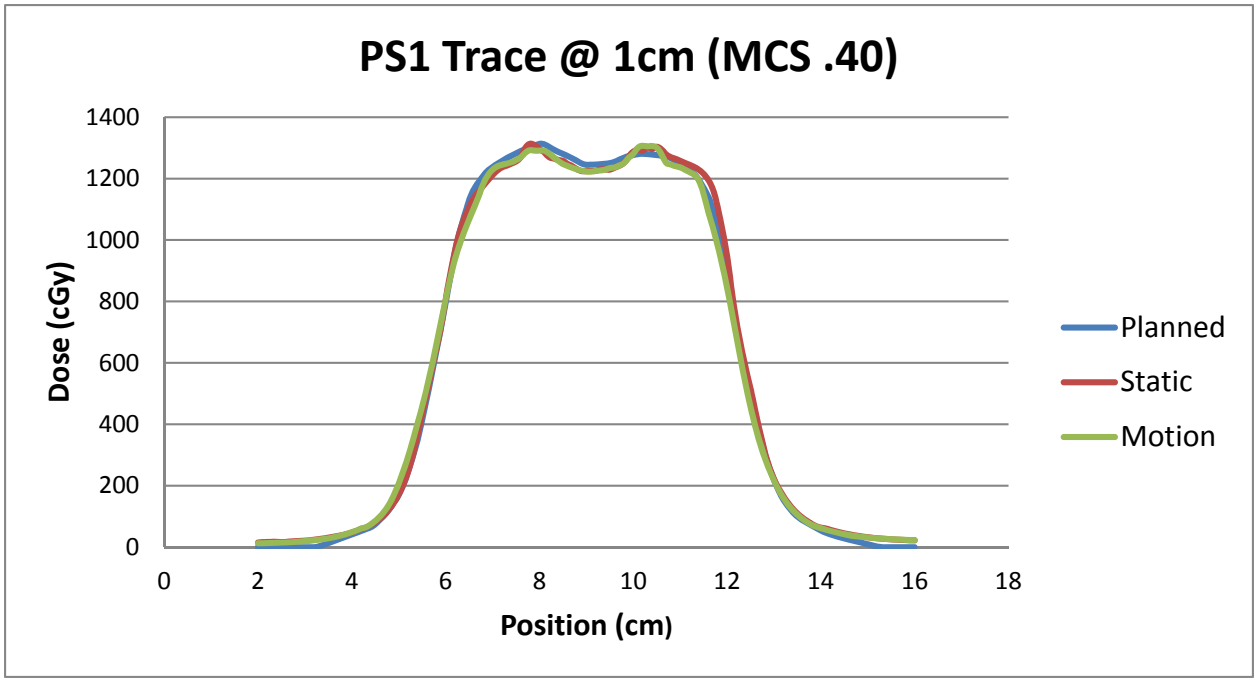

Figure 55: Longitudinal profiles for patient trace #1 at 1 cm amplitude with a plan MCS of 0.40.

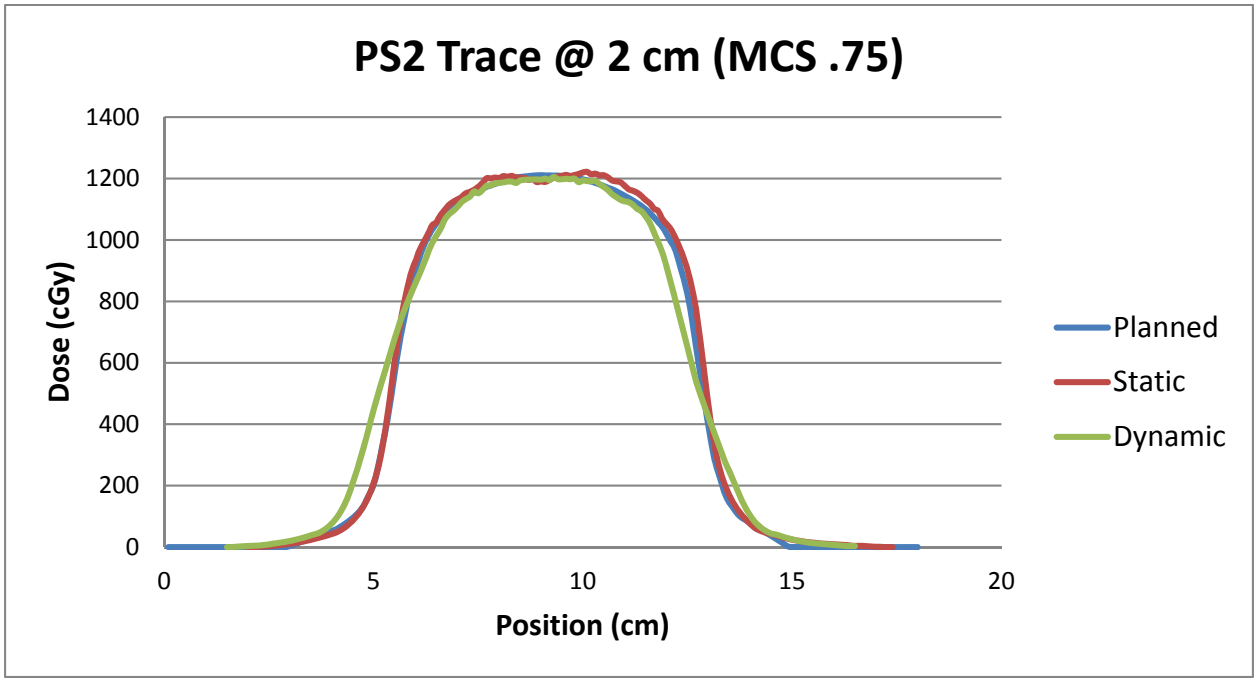

Figure 56: Longitudinal profiles for patient trace #2 at 2 cm amplitude with a plan MCS of 0.75.

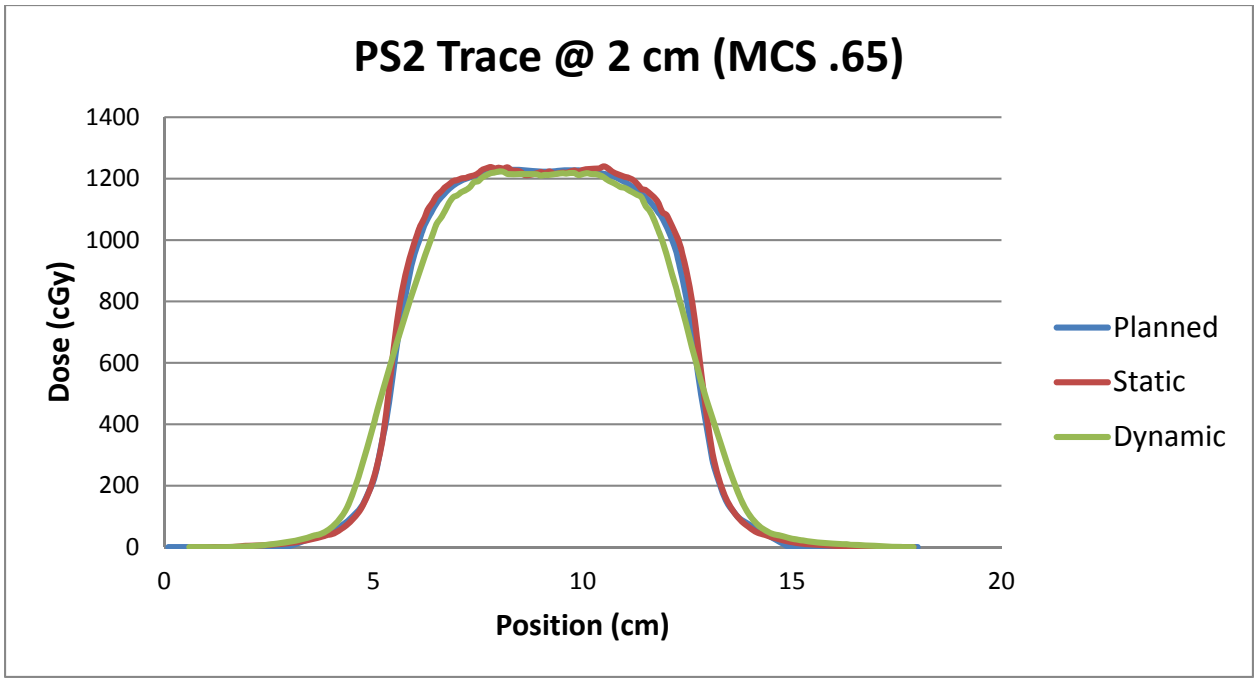

Figure 57: Longitudinal profiles for patient trace #2 at 2 cm amplitude with a plan MCS of 0.65.

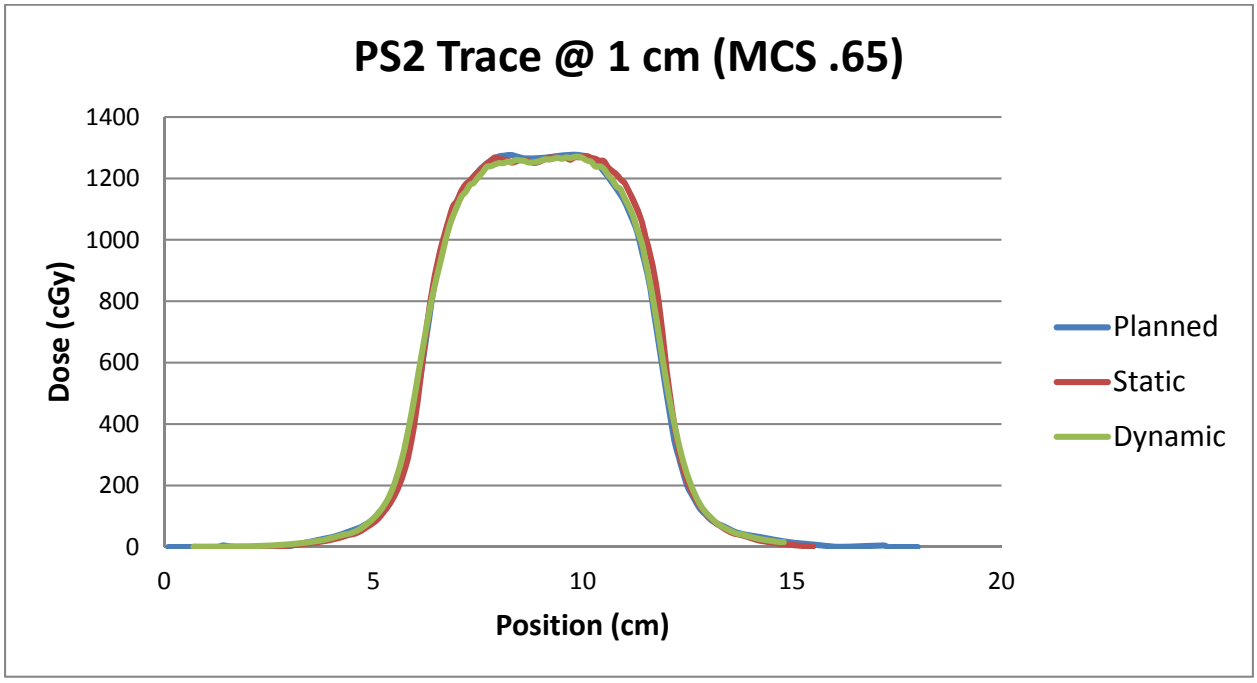

Figure 58: Longitudinal profiles for patient trace #2 at 1 cm amplitude with a plan MCS of 0.65.

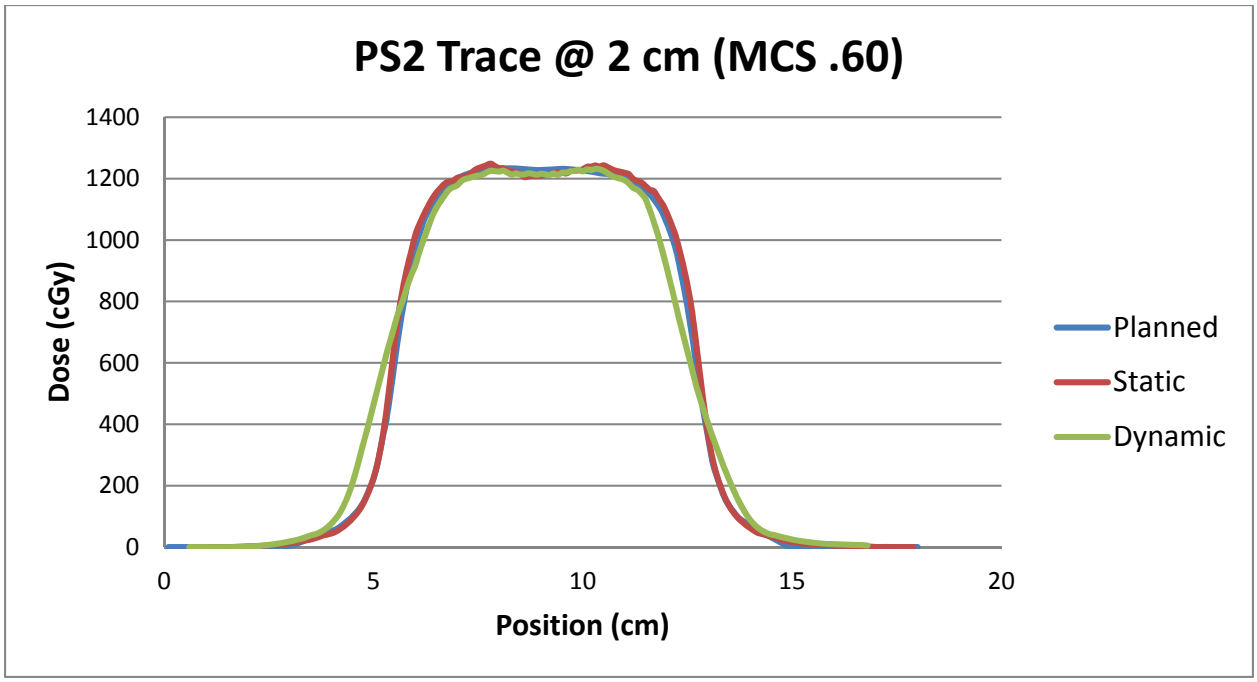

Figure 59: Longitudinal profiles for patient trace #2 at 2 cm amplitude with a plan MCS of 0.60.

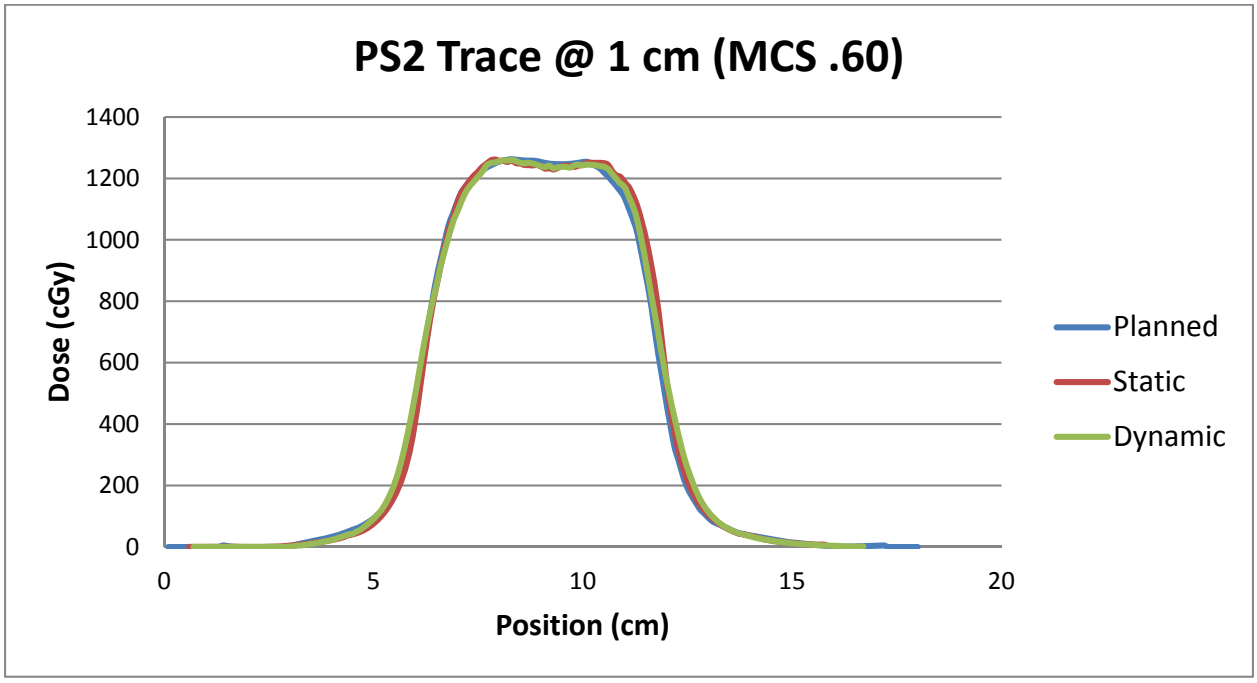

Figure 60: Longitudinal profiles for patient trace #2 at 1 cm amplitude with a plan MCS of 0.60.

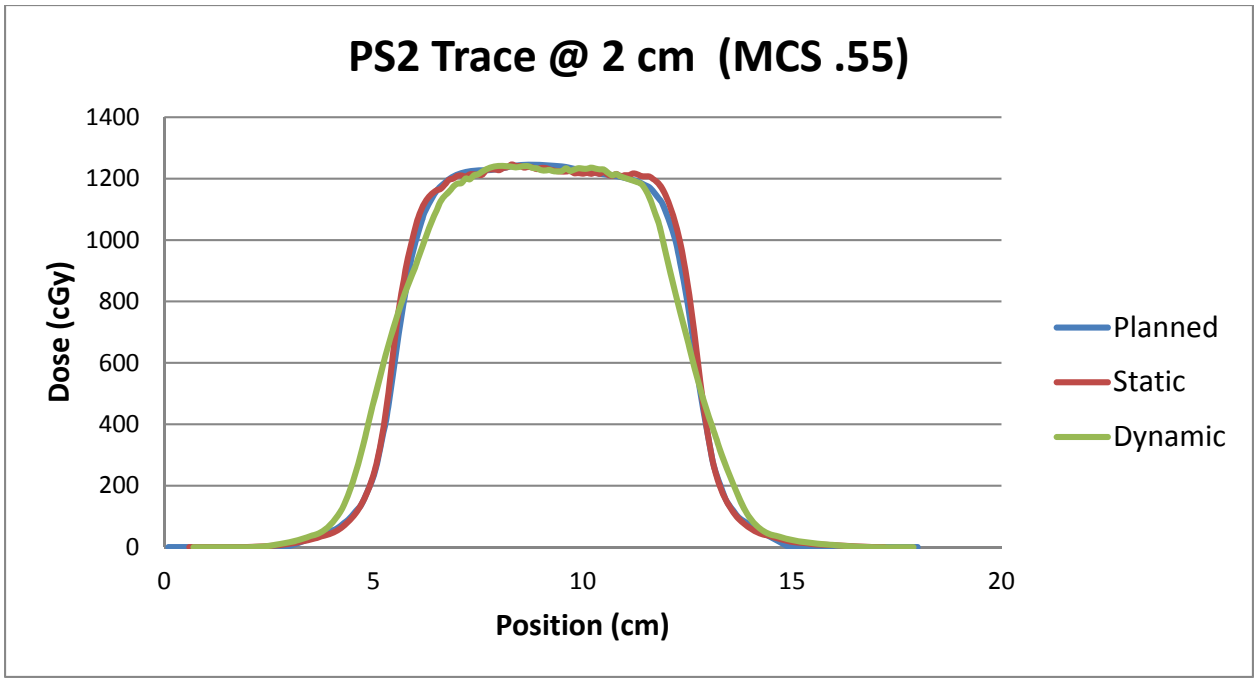

Figure 61: Longitudinal profiles for patient trace #2 at 2 cm amplitude with a plan MCS of 0.55.

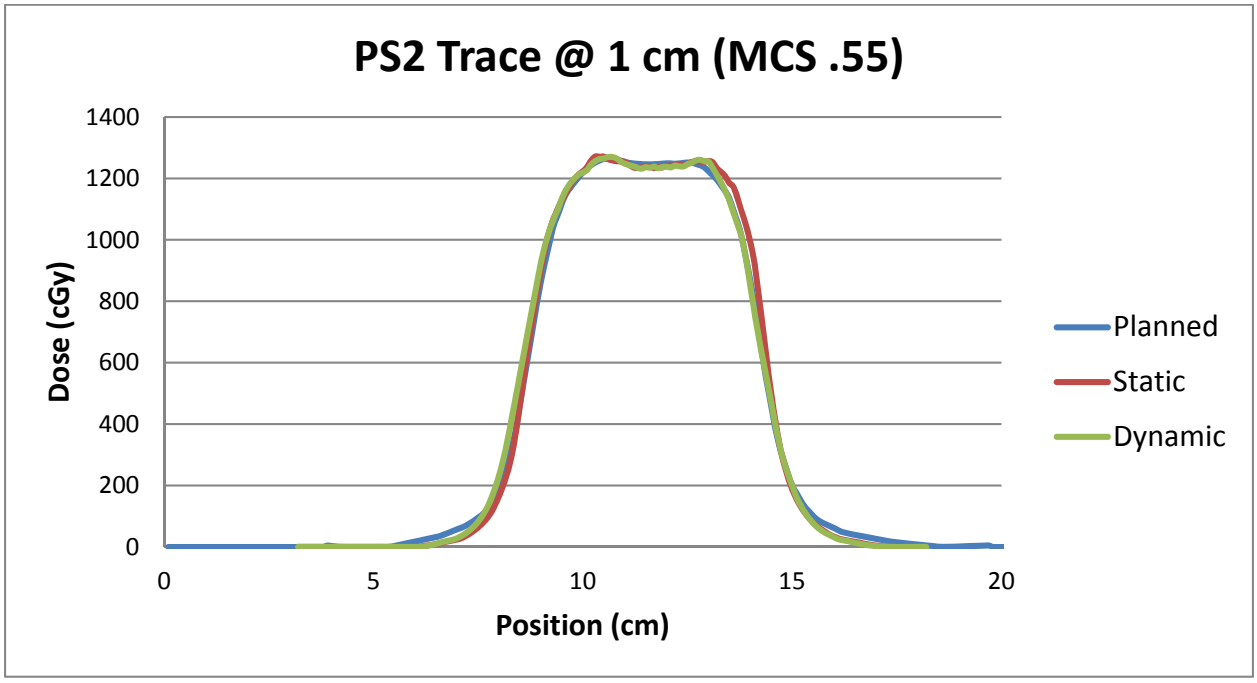

Figure 62: Longitudinal profiles for patient trace #2 at 1 cm amplitude with a plan MCS of 0.55.

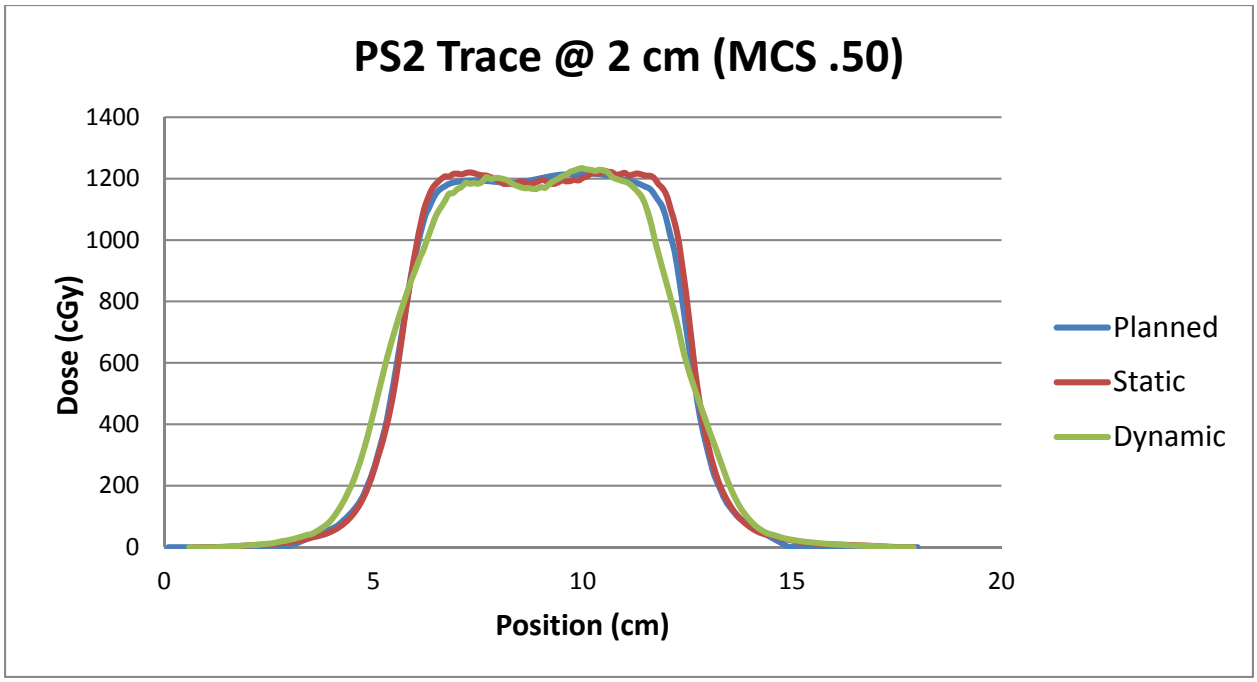

Figure 63: Longitudinal profiles for patient trace #2 at 2 cm amplitude with a plan MCS of 0.50.

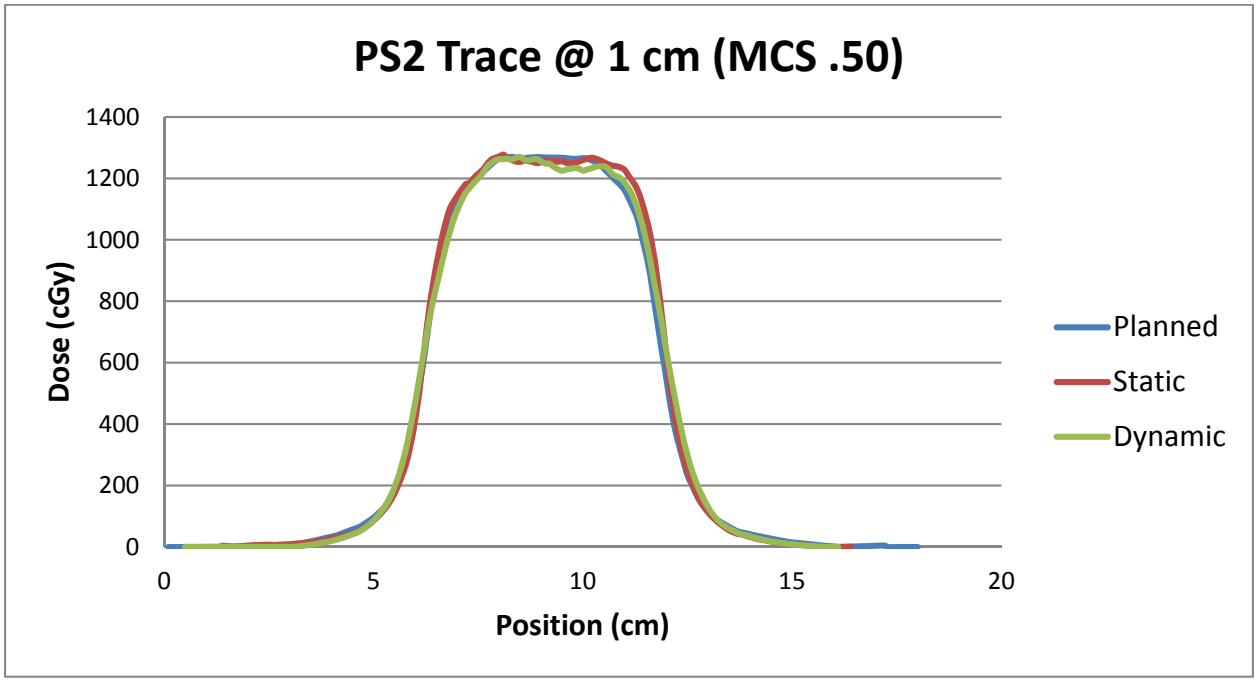

Figure 64: Longitudinal profiles for patient trace #2 at 1 cm amplitude with a plan MCS of 0.50.

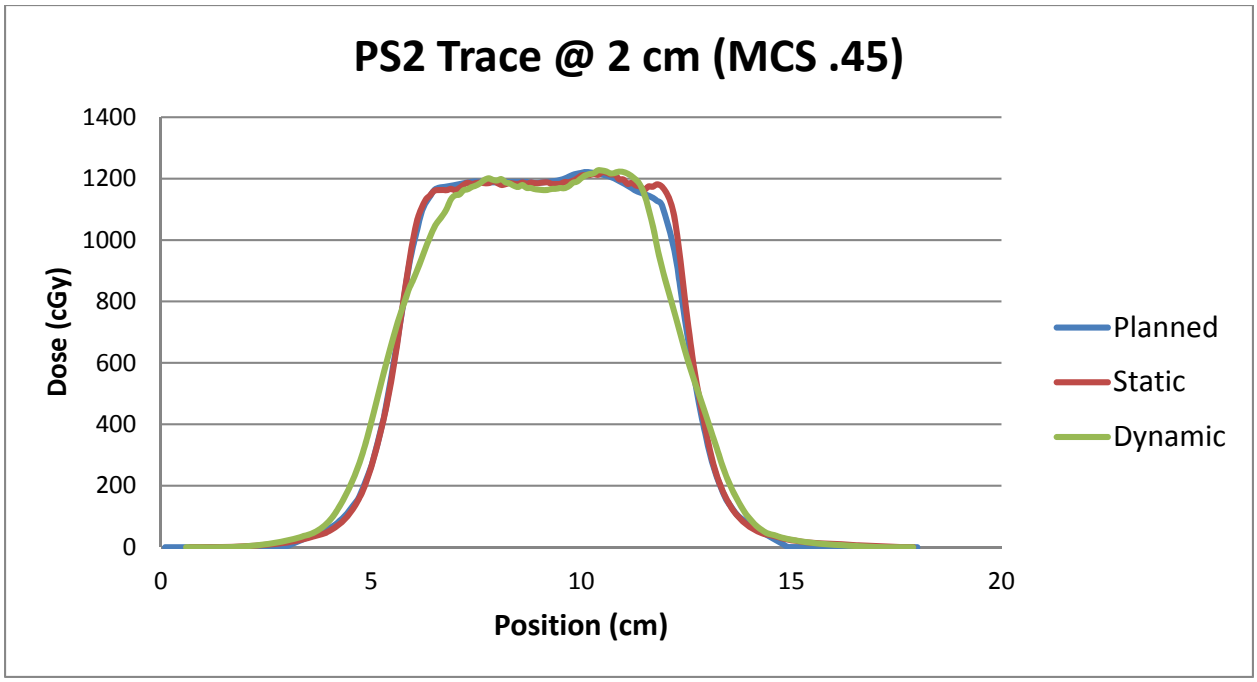

Figure 65: Longitudinal profiles for patient trace #2 at 2 cm amplitude with a plan MCS of 0.45.

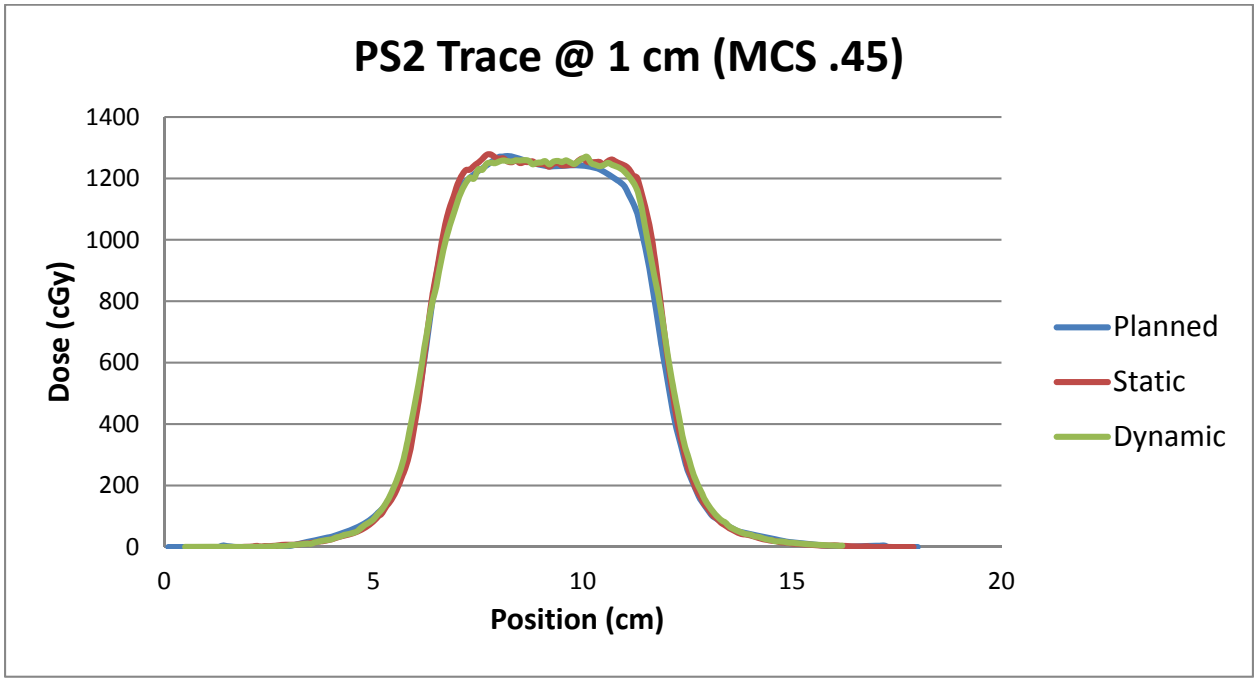

Figure 66: Longitudinal profiles for patient trace #2 at 1 cm amplitude with a plan MCS of 0.45.

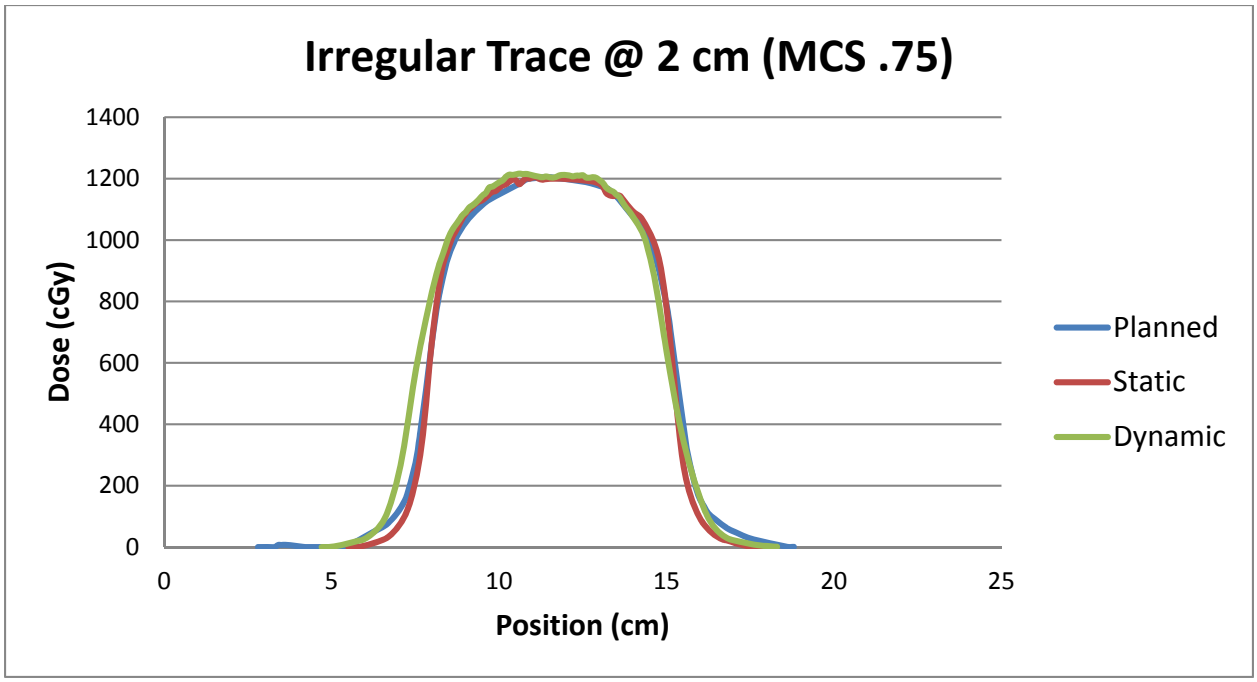

Figure 67: Longitudinal profiles for irregular patient trace at 2 cm amplitude with a plan MCS of 0.75.

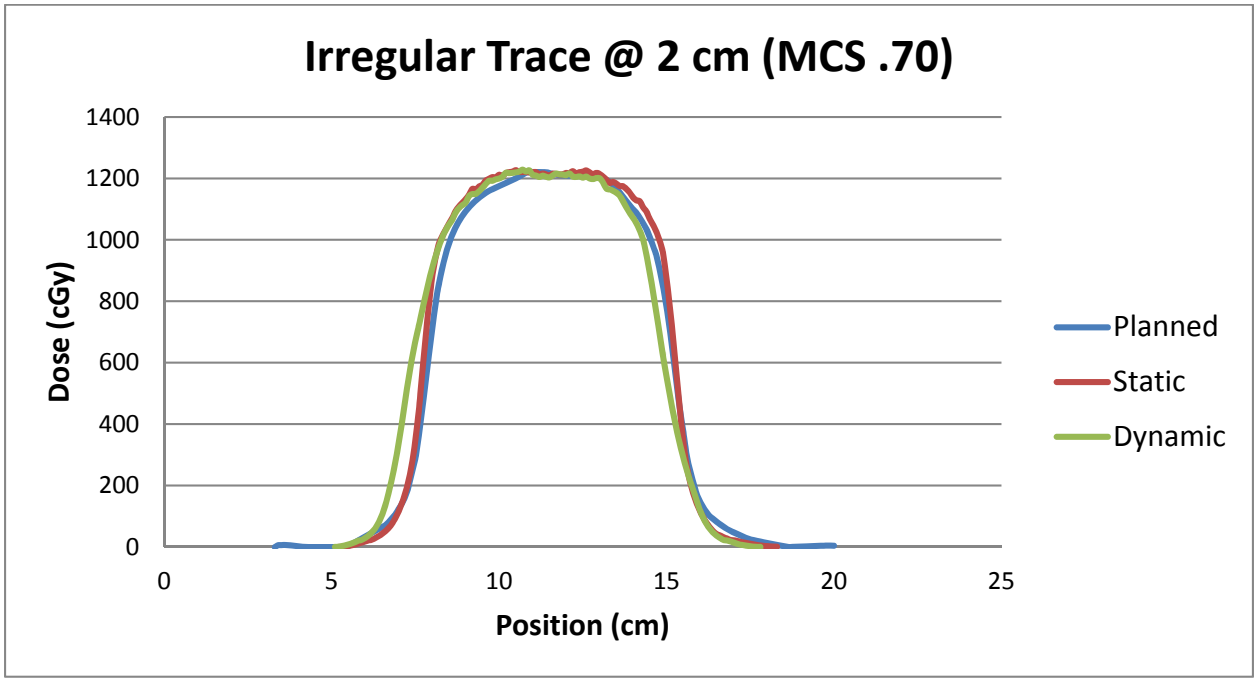

Figure 68: Longitudinal profiles for irregular patient trace at 2 cm amplitude with a plan MCS of 0.70.

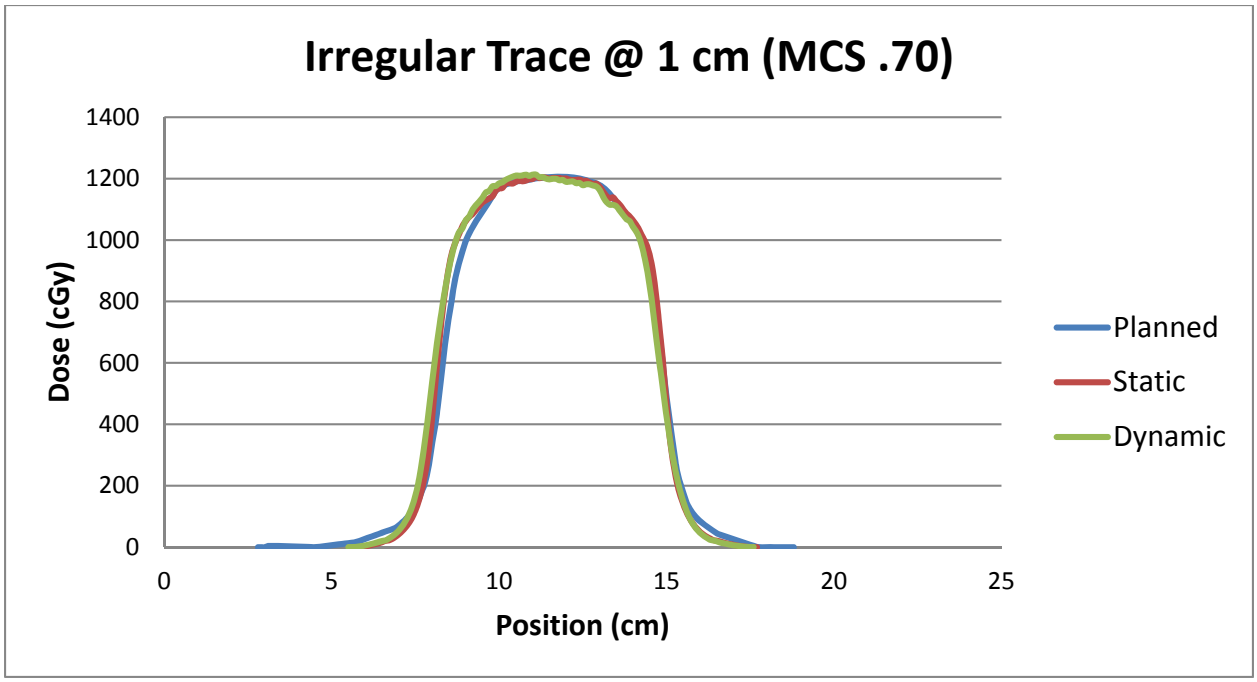

Figure 69: Longitudinal profiles for irregular patient trace at 1 cm amplitude with a plan MCS of 0.70.

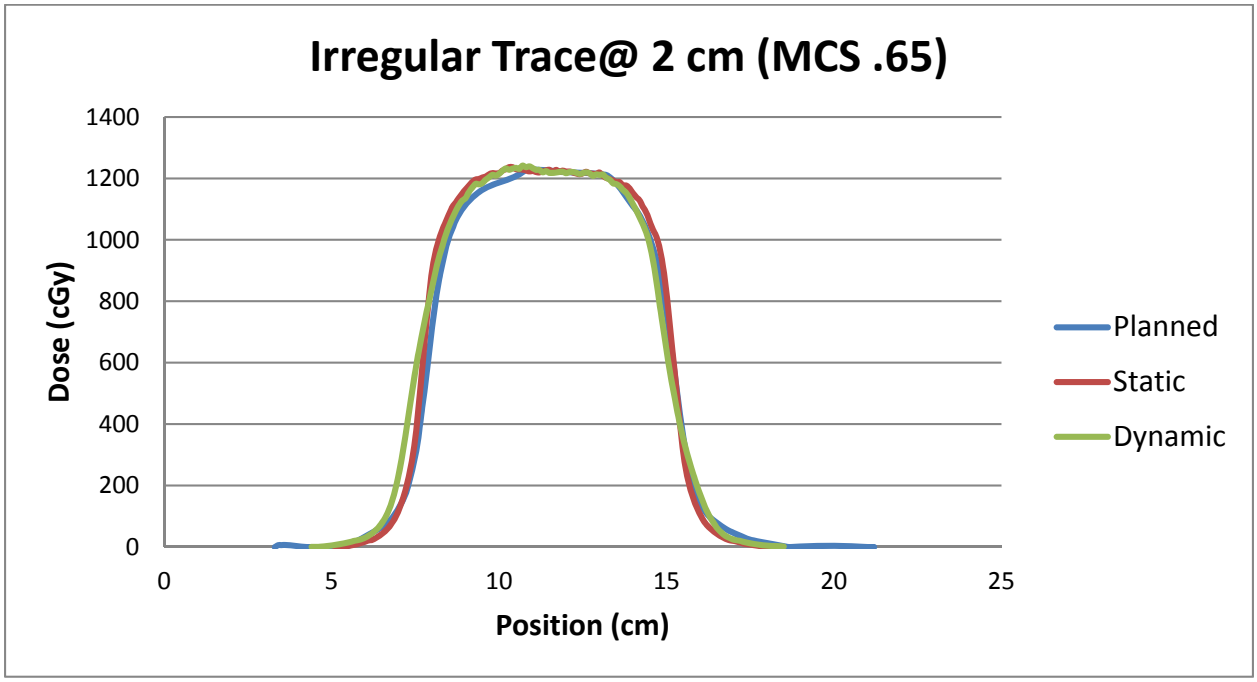

Figure 70: Longitudinal profiles for irregular patient trace at 2 cm amplitude with a plan MCS of 0.65.

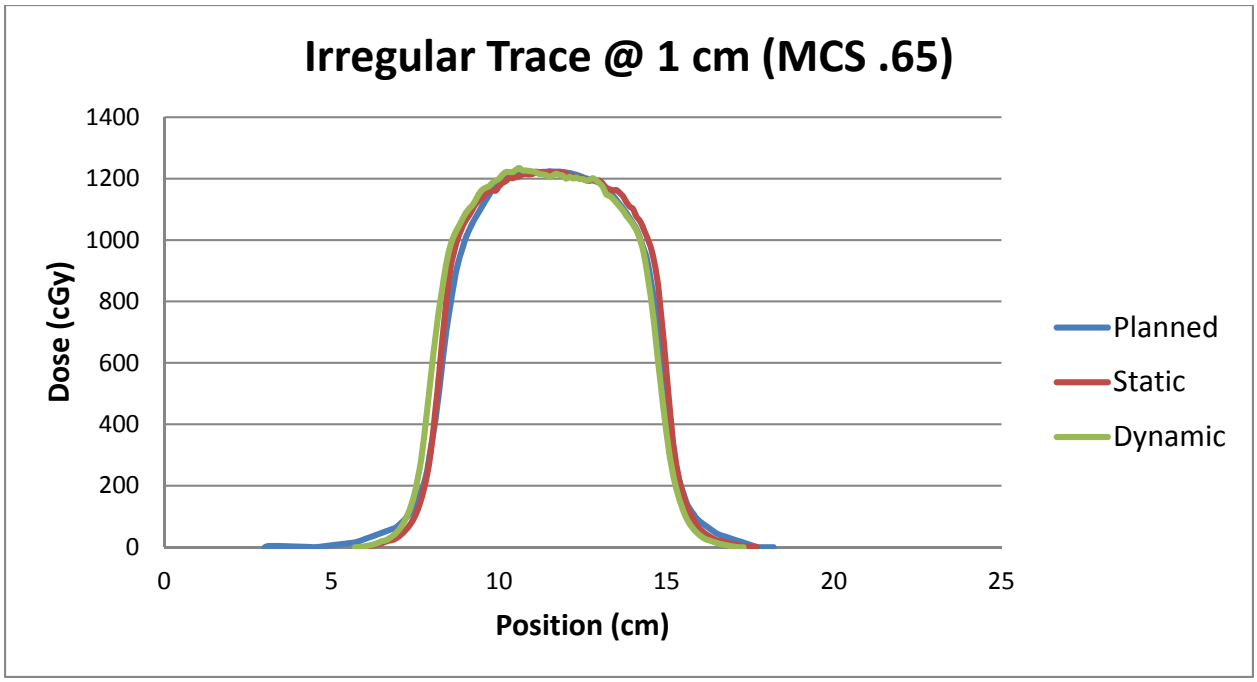

Figure 71: Longitudinal profiles for irregular patient trace at 1 cm amplitude with a plan MCS of 0.65.

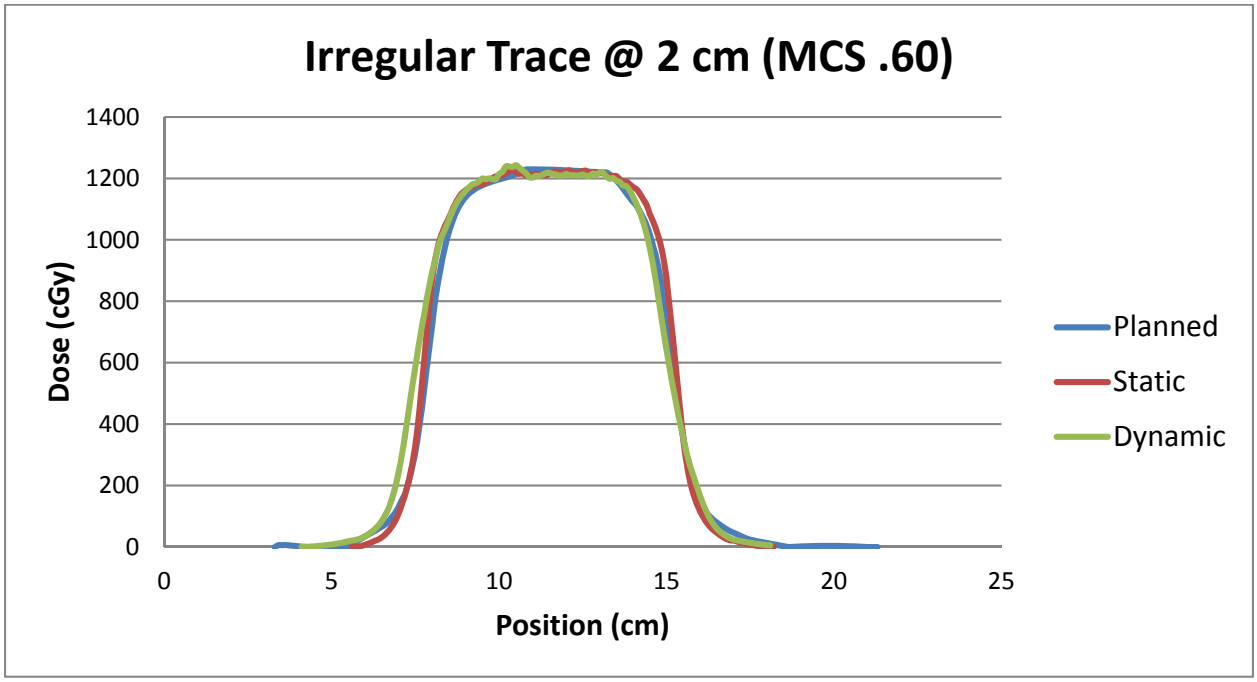

Figure 72: Longitudinal profiles for irregular patient trace at 2 cm amplitude with a plan MCS of 0.60.

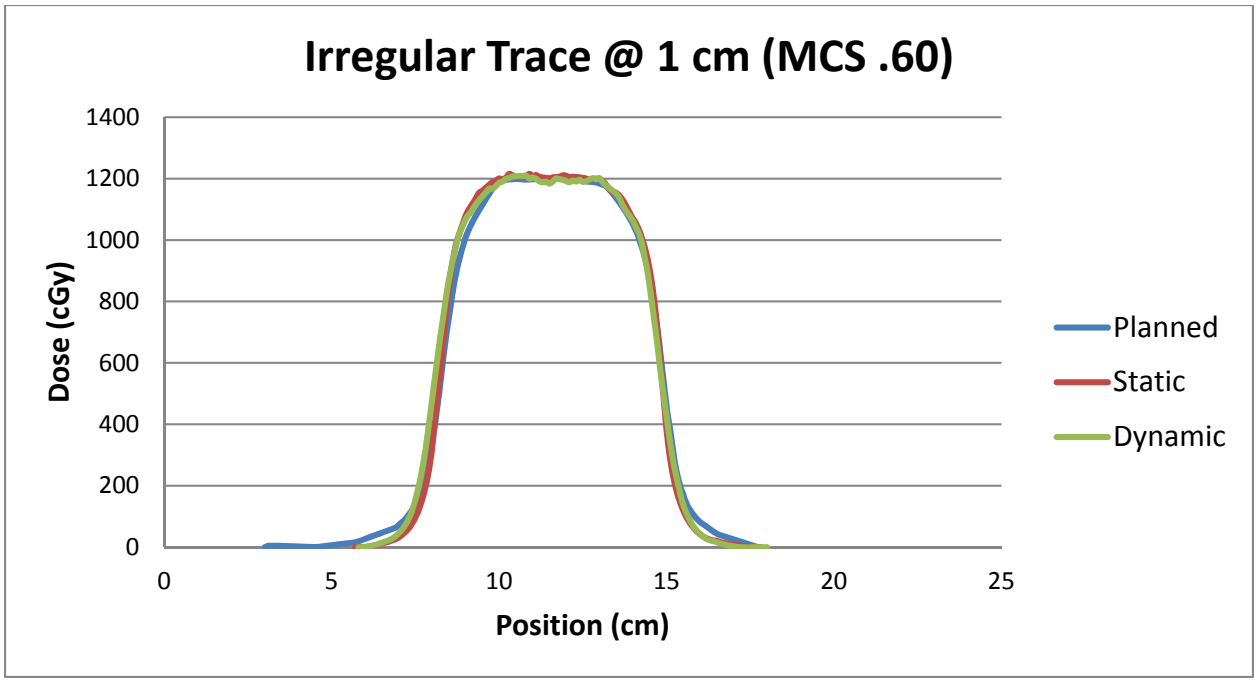

Figure 73: Longitudinal profiles for irregular patient trace at 1 cm amplitude with a plan MCS of 0.60.

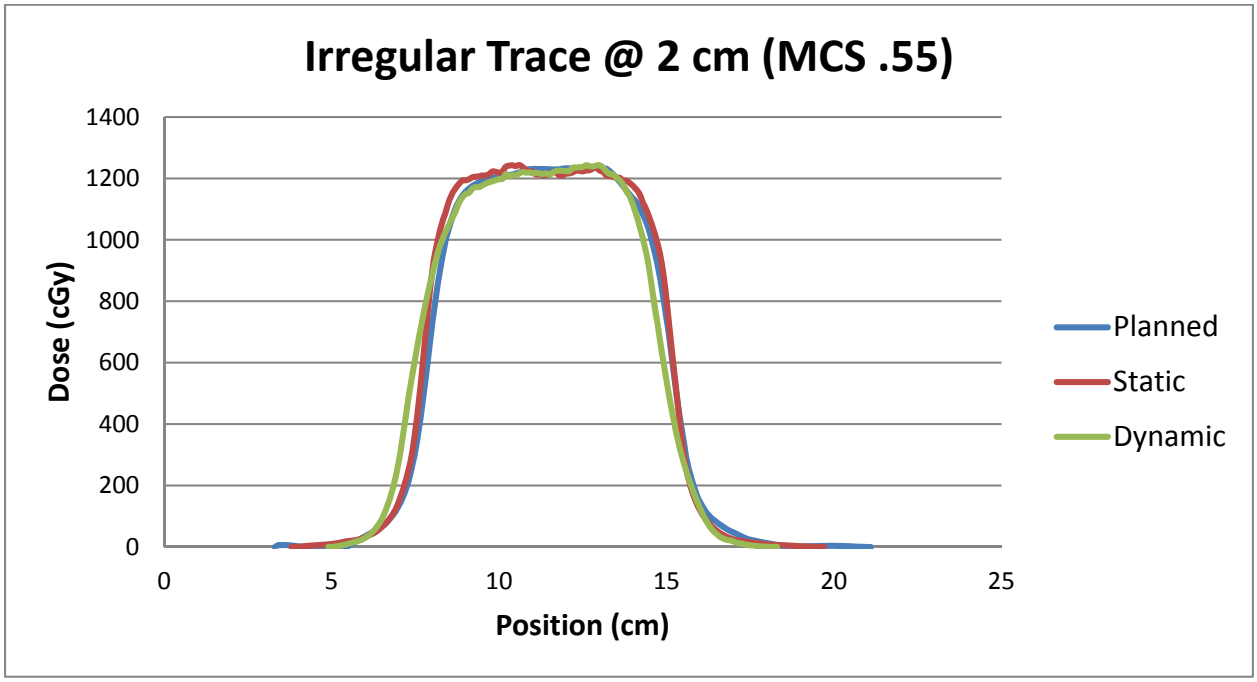

Figure 74: Longitudinal profiles for irregular patient trace at 2 cm amplitude with a plan MCS of 0.55.

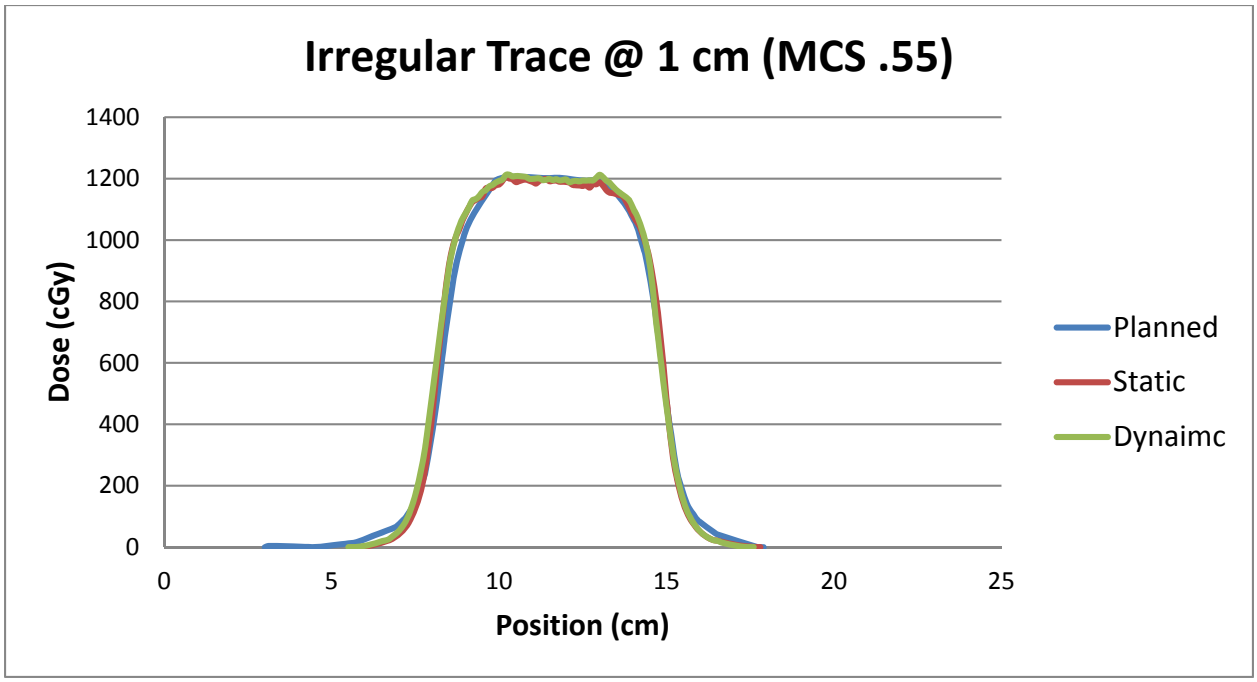

Figure 75: Longitudinal profiles for irregular patient trace at 1 cm amplitude with a plan MCS of 0.55.

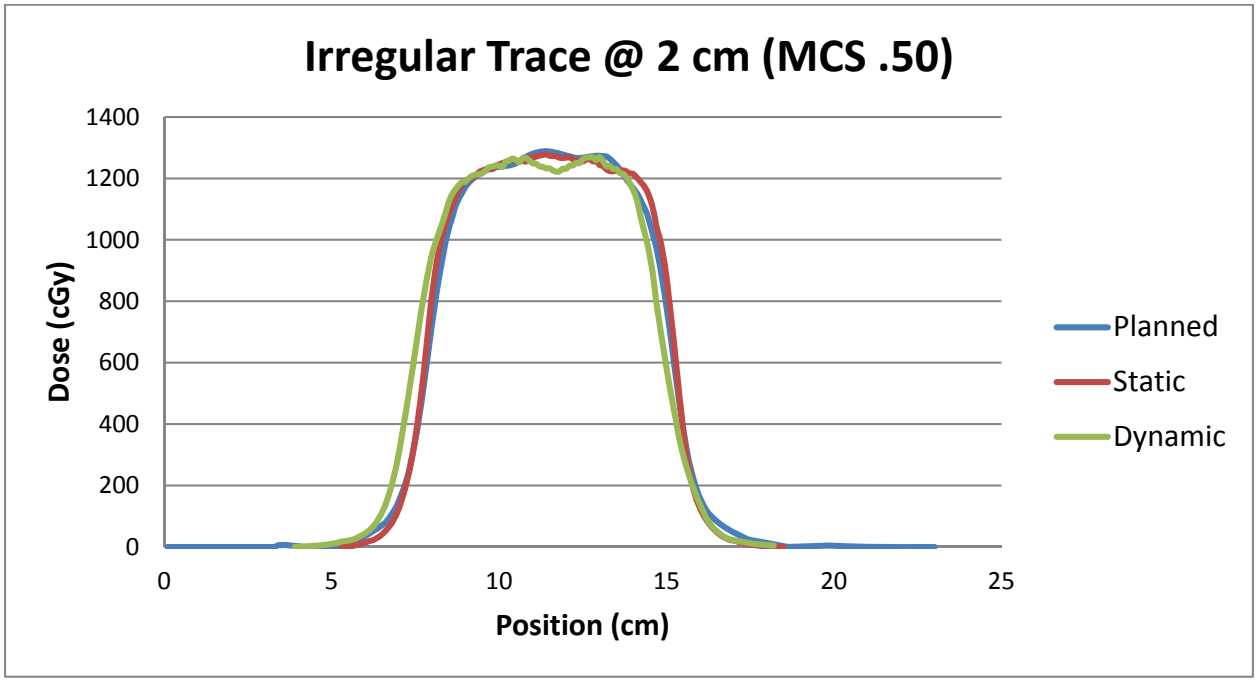

Figure 76: Longitudinal profiles for irregular patient trace at 2 cm amplitude with a plan MCS of 0.50.

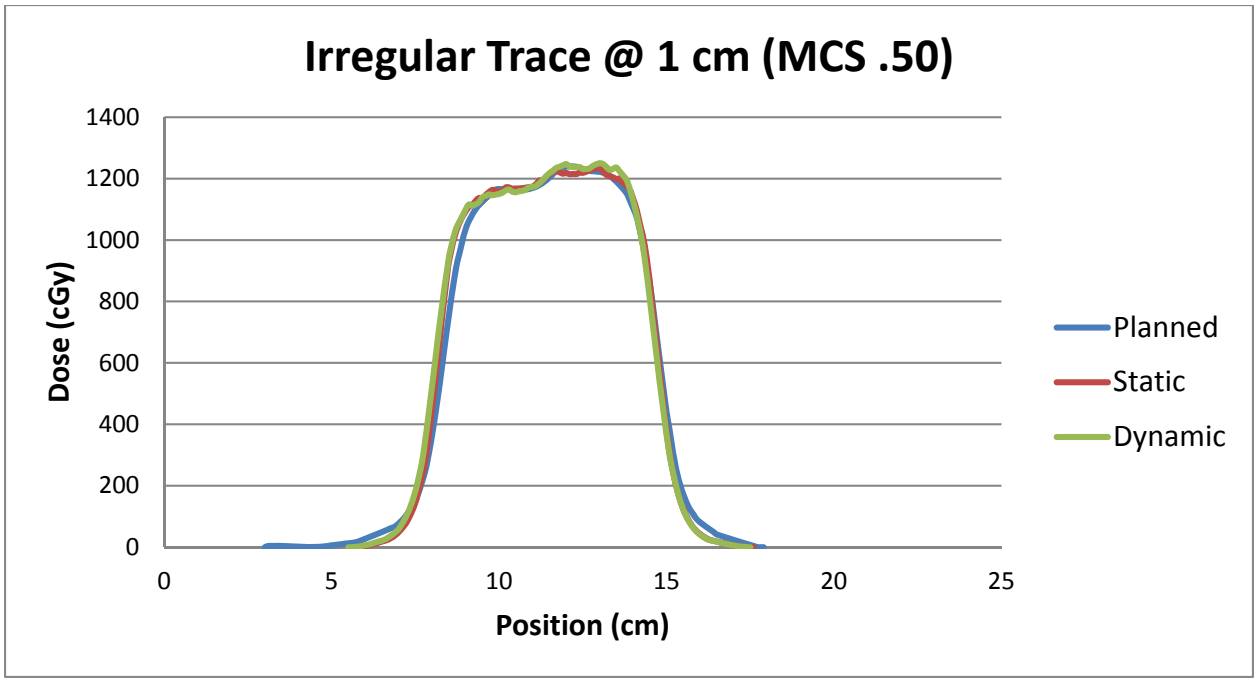

Figure 77: Longitudinal profiles for irregular patient trace at 1 cm amplitude with a plan MCS of 0.50.

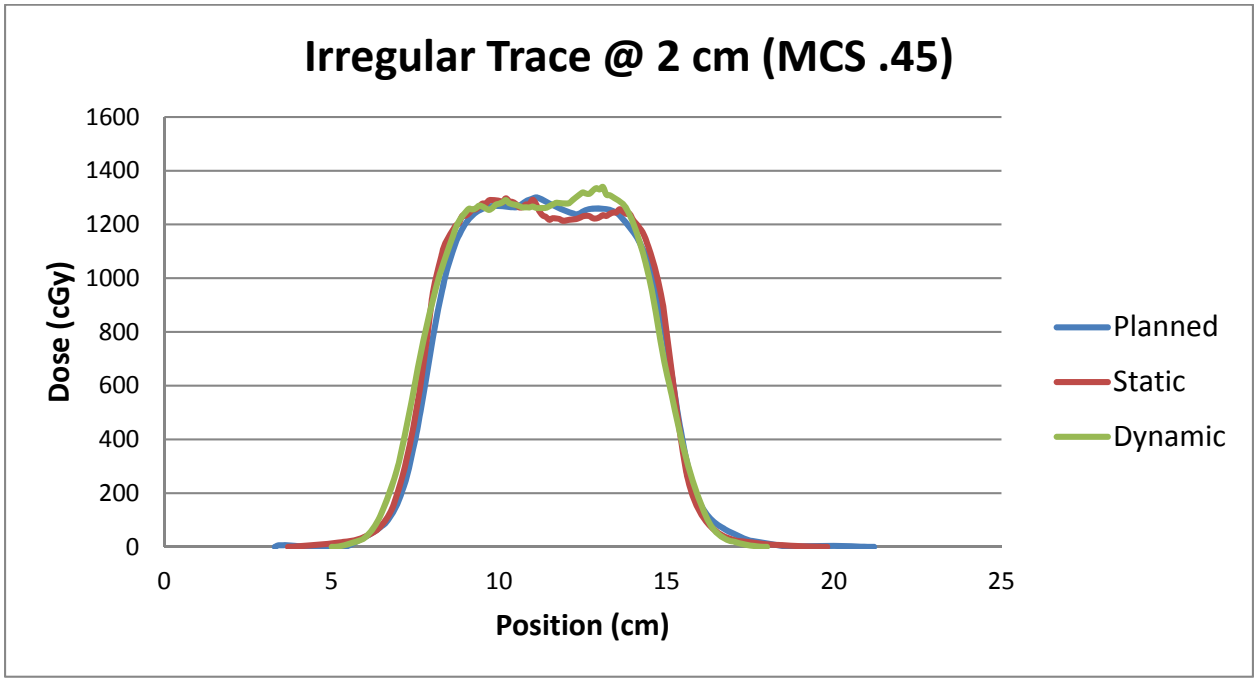

Figure 78: Longitudinal profiles for irregular patient trace at 2 cm amplitude with a plan MCS of 0.45.

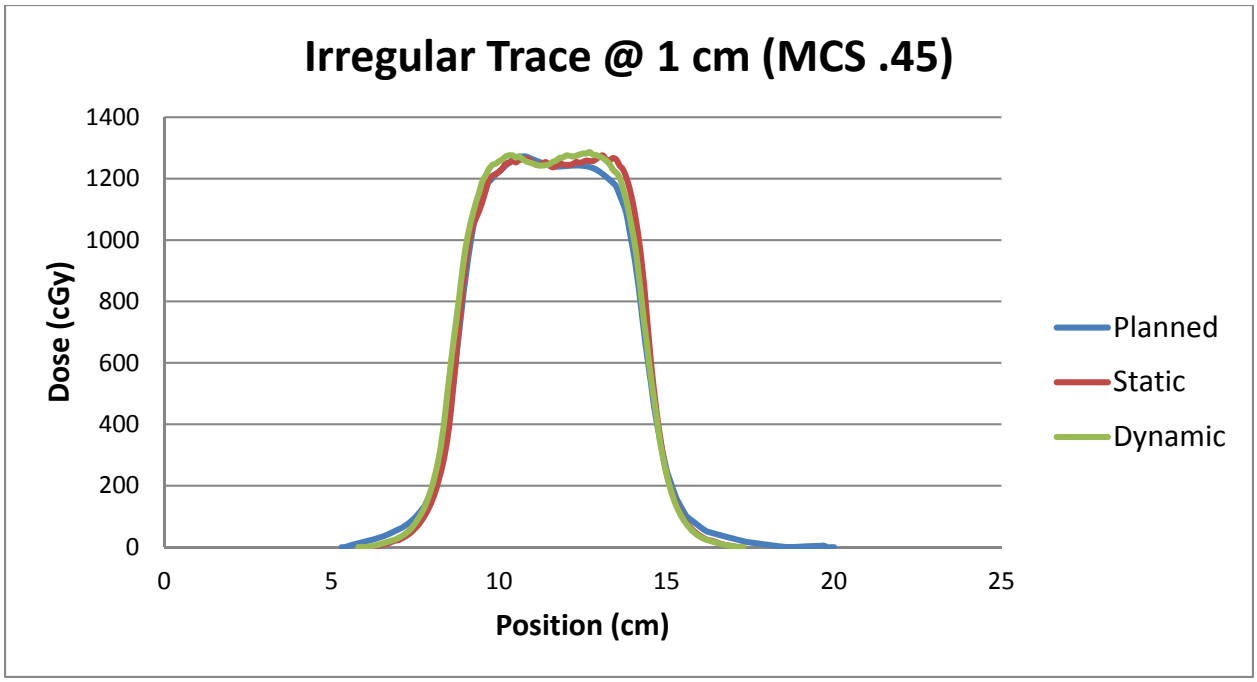

Figure 79: Longitudinal profiles for irregular patient trace at 1 cm amplitude with a plan MCS of 0.45.

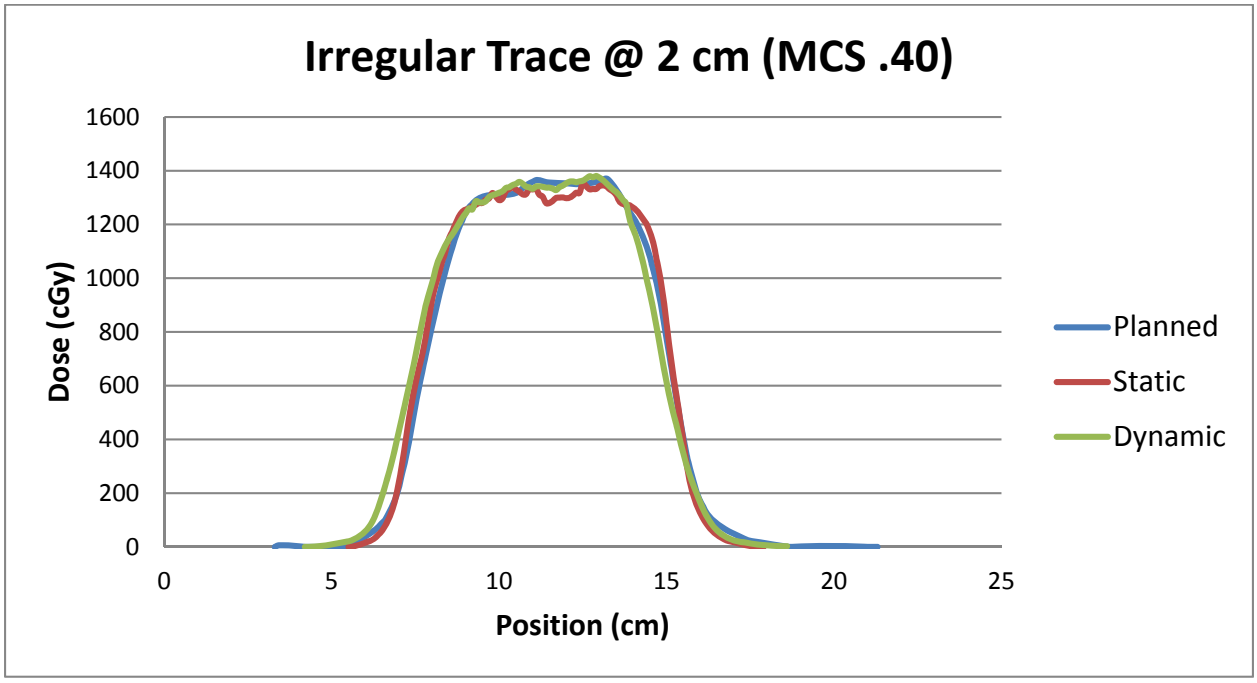

Figure 80: Longitudinal profiles for irregular patient trace at 2 cm amplitude with a plan MCS of 0.40.

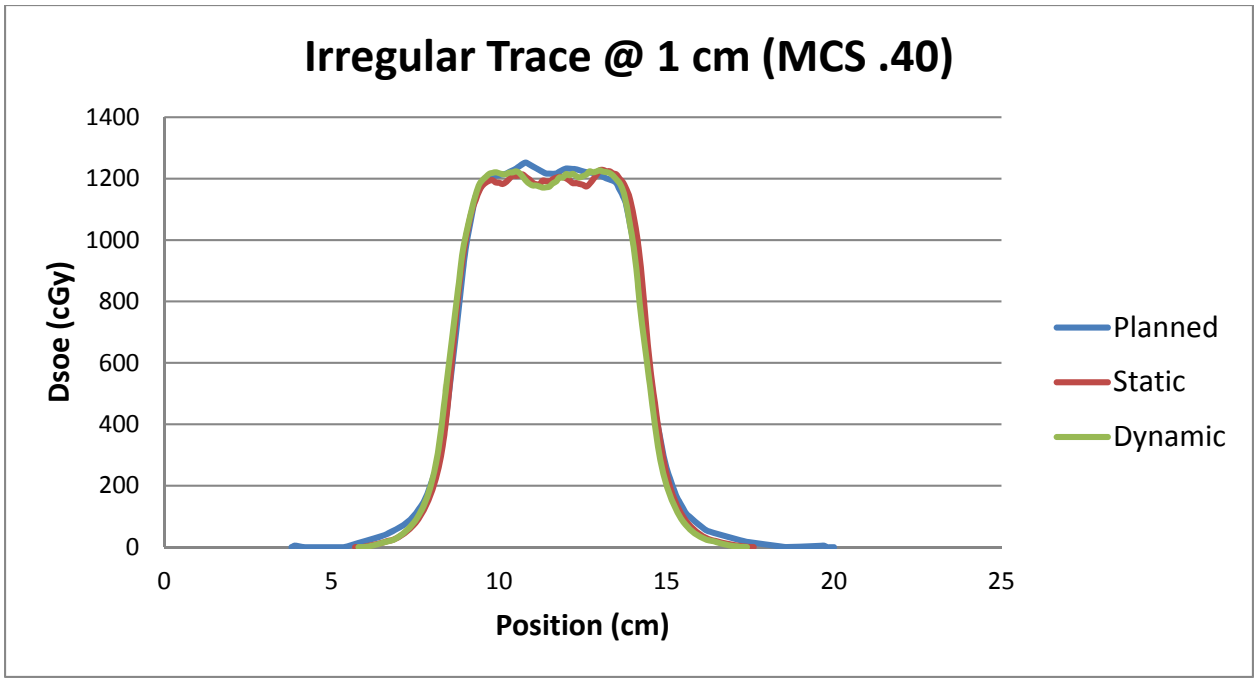

Figure 81: Longitudinal profiles for irregular patient trace at 1 cm amplitude with a plan MCS of 0.40.

Appendix B. Lateral Profiles

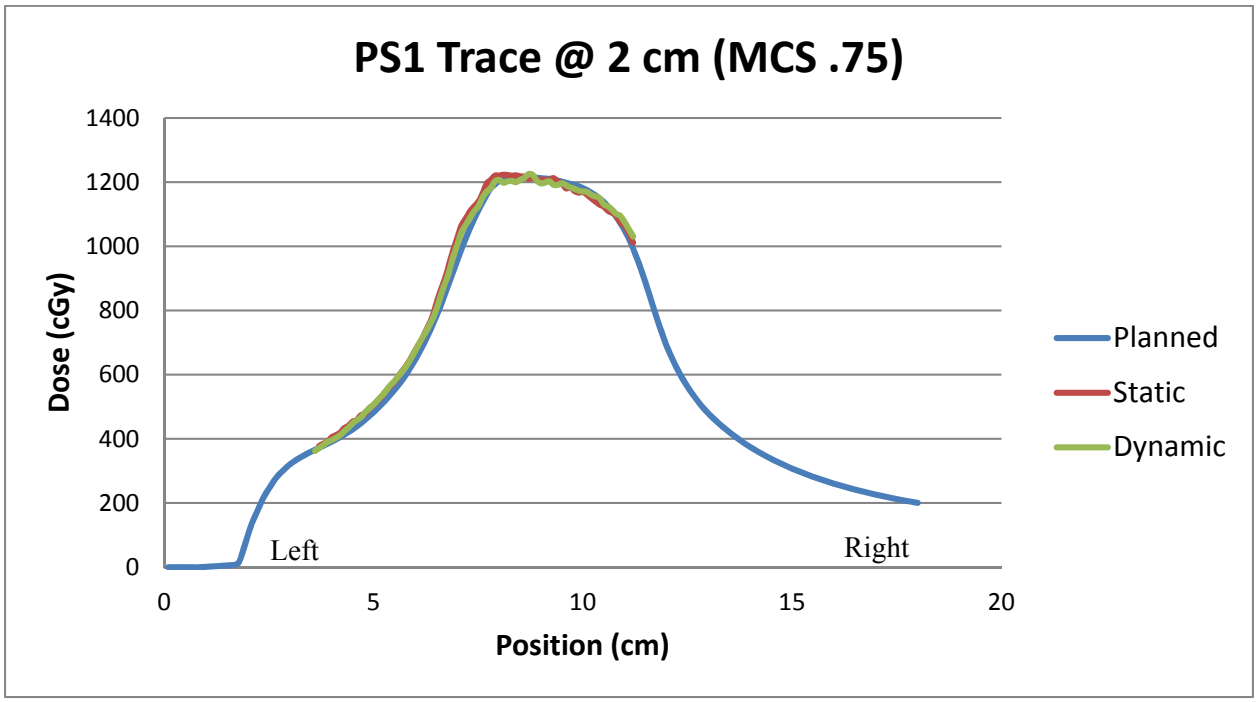

Figure 82: Lateral profiles for patient trace 1 at 2 cm amplitude with a plan MCS of 0.75.

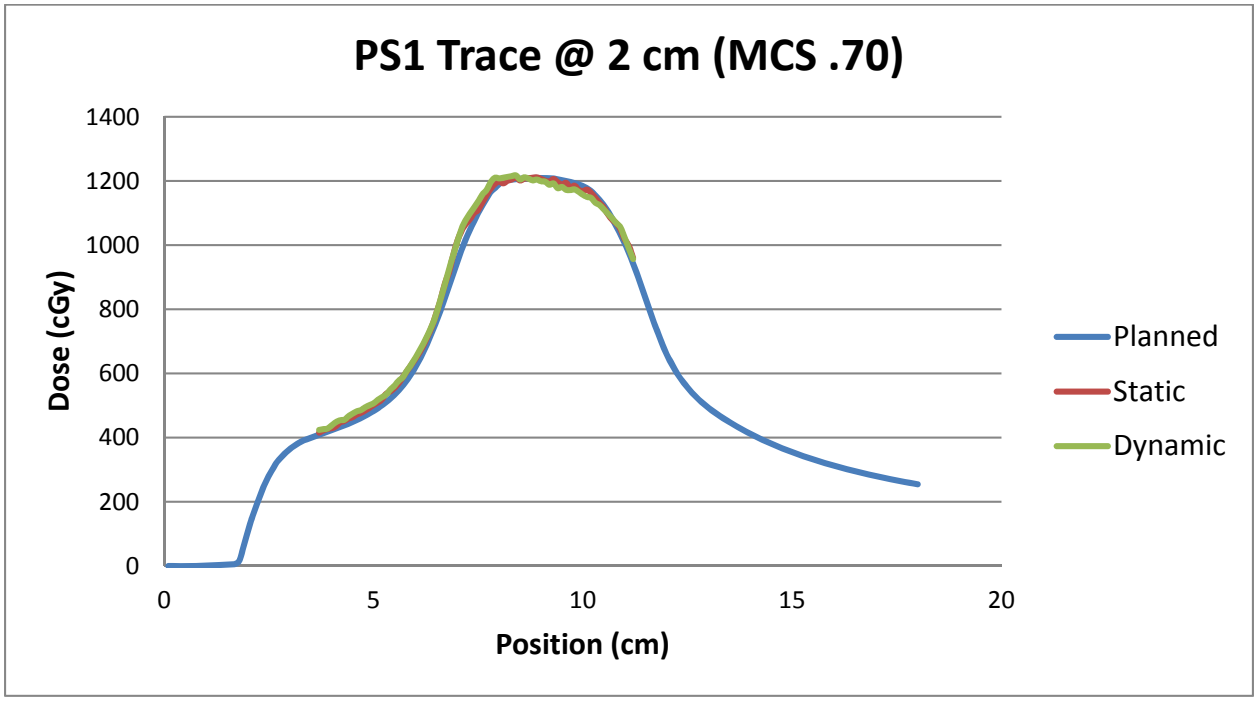

Figure 83: Lateral profiles for patient trace 1 at 2 cm amplitude with a plan MCS of 0.70.

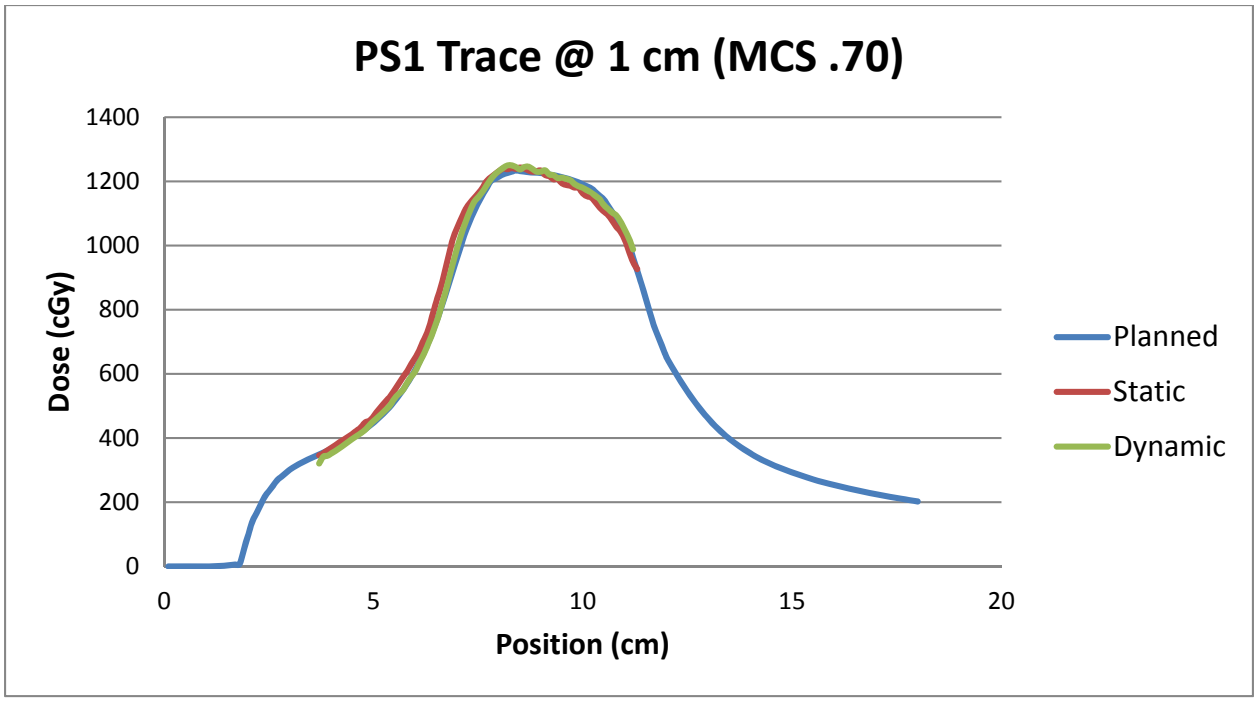

Figure 84: Lateral profiles for patient trace 1 at 1 cm amplitude with a plan MCS of 0.70.

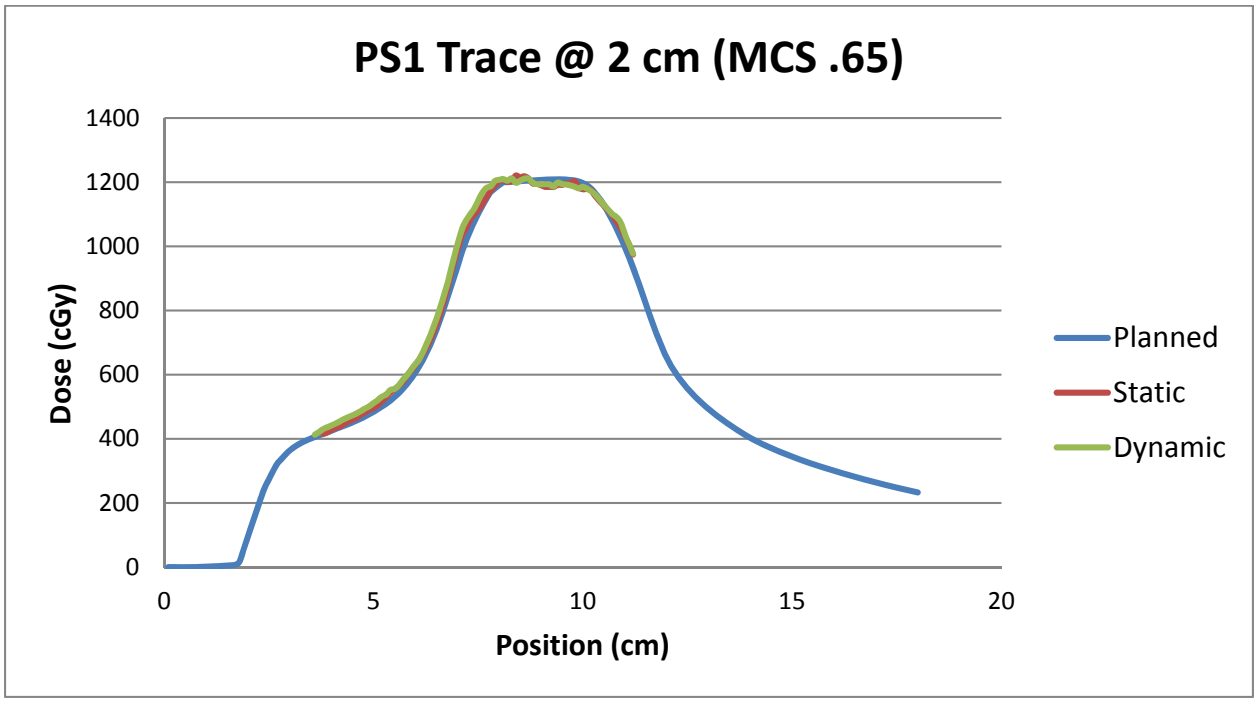

Figure 85: Lateral profiles for patient trace 1 at 2 cm amplitude with a plan MCS of 0.65.

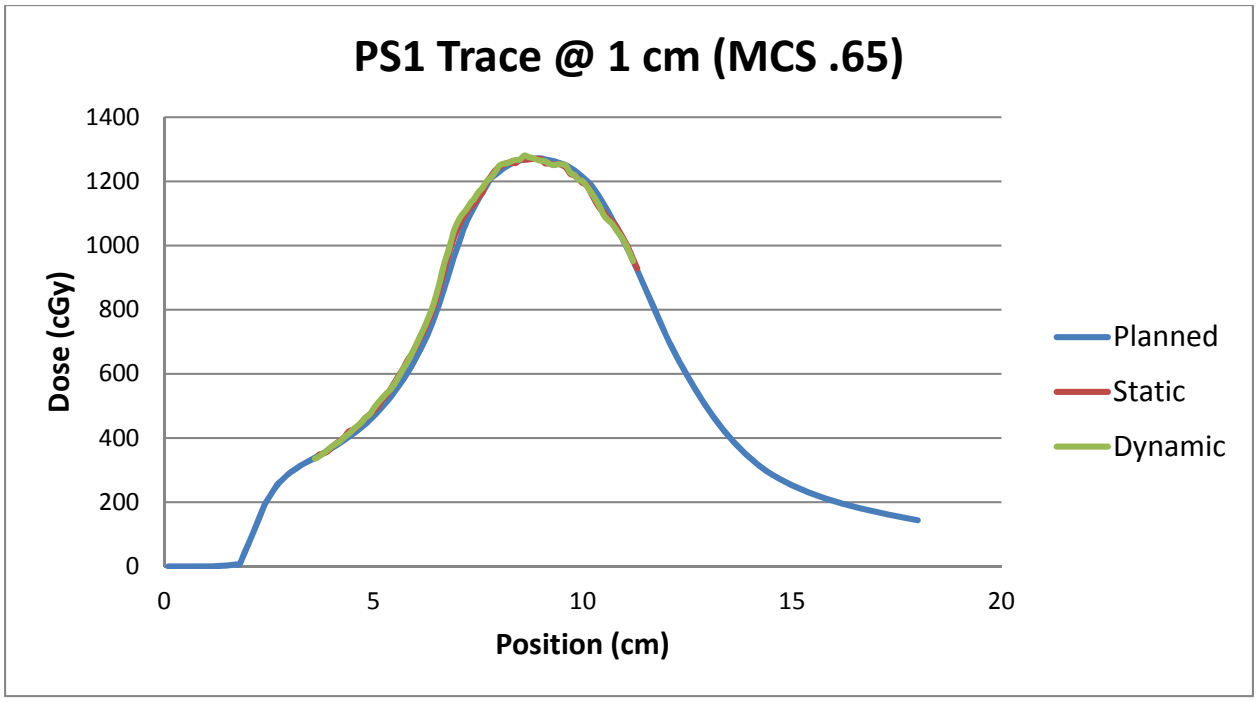

Figure 86: Lateral profiles for patient trace 1 at 1 cm amplitude with a plan MCS of 0.65.

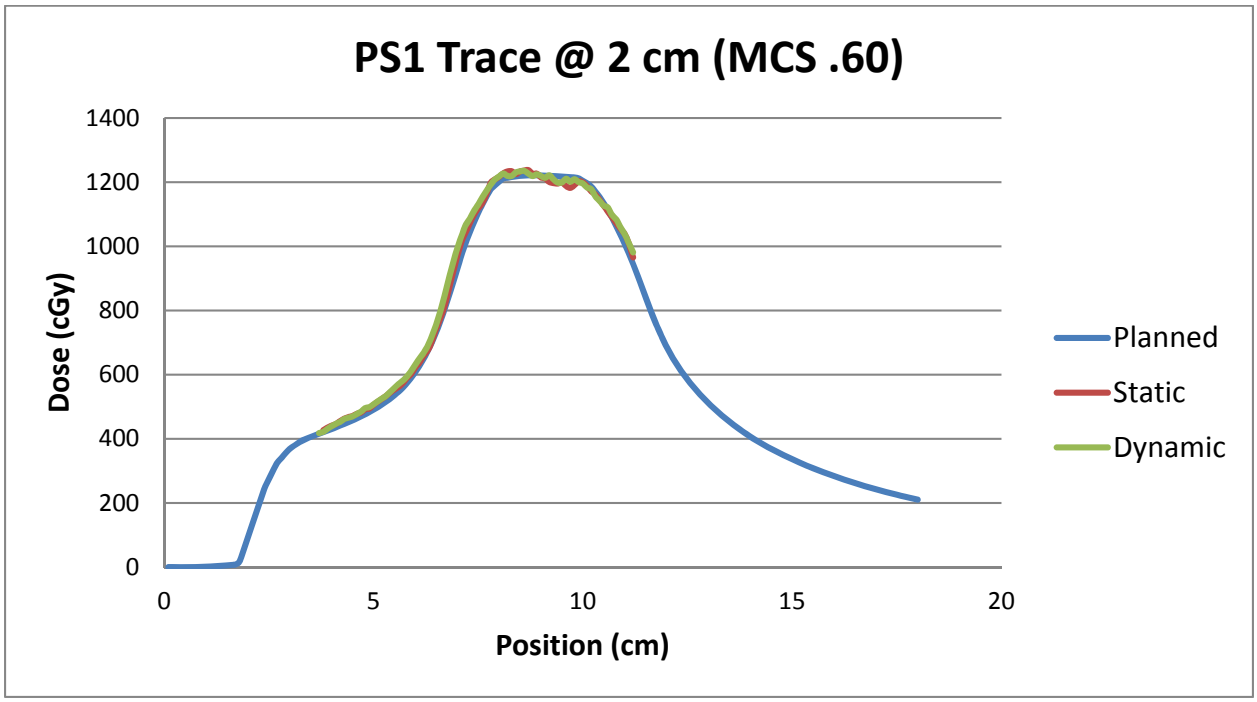

Figure 87: Lateral profiles for patient trace 1 at 2 cm amplitude with a plan MCS of 0.60.

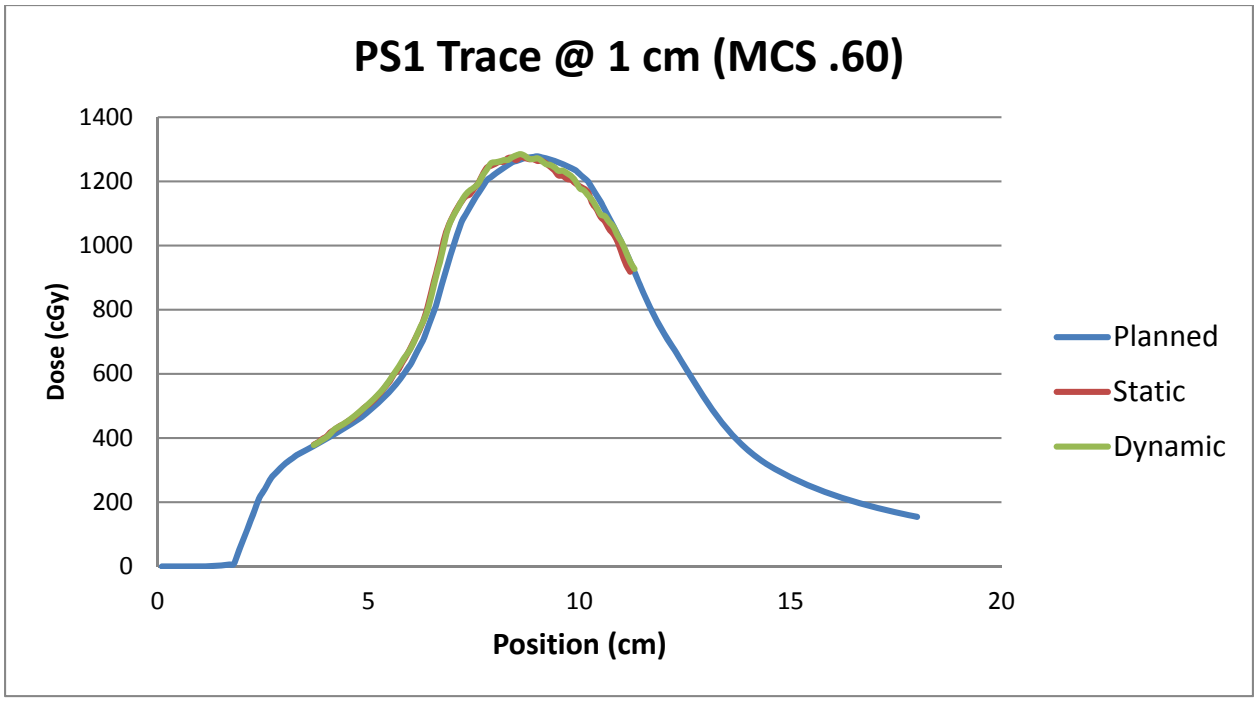

Figure 88: Lateral profiles for patient trace 1 at 1 cm amplitude with a plan MCS of 0.60.

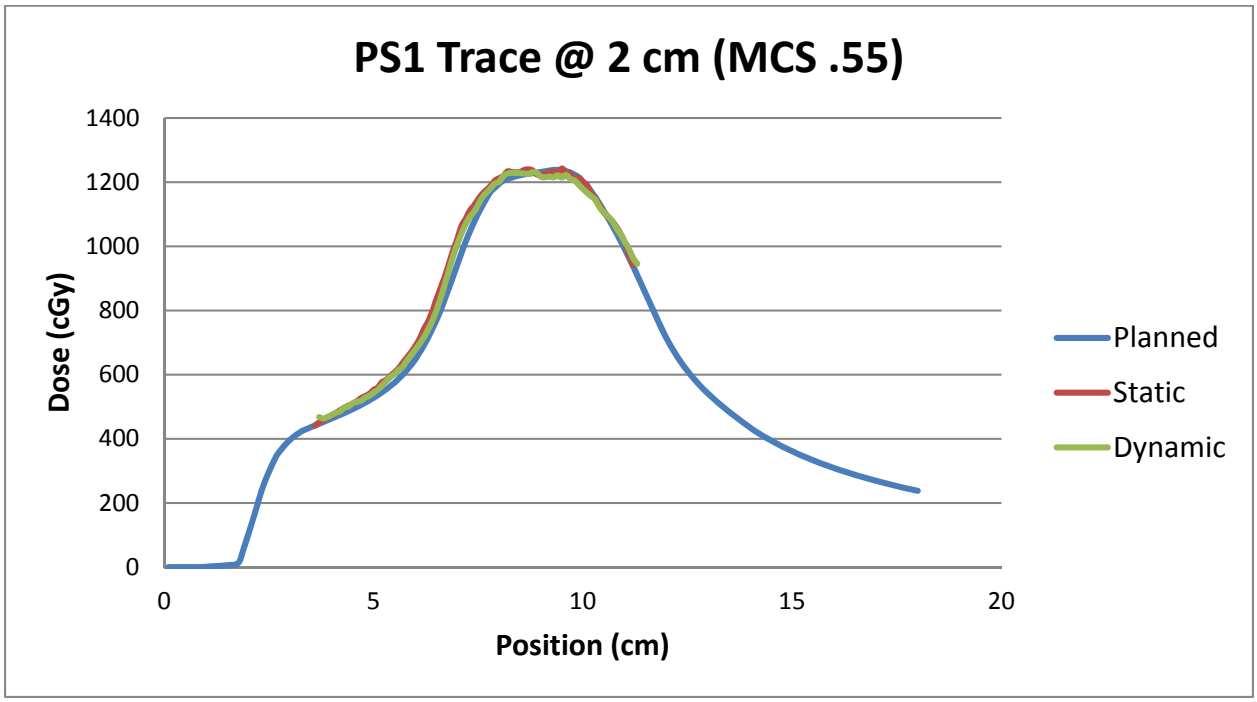

Figure 89: Lateral profiles for patient trace 1 at 2 cm amplitude with a plan MCS of 0.55.

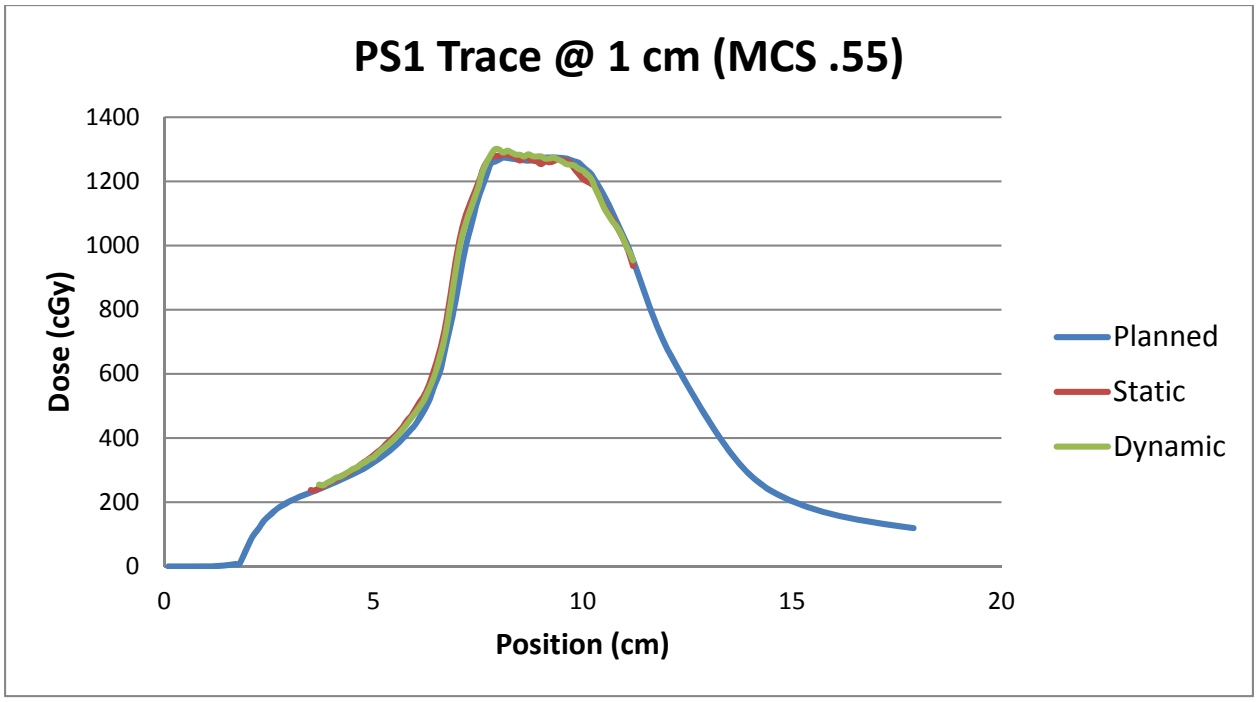

Figure 90: Lateral profiles for patient trace 1 at 1 cm amplitude with a plan MCS of 0.55.

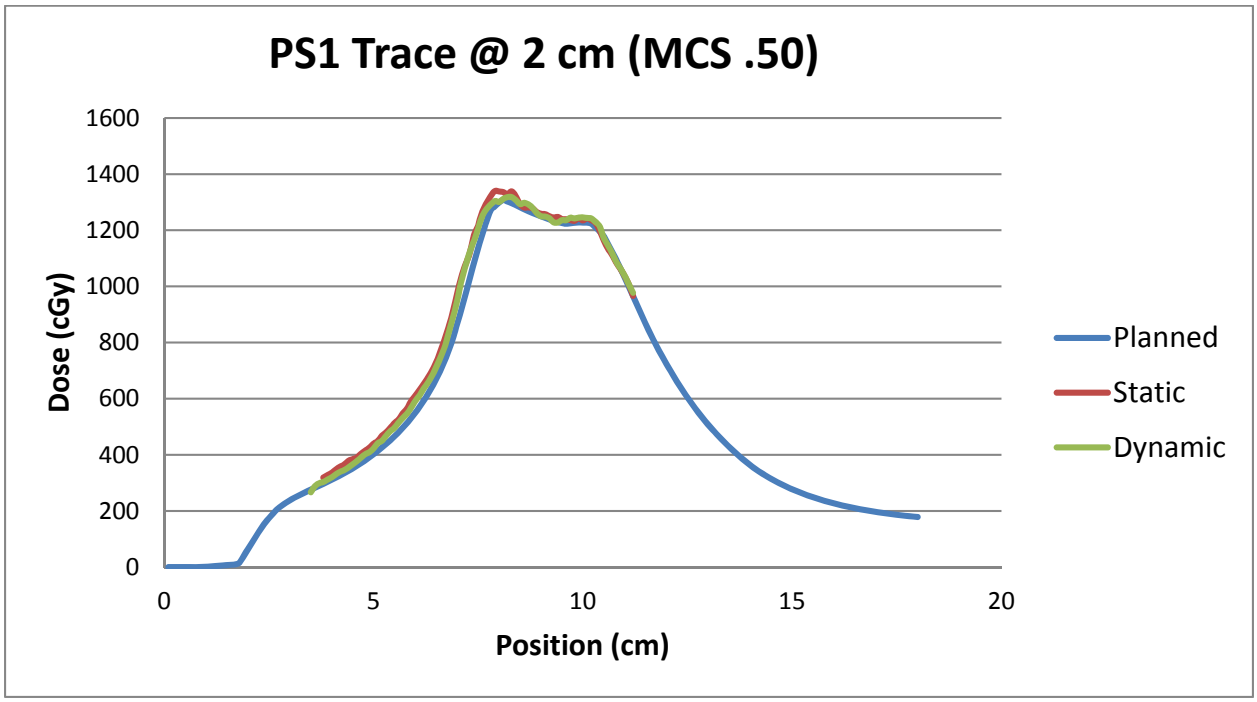

Figure 91: Lateral profiles for patient trace 1 at 2 cm amplitude with a plan MCS of 0.50.

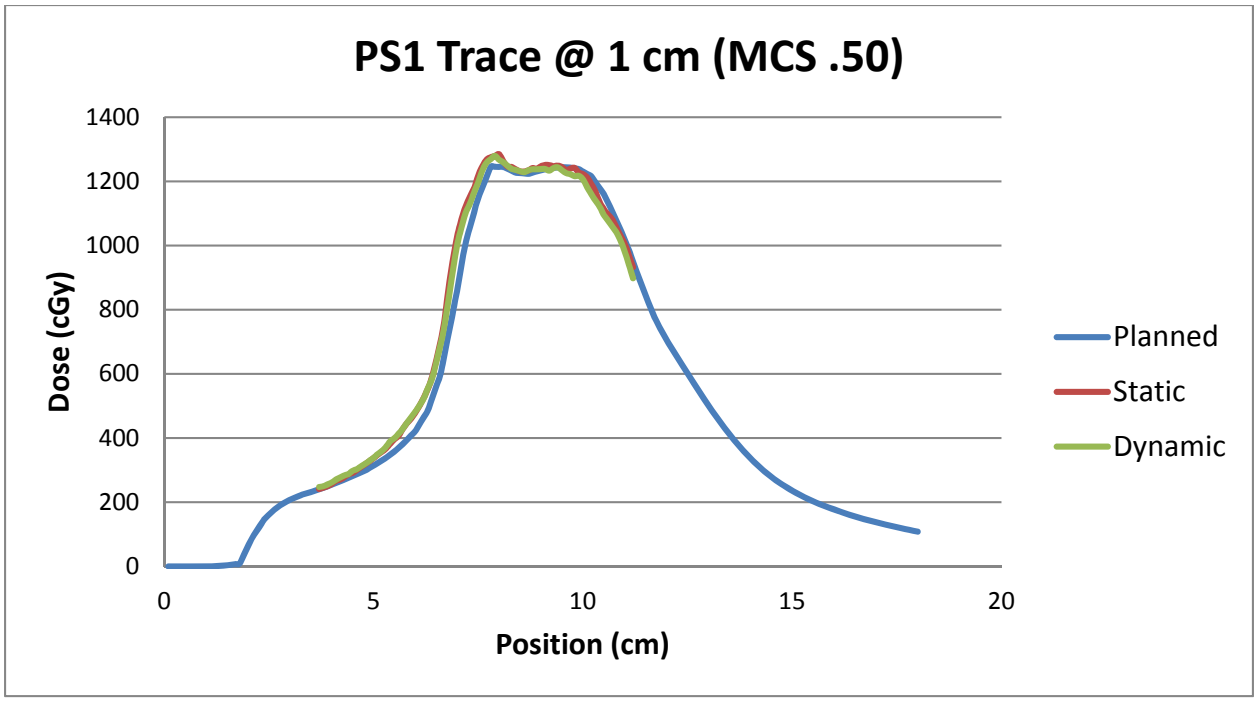

Figure 92: Lateral profiles for patient trace 1 at 1 cm amplitude with a plan MCS of 0.50.

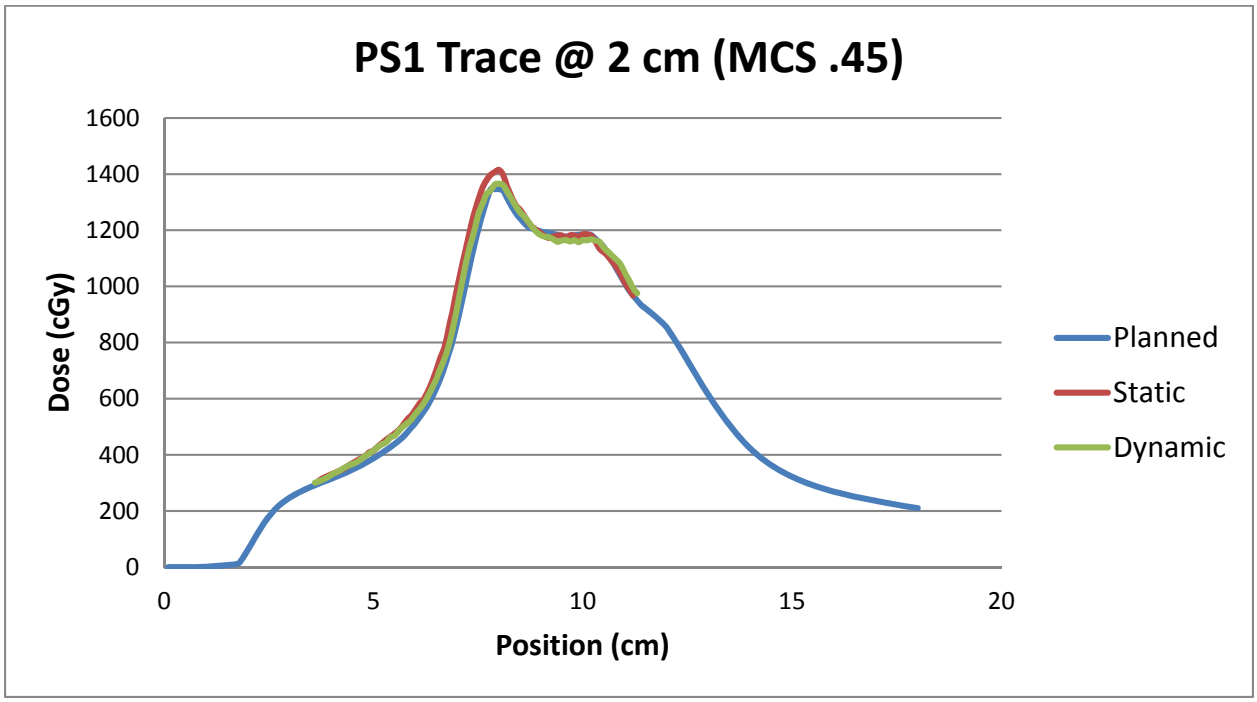

Figure 93: Lateral profiles for patient trace 1 at 2 cm amplitude with a plan MCS of 0.45.

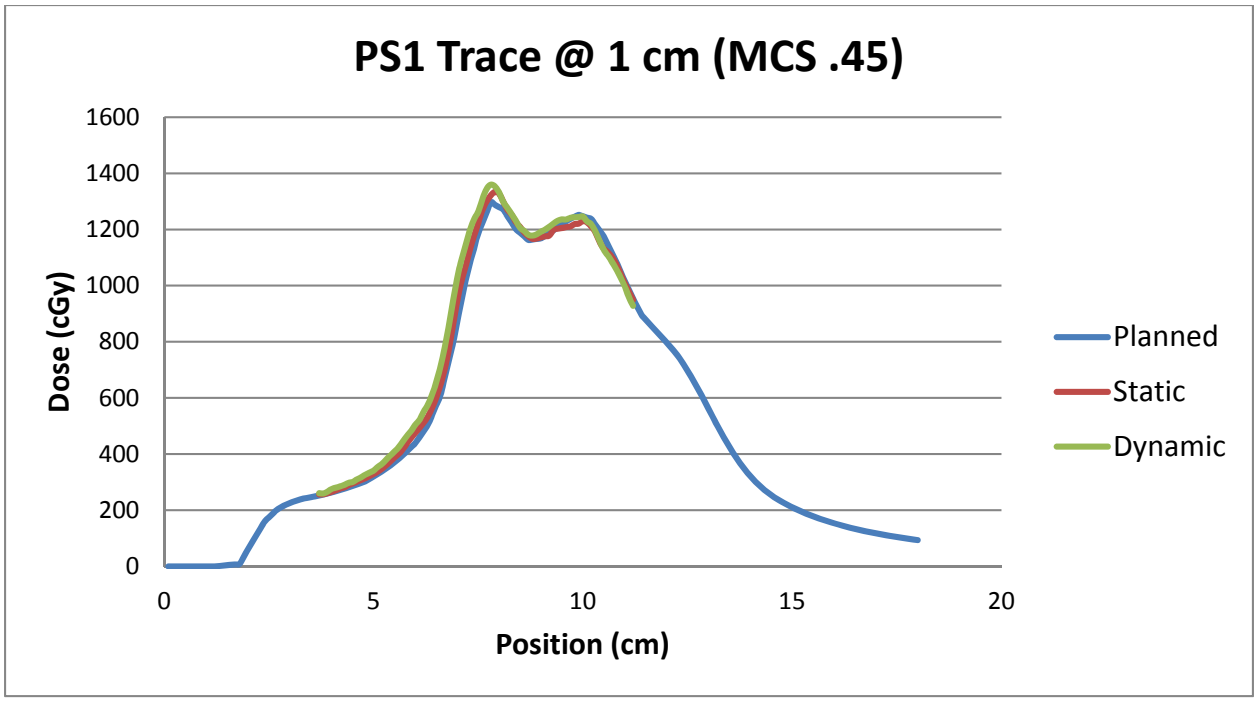

Figure 94: Lateral profiles for patient trace 1 at 1 cm amplitude with a plan MCS of 0.45.

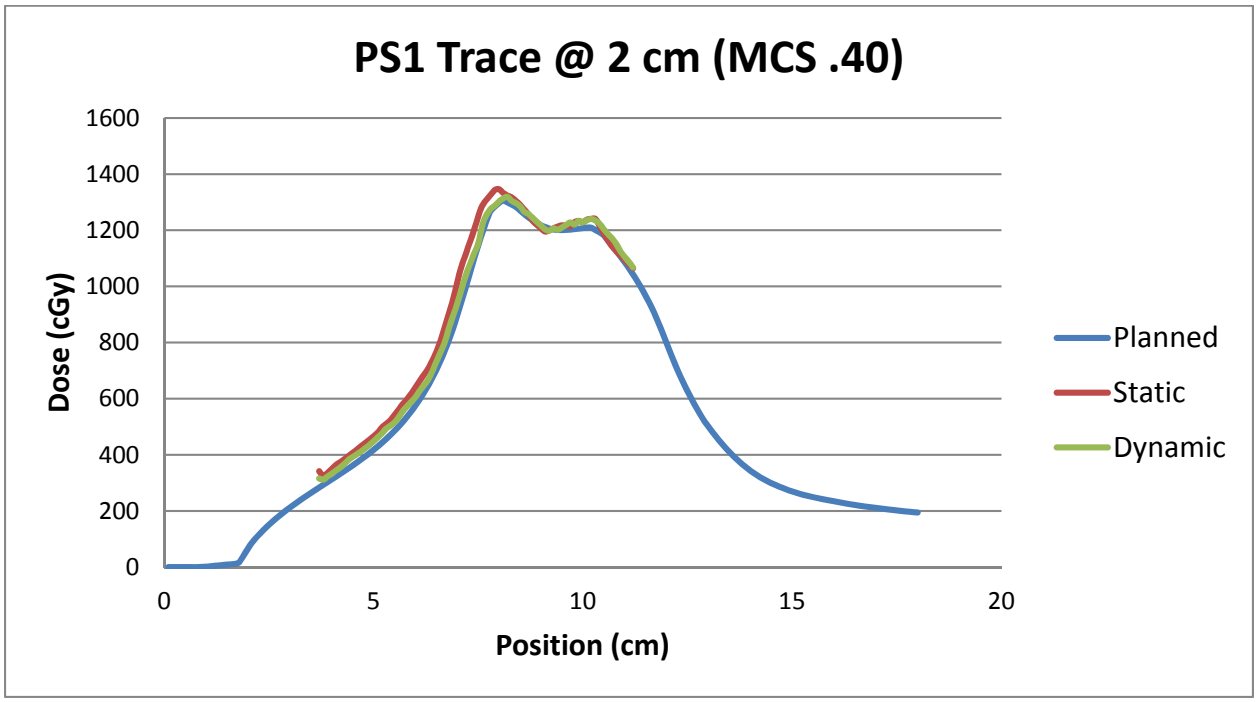

Figure 95: Lateral profiles for patient trace 1 at 2 cm amplitude with a plan MCS of 0.40.

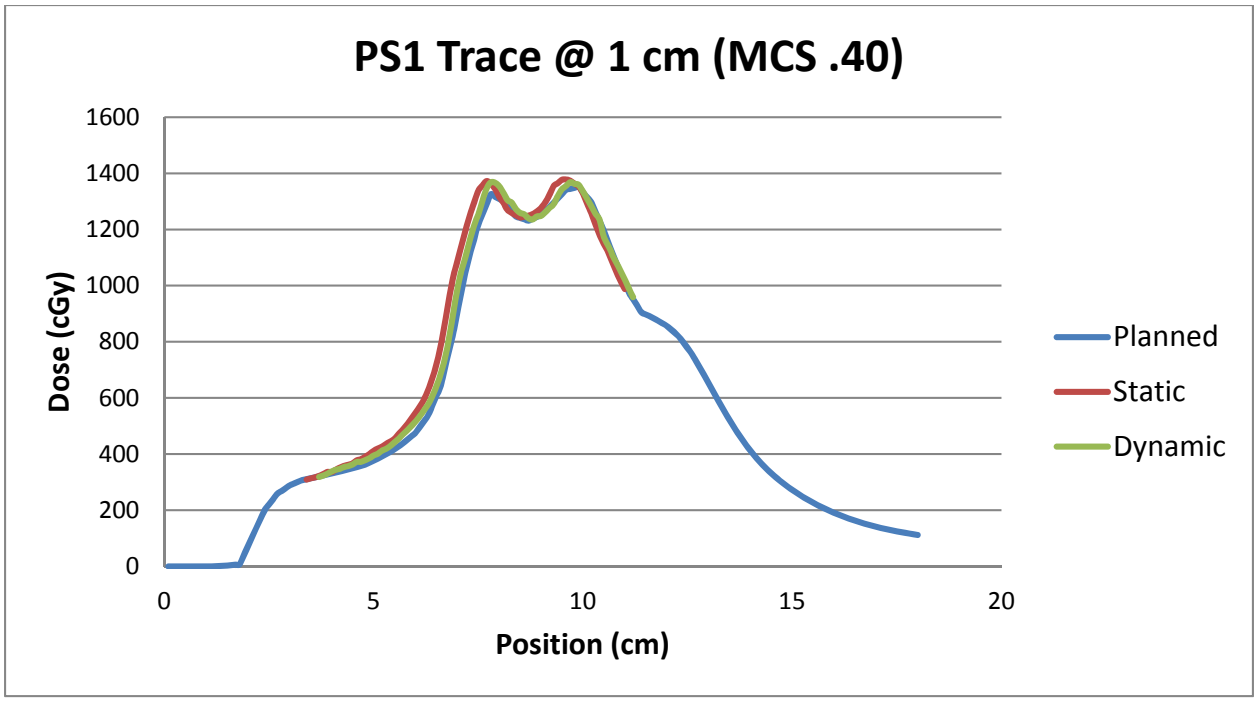

Figure 96: Lateral profiles for patient trace 1 at 1 cm amplitude with a plan MCS of 0.40.

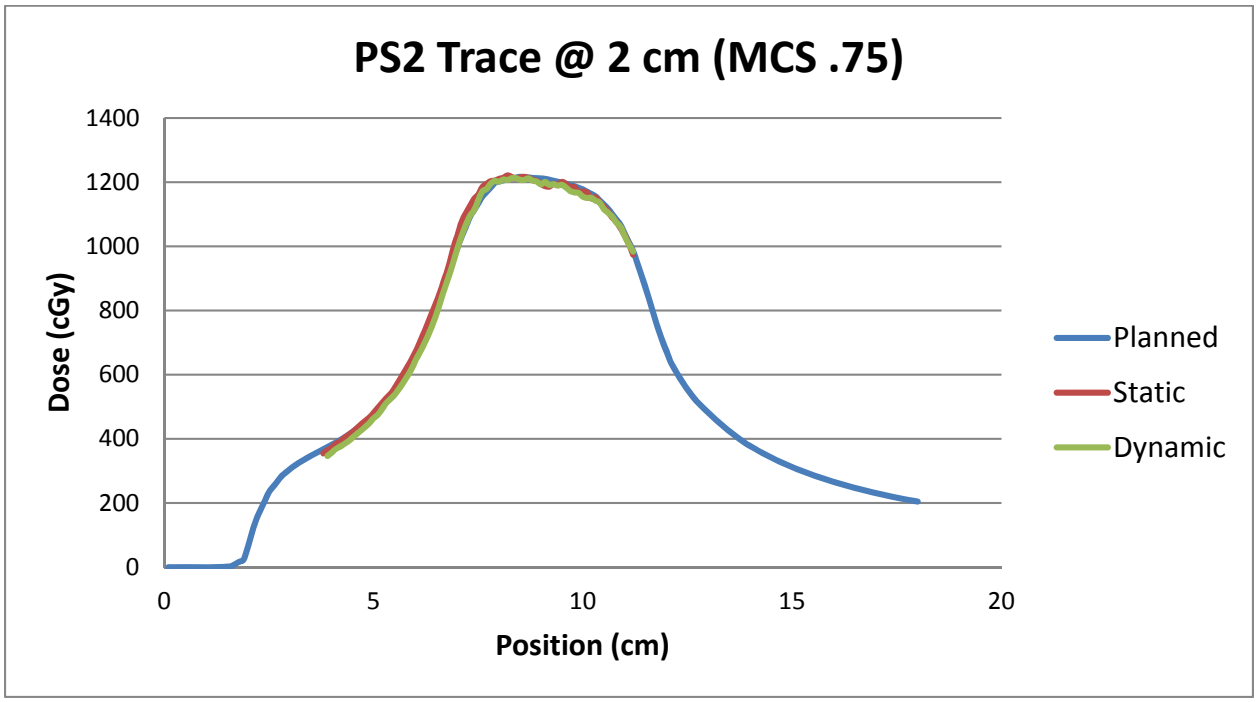

Figure 97: Lateral profiles for patient trace 2 at 2 cm amplitude with a plan MCS of 0.75.

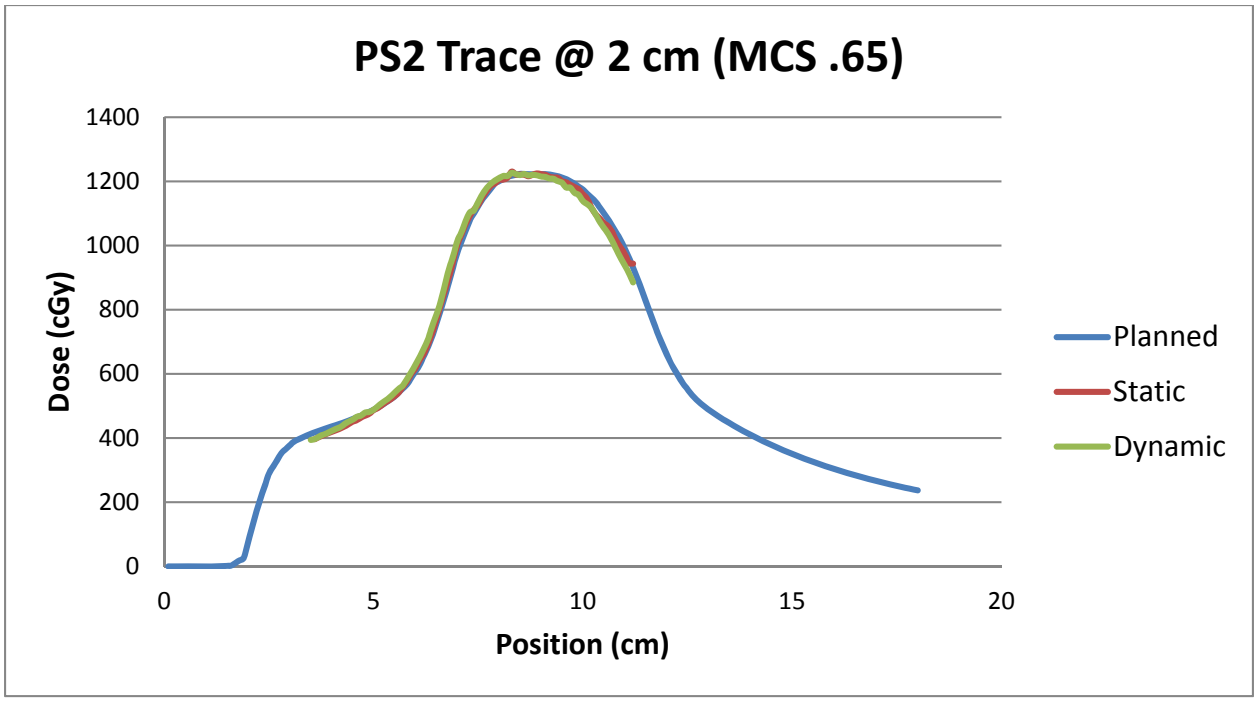

Figure 98: Lateral profiles for patient trace 2 at 2 cm amplitude with a plan MCS of 0.65.

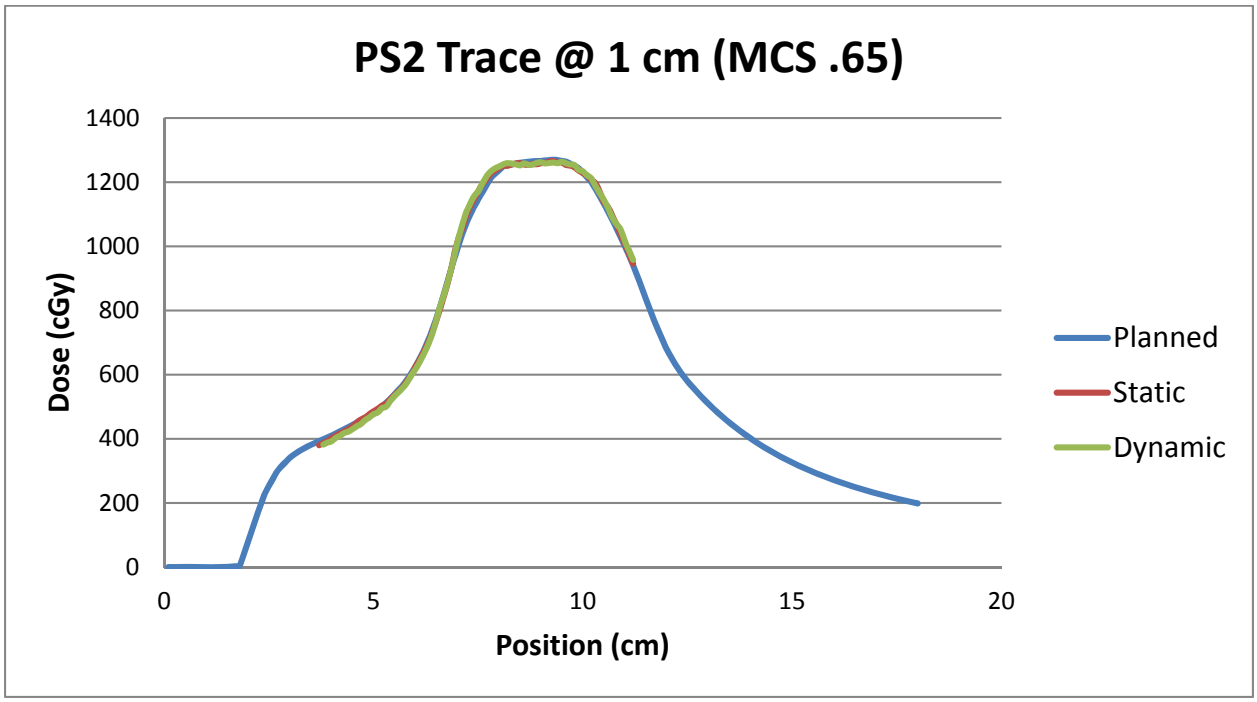

Figure 99: Lateral profiles for patient trace 2 at 1 cm amplitude with a plan MCS of 0.65.

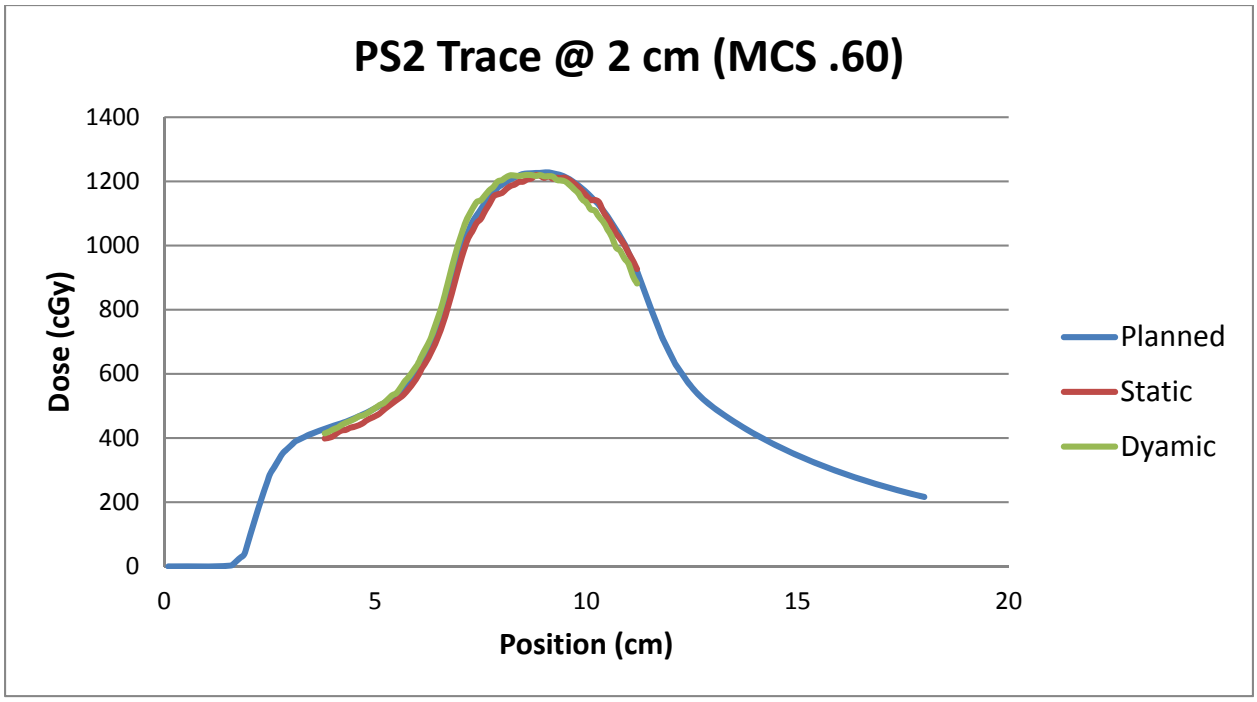

Figure 100: Lateral profiles for patient trace 2 at 2 cm amplitude with a plan MCS of 0.60.

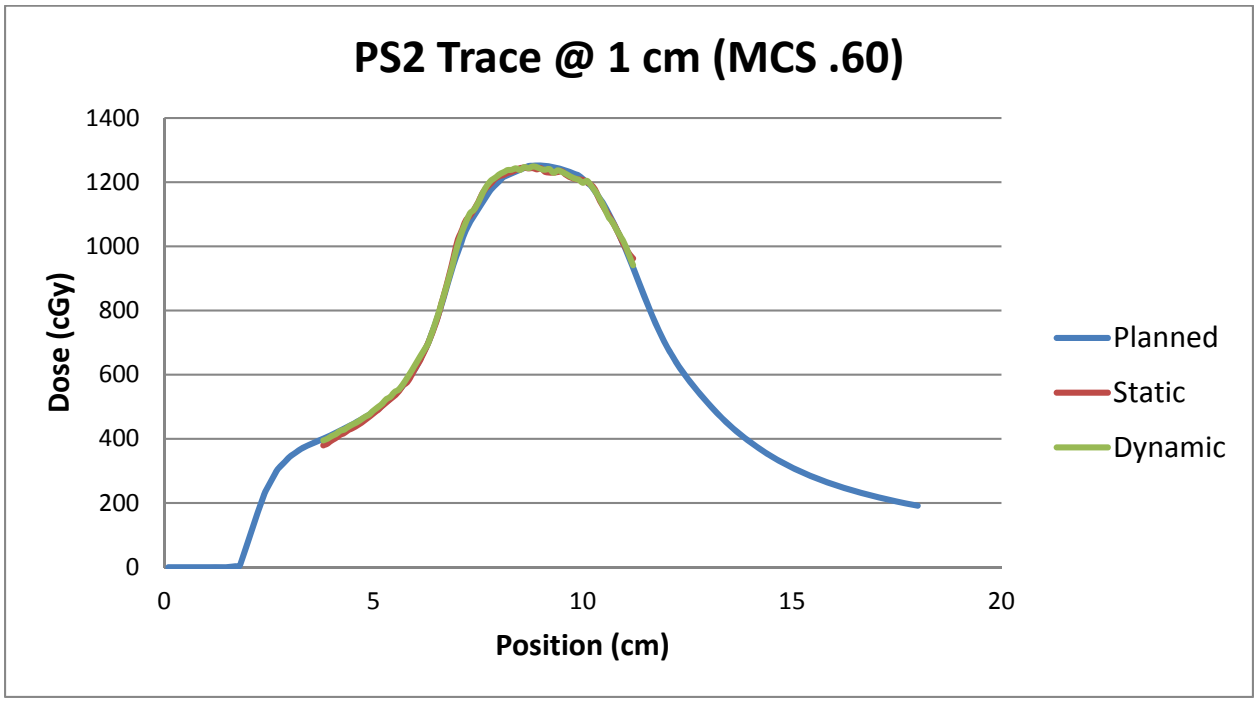

Figure 101: Lateral profiles for patient trace 2 at 1 cm amplitude with a plan MCS of 0.60.

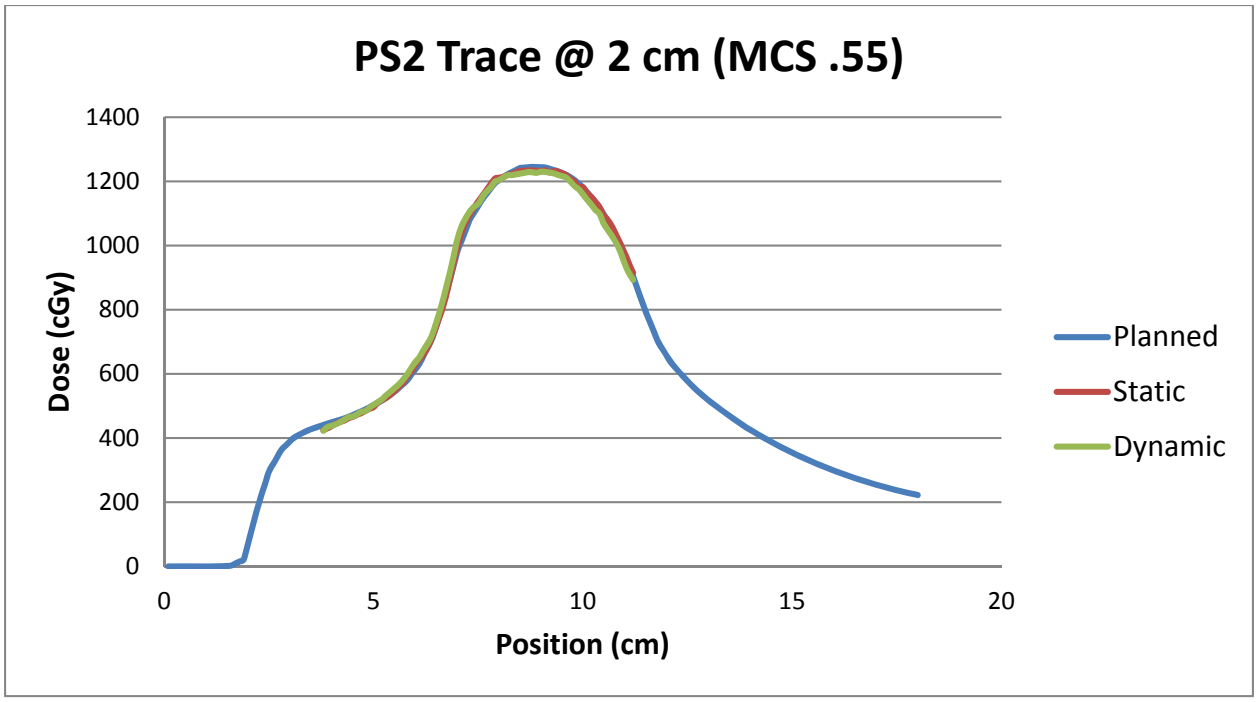

Figure 102: Lateral profiles for patient trace 2 at 2 cm amplitude with a plan MCS of 0.55.

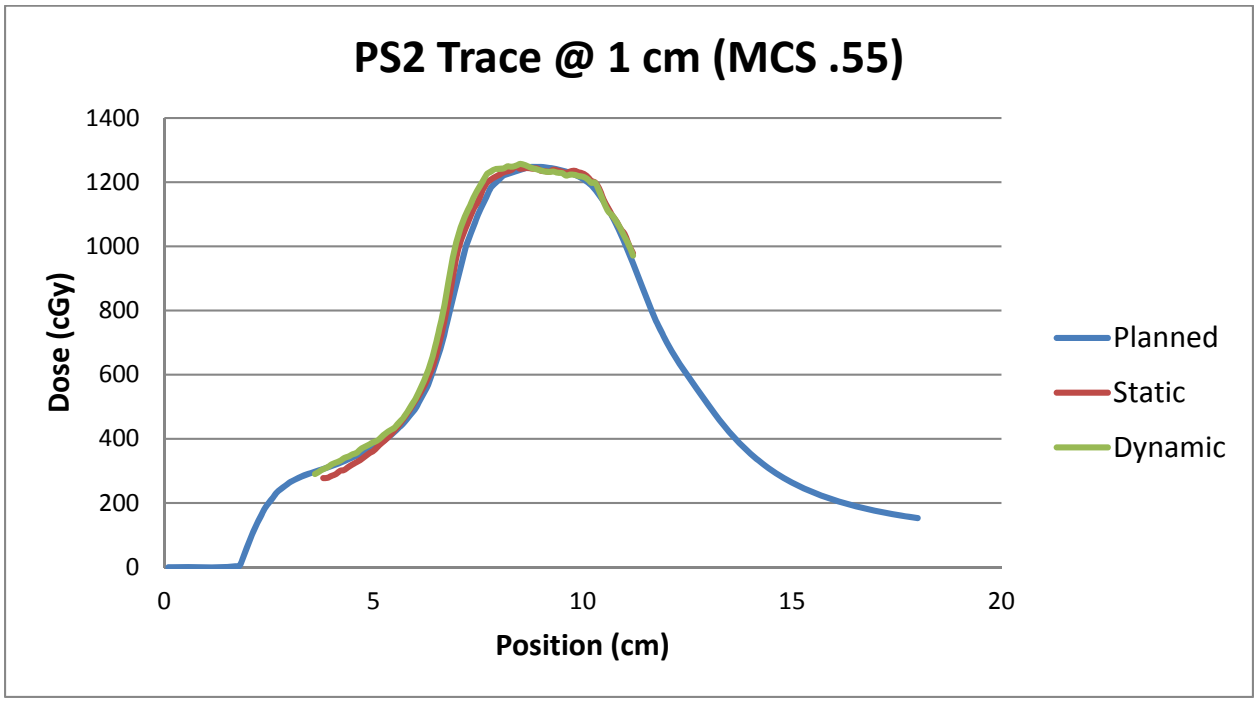

Figure 103: Lateral profiles for patient trace 2 at 1 cm amplitude with a plan MCS of 0.55.

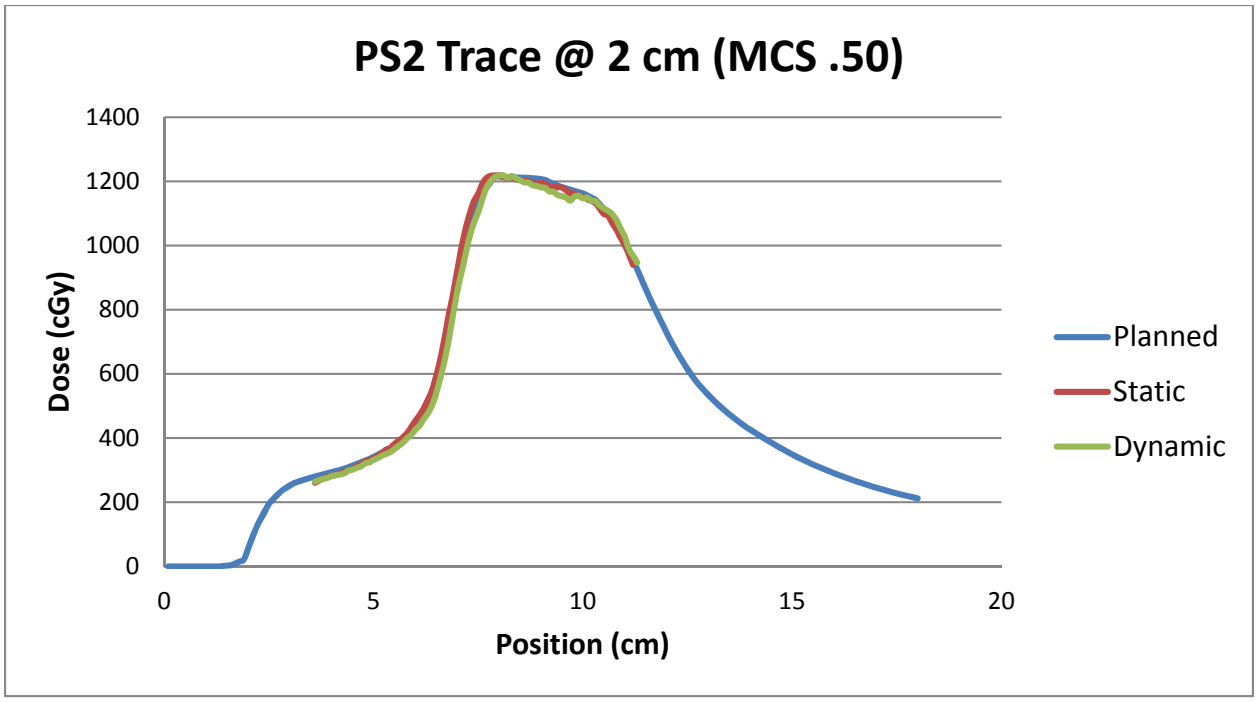

Figure 104: Lateral profiles for patient trace 2 at 2 cm amplitude with a plan MCS of 0.50.

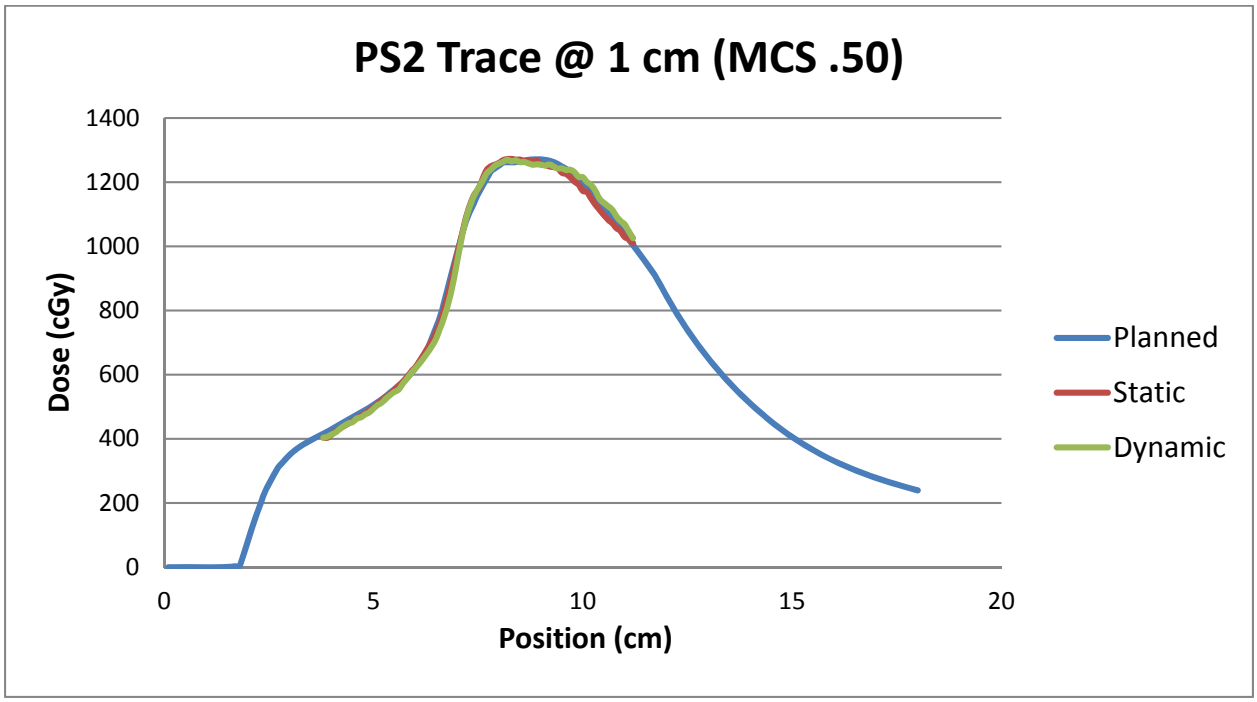

Figure 105: Lateral profiles for patient trace 2 at 1 cm amplitude with a plan MCS of 0.50.

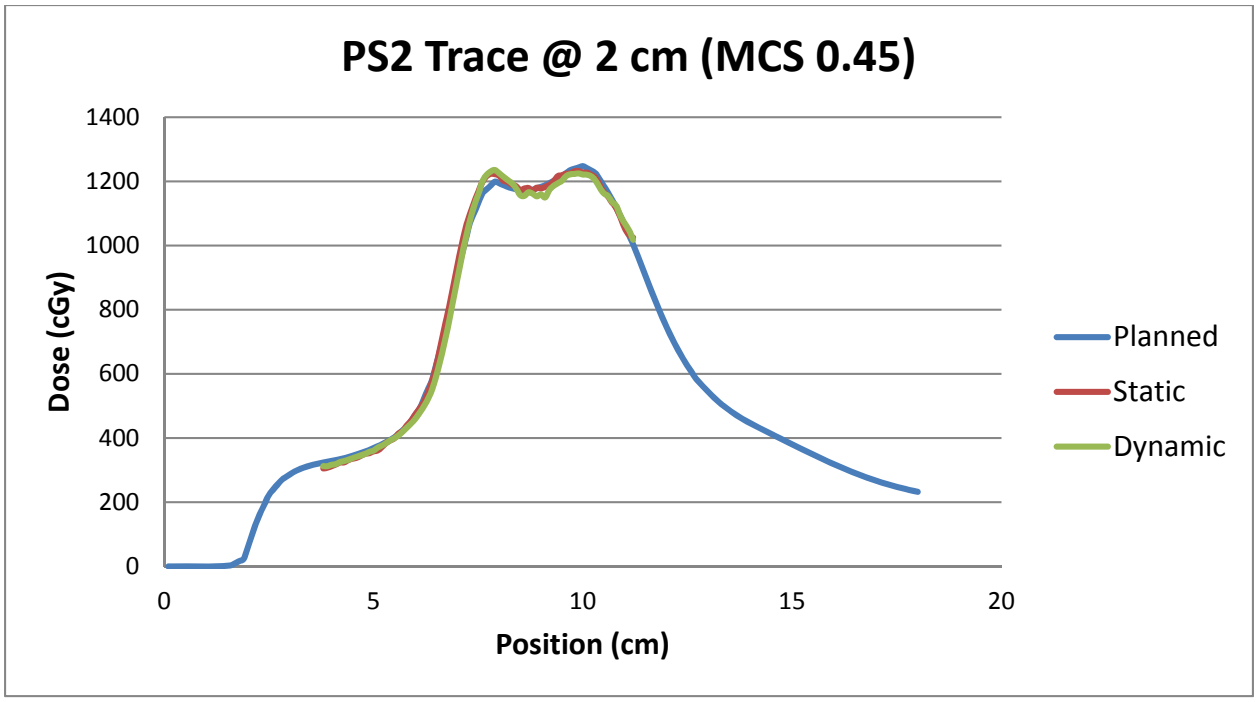

Figure 106: Lateral profiles for patient trace 2 at 2 cm amplitude with a plan MCS of 0.45.

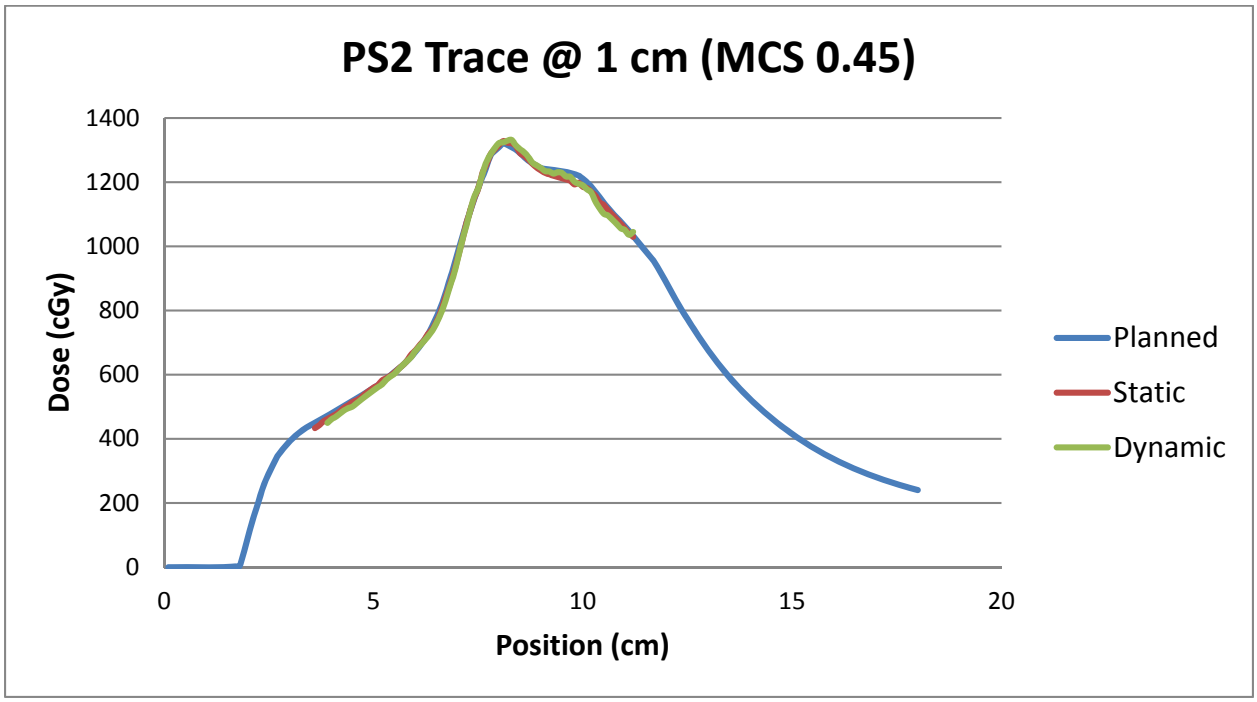

Figure 107: Lateral profiles for patient trace 2 at 1 cm amplitude with a plan MCS of 0.45.

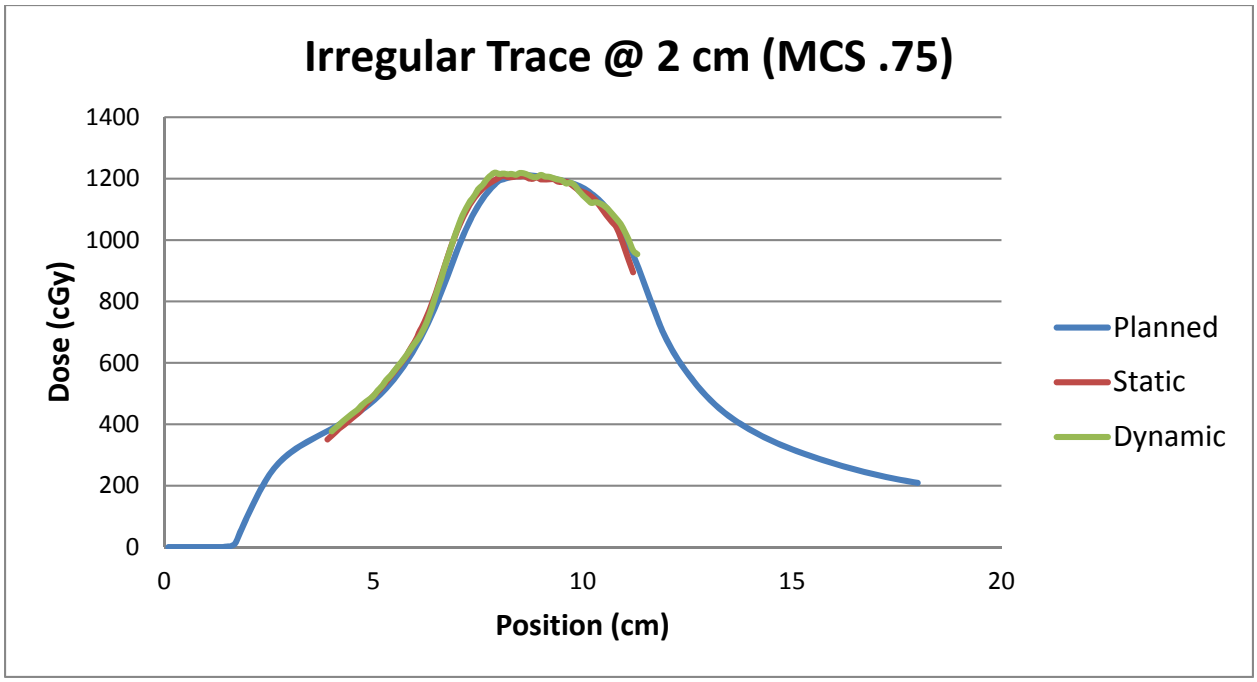

Figure 108: Lateral profiles for irregular patient trace at 2 cm amplitude with a plan MCS of 0.75.

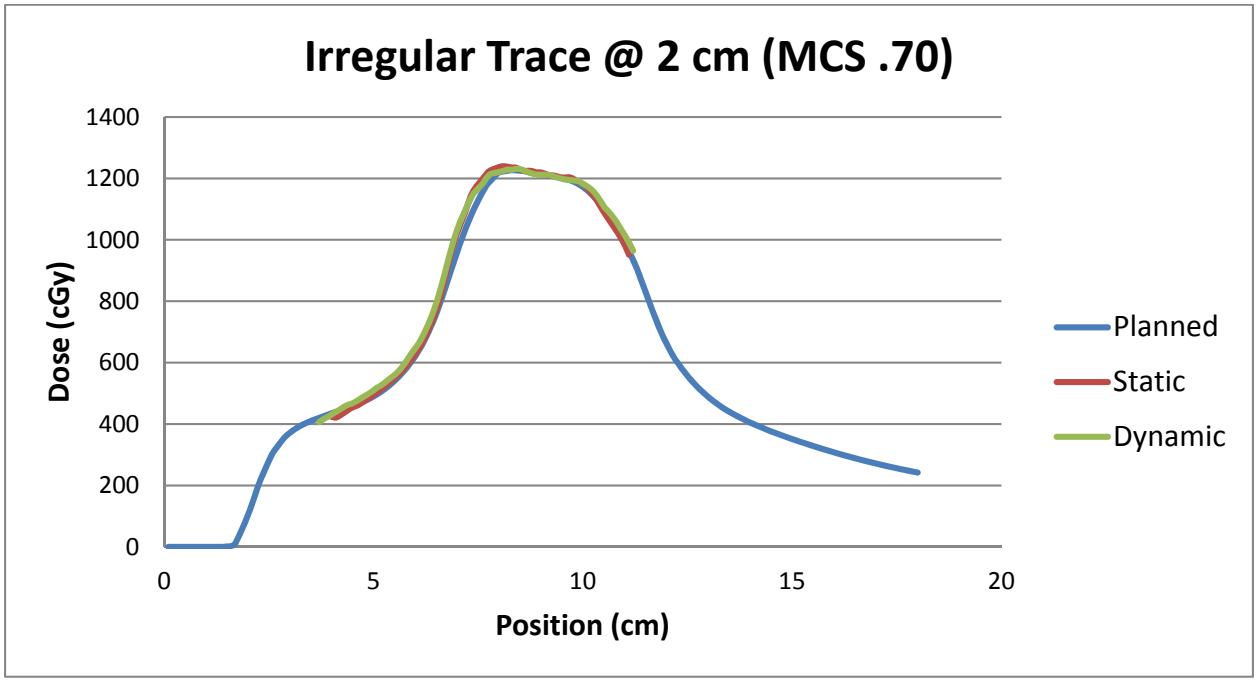

Figure 109: Lateral profiles for irregular patient trace at 2 cm amplitude with a plan MCS of 0.70.

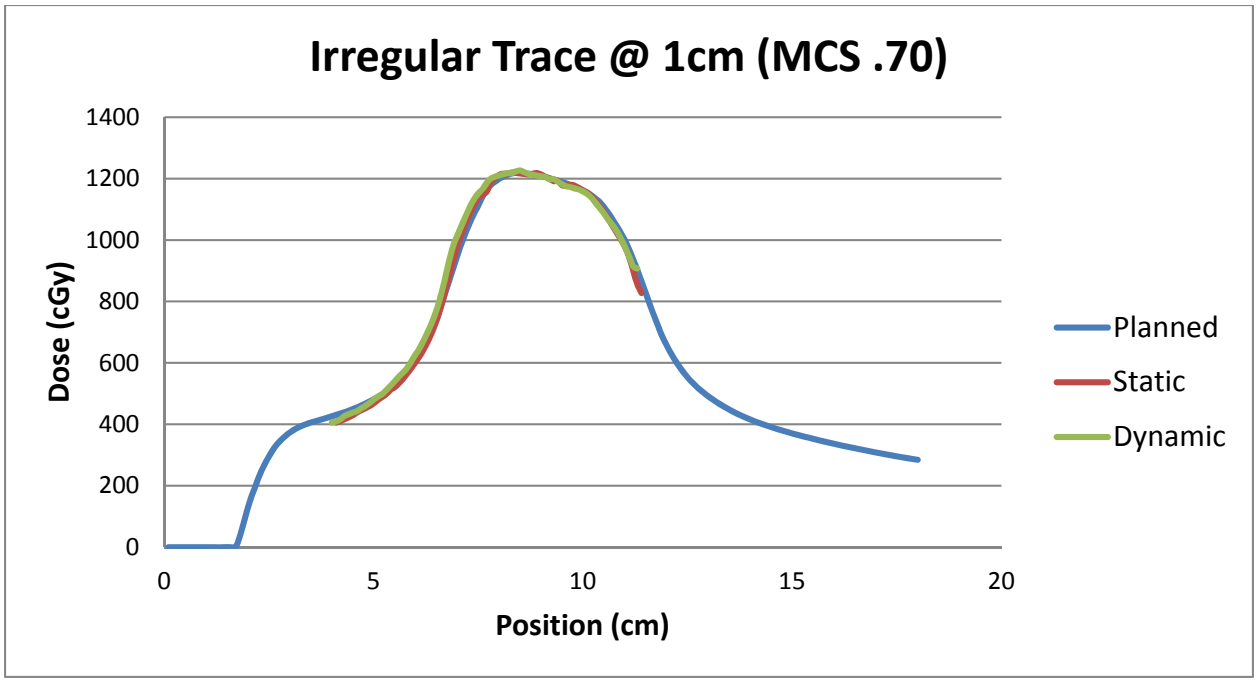

Figure 110: Lateral profiles for irregular patient trace at 1 cm amplitude with a plan MCS of 0.70.

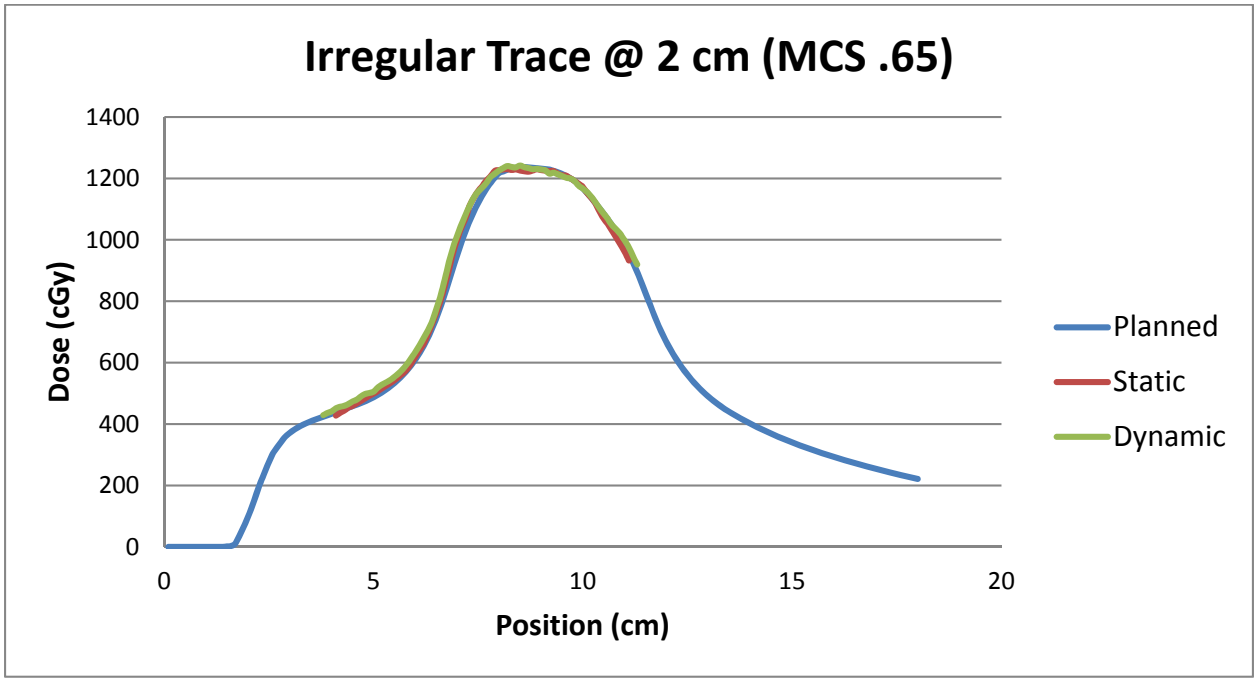

Figure 111: Lateral profiles for irregular patient trace at 2 cm amplitude with a plan MCS of 0.65.

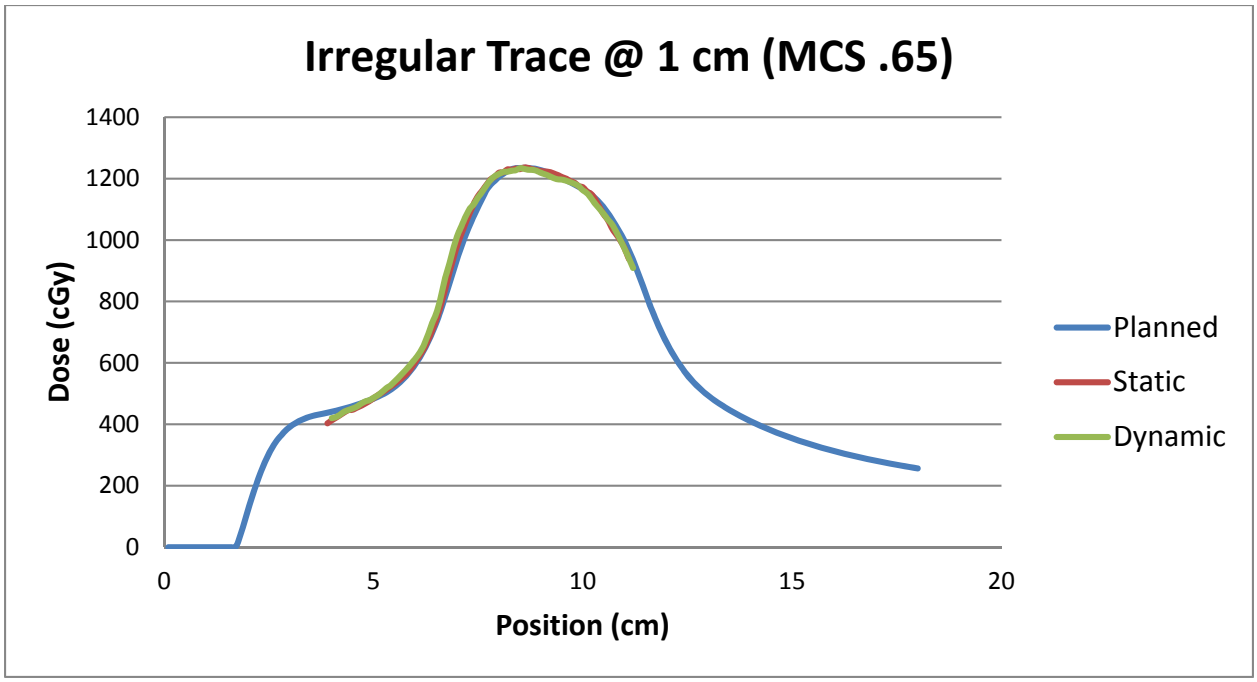

Figure 112: Lateral profiles for irregular patient trace at 1 cm amplitude with a plan MCS of 0.65.

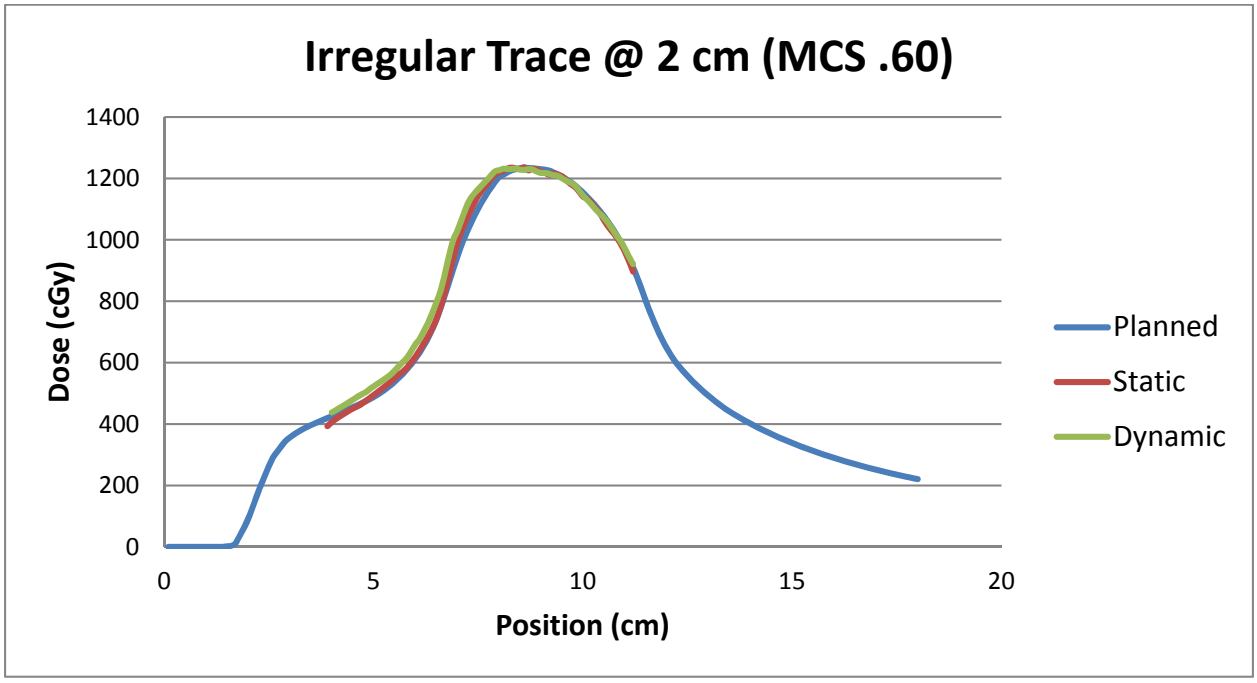

Figure 113: Lateral profiles for irregular patient trace at 2 cm amplitude with a plan MCS of 0.60.

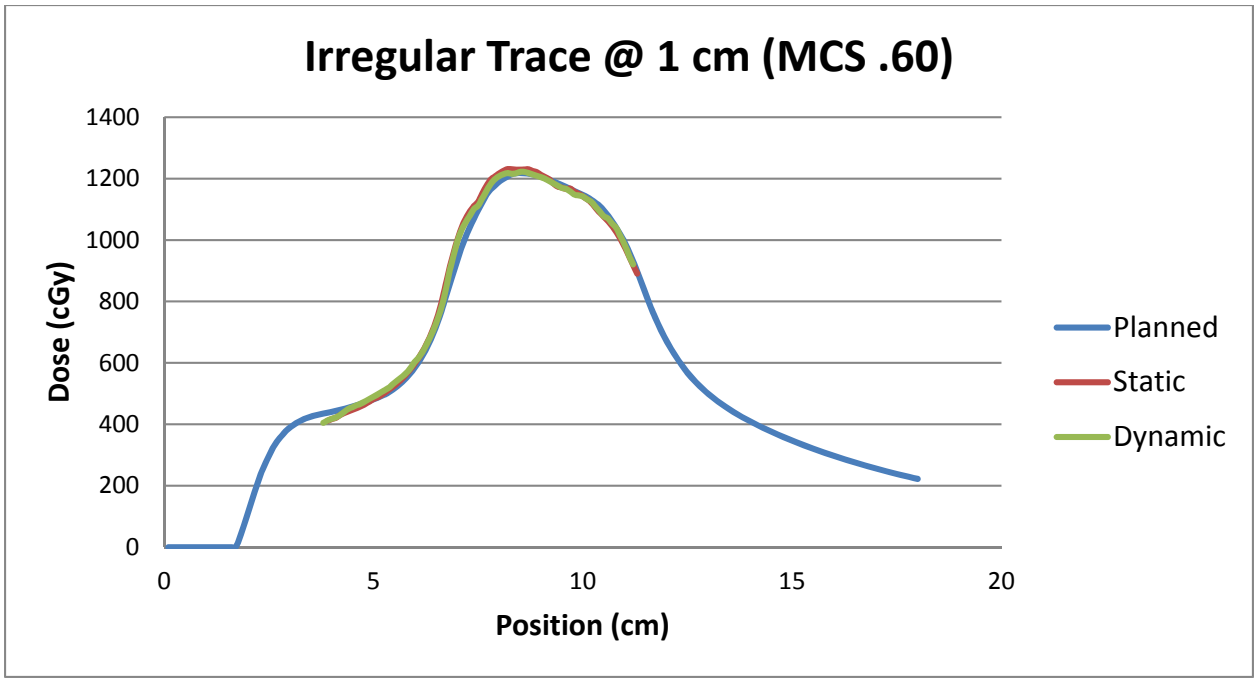

Figure 114: Lateral profiles for irregular patient trace at 1 cm amplitude with a plan MCS of 0.60.

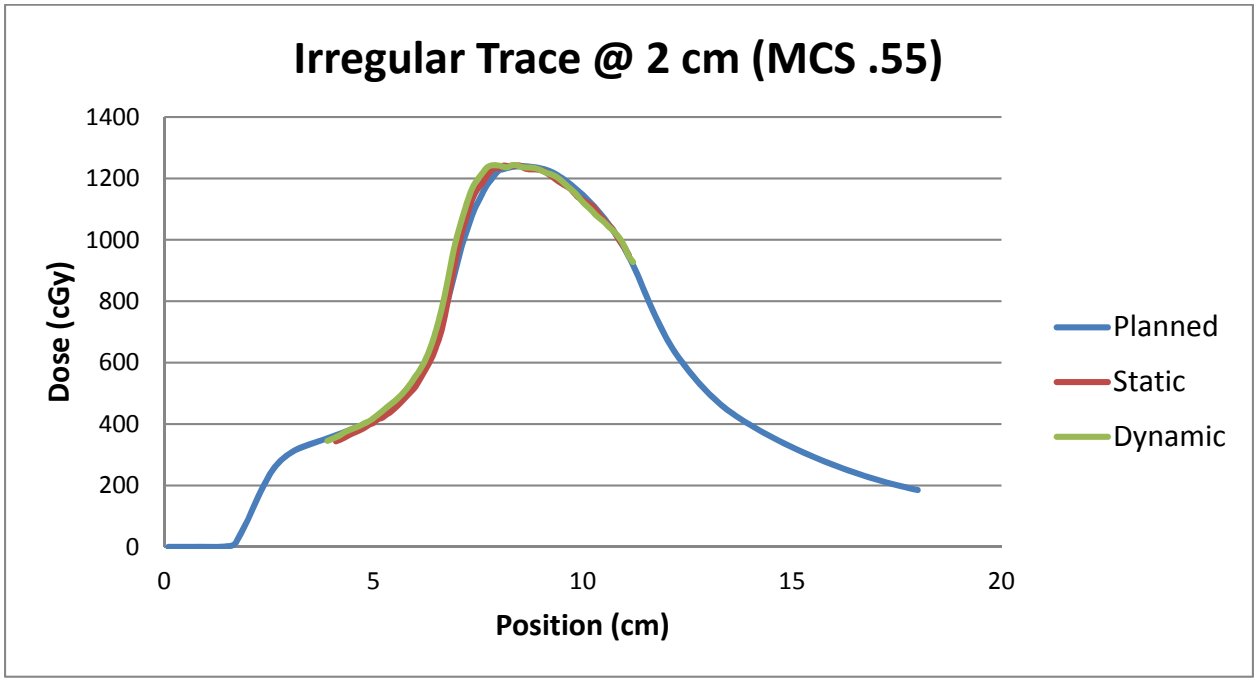

Figure 115: Lateral profiles for irregular patient trace at 2 cm amplitude with a plan MCS of 0.55.

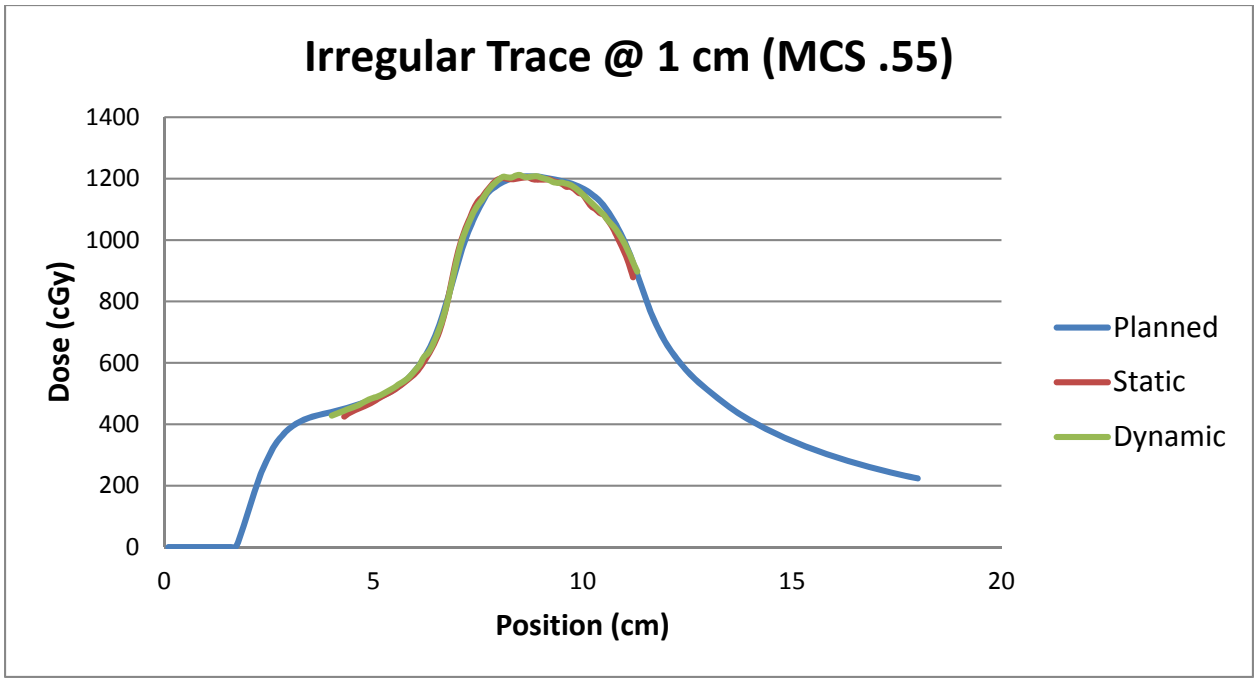

Figure 116: Lateral profiles for irregular patient trace at 1 cm amplitude with a plan MCS of 0.55.

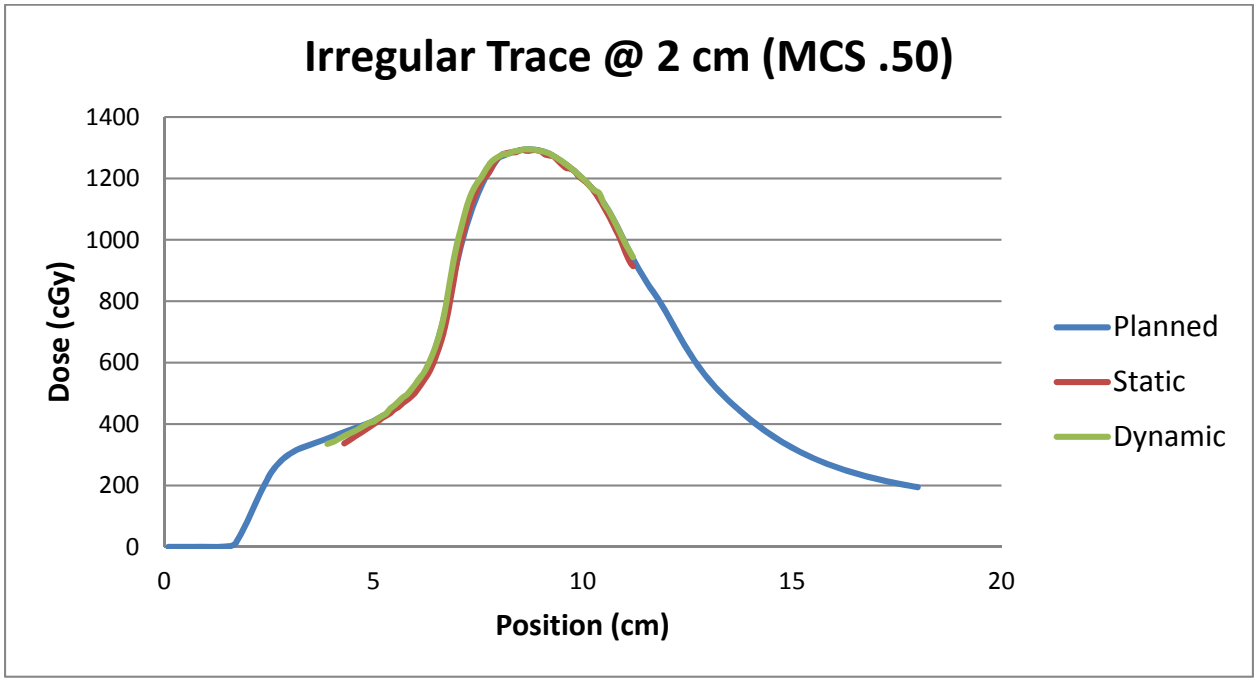

Figure 117: Lateral profiles for irregular patient trace at 2 cm amplitude with a plan MCS of 0.50.

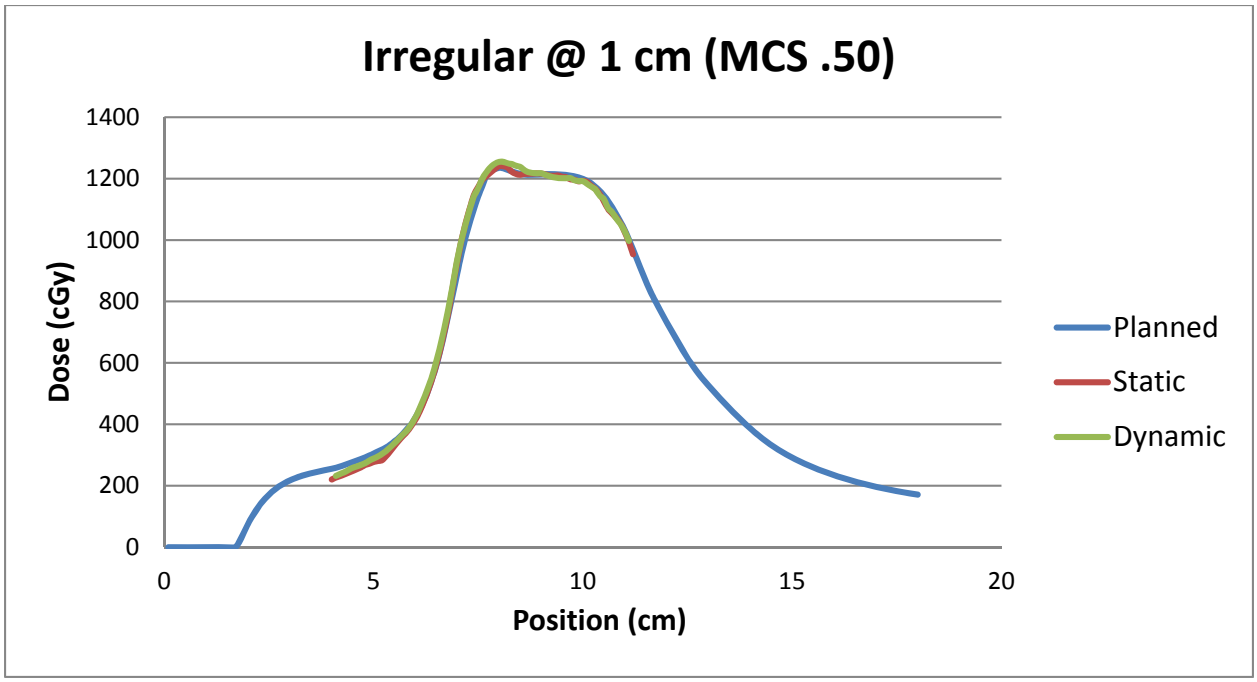

Figure 118: Lateral profiles for irregular patient trace at 1 cm amplitude with a plan MCS of 0.50.

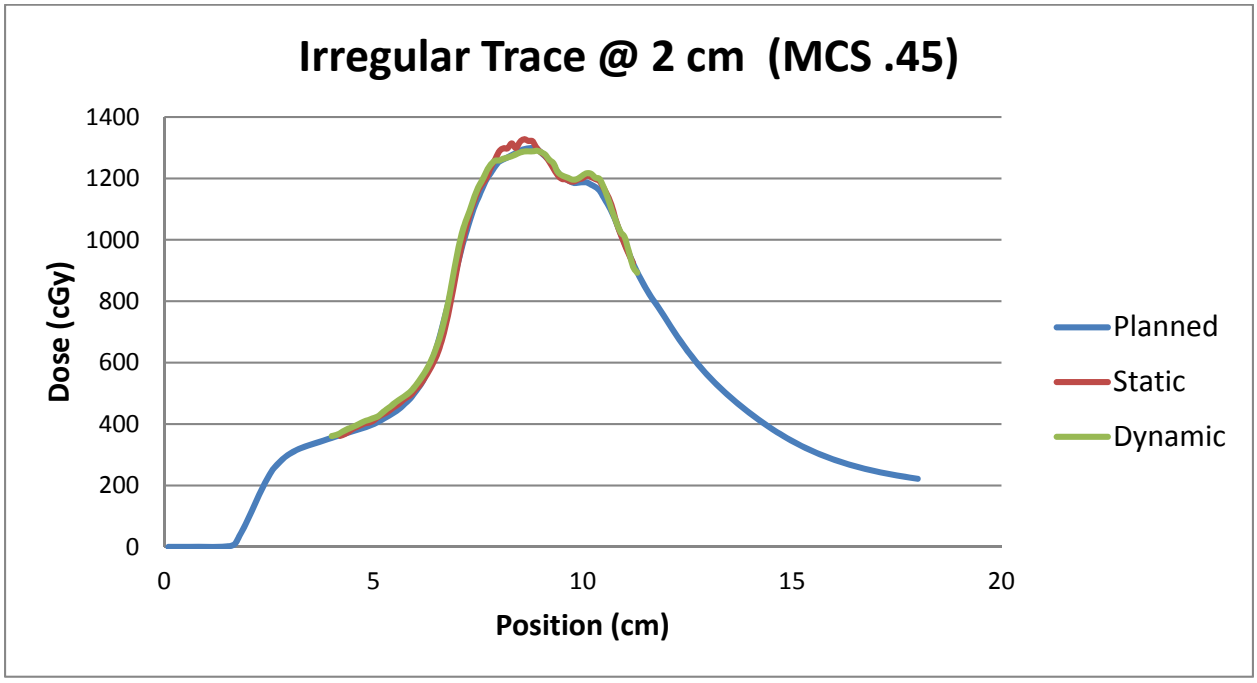

Figure 119: Lateral profiles for irregular patient trace at 2 cm amplitude with a plan MCS of 0.45.

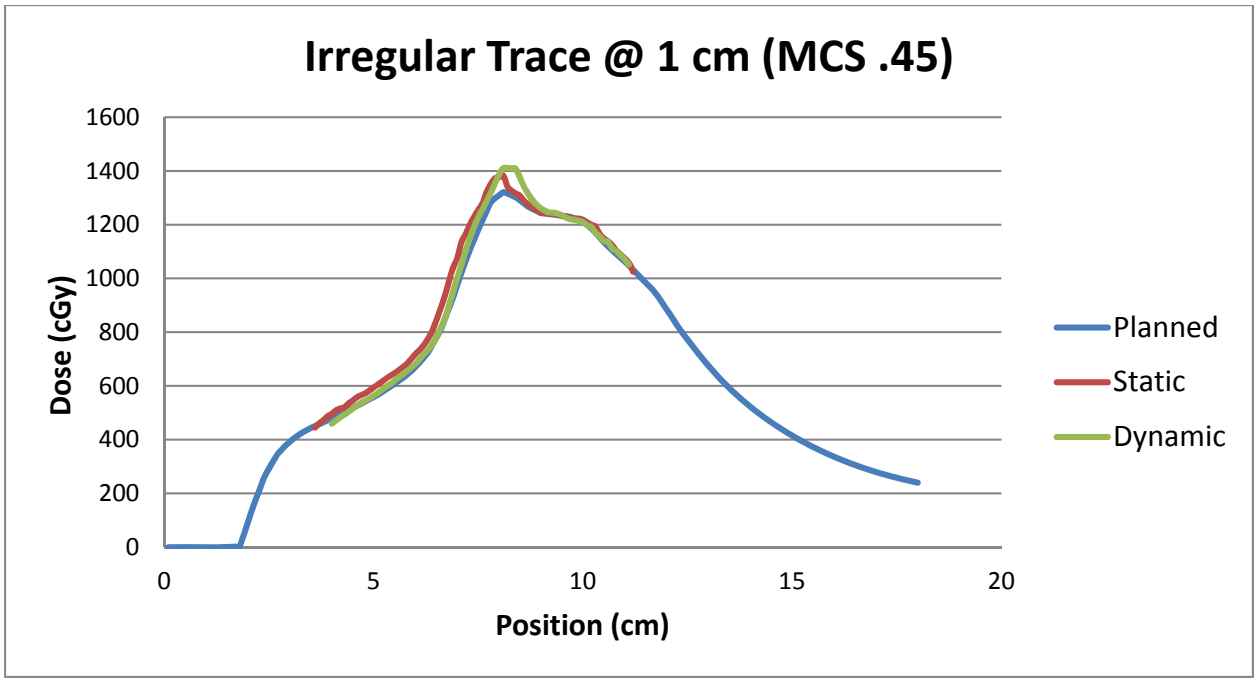

Figure 120: Lateral profiles for irregular patient trace at 1 cm amplitude with a plan MCS of 0.45.

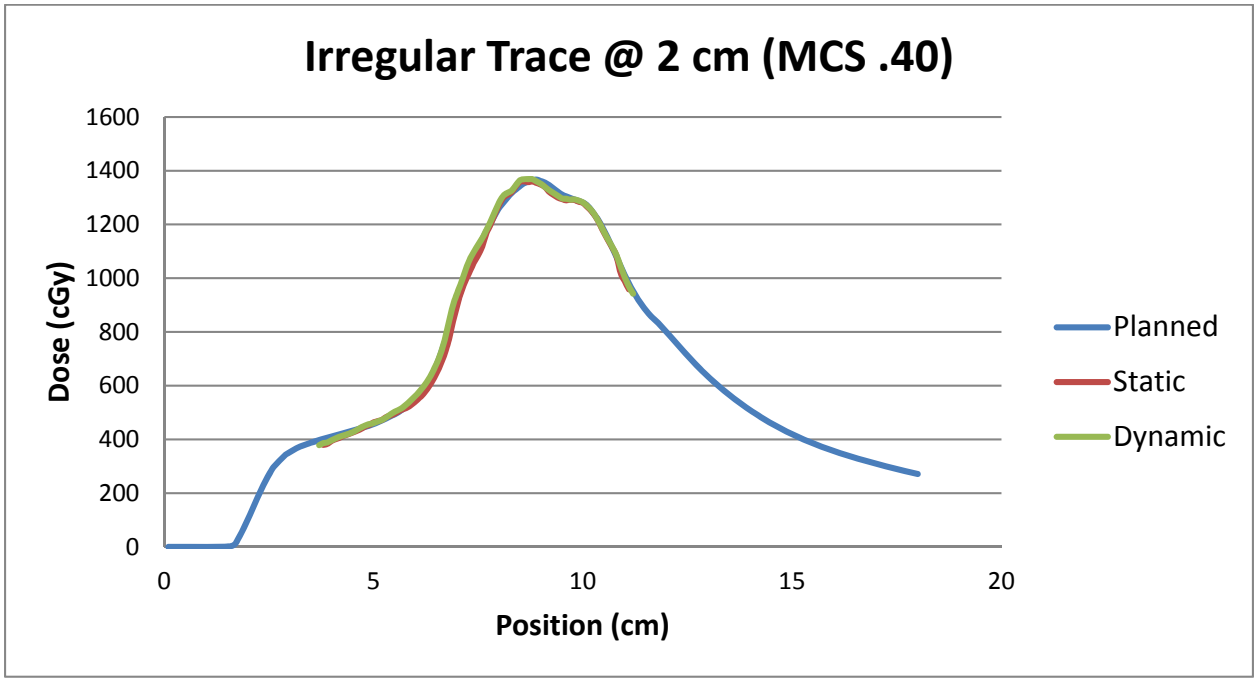

Figure 121: Lateral profiles for irregular patient trace at 2 cm amplitude with a plan MCS of 0.40.

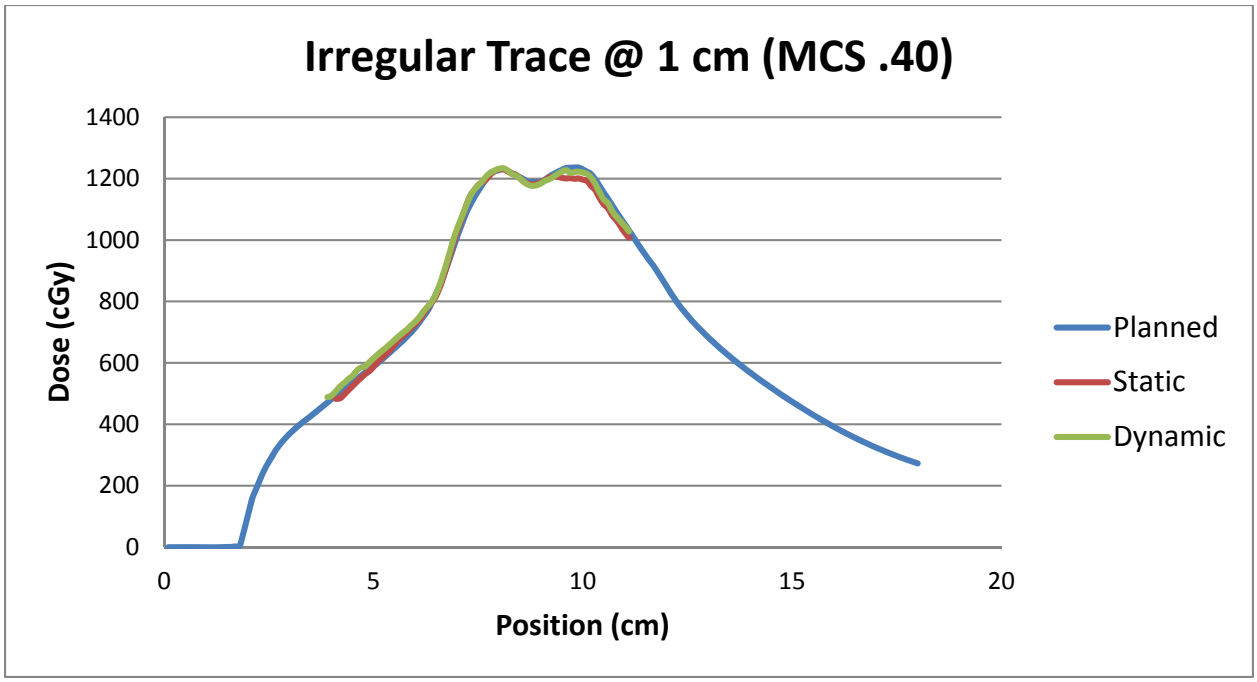

Figure 122: Lateral profiles for irregular patient trace at 1 cm amplitude with a plan MCS of 0.40.

Appendix C. Mean, Minimum and Maximum Plots

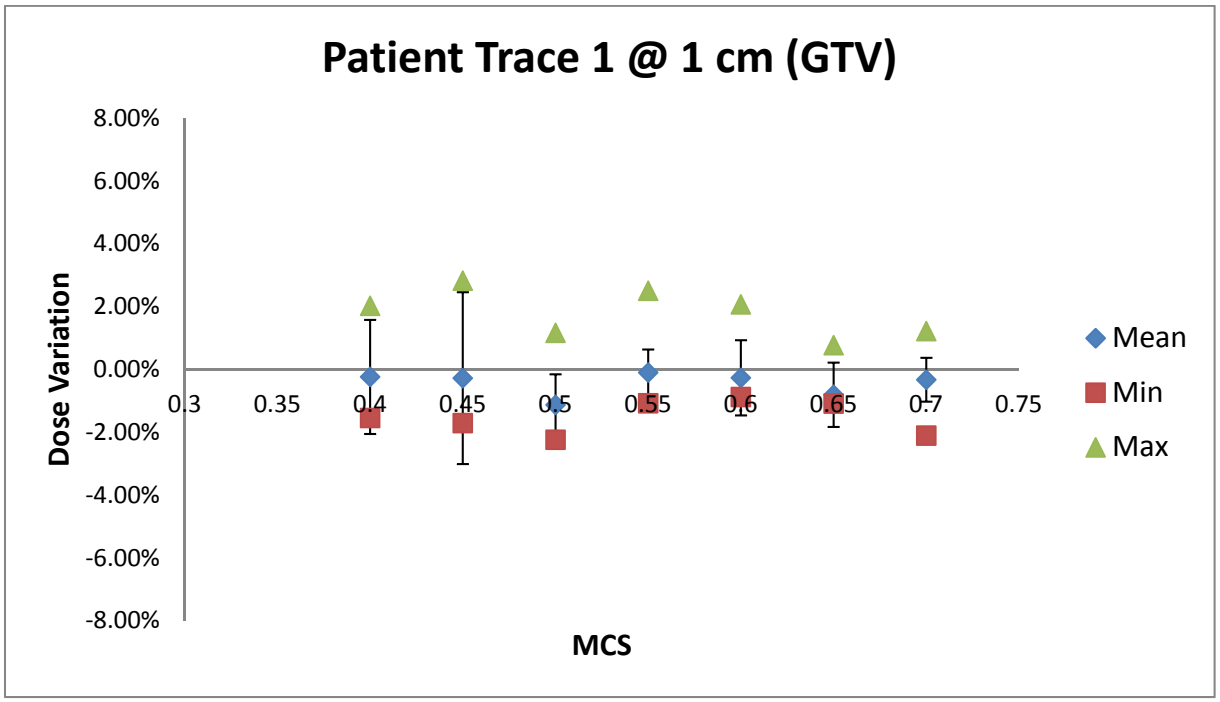

Figure 123: Percent dose error of dynamic delivery for patient trace 1 at 1 cm

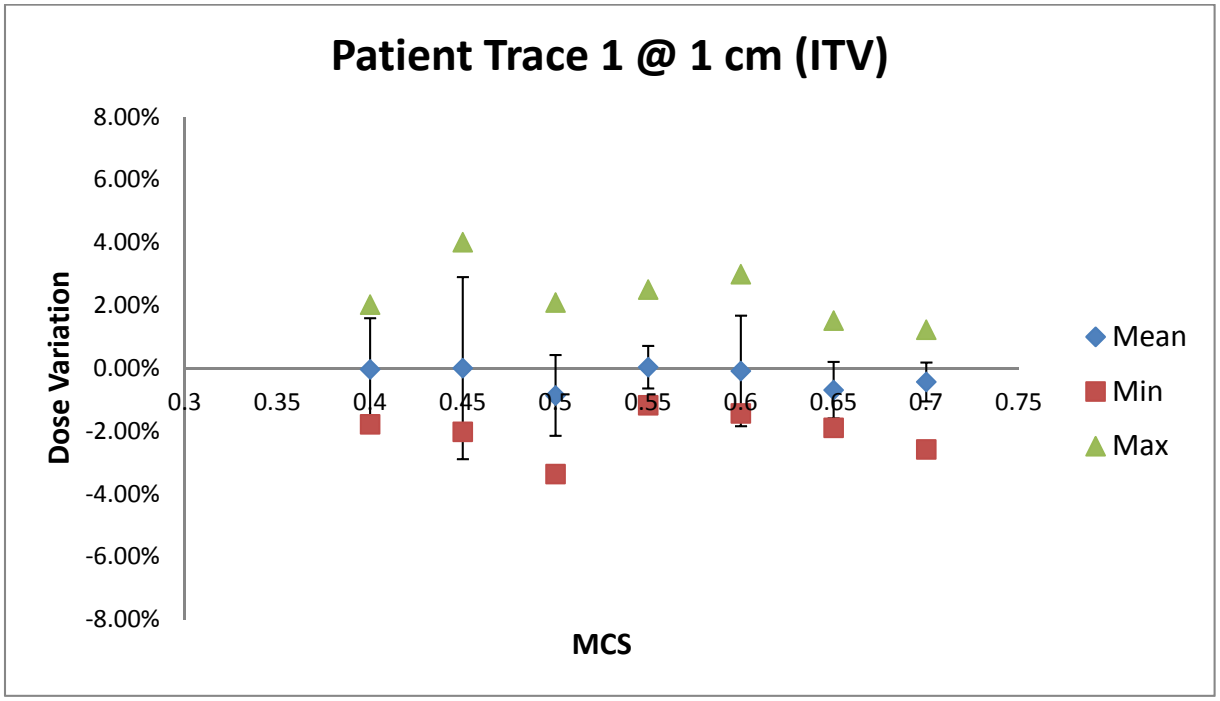

Figure 124: Percent dose error of dynamic delivery for patient trace 1 at 1 cm

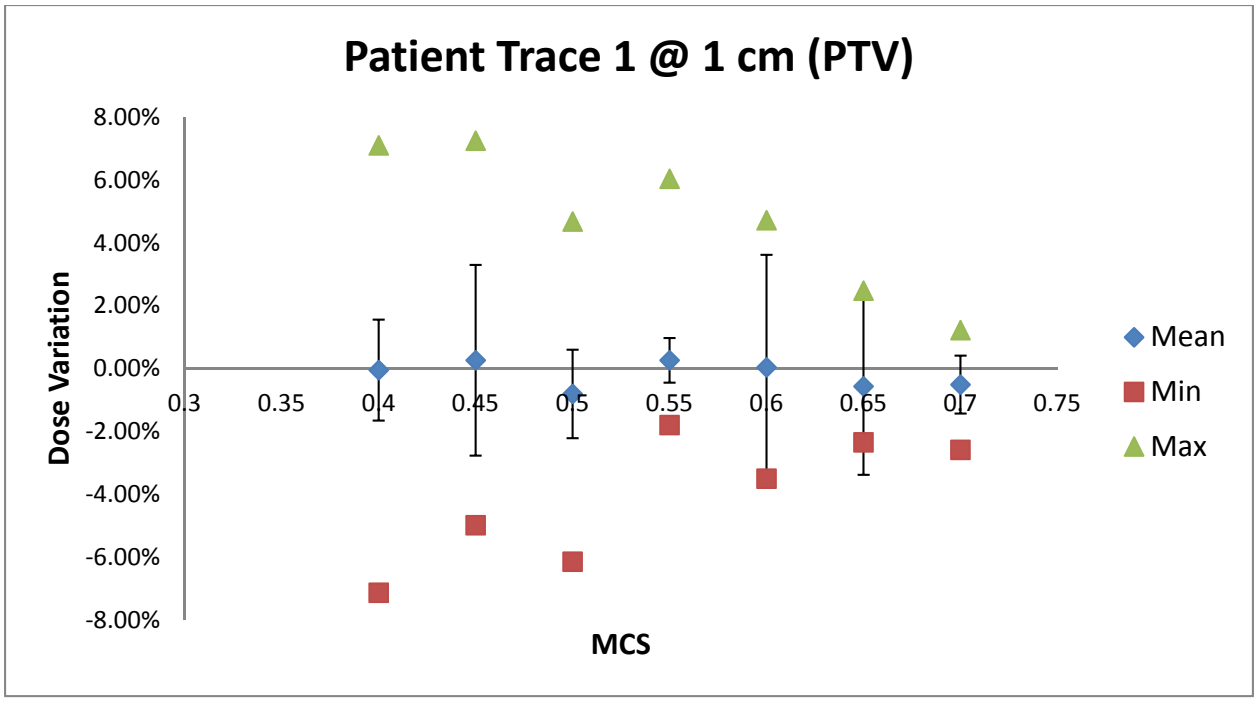

Figure 125: Percent dose error of dynamic delivery for patient trace 1 at 1 cm

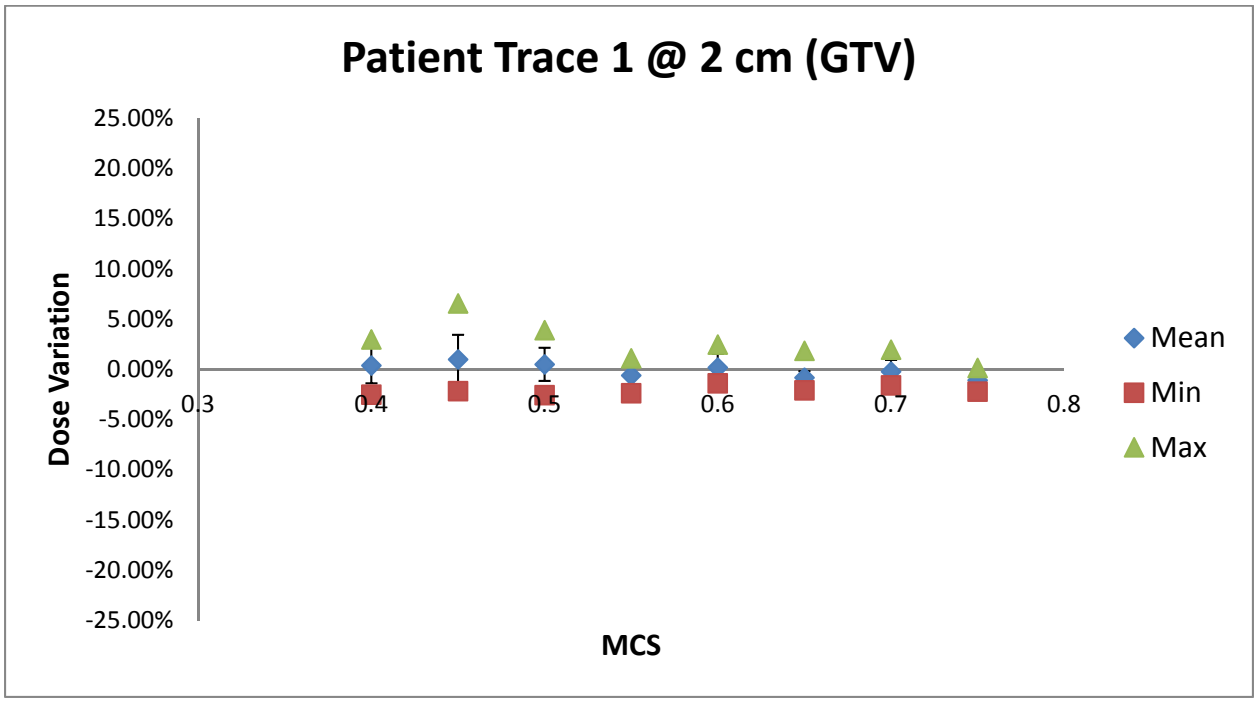

Figure 126: Percent dose error of dynamic delivery for patient trace 1 at 2 cm

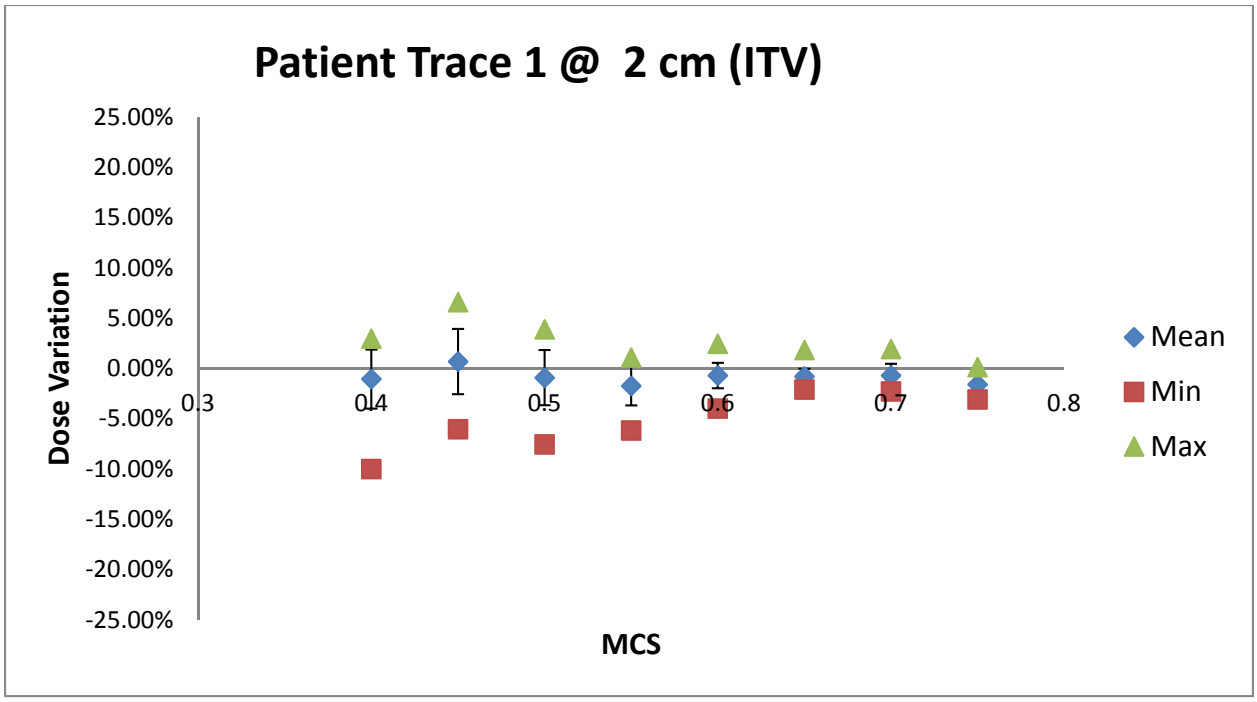

Figure 127: Percent dose error of dynamic delivery for patient trace 1 at 2 cm

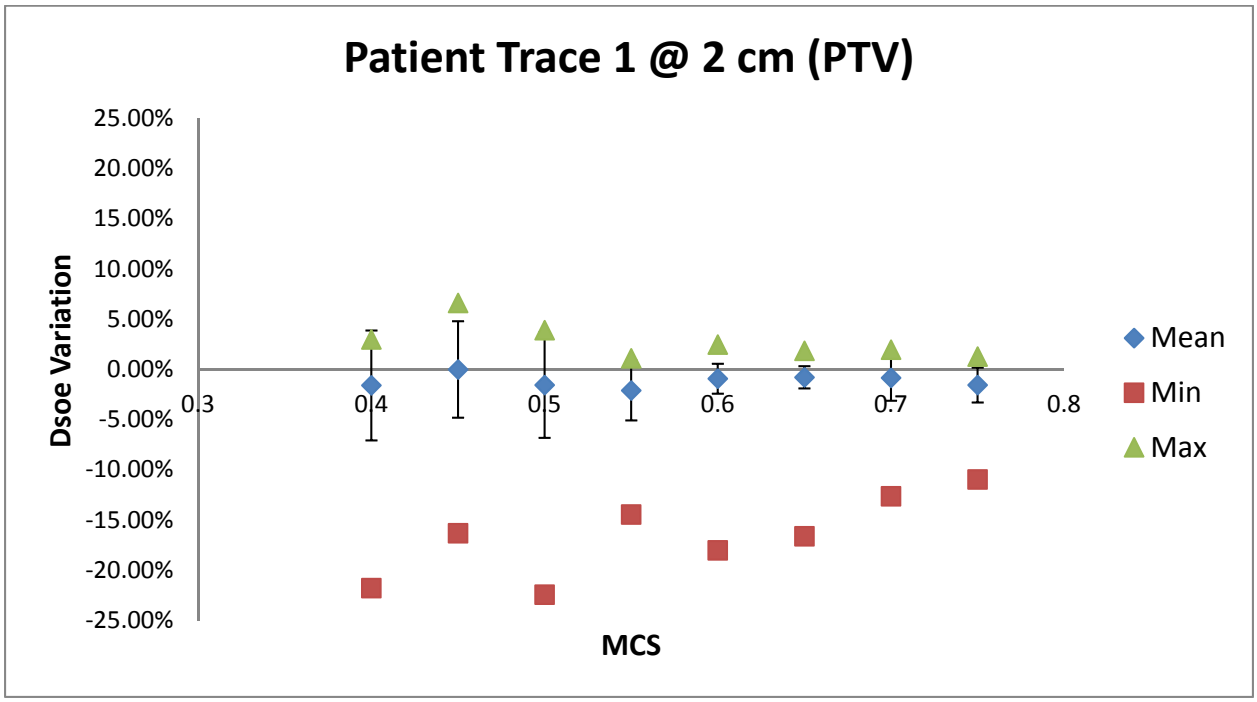

Figure 128: Percent dose error of dynamic delivery for patient trace 1 at 2 cm

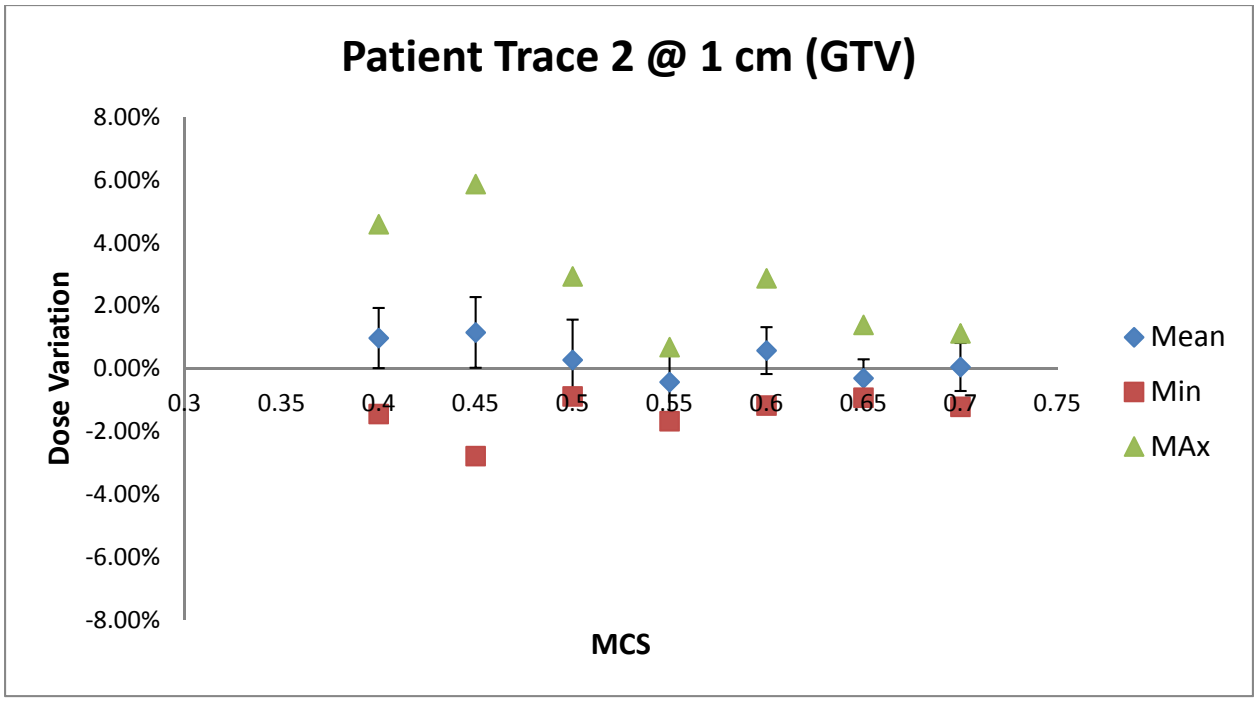

Figure 129: Percent dose error of dynamic delivery for patient trace 2 at 1 cm

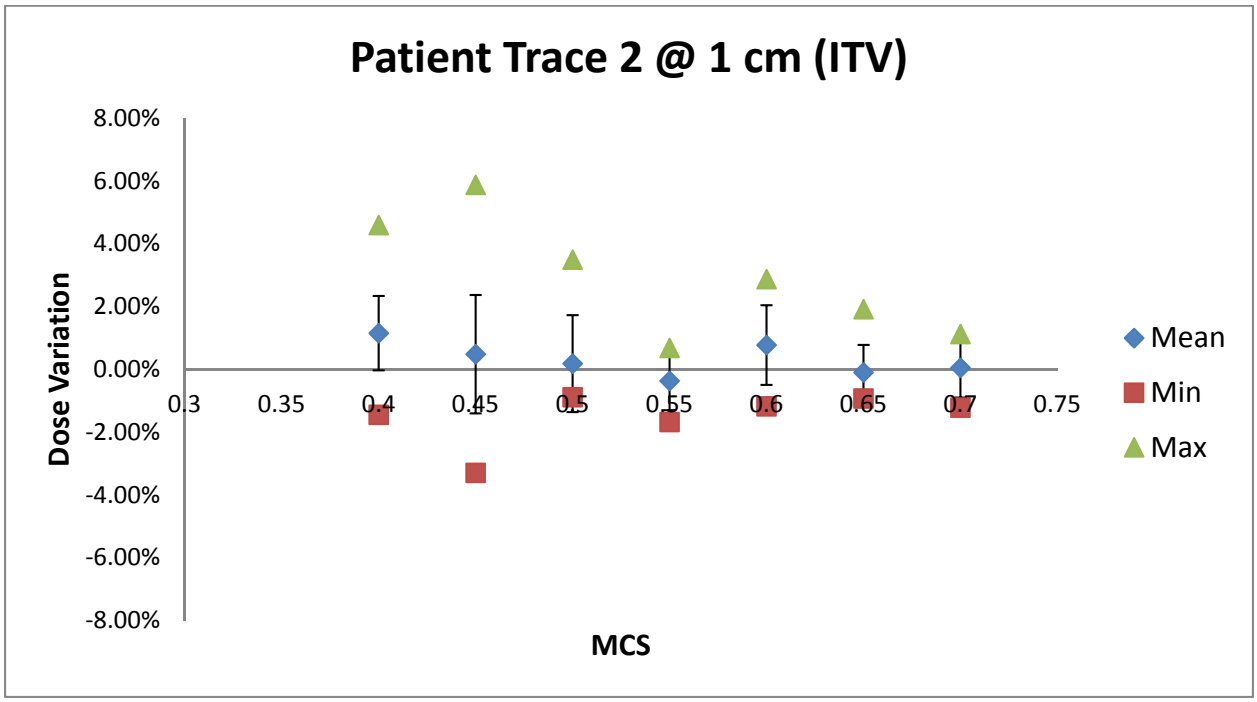

Figure 130: Percent dose error of dynamic delivery for patient trace 2 at 1 cm

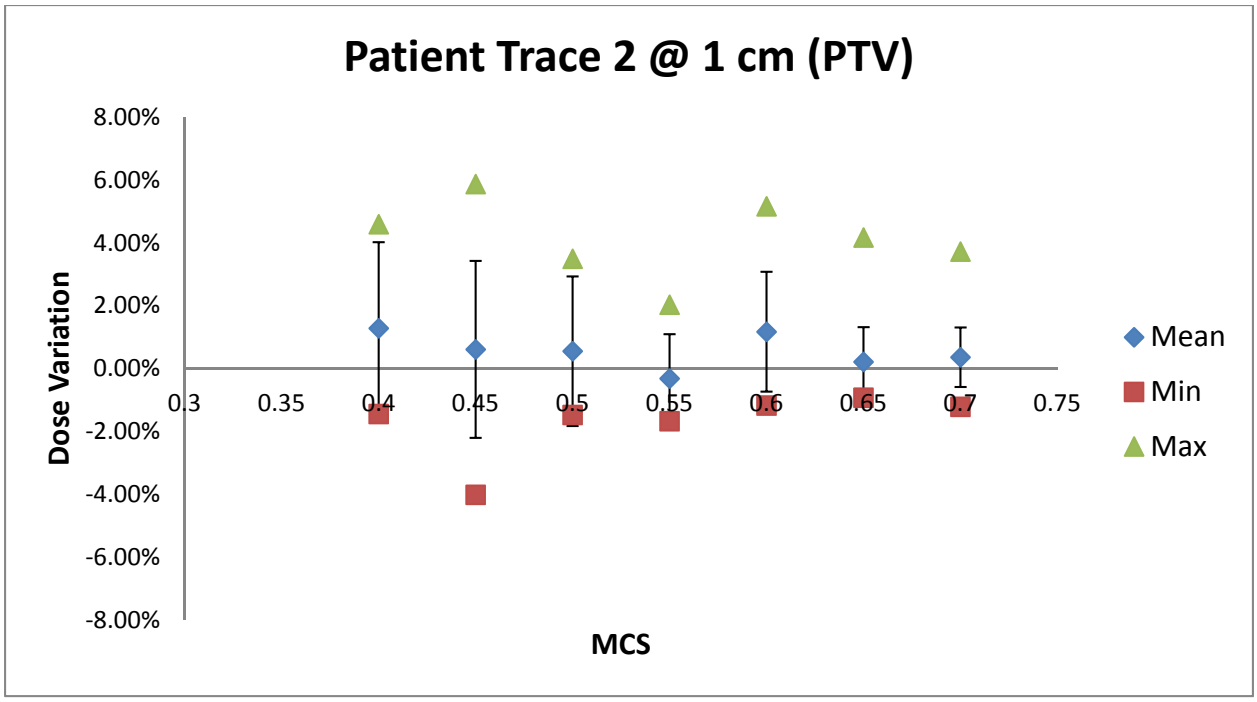

Figure 131: Percent dose error of dynamic delivery for patient trace 2 at 1 cm

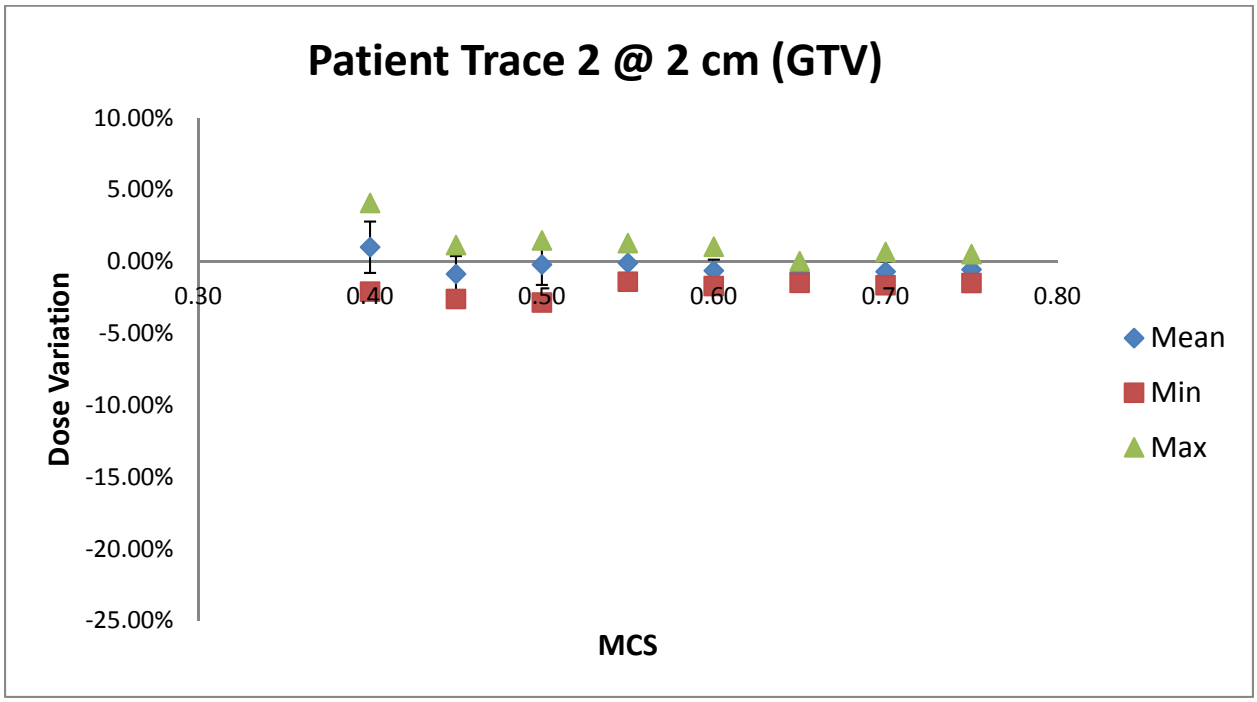

Figure 132: Percent dose error of dynamic delivery for patient trace 2 at 2 cm

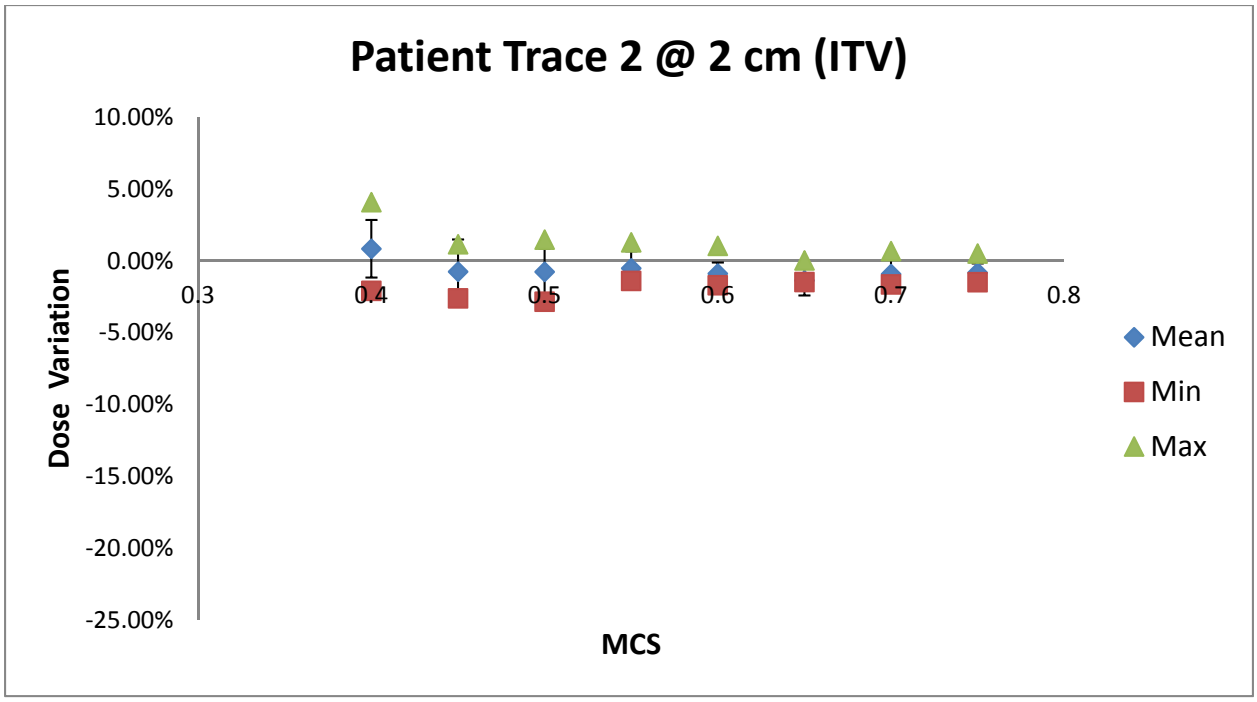

Figure 133: Percent dose error of dynamic delivery for patient trace 2 at 2 cm

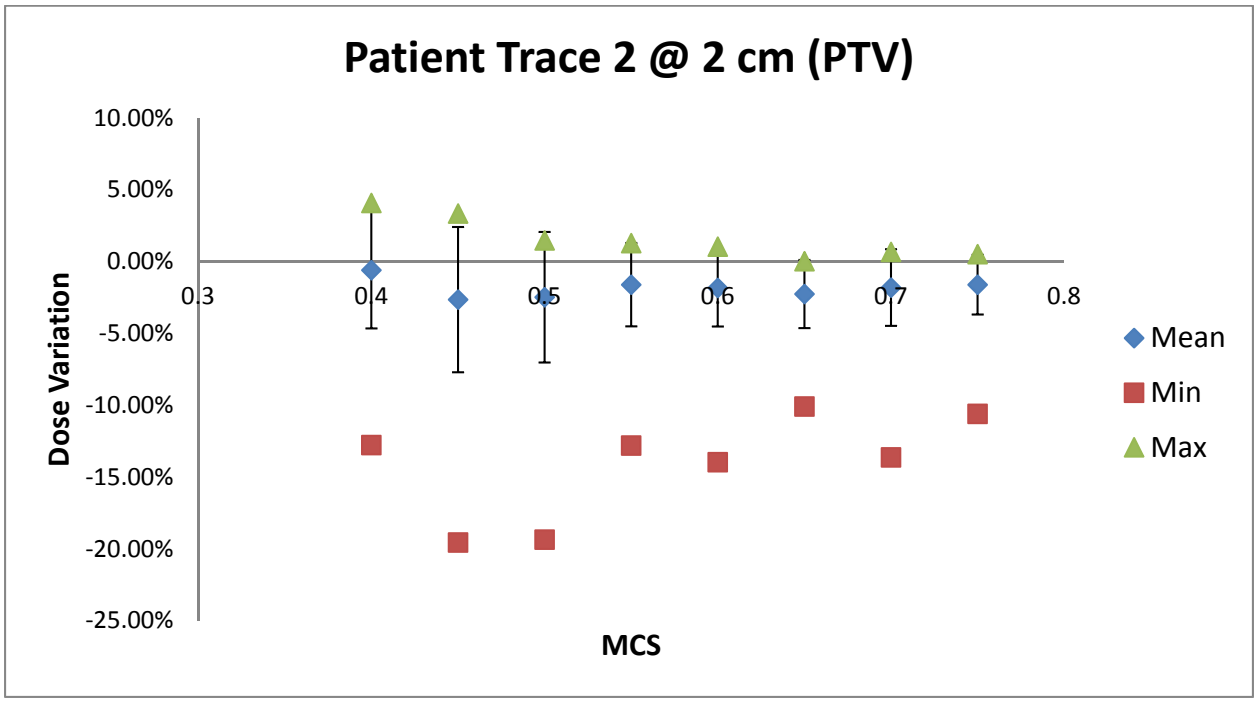

Figure 134: Percent dose error of dynamic delivery for patient trace 2 at 2 cm

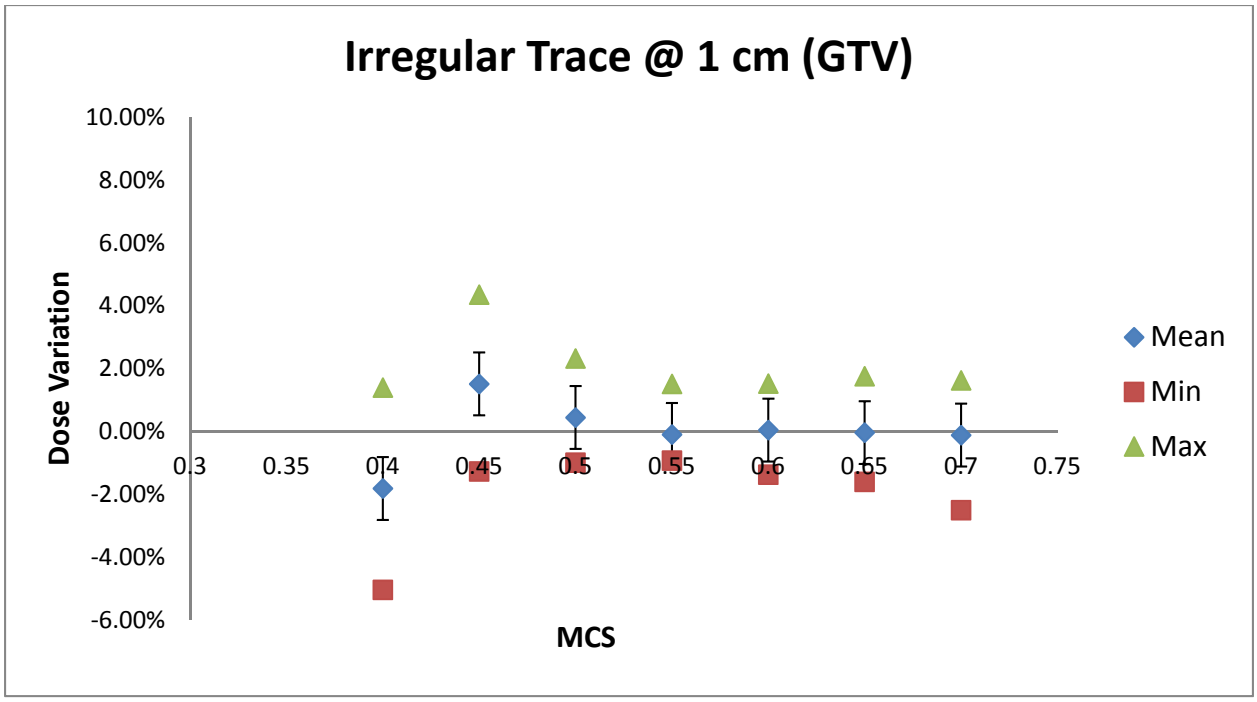

Figure 135: Percent dose error of dynamic delivery for irregular trace at 1 cm

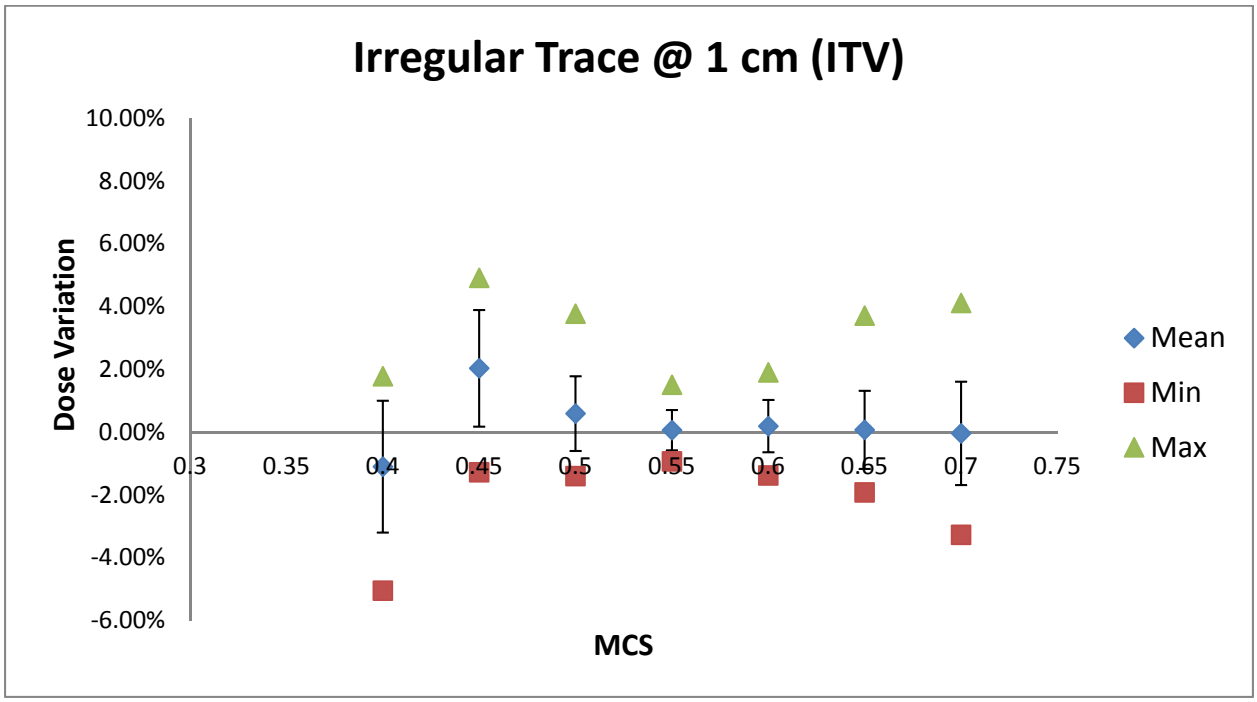

Figure 136: Percent dose error of dynamic delivery for irregular trace at 1 cm

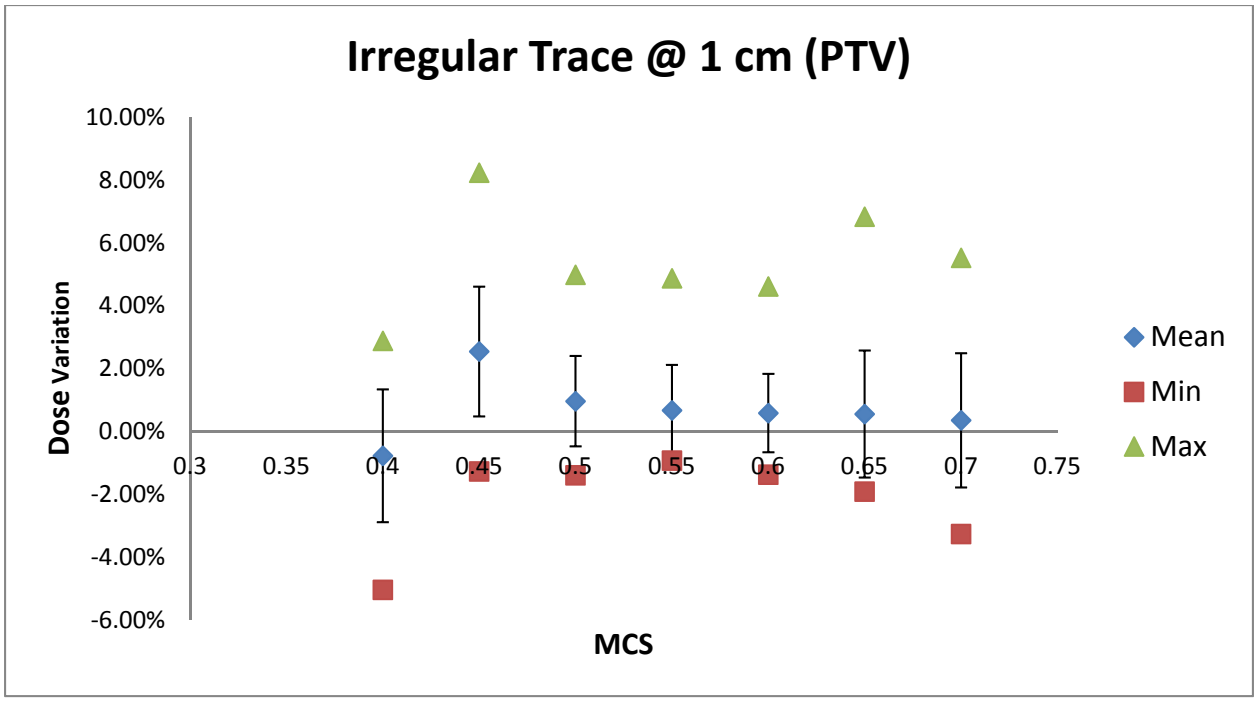

Figure 137: Percent dose error of dynamic delivery for irregular trace at 1 cm

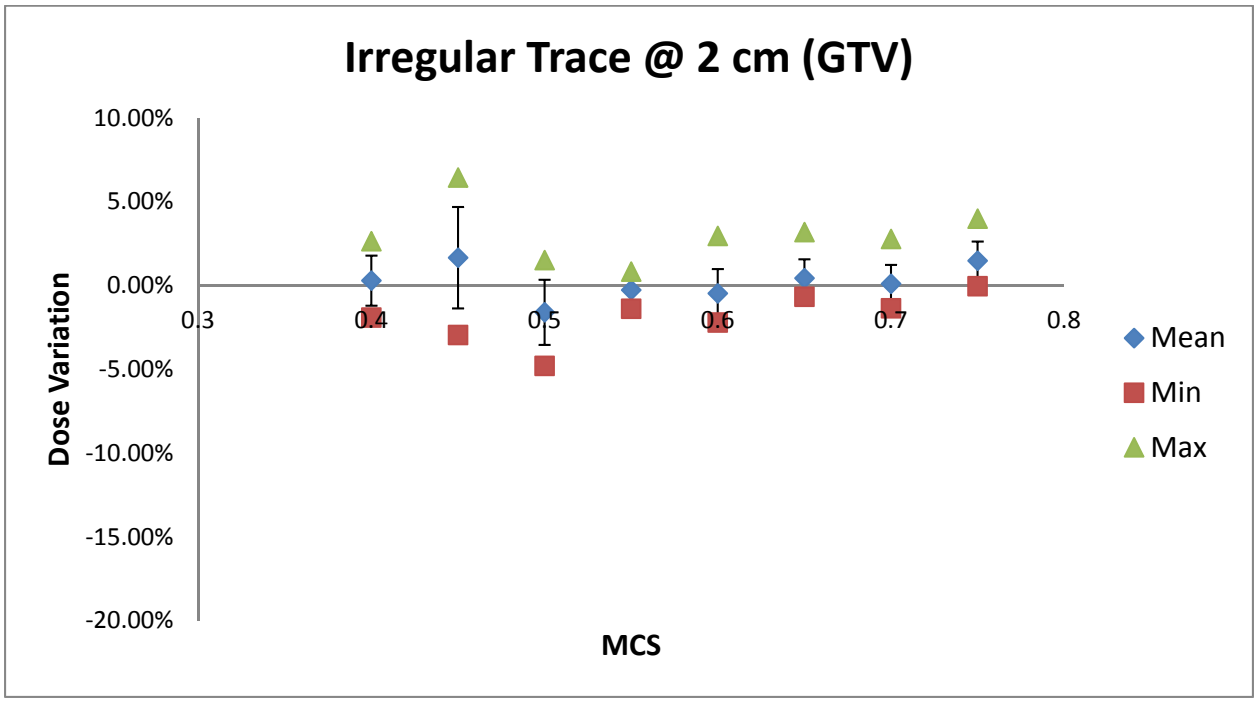

Figure 138: Percent dose error of dynamic delivery for irregular trace at 2 cm

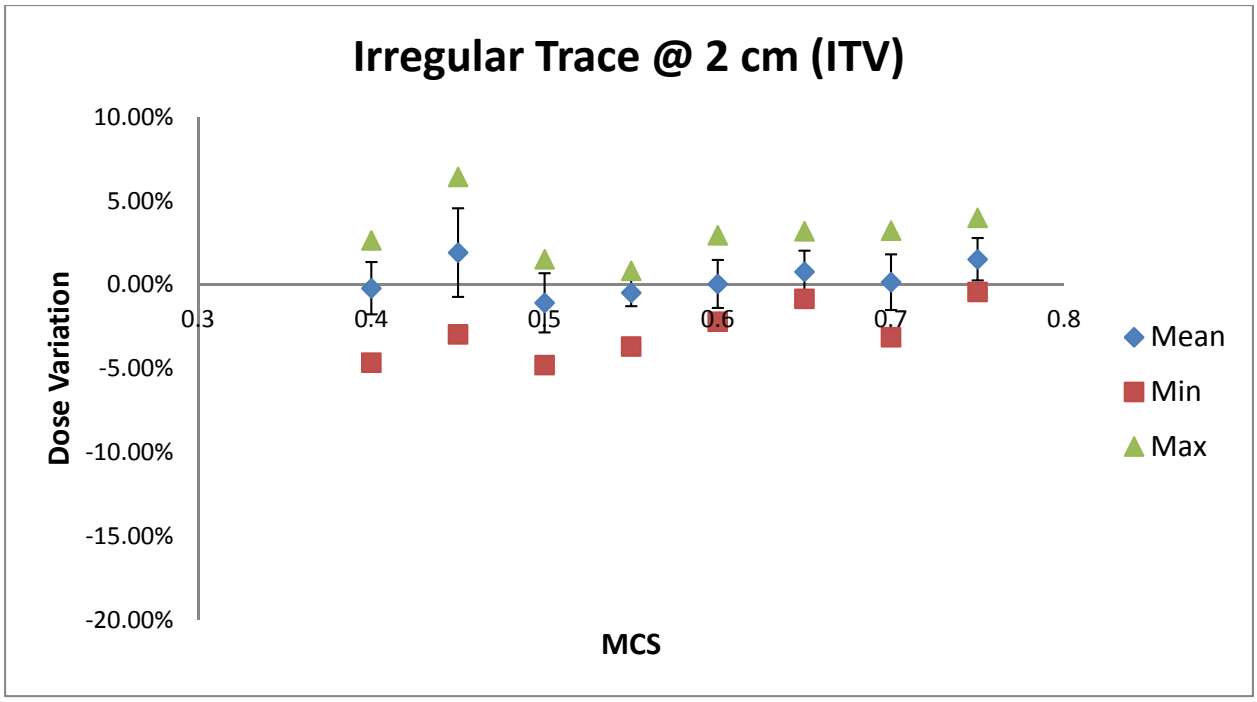

Figure 139: Percent dose error of dynamic delivery for irregular trace at 2 cm

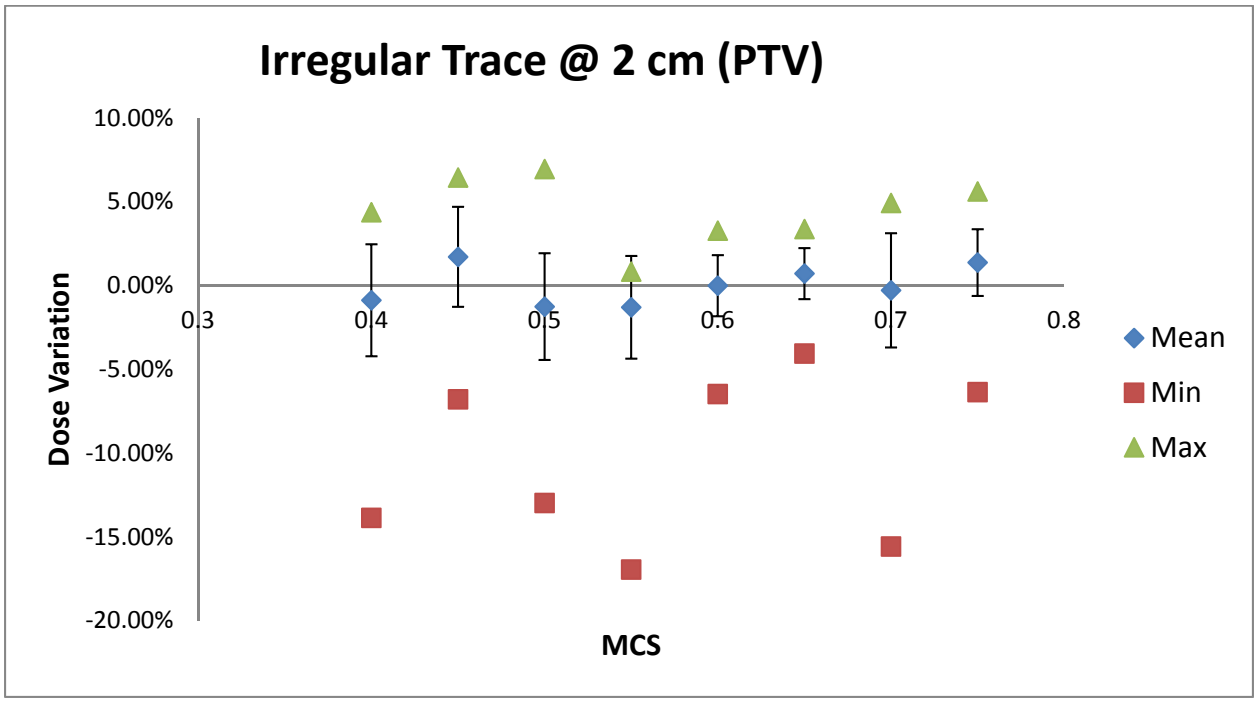

Figure 140: Percent dose error of dynamic delivery for irregular trace at 2 cm

Appendix D. Dose Distribution Width Supplemental Plots

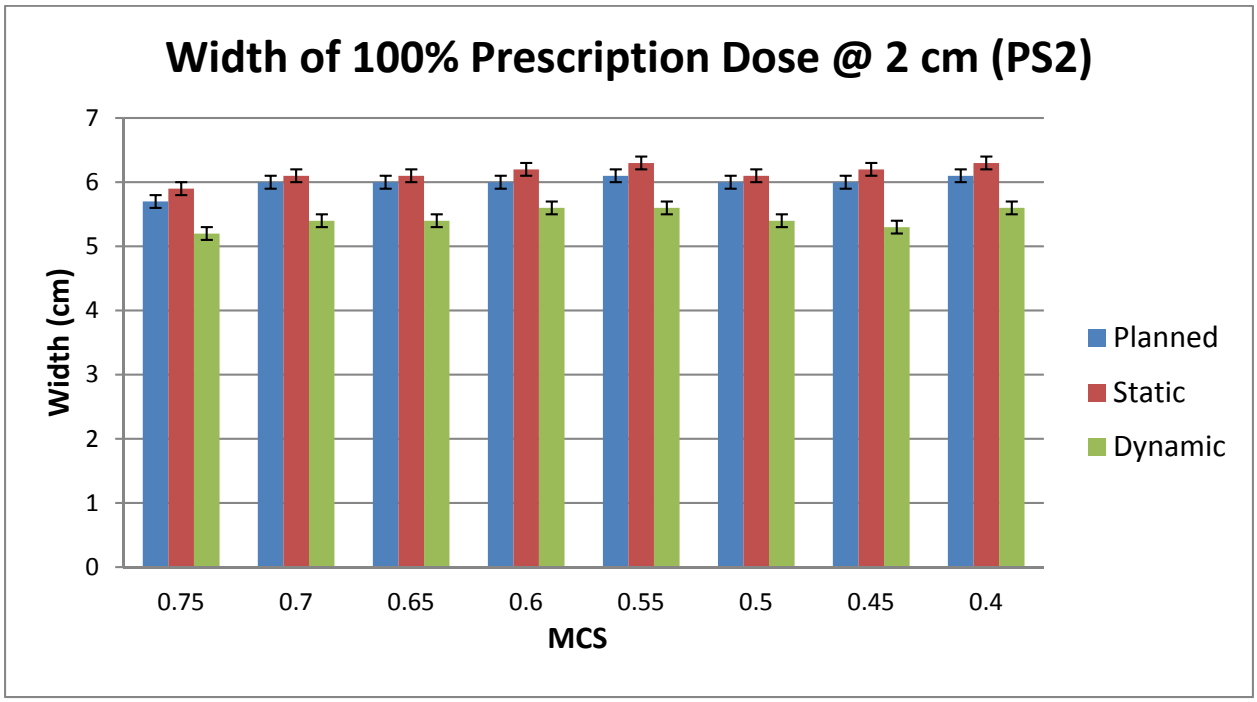

Figure 141: Width of the 100% prescription dose (1000 cGy) of planned, static and dynamic dose distribution for patient trace 2 at an amplitude of 2 cm.

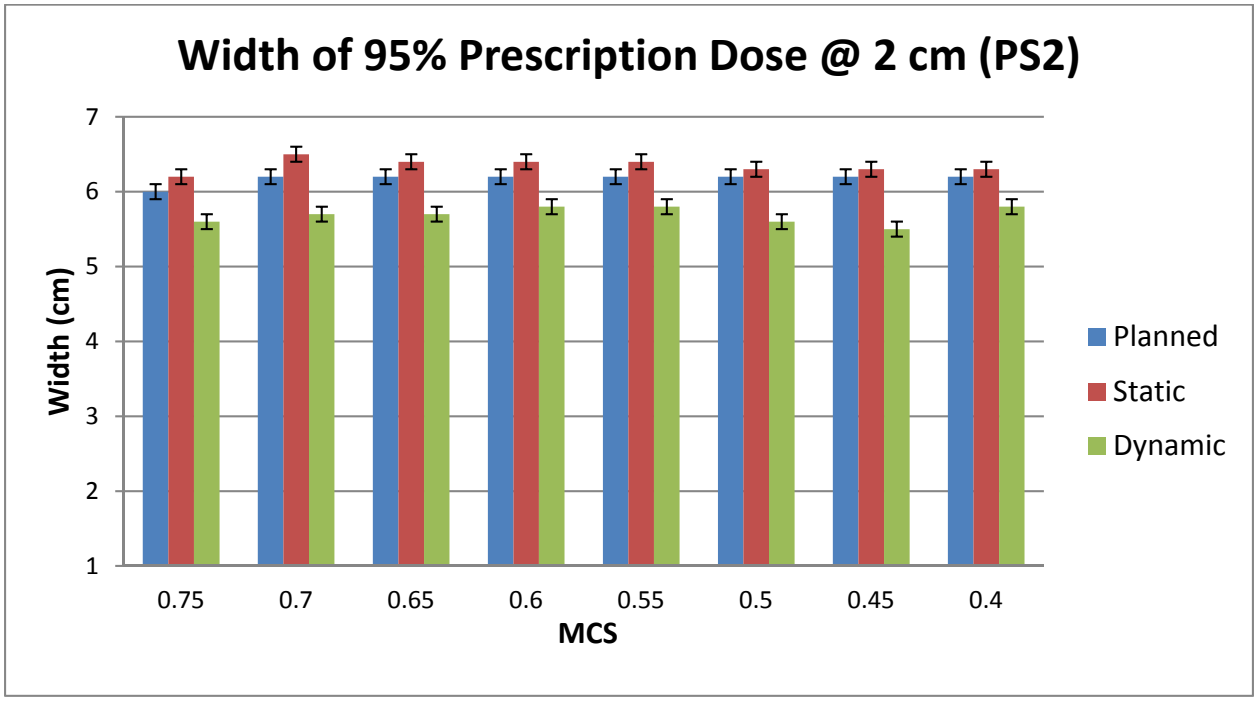

Figure 142: Width of the 95% prescription dose (950 cGy) of planned, static and dynamic dose distribution for patient trace 2 at an amplitude of 2 cm.

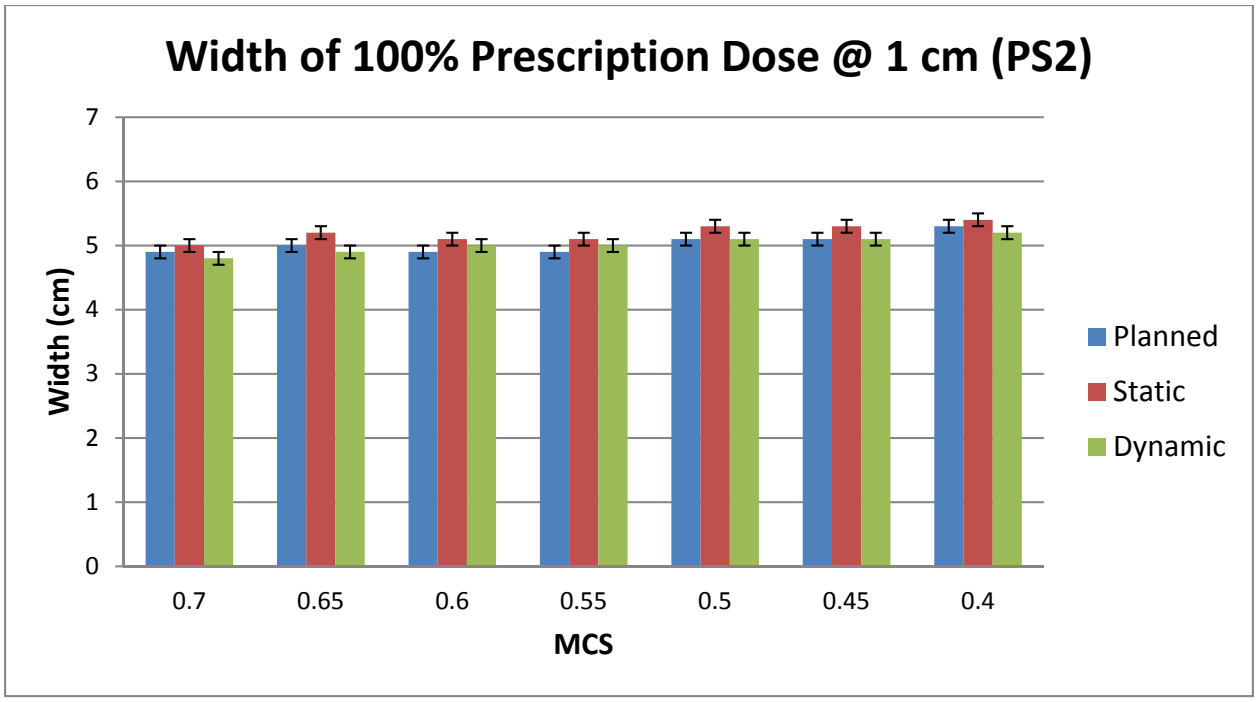

Figure 143: Width of the 100% prescription dose (1000 cGy) of planned, static and dynamic dose distribution for patient trace 2 at an amplitude of 1 cm.

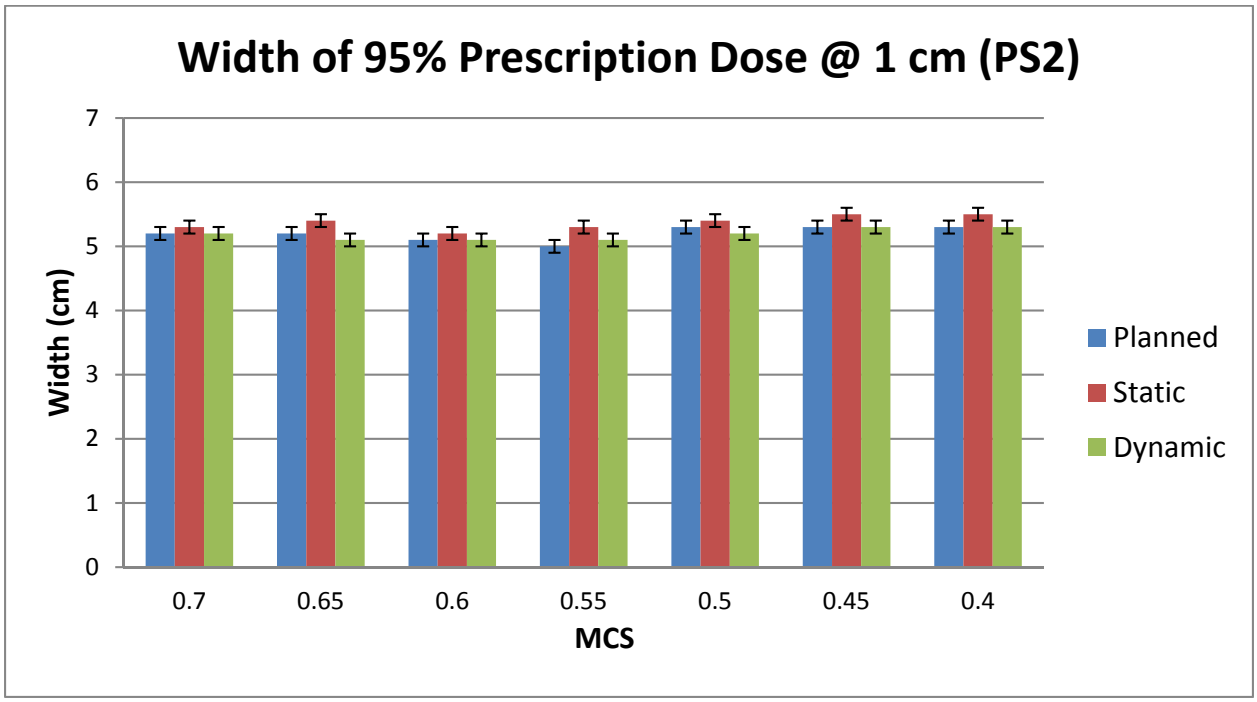

Figure 144: Width of the 95% prescription dose (950 cGy) of planned, static and dynamic dose distribution for patient trace 2 at an amplitude of 1 cm.

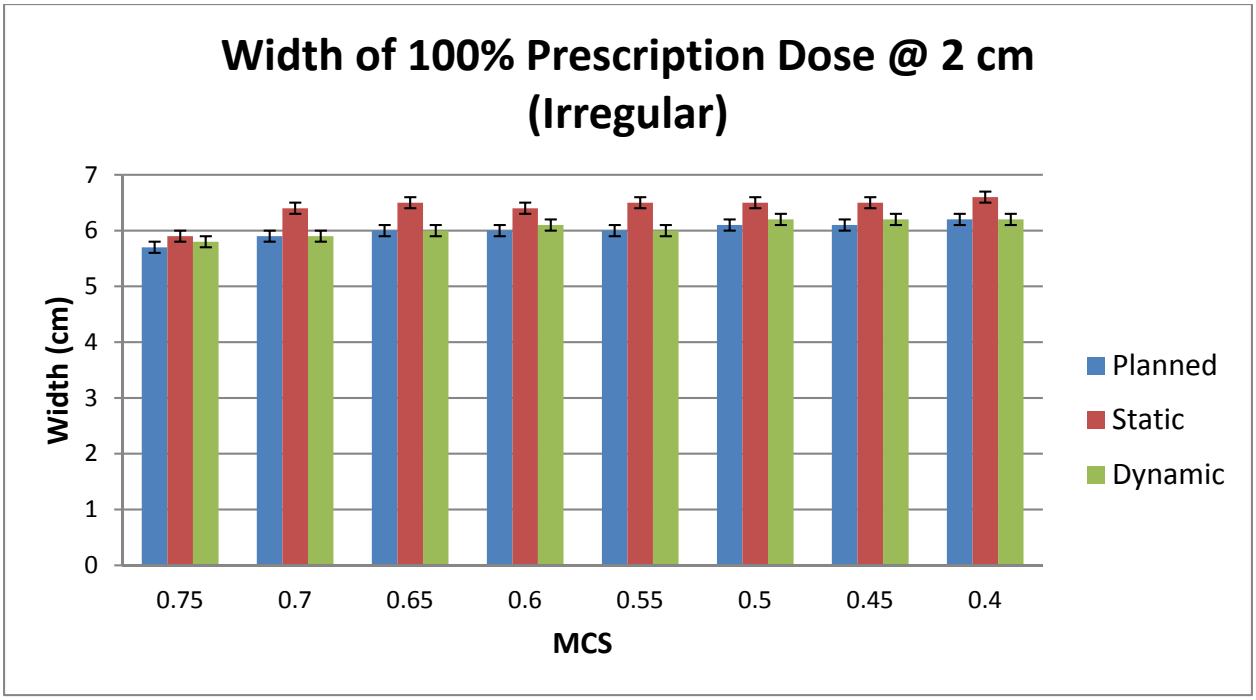

Figure 145: Width of the 100% prescription dose (1000 cGy) of planned, static and dynamic dose distribution for irregular trace at an amplitude of 2 cm.

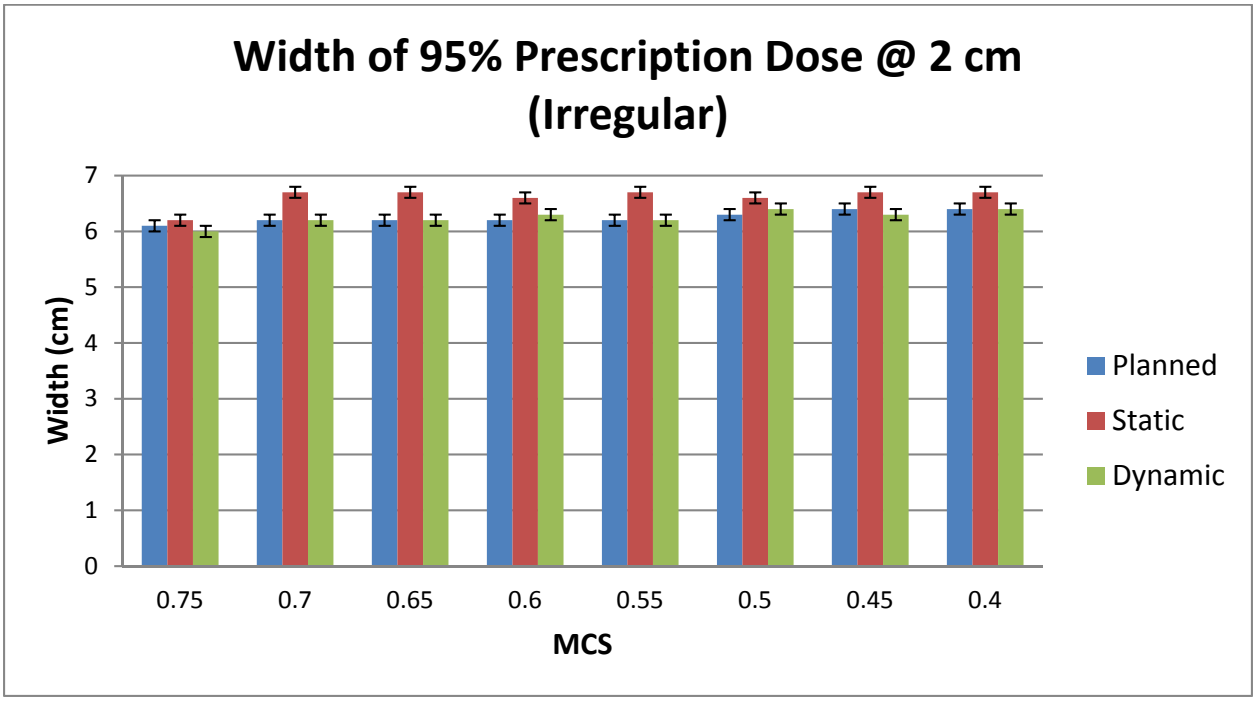

Figure 146: Width of the 95% prescription dose (950 cGy) of planned, static and dynamic dose distribution for irregular trace at an amplitude of 2 cm.

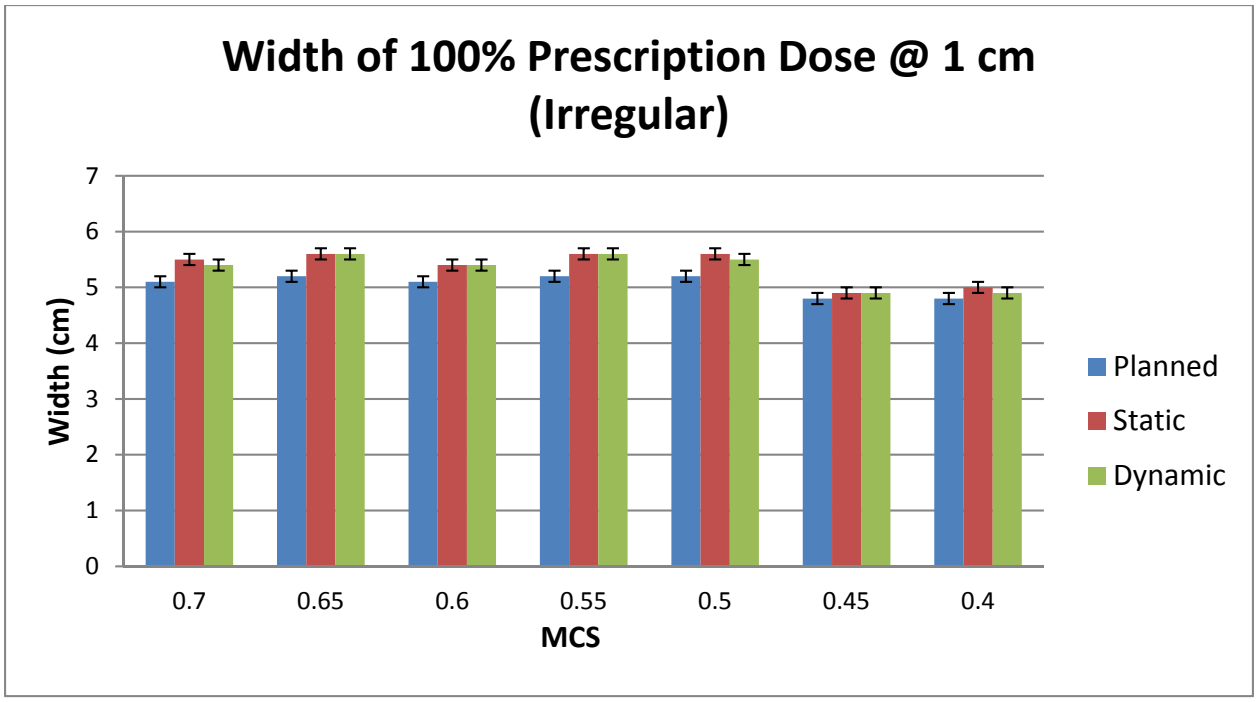

Figure 147: Width of the 100% prescription dose (1000 cGy) of planned, static and dynamic dose distribution for irregular trace at an amplitude of 1 cm.

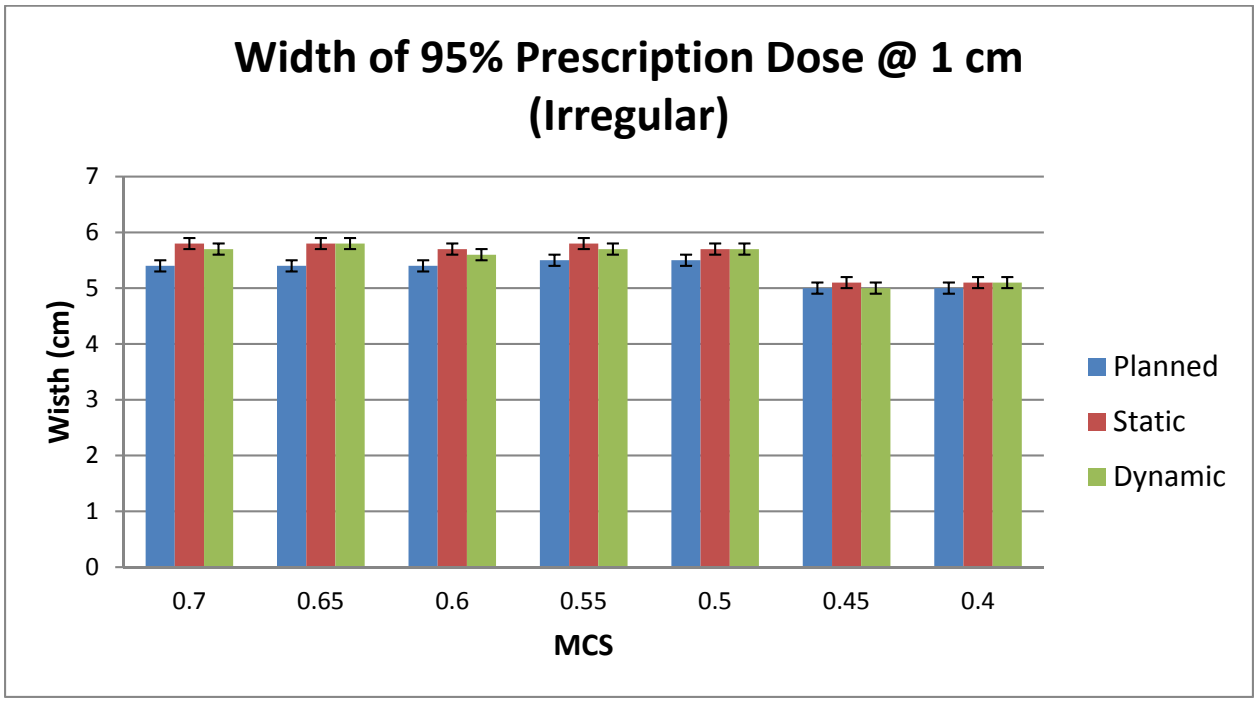

Figure 148: Width of the 95% prescription dose (950 cGy) of planned, static and dynamic dose distribution for irregular trace at an amplitude of 1 cm.

Appendix E. Gamma Analysis Supplemental Tables

Table 31: Patient trace 1 ITV gamma analysis results (1 cm)

MCS	Static Gamma (3%/3mm)	Dynamic Gamma (3%/3mm)	Static Gamma (5%/3mm)	Dynamic Gamma (5%/3mm)
0.70	91.42	88.04	92.53	88.99
0.65	95.04	94.96	95.28	95.83
0.60	91.97	84.03	92.53	84.82
0.55	86.86	91.90	87.49	92.45
0.50	88.01	85.85	88.49	87.03
0.45	79.84	85.36	80.28	86.15
0.40	80.25	80.48	80.65	80.56

Table 32: Patient trace 1 ITV gamma analysis results (2 cm)

MCS	Static Gamma (3%/3mm)	Dynamic Gamma (3%/3mm)	Static Gamma (5%/3mm)	Dynamic Gamma (5%/3mm)
0.75	90.26	88.41	90.39	90.65
0.70	90.06	88.28	91.05	89.34
0.65	86.90	86.37	88.22	87.16
0.60	85.52	86.04	86.31	87.16
0.55	84.27	82.36	85.12	83.87
0.50	82.49	67.15	82.82	67.81
0.45	81.47	64.32	82.42	65.52
0.40	87.10	75.64	88.22	76.50

Table 33: Patient trace 2 ITV gamma analysis results (1 cm)

MCS	Static Gamma (3%/3mm)	Dynamic Gamma (3%/3mm)	Static Gamma (5%/3mm)	Dynamic Gamma (5%/3mm)
0.70	95.12	97.02	95.62	98.59
0.65	90.16	95.04	90.82	96.28
0.60	89.66	94.46	90.16	95.45
0.55	85.13	82.45	86.31	83.87
0.50	85.53	84.37	85.69	85.03
0.45	81.80	84.45	82.80	85.36
0.40	78.33	79.98	79.49	82.38

Table 34: Patient trace 2 ITV gamma analysis results (2 cm)

MCS	Static Gamma (3%/3mm)	Dynamic Gamma (3%/3mm)	Static Gamma (5%/3mm)	Dynamic Gamma (5%/3mm)
0.75	89.07	98.75	90.65	99.14
0.70	94.67	94.27	96.77	95.19
0.65	92.50	93.09	93.09	94.34
0.60	96.58	95.52	97.56	96.58
0.55	93.22	90.13	94.47	91.05
0.50	82.23	83.75	83.26	84.46
0.45	88.02	81.90	89.27	83.21
0.40	85.25	70.44	85.85	71.63

Table 35: Irregular trace ITV gamma analysis results (1 cm)

MCS	Static Gamma (3%/3mm)	Dynamic Gamma (3%/3mm)	Static Gamma (5%/3mm)	Dynamic Gamma (5%/3mm)
0.70	93.78	83.40	94.11	83.99
0.65	96.32	84.69	96.79	85.38
0.60	90.62	79.35	90.98	80.28
0.55	91.15	85.62	91.88	86.21
0.50	81.56	73.29	82.14	74.54
0.45	82.90	78.48	83.21	78.76
0.40	80.65	75.84	81.91	75.93

Table 36: Irregular trace ITV gamma analysis results (2 cm)

MCS	Static Gamma (3%/3mm)	Dynamic Gamma (3%/3mm)	Static Gamma (5%/3mm)	Dynamic Gamma (5%/3mm)
0.75	90.01	80.14	90.28	81.65
0.70	88.06	86.37	88.22	87.52
0.65	87.56	77.90	89.24	80.57
0.60	87.98	78.52	88.13	79.16
0.55	86.90	76.12	87.22	78.22
0.50	81.62	78.51	81.93	79.31
0.45	85.72	76.89	86.25	78.34
0.40	81.10	64.75	82.42	67.81

Table 37: Patient trace 1 PTV gamma analysis results (1 cm)

MCS	Static Gamma (3%/3mm)	Dynamic Gamma (3%/3mm)	Static Gamma (5%/3mm)	Dynamic Gamma (5%/3mm)
0.70	85.94	85.32	86.51	85.84
0.65	92.01	91.49	92.30	92.64
0.60	90.77	85.99	91.58	86.56
0.55	87.57	93.74	87.90	93.97
0.50	83.34	85.41	83.59	86.18
0.45	78.14	70.83	78.77	71.45
0.40	85.03	84.07	85.41	84.27

Table 38: Patient trace 1 PTV gamma analysis results (2 cm)

MCS	Static Gamma (3%/3mm)	Dynamic Gamma (3%/3mm)	Static Gamma (5%/3mm)	Dynamic Gamma (5%/3mm)
0.75	86.56	83.59	86.90	84.66
0.70	87.23	86.73	87.72	88.05
0.65	86.19	88.59	86.61	89.29
0.60	86.03	87.43	86.52	87.97
0.55	82.22	79.62	83.01	80.53
0.50	82.55	72.22	83.63	73.05
0.45	80.32	75.24	81.11	75.86
0.40	80.12	78.09	80.94	78.68

Table 39: Patient trace 2 PTV gamma analysis results (1 cm)

MCS	Static Gamma (3%/3mm)	Dynamic Gamma (3%/3mm)	Static Gamma (5%/3mm)	Dynamic Gamma (5%/3mm)
0.70	95.57	97.96	96.17	98.86
0.65	93.28	94.92	93.68	95.37
0.60	94.67	96.86	94.92	97.31
0.55	88.67	86.18	89.24	87.09
0.50	87.41	90.64	87.51	91.09
0.45	83.62	90.54	84.02	91.14
0.40	84.17	88.30	84.82	89.50

Table 40: Patient trace 2 PTV gamma analysis results (2 cm)

MCS	Static Gamma (3%/3mm)	Dynamic Gamma (3%/3mm)	Static Gamma (5%/3mm)	Dynamic Gamma (5%/3mm)
0.75	91.94	99.17	93.01	99.46
0.70	95.74	94.07	96.94	95.33
0.65	94.92	94.42	95.29	95.08
0.60	96.55	96.94	97.27	97.60
0.55	94.09	95.78	94.87	96.36
0.50	89.17	84.08	89.83	84.58
0.45	91.90	85.86	92.39	86.44
0.40	88.18	81.77	88.51	82.55

Table 41: Irregular trace PTV gamma analysis results (1 cm)

MCS	Static Gamma (3%/3mm)	Dynamic Gamma (3%/3mm)	Static Gamma (5%/3mm)	Dynamic Gamma (5%/3mm)
0.70	94.26	86.78	94.92	86.99
0.65	91.49	90.63	92.65	91.25
0.60	88.34	87.18	88.56	87.84
0.55	85.12	88.51	87.01	88.67
0.50	86.24	82.34	87.51	82.76
0.45	83.45	79.24	83.45	80.54
0.40	79.23	75.63	80.32	78.17

Table 42: Irregular trace PTV gamma analysis results (2 cm)

MCS	Static Gamma (3%/3mm)	Dynamic Gamma (3%/3mm)	Static Gamma (5%/3mm)	Dynamic Gamma (5%/3mm)
0.75	86.90	89.25	87.20	90.10
0.70	90.15	82.64	90.37	83.01
0.65	86.23	84.25	86.52	84.71
0.60	83.78	82.69	84.31	83.36
0.55	85.30	76.23	85.62	77.77
0.50	79.29	71.45	82.36	71.83
0.45	74.81	77.24	75.41	78.56
0.40	75.84	71.31	76.23	72.49

Vita

Desmond Fernandez was born in Baton Rouge, Louisiana in 1991. He is the son of Donald and Patricia Fernandez. Desmond grew up in Plaquemine, Louisiana where he attended Plaquemine High School. He graduated from Plaquemine High School in 2009 and enrolled at Southern University A&M College, where he received his Bachelor of Science degree in physics. After graduating from Southern University in the spring of 2013, he matriculated into LSU's medical physics M.S. program. Following graduation from the medical physics program, he expects to begin his medical physics residency at Mary Bird Perkins Cancer Center.